

# Plastic Shrinkage Behaviour and Mitigation Measures for Fibre Reinforced Concrete



A thesis presented for the degree of  
*Doctor of Philosophy in Civil and Structural Engineering*  
at The University of Sheffield

**By**  
**Talal O Alshammari**

Sheffield  
March 2023

## Abstract

Plastic shrinkage (in fresh concrete) can cause the initiation of early-age cracking, which can eventually evolve into larger cracks, compromising durability and reducing overall service-life. Plastic shrinkage cracks can also facilitate the ingress of harmful chemicals (e.g. chlorides) into the concrete and increase the possibility of corrosion of steel bars.

Plastic shrinkage is affected by various parameters, including the properties and proportions of the concrete constituents, as well the environmental conditions (temperature, relative humidity, and wind speed). These parameters affect the bleeding and evaporation rates of surface water, and are thus directly related to the formation of plastic shrinkage cracks. This research aims to investigate the mechanisms of plastic shrinkage and plastic shrinkage cracking, with a view of developing cost-effective and sustainable mitigation strategies to control early-age cracking.

The main parameters investigated in this research study are: 1) fibre type (i.e. manufactured steel fibres (MSF) and recycled tyre steel fibre (RTSF) from post-consumer tyres) and fibre content (10, 20, and 30 kg/m<sup>3</sup>); 2) water to cement ratio (0.5 – 0.6); 3) environmental conditions (wind speed and temperature); and 4) concrete curing methods and use of admixtures.

RTSF was found more effective in preventing crack development than MSF, at the same fibre content. When fresh concrete was exposed to environmental conditions typical of Saudi Arabia (high temperatures and wind speed), it was found that while 30 kg/m<sup>3</sup> of RTSF can control plastic shrinkage cracks at lower w/c ratios (0.5 and 0.55) and in low and mid environmental conditions (T=28-36 °C, and wind speed=3-4.6 m/s), for higher w/c ratio (0.6) and in more extreme conditions (T=45 °C and wind speed=7 m/s), the use of 40 kg/m<sup>3</sup> of RTSF fibre was required to completely eliminate surface plastic shrinkage cracks. All of the different mitigation strategies commonly used in construction were successful in restraining plastic shrinkage cracks, albeit with different associated cost and efficiency. The use of cold water (7 °C) in the mix, showed the most benefits in terms of cost, quality, and time, while the use of RTSF gave optimal results in terms of performance and overall structural benefits.

Based on the main results of this study, recommendations are made to control plastic shrinkage in pavements. The recommendations consider not only the overall mechanical performance of the concrete (crack initial time, crack reduction ratio) and construction method, but also cost, speed of construction/application, and sustainable.

## **Acknowledgement**

This work would have not been possible without the support that I have received from a few people that I would include here:

First and foremost, I would like to express my deepest gratitude to my supervisors Professor Kypros Pilakoutas and Dr. Maurizio Guadagnini for their assistance, encouragement, guidance, patience, support, and their help to complete this work. Without their invaluable support and endless enthusiasm, this work would have not done. Many thanks.

I would thank Al-jouf University and the Ministry of Education of Saudi Arabia for their financial support for this research.

Many thanks for the technical staff of the Concrete and Heavy Structures Lab to their help, support, and patience during this research.

I would thank all the members of Concrete and Earthquake Engineering (CEE) group for their encouragement and help during the meetings of this work.

I would thank all my PhD mates in our office (E110) for the good time we had together, and for their continuous support.

Finally, I would like to thank all my family for their tremendous support, love, care, patience and encouragement during my study.

# Table of Contents

<b>Abstract.....</b>	<b>ii</b>
<b>Acknowledgement.....</b>	<b>iii</b>
<b>Chapter 1 : Introduction</b>	<b>1</b>
1.1. Introduction	2
1.2. Research motivation	2
1.3. Research aim and objectives	3
1.4. Research significance	3
1.5. Thesis layout	4
1.6. References	6
<b>Chapter 2 : Literature review</b>	<b>9</b>
2.1. Research background	10
2.1.1. Brief literature review on shrinkage cracks	10
2.1.2. Plastic shrinkage	10
2.1.3. Autogenous shrinkage	11
2.1.4. Chemical shrinkage	12
2.1.5. Drying shrinkage	13
2.1.6. The phenomena and the mechanism of plastic shrinkage cracking	13
2.1.7. Influencing factors of plastic shrinkage cracking	14
2.1.8. Plastic shrinkage testing techniques	17
2.2. Materials properties	23
2.2.1. Cement	23
2.2.2. Water	23
2.2.3. Aggregates	23
2.2.4. Admixture	30
2.3. References	31
<b>Chapter 3 : Performance of Manufactured and Recycled Steel Fibres in Restraining Concrete Plastic Shrinkage Cracks</b>	<b>37</b>
3.1. Introduction	39
3.1.1. Plastic Shrinkage Phenomenon	39
3.1.2. Use of Fibres to Mitigate Shrinkage-Induced Cracking	41
3.1.3. Restrained Plastic Shrinkage Testing Techniques	43
3.1.4. Measurements	44
3.1.5. Significance of Research	44
3.2. Experimental Program	45

3.2.1. Materials	45
3.2.2. Mix Design	48
3.2.3. Mixing and Casting Procedure	49
3.3. Methodology	49
3.3.1. Workability	49
3.3.2. Compressive Strength	49
3.3.3. Evaporation Rate	49
3.3.4. Plastic Shrinkage Test	50
3.4. Experimental Results and Discussion	53
3.4.1. Workability	53
3.4.2. Compressive Strength	54
3.4.3. Evaporation Rate	55
3.4.4. Plastic Shrinkage Test Results	57
3.5. Conclusions	62
3.6. References	64
<b>Chapter 4 : The Effect of Harsh Environmental Conditions on Concrete Plastic Shrinkage Cracks: Case Study Saudi Arabia</b>	<b>72</b>
4.1. Introduction	74
4.1.1. Problem Statement	77
4.1.2. Selection of Environmental Conditions	77
4.1.3. Significance of Research	80
4.2. Materials	80
4.2.1. Concrete and Specimen Preparations	80
4.2.2. Recycled Tire Steel Fibre (RTSF)	81
4.3. Methodology	83
4.3.1. Compressive Strength	83
4.3.2. Evaporation Rate	83
4.3.3. Plastic Shrinkage Test	83
4.3.4. Measurement of the Cracks	84
4.3.5. Examined Environmental Conditions	84
4.4. Experimental Results and Discussion	85
4.4.1. Compressive Strength	85
4.4.2. Evaporation Rate	86
4.4.3. Crack Measurements and Results	88
4.4.4. Influence of Environmental Conditions on Evaporation Rate and Cracking	91
4.4.5. Crack Reduction Ratio (CRR)	92

4.5. Conclusions	94
4.6. References	96
<b>Chapter 5 : Effect of Curing Methods on Plastic Shrinkage Cracking</b>	<b>104</b>
5.1. Introduction	106
5.1.1. Concrete curing methods	106
5.1.2. Significance of research	108
5.2. Materials and experimental methods	108
5.2.1. Mixture proportioning	108
5.2.2. Mixing and placing	109
5.2.3. Experimental methods	109
5.3. Experimental results and discussion	113
5.3.1. Evaporation rate	115
5.3.2. Crack width development	118
5.3.3. Comparison of the concrete curing methods	121
5.4. Conclusion	124
5.5. References	126
<b>Chapter 6 : Conclusions and Recommendations for Future Work</b>	<b>131</b>
6.1. Conclusions	132
6.1.1. Performance of RTSF and MSF in restraining plastic shrinkage cracking (Chapter 3).	132
6.1.2. The Effect of Harsh Environmental Conditions on Concrete Plastic Shrinkage Cracks: Case Study Saudi Arabia (Chapter 4).	132
6.1.3. Effect of various curing methods on plastic shrinkage cracking (Chapter 5).	133
6.2. Recommendations for Future Work	134
6.2.1. Fibre length distribution and hybrid blends	134
6.2.2. Modifications to the plastic shrinkage cracking test	134
6.2.3. Concrete curing methods	134
<b>Appendix A: Literature review.....</b>	<b>137</b>
<b>Appendix B: Experimental Results for Chapter 2 "Performance of SFRC for Restraining Concrete Plastic Shrinkage Cracks" .....</b>	<b>145</b>
<b>Appendix C: Experimental Results for Chapter 3 " Influence of Environmental Conditions on Concrete Plastic Shrinkage Cracks ".....</b>	<b>183</b>
<b>Appendix D: Experimental Results for Chapter 4 "Effects of Concrete Curing Methods on Plastic Shrinkage Cracking".....</b>	<b>239</b>

## List of Figures

Figure 2.1: Typical plastic shrinkage cracks [5].	11
Figure 2.2: Principal measurement methods for chemical shrinkage of cementitious materials [21,22]	12
Figure 2.3: Stages during capillary pressure build-up [33].	14
Figure 2.4: Effect of w/c on time to initiation of cracks [7].	16
Figure 2.5: Effect of cement content on total area of cracks [7].	16
Figure 2.6: Test specimen dimensions [46].	17
Figure 2.7: Restrained ring shrinkage test setup [47].	18
Figure 2.8: Steel slab mould [48]	19
Figure 2.9: A substrate base with protuberances [49].	20
Figure 2.10: Schematic of plastic shrinkage cracking test setup: a) side view; b) top view; and c) concrete substrate geometry [50].	21
Figure 2.11: Schematic of the chamber as suggested by the [35].	22
Figure 2.12: Left and right path in the chamber [35].	22
Figure 2.13: Particle size of fine aggregates with limitations.	24
Figure 2.14: Particle size of 10 mm aggregates with limitations.	25
Figure 2.15: Particle size of 20 mm aggregates with limitations.	25
Figure 2.16: Coarse aggregates weight in the water (10 mm, and 20 mm size)	27
Figure 2.17: Fine aggregates weight in the water	27
Figure 2.18: Tamping the aggregate into the mold (core test)	28
Figure 2.19: Dry the coarse aggregates 10 mm size by towel	28
Figure 2.20: Dry the coarse aggregates 20 mm size in the oven	29
Figure 2.21: Oven dry of the aggregates.	29
Figure 3.1: Evaporation and bleeding of concrete [17].	40
Figure 3.2: Typical behaviour of plastic shrinkage cracking [20].	41
Figure 3.3 : Appearance of (a) RTSF and (b) MSF.	46
Figure 3.4: Average (a) length, (b) diameter, and (c) tensile strength of the RTSF.	46
Figure 3.5: Set-up for tensile testing of RTSF.	47
Figure 3.6: RTSF length distribution.	47
Figure 3.7: Schematic section of the chamber.	50
Figure 3.8: Schematic plan of the contents of the chamber.	50
Figure 3.9: Geometry of the stress riser and internal restraints [53].	51
Figure 3.10: The complete mould.	51
Figure 3.11: Set-up for plastic shrinkage test.	52
Figure 3.12: Image processing steps.	53
Figure 3.13: Effect of fibre type and dosage on slump of concrete.	54
Figure 3.14: Compressive strength and normalized ratio of PC and FRC at 1 day (a, c) and 28 days (b, d) for cubes inside (In) and outside (Out) the chamber.	55
Figure 3.15: Environmental conditions for all mixes.	56
Figure 3.16: Evaporation rate of the various mixes compared to PC: (a) RTSFC10; (b) MSFC10; (c) RTSFC20; (d) MSFC20; (e) RTSFC30; (f) MSFC30.	57

Figure 3.17: Crack width evolution for all specimens compared to their PC counterpart: (a) RTSFC10; (b) MSFC10; (c) RTSFC20; (d) MSFC20; (e) RTSFC20; (f) MSFC30. ....	58
Figure 3.18: Crack reduction ratio (CRR) in specimens containing RTSF and MSF at 24 h. ....	59
Figure 3.19: Evolution of crack reduction ratio (CRR) for specimens containing RTSF and MSF at 6 h.....	59
Figure 3.20: Location of the cross-section of RTSF and MSF slabs (red dashed line).....	60
Figure 3.21: (a) Cross-section of specimen RTSFC30 and selected region of interest (ROI). (b). Magnified ROI of cross-section of specimen RTSFC30 (left) and distribution of aggregates and fibres (right). (c). Cross-section of specimen MSFC30 and selected region of interest (ROI). (d). Magnified ROI of cross-section of specimen MSFC30 (left) and distribution of aggregates and fibres (right). ....	61
Figure 4.1: Factors affecting plastic shrinkage cracking. ....	75
Figure 4.2: Map of the three selected cities of Saudi Arabia.....	78
Figure 4.3: Selected environments climate graphs [41].....	80
Figure 4.4: RTSF.....	82
Figure 4.5: (a) Tensile strength; and (b) RTSF length distributions.....	82
Figure 4.6: Schematic section of the chamber.....	84
Figure 4.7: Examined sets of environmental conditions.....	85
Figure 4.8: Compressive strength of PC and FRC at 28 days of curing for cubes inside and outside the chamber. * higher content of RTSF (40 kg/m <sup>3</sup> ). ....	86
Figure 4.9: Effect of temperature on evaporation rates (wind speed = 4.7 m/s).....	87
Figure 4.10: Effect of wind speed on evaporation rates (T = 36 °C).....	87
Figure 4.11: Effect of water cement ratio on evaporation rates (T = 36 °C, Wind speed = 4.7 m/s).....	88
Figure 4.12: Typical crack pattern in plain concrete (PC) specimens of high temperature examined at 24 h.....	88
Figure 4.13: Crack evolution for the specimens subjected to the examined temperatures. ....	89
Figure 4.14: Crack evolution for the specimens subjected to the examined wind speeds. ....	90
Figure 4.15: Crack evolution for the specimens manufactured using different w/c ratios.....	90
Figure 4.16: Effect of (a) temperature; (b) wind speed; and (c) w/c ratio on evaporation rate at crack initiation and time of crack initiation. * higher content of RTSF (40 kg/m <sup>3</sup> ). ....	91
Figure 4.17: Crack reduction ratio for all temperatures.....	92
Figure 4.18: Crack reduction ratio for all wind speeds.....	93
Figure 4.19: Crack reduction ratio for all water cement ratio.....	94
Figure 5.1: Plastic shrinkage test chamber .....	109
Figure 5.2: Schematic of inside the chamber.....	110
Figure 5.3: RTSF length distribution.....	113
Figure 5.4: Environmental conditions of all concrete curing methods. ....	114
Figure 5.5: Concrete temperature of all concrete curing methods. ....	114
Figure 5.6: Evaporation rate of the various curing methods compared to PC. ....	117
Figure 5.7: Temperature (red curves) and crack width (blue curves) evolution for all curing methods compared to their PC counterpart. ....	119
Figure 5.8: Crack reduction ratio of all concrete curing methods .....	120
Figure 5.9: Power floating concrete of big scale. ....	120



Figure 5.10: Comparison between concrete curing methods..... 124

## List of Tables

Table 2.1 Concrete mix proportions. ....	48
Table 2.2 Physical properties of fine and coarse aggregates. ....	48
Table 3.1: Parameters of the study. ....	81
Table 4.1: Concrete mix proportions. ....	108
Table 4.2: Comparison of concrete curing methods (in brackets the efficiency index used in Figure 4.10) .....	122

**This page is intentionally left blank**

## **Chapter 1 : Introduction**

This chapter provides the motivation and introduces the aim, objectives, and the layout of this thesis.

## 1.1. Introduction

Concrete is one of the most used structural materials owing to its low cost and overall good performance and durability. However, when exposed to harsh environmental conditions, several aspects can affect its long-term performance, and its deterioration can lead to costly maintenance [1,2]. One of the main factors affecting concrete durability and long-term performance is surface cracking [3].

Cracking in concrete, though unavoidable, is a universal problem [4] and considerable research has been carried out to understand its development. The development of concrete cracks can be attributed to structural and non-structural causes [5]. Structural cracking in concrete usually occurs as a result of external loading and much of the existing research has focused on examining this aspect. Non-structural cracking in concrete is mainly associated with the nature of the mix design, casting and curing, and environmental exposure [6]. Under normal circumstance, non-structural cracking does not lead to structural failure, but it can reduce service life by promoting corrosion of the reinforcing steel and accelerate concrete deteriorations [7].

Non-structural cracks can appear in concrete at both plastic and hardened state, and are known as shrinkage cracks. When the concrete is still in its plastic state, within a few hours from casting and before reaching the hardened state, cracks can develop at the surface of the concrete due to plastic shrinkage caused by excessive bleeding and evaporation. Cracks that initiate during the plastic state can progress until the final setting time and continue to develop in the hardened state due to drying shrinkage.

## 1.2. Research motivation

The aim of this research work is to understand and improve the performance of fresh concrete under different environmental conditions against non-structural plastic shrinkage cracks, and provide a more sustainable concrete. First, an in-depth understanding needs to be made on the mechanisms of plastic shrinkage cracking and associated phenomena. For many decades, the use of different types of fibres in concrete has been found to provide the most effective solution to mitigate plastic shrinkage cracks [8–12]. However, as one of the objectives of this research is to find a potential and sustainable alternative to manufactured fibres, the effectiveness of recycled tyre steel fibres is examined to reduce overall costs and improve the environmental credentials of concrete. Also, as harsher environmental conditions are expected to develop due to climate change, an investigation on the performance of concrete at its plastic

state is carried out under high, mid, and low environmental conditions to assess the impact of environmental exposure on plastic shrinkage and associated cracking. Finally, as concrete curing can critically affect plastic shrinkage, different methods are examined and assessed in terms of their effectiveness and sustainability credential, including time, quality, and overall costs.

### **1.3. Research aim and objectives**

The aim of this research is to investigate the plastic shrinkage of concrete exposed to different environmental conditions and examine the impact of steel fibres and other curing methods on restraining plastic shrinkage cracking.

To achieve the above aim, the following objectives are identified:

Obj1. To identify the mechanisms contributing for the development of suitable testing methods to examine plastic shrinkage cracking.

Obj2. To examine the effects of manufactured and recycled tyre steel fibres on the performance of concrete at the plastic state (plastic shrinkage cracking).

Obj3. To evaluate the impact of environmental conditions on early age strength evolution of concrete containing manufactured and recycled tyre steel fibres.

Obj4. To study the effects of environmental conditions typical of Middle Eastern regions on the plastic shrinkage behaviour of concrete.

Obj5. To study the effects of different curing methods and surface finishes on plastic shrinkage induced cracking in concrete.

Obj6. To assess the environmental benefits and cost implications of different curing methods and mitigation strategies to control plastic shrinkage cracking.

### **1.4. Research significance**

This work will develop further understanding on the cracking behaviour of concrete at the plastic state and provide key experimental data that will enable a more reliable assessment of the effect of environmental conditions on plastic shrinkage cracking. In turn, this will enable the development of more cost-effective and sustainable solutions to control plastic shrinkage cracking in concrete and increase the service life of concrete structures.

Recycled tyre steel fibres (RTSF) possess excellent mechanical characteristics and provide a valid alternative to manufactured steel fibres in structural applications. Their use in concrete pavements can reduce the demand on natural resources, eliminate issues related to

their disposal, and offer a promising solution for the development of more sustainable, durable and economic concrete pavements.

## 1.5. Thesis layout

This thesis consists of six chapters, including an introductory section in chapter 1 and a brief literature review of this research in chapter 2, followed by three paper-style chapters and a concluding section with recommendations for future work. Four Appendixes are also included the relevant experimental data.

**Chapter 1** This chapter provides an introductory section including motivation, aim, objectives, and significance of this research.

**Chapter 2** This chapter provides a brief literature review of this research and introduces the initial tests for the materials that were used in this study.

**Chapter 3** Titled “Performance of Manufactured and Recycled Steel Fibres in Restraining Concrete Plastic Shrinkage Cracks” is based on Alshammari et al. [13] published in “Materials” and addresses Objectives 1, 2, and 3. This study evaluates the performance of recycled tyre steel fibre (RTSF) and manufactured steel fibre (MSF) to restrain plastic shrinkage cracks. Different doses of RTSF, and MSF were added to the concrete at 0, 10, 20, 30 kg/m<sup>3</sup> to mitigate plastic shrinkage cracking. The compressive strength was also tested at the age of one-day, to assess the effects of environmental conditions on early hydration, and at 28 days. The influence of RTSF and MSF on workability is discussed.

**Chapter 4** Titled “The Effect of Harsh Environmental Conditions on Concrete Plastic Shrinkage Cracks: Case Study Saudi Arabia” is based on Alshammari et al. [14] published in “Materials” and addresses Objectives 1-4. This study examines the effects of high, mid, and low—wind speed, air temperature, and relative humidity on plastic shrinkage. Saudi Arabia was used in a case study as a hot weather country. Three of its main cities were selected as representative of typical environmental conditions and such conditions were replicated in the laboratory to study their effect on plastic shrinkage induced cracking. The concrete specimens were exposed to three different air temperatures (28 °C, 36 °C, and 45 °C and wind speeds (3 m/s, 4.7 m/s, and 7 m/s). The effect of different water to cement ratios on plastic shrinkage was also examined.

**Chapter 5** Titled “Effect of Curing Methods on Plastic Shrinkage Cracking” is based on Alshammari et al. [15] published in “Construction materials” and addresses Objectives 1, 2, 5, and 6. This study assesses the effects of concrete curing methods to avoid or reduce plastic shrinkage cracking in concrete. The concrete curing methods are compared in terms of mechanical performance, sustainability, cost, and time of application. The concrete curing methods that were used in this study included: covering the concrete with plastic sheet or wet-hessian fabric; finishing the surface using a power float; using cold mixing water; adding three curing concrete admixtures (Safecure Super, Safecure Super 90W-10%, and Superplastizer); and adding 40 kg/m<sup>3</sup> of RTSF.

**Chapter 6** This chapter summarizes the main conclusions from all chapters and provides recommendations for future work.



## 1.6. References

- [1] N. Renne, P. Kara De Maeijer, B. Craeye, M. Buyle, A. Audenaert, Sustainable Assessment of Concrete Repairs through Life Cycle Assessment (LCA) and Life Cycle Cost Analysis (LCCA), *Infrastructures*. 7 (2022).  
<https://doi.org/10.3390/infrastructures7100128>.
- [2] S.T. Li, C.Q. and Yang, Prediction of concrete crack width under combined reinforcement corrosion and applied load, *J. Eng. Mech.* 137 (2011) 722–731.
- [3] P. min Zhan, Z. hai He, Application of shrinkage reducing admixture in concrete: A review, *Constr. Build. Mater.* 201 (2019) 676–690.  
<https://doi.org/10.1016/j.conbuildmat.2018.12.209>.
- [4] G.W. Scherer, Drying, Shrinkage, and Cracking of Cementitious Materials, *Transp. Porous Media*. 110 (2015) 311–331. <https://doi.org/10.1007/s11242-015-0518-5>.
- [5] CCIP-048, Technical Report No.22: Non-structural cracks in concrete (4th ed), Surrey: The Concrete Society: A Cement and Concrete Industry Publication, (2010).
- [6] H.G. Kwak, S.J. Ha, J.K. Kim, Non-structural cracking in RC walls: Part I. Finite element formulation, *Cem. Concr. Res.* 36 (2006) 749–760.  
<https://doi.org/10.1016/j.cemconres.2005.12.001>.
- [7] P. Arito, Influence of mix design parameters on restrained shrinkage cracking in non-structural concrete patch repair mortars, (2018).
- [8] C. Qi, J. Weiss, J. Olek, Statistical significance of the restrained slab test for quantifying plastic cracking in fiber reinforced concrete, *J. ASTM Int.* 2 (2005) 105–122.  
<https://doi.org/10.1520/jai12242>.
- [9] I.M.G. Bertelsen, L.M. Ottosen, G. Fischer, Influence of fibre characteristics on plastic shrinkage cracking in cement-based materials: A review, *Constr. Build. Mater.* (2020).  
<https://doi.org/10.1016/j.conbuildmat.2019.116769>.
- [10] N. Pešić, S. Živanović, R. Garcia, P. Papastergiou, Mechanical properties of concrete reinforced with recycled HDPE plastic fibres, *Constr. Build. Mater.* 115 (2016) 362–370. <https://doi.org/10.1016/j.conbuildmat.2016.04.050>.
- [11] G. Olivier, R. Combrinck, M. Kayondo, W.P. Boshoff, Combined effect of nano-silica, super absorbent polymers, and synthetic fibres on plastic shrinkage cracking in concrete, *Constr. Build. Mater.* 192 (2018) 85–98.  
<https://doi.org/10.1016/j.conbuildmat.2018.10.102>.
- [12] Soroushian, P., Mirza, F. and Alhozajiny, A., Plastic shrinkage cracking of

- polypropylene fiber reinforced concrete., *Mater. J.* 92 (1993) 553–560.
- [13] T.O. Alshammari, M. Guadagnini, K. Pilakoutas, Performance of Manufactured and Recycled Steel Fibres in Restraining Concrete Plastic Shrinkage Cracks, *Materials (Basel)*. 16 (2023) 713. <https://doi.org/10.2139/ssrn.4232808>.
- [14] T.O. Alshammari, M. Guadagnini, K. Pilakoutas, The Effect of Harsh Environmental Conditions on Concrete Plastic Shrinkage Cracks: Case Study Saudi Arabia, *Materials (Basel)*. 15 (2022). <https://doi.org/10.3390/ma15238622>.
- [15] T.O. Alshammari, K. Pilakoutas, M. Guadagnini, Effect of Curing Methods on Plastic Shrinkage Cracking, *Constr. Mater.* (2023) 244–258.

**This page is intentionally left blank**

## **Chapter 2 : Literature review**

This chapter provides a brief literature review of this research and introduces the initial tests for the materials that were used in this study.

**Appendix A** has provided the relevant experimental data of this chapter.

## **2.1. Research background**

### **2.1.1. Brief literature review on shrinkage cracks**

Concrete starts changing its volume soon after casting due to many reasons. Following vibration, the heavy aggregates tend to sink down while lighter materials, including water, tend to rise and some water comes out of the mix on the surface as bleed water. Hydration of cement leads to the development of chemical compounds that occupy less volume than the original unbound materials. The surrounding environmental conditions also play a critical role as they affect the initial and final setting of concrete. The volume change of concrete during both the plastic and hardened stage can cause shrinkage cracking [1] and can have a significant impact on the long-term performance and durability of structures. These surface shrinkage cracks are usually divided into two categories (plastic, and drying) [2]. In the following sections, the different types of shrinkage cracks that occur on the surface of the concrete are briefly described, and a detailed explanation of the phenomena of plastic shrinkage cracks is given.

### **2.1.2. Plastic shrinkage**

Within the first few hours from casting, and before the concrete begins the final set, plastic shrinkage cracks may appear in fresh concrete. Plastic shrinkage cracking starts when all the bleeding water starts to evaporate from the surface of the concrete due to the environmental conditions [3,4]. Cracks can develop as single or multiple cracks with a length varying between a few centimetres to a few metres (see Figure 2.1) [5]. The occurrence of plastic shrinkage is highly likely at high temperatures and wind speed, and low humidity [6,7]. However, there are other factors that make the plastic shrinkage more likely to occur, including high w/c ratio and high content of fine materials within the mix [8]. After final setting time, plastic shrinkage cracks will become drying shrinkage cracks [9].



Figure 2.1: Typical plastic shrinkage cracks [5].

### 2.1.3. Autogenous shrinkage

The autogenous shrinkage is known as a volume change that is a reason for self-desiccation and chemical process of cement hydration due to the capillary pressure [10]. Autogenous shrinkage is a macroscopic reduction in length without any moisture loss to or from the concrete [11]. The autogenous shrinkage concrete is usually caused by the use of high binder content and low water-to-binder ratio [12]. Altoubat, and Lange [13] made a study that discusses the water-to-binder ratio (w/b) effects in autogenous shrinkage and reported that the autogenous shrinkage increased in concrete with the decrease of water-to-binder ratio and is familiar to occur with less than 0.42 of water-to-binder ratio. In addition to the effects of w/b on autogenous shrinkage, it also depends on the curing time and condition, and mixture composition. Most early-age autogenous shrinkage can develop to a potential cracking on concrete which reduces the durability and mechanical properties of concrete [14].

Fibres were found to resist the autogenous shrinkage on concrete at an early age and delay the occurrence of cracking. It greatly affects the autogenous shrinkage in terms of their size, type and content, dispersion and orientation, elastic modulus, and aspect ratio. Wu et al. [15] investigated the effects of steel fibres (straight, corrugated, and hooked) on restrain autogenous and drying shrinkage cracks. The volume fraction used in this study was (0%, 1%, 2%, and 3%) of steel fibres. The result showed that the use of hooked fibres was most effective in reducing autogenous and drying shrinkage and the optimum fibre content was found at 2% compared to the volume fraction used. Using a combination of steel and polyvinyl alcohol fibres was found more beneficial in restraining autogenous shrinkage than the use of steel fibre only [16,17]. Ma et al. [18] evaluated the effects of cellulose fibres by different volume on

autogenous shrinkage. The results indicated that the cellulose fibres reduced the autogenous shrinkage values up to 70% and 33% lower than control mix.

#### 2.1.4. Chemical shrinkage

Chemical shrinkage is not at all related to the macroscopic volume change of cement or concrete like autogenous shrinkage. It is produced by the reaction between un-hydrated cement and water [11]. The chemical shrinkage was found to be affected by a low water to cement ratio, and a high thickness of cement paste [19]. The results of early volume change of concrete as a result of the chemical shrinkage is generally considered a reduction of durability of concrete structures due to early age cracking [20].

Over the past decades, three measurement methods for chemical shrinkage had outlined in the literature: dilatometry, pycnometry and gravimetry as shown in Figure 2.2 [21,22]. ASTM C1608 [23] had recommended both dilatometry and pycnometry methods as a reliable test method to find chemical shrinkage of cementitious materials. Zhang et al. [19] compared the two methods with a presented method of the chemical shrinkage measurement. The improved method was much higher precision and repeatability than ASTM C 1608 methods.

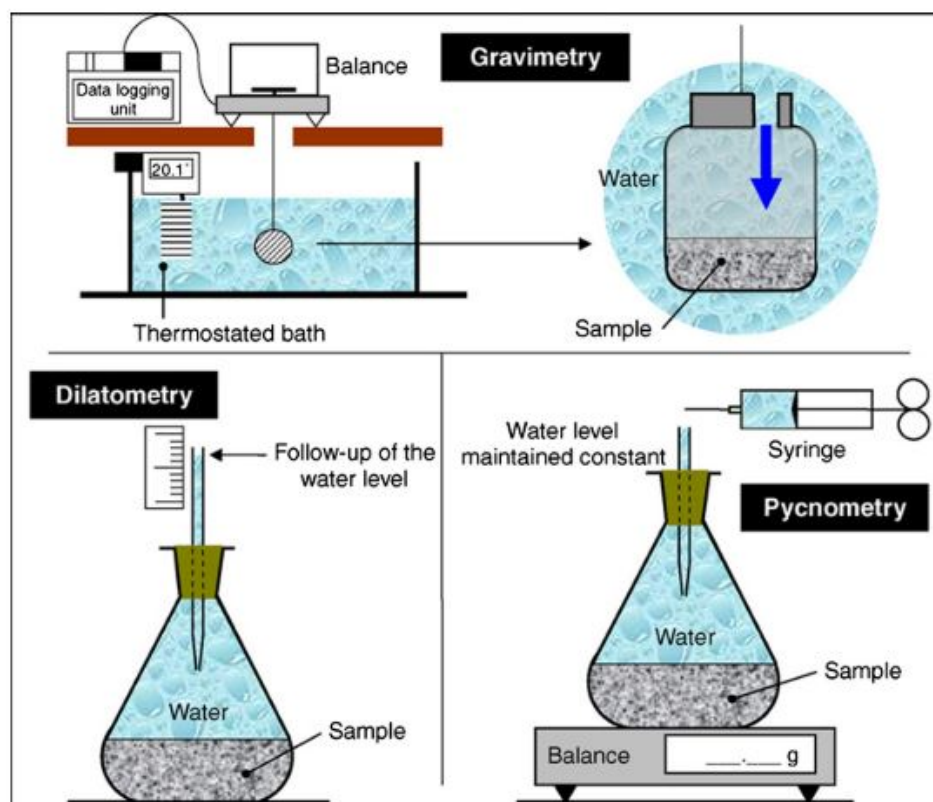


Figure 2.2: Principal measurement methods for chemical shrinkage of cementitious materials [21,22]

### 2.1.5. Drying shrinkage

Drying shrinkage cracks start to develop as early as the first week after casting and continue for months and years. Most often they develop from cracks that started at the plastic stage [24]. Relative humidity and temperature are the main factors affecting drying shrinkage cracks. Saliba et al. [25] explained that plastic shrinkage cracks evolve into drying shrinkage crack as the larger pores in concrete lose their internal water and dry. The internal change in relative humidity caused by drying also contributes to accelerate the rate of cracking. Furthermore, the properties of the concrete constituents, including cement type, aggregates, w/c ratio, and admixtures also affect drying shrinkage [26].

Most recent studies have focused on drying shrinkage cracks and in finding solutions to this practical problem. The use of shrinkage reducing admixtures was found to be very effective in mitigating drying shrinkage as these successfully reduce the surface tension of water [27]. Many studies have also examined reducing drying shrinkage by adding fibres to the concrete. It is reported that the use of steel fibres can reduce drying shrinkage by up to 40% [28]. Younis et al. [29] tested the effects of incorporating short and long recycled steel fibres (with total RSF content of 60 kg/m<sup>3</sup> at contents of 30, 50 and 70%) in self-compacting concrete on drying shrinkage. The results showed that recycled steel fibres reduced and delayed the drying shrinkage in most of the percentages applied, but the 70% showed the best behaviour to eliminate the cracks. Glass fibres have also been shown to be effective at mitigating drying shrinkage cracks and reductions in crack width by up to 20-30% were shown by [30].

### 2.1.6. The phenomena and the mechanism of plastic shrinkage cracking

Plastic shrinkage occurs when concrete starts to lose (bleed) water from its surface due to environmental conditions before the concrete sets. As aggregates and binders are heavier than water, they tend to sink while some matrix with water migrates to the surface and some of the water bleeds to the surface. The rate of bleeding depends on the water content, particle size distribution, viscosity and rate of hydration of cement. When the surface water evaporation rate is higher than the bleeding rate, drying begins. Boshoff and Combrinck [31] and Sayahi et al. [32] studied the behaviour of plastic shrinkage cracks and found that the capillary pressure develops rapidly once the drying time begins, but reduces suddenly when air enters the pores, before initial setting time begins. When initial setting time starts, bleeding is slowed down and can be considered to end. Soon after the initial setting time, the onset of cracking begins and the crack width increases up to the final setting time. After the final setting time is reached, crack growth reduces as the temperature decreases and drying slows down.



Capillary pressure builds up as air enters the concrete from some weak points on the surface [33], and drops when the air has penetrated the concrete. As shown in Figure 2.3, six stages (A - F) can be identified to explain the evolution of capillary pressure inside the concrete during plastic shrinkage cracking.

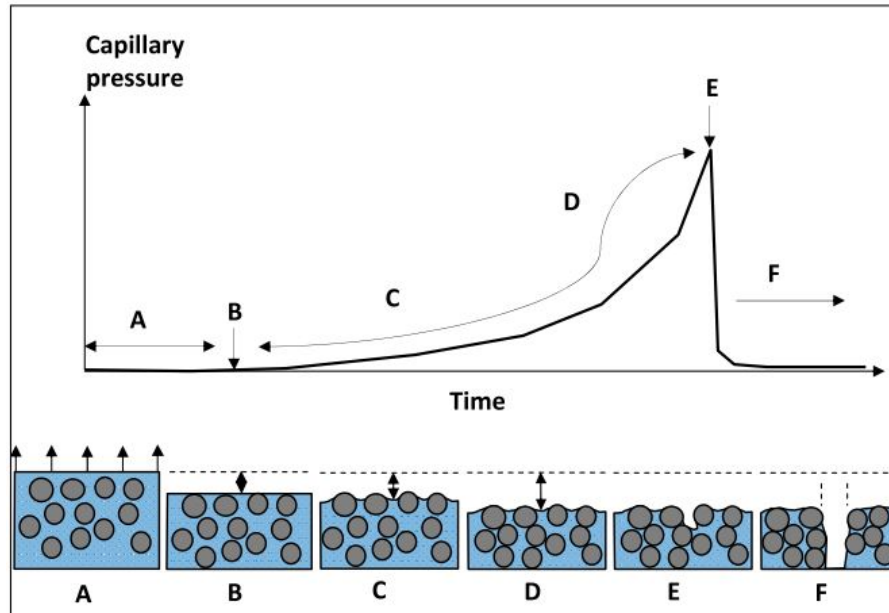


Figure 2.3: Stages during capillary pressure build-up [33].

As shown in Figure 2.3, at stage A, just after casting and bleeding starts, a thin film of water is formed on the surface. At this point the bleeding rate is higher than the evaporation rate. At stage B, the bleeding water accumulates on the concrete surface as the heavier materials sink to the bottom of the concrete due to gravity. At this point the additional pressure created by the bleeding water increases the capillary pressure. At stage C, the bleeding water starts to evaporate and the particles are pulled close together by the water menisci. At stage D, the capillary pressure keeps increasing until the air starts to enter the concrete (stage E). The entry points for the air are weakened by this pressure build-up and coincide with crack openings. At the stage (F), more air penetrates the concrete and plastic shrinkage cracks increase.

### 2.1.7. Influencing factors of plastic shrinkage cracking

Many factors can negatively affect the performance of freshly placed concrete during mixing, casting, and curing. Factors such as environmental conditions, type and quantity of constituent materials (i.e. mix design) affect directly evaporation rate and bleeding rate, respectively, and in turn plastic shrinkage cracking [34]. According to ASTM C1579 [35] and

Uno [36], plastic shrinkage cracking is expected to initiate when the evaporation rate exceeds  $1.0 \text{ kg/m}^2/\text{h}$ .

#### **2.1.7.1. Environmental conditions**

Air and concrete temperature, relative humidity, and wind velocity are the key parameters that affect the evaporation rate of concrete during mixing, casting and curing. Kosmatka et al. [5] observed that plastic shrinkage cracking is more likely to occur in hot weather concreting. ASTM C1579 [35] recommends that concrete should be appropriately cured to avoid cracking associated with plastic shrinkage when the air temperature is higher than  $(36 \pm 3 \text{ }^\circ\text{C})$ , relative humidity higher than  $(30 \pm 10 \%)$ , and wind velocity faster than  $4.7 \text{ m/s}$ . Moreover, ASTM C192/C192M [37] suggests that, before mixing, the temperature of the concrete constituent materials (cement, aggregates, and water) should be in the range of  $20$  to  $30 \text{ }^\circ\text{C}$  to avoid affecting negatively the performance of the resulting concrete.

Wind speed affects the evaporation rate as the bleeding water is quickly removed from the concrete surface [36], with higher wind speeds leading to higher evaporation rates [38]. Exposure of concrete to high ambient temperatures, which are typically associated with lower relative humidity, results in an increase in evaporated water and can accelerate plastic shrinkage [36], and increase the risk of plastic shrinkage cracking [39]. High ambient temperatures also increase the temperature of concrete as they speed up concrete hydration and affect final setting time [40]. To summarize, exposure to high ambient temperature increases evaporation rate, which in turn accelerates the onset of plastic shrinkage cracking.

#### **2.1.7.2. Mix design**

The type and amount of the concrete constituent materials (water, cement, fine and coarse aggregates) affect plastic shrinkage cracking as their distribution within the concrete volume affects the resulting amount of bleeding water [41], which will eventually evaporate.

Almusallam et al. [7] examined the effect of different w/c and cement contents on plastic shrinkage cracking and found that the total area of crack and the crack initial time increase with increasing w/c ratio and cement contents (Figure 2.4, and Figure 2.5). This increment was related to the higher bleeding and evaporation rates associated to the higher w/c ratios.

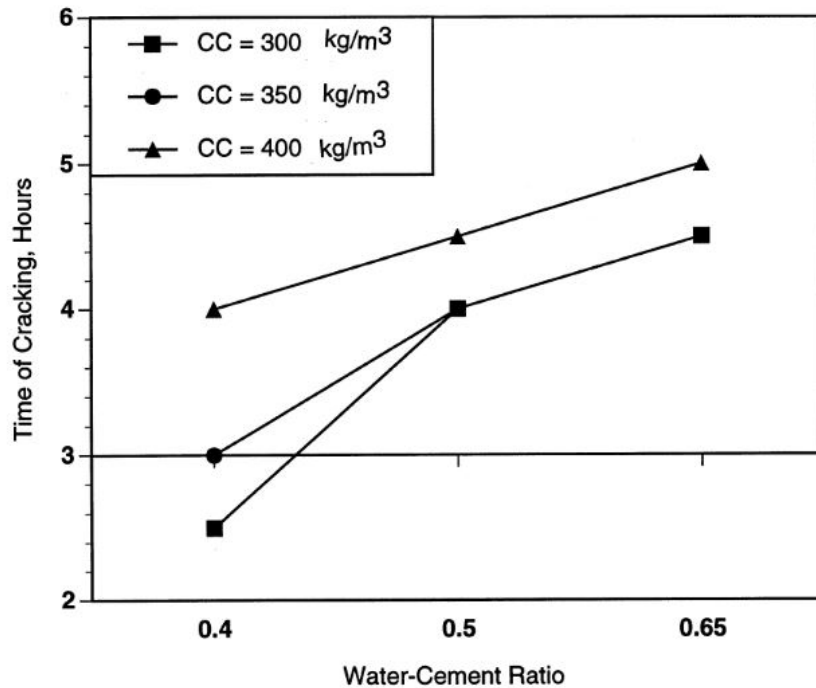


Figure 2.4: Effect of w/c on time to initiation of cracks [7].

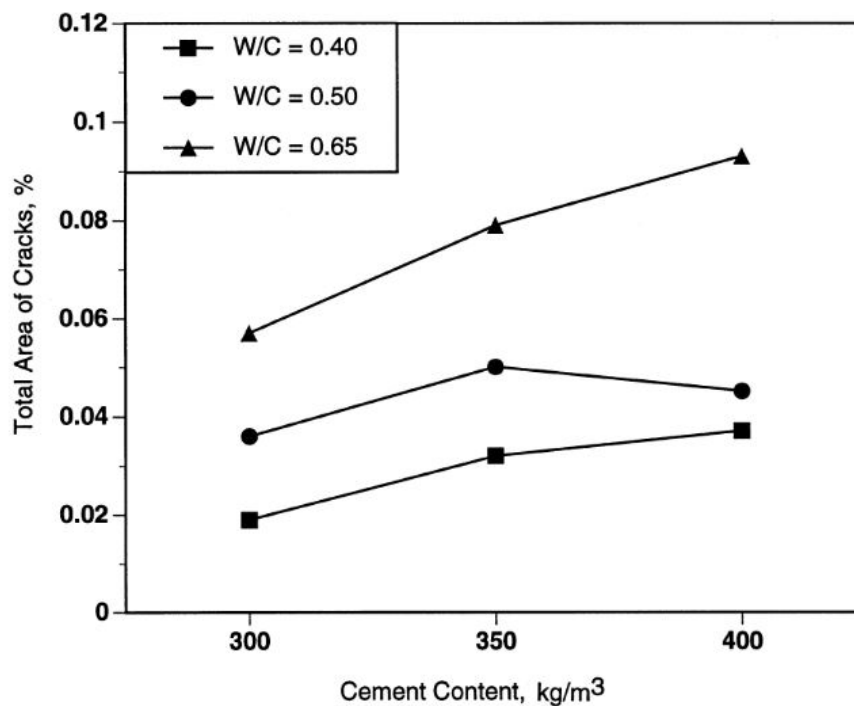


Figure 2.5: Effect of cement content on total area of cracks [7].

The effects of aggregates on plastic shrinkage cracks were investigated by Banthia et al. [42], who found that higher amounts of fine and coarse aggregates can mitigate plastic shrinkage cracking. The use of higher amounts of binders (including cement, silica fume, fly ash, and granulated blast furnace slag) decreases the bleeding rate during setting, and this can more easily result in higher evaporation rates and thus increase the risk of plastic shrinkage

cracks [43,44]. According to CSA A23.1 [45], appropriate measures to mitigate the occurrence of plastic shrinkage cracking should be put in place when finer binders, like silica fume and fly ash, are used as cement replacements and the evaporation rate is more than  $0.25 \text{ kg/m}^2/\text{h}$ .

### 2.1.8. Plastic shrinkage testing techniques

There are different types of plastic shrinkage cracks in fresh concrete specimens. These tests are restrained and designed in specific conditions to induce cracks in fresh concrete. The next following sections will give explanations and examples for those tests and the test methodology that used in this research.

#### 2.1.8.1. Ring test

According to ASTM C1581/C1581M [46], the ring test should be applied to the freshly concrete. The test procedure is when the concrete has mixed and casted, it should be compacted in a circular mould in a steel ring to the dimensions as shown in Figure 2.6. After placing the concrete in the ring specimens should vibrate for 5 seconds and have covered with plastic and wet burlap as recommended in ASTM C1581/C1581M [46]. The ring specimens should be stored in a controlling environmental conditions room of  $23 \pm 2 \text{ }^\circ\text{C}$  and RH of  $50 \pm 4\%$  as mentioned in ASTM C1581/C1581M [46]. The measurement of the cracks should take after 6 hours of the casting and 24 hours.

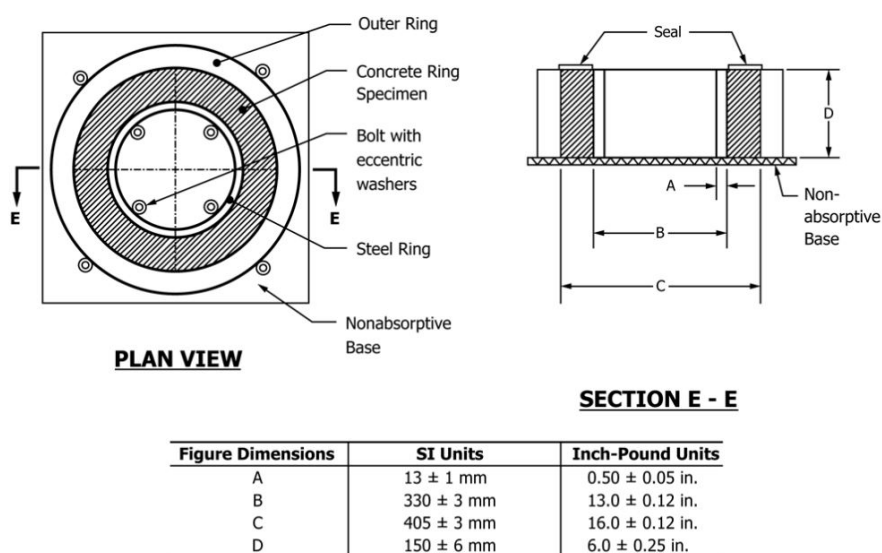


Figure 2.6: Test specimen dimensions [46].

Ling et al. [47] carried out a restrained ring test to examine plastic shrinkage cracking of fly ash based geopolymer pastes with and without shrinkage reducing admixture as shown in Figure 2.7. The result found that the use of shrinkage reducing admixtures can significantly

reduce free plastic shrinkage cracks and restrained shrinkage, distinctly delaying crack initiation and reducing crack width. However, the appearance of the cracks could be prevented completely.

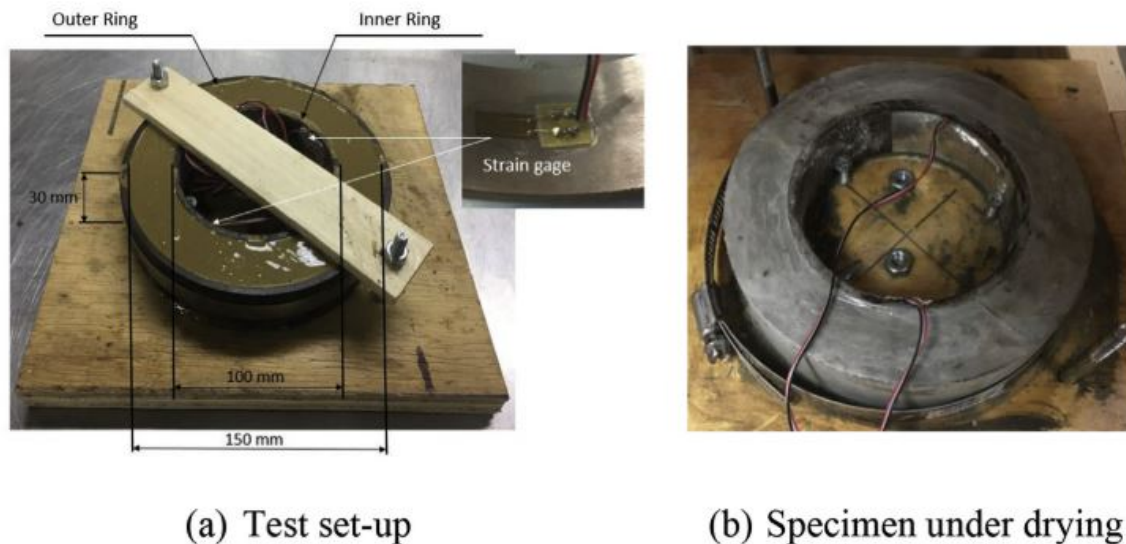


Figure 2.7: Restrained ring shrinkage test setup [47].

### 2.1.8.2. Slab test

It can be noticed that the plastic shrinkage is highly expected in concrete that has a large exposed surface area like slabs and pavements. Recently published research has developed different types of plastic shrinkage slabs test, therefore in this section all of plastic shrinkage slab tests will explain in detail.

Cao et al. [48] investigated the effects of expansive agents (EA), different types of fibres, and the interaction between EA and fibre on the cracking behaviour of restrained self-consolidating concrete (SCC). The study used a slab test which is a simulating concrete restrained by external formwork and internal reinforcement as shown in Figure 2.8. The volume of steel and polypropylene fibre used was 0.25, 0.50, and 0.75%, and 0.05, 0.10, and 0.15%, respectively. After placement, each concrete slab was exposed to fan generated airflow, at ambient temperature and relative humidity for 24 hours. The results showed that polypropylene fibres were more effective in reducing the nominal total crack area than steel fibres. Additionally, the combination of EA and fibres enabled SCC to present good early-age cracking resistance.

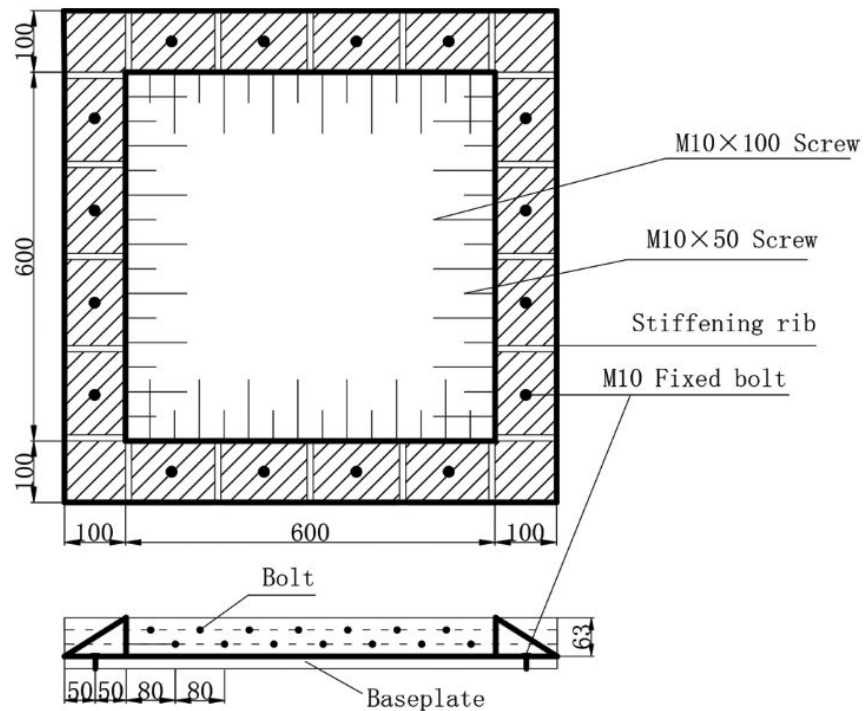


Figure 2.8: Steel slab mould [48]

Banthia et al. [49] made a study in concrete slabs to restrain plastic shrinkage cracks in fresh concrete. The study had used substrate bases with dimensions of  $40 \times 95 \times 325$  mm as shown in Figure 2.9. To restrain plastic shrinkage cracks, a 10 mm rebar and polypropylene fibres have used as reinforcement in the substrate bases. After concrete has been casted, the substrate bases had covered with a plastic sheet and stored in an attempt environmental room for 24 hours. Then, the substrate bases should transfer to a tank of lime-saturated water until used in the tests. For cracks measurement, a high magnification microscope was used to find the locations and average of crack length and width. In general, the results indicated that polypropylene fibres for both lengths had affected in controlling plastic shrinkage cracks. Specifically, the finer and larger fibres were most effective to hide cracks at the concrete more than coarser and shorter fibres.

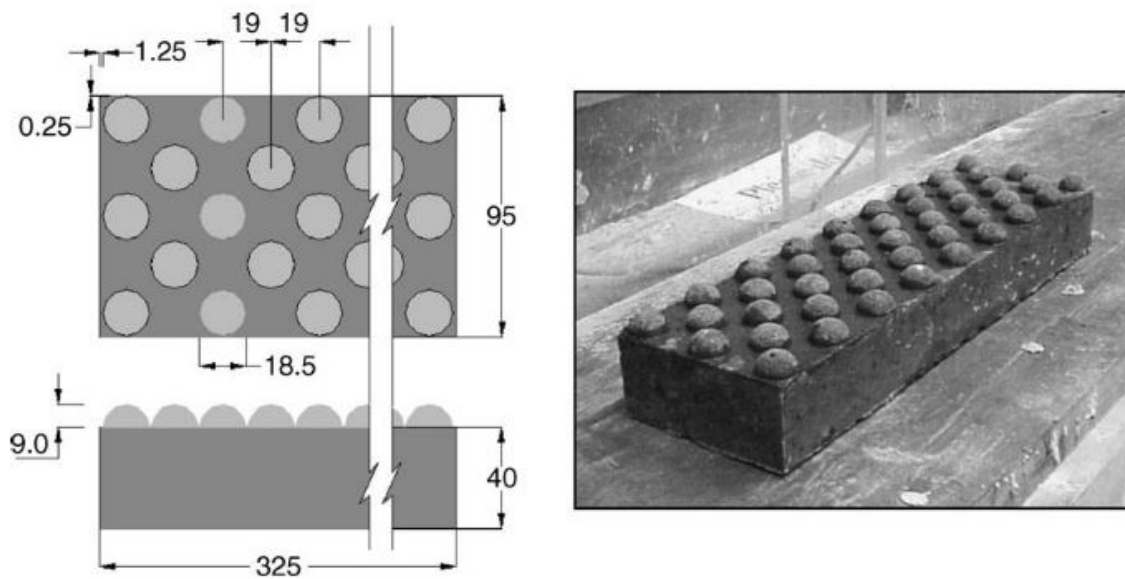


Figure 2.9: A substrate base with protuberances [49].

Naaman et al. [50] had provided a method to restrain plastic shrinkage cracks in slab which is a substrate into methylnmethacrylate mould of dimensions of  $38.1 \times 76.2 \times 1016$  mm as shown in Figure 2.10. Four types of fibre had investigated (polypropylene, polyvinyl alcohol, high-density polyethylene, and carbon) with volume fractions varied from 0.05 to 0.4%. By using handheld microscope, and a magnifying glass, the crack width and length were measured every 30 minutes since casted in the first 4 hours of the test. Then, the crack was measured every hour in the last 4 hours of the test. The typical time of the test was 8 hours, and then slabs were covered and measured again at 24 hours by using a microscope. The results showed that the cracks were almost stabilised at the second 4 hours of the test. In addition, both fibres used in the study have provided positive effects to control of plastic shrinkage cracking and the micro fibre were most effective to reduce cracks at the surface of the concrete.

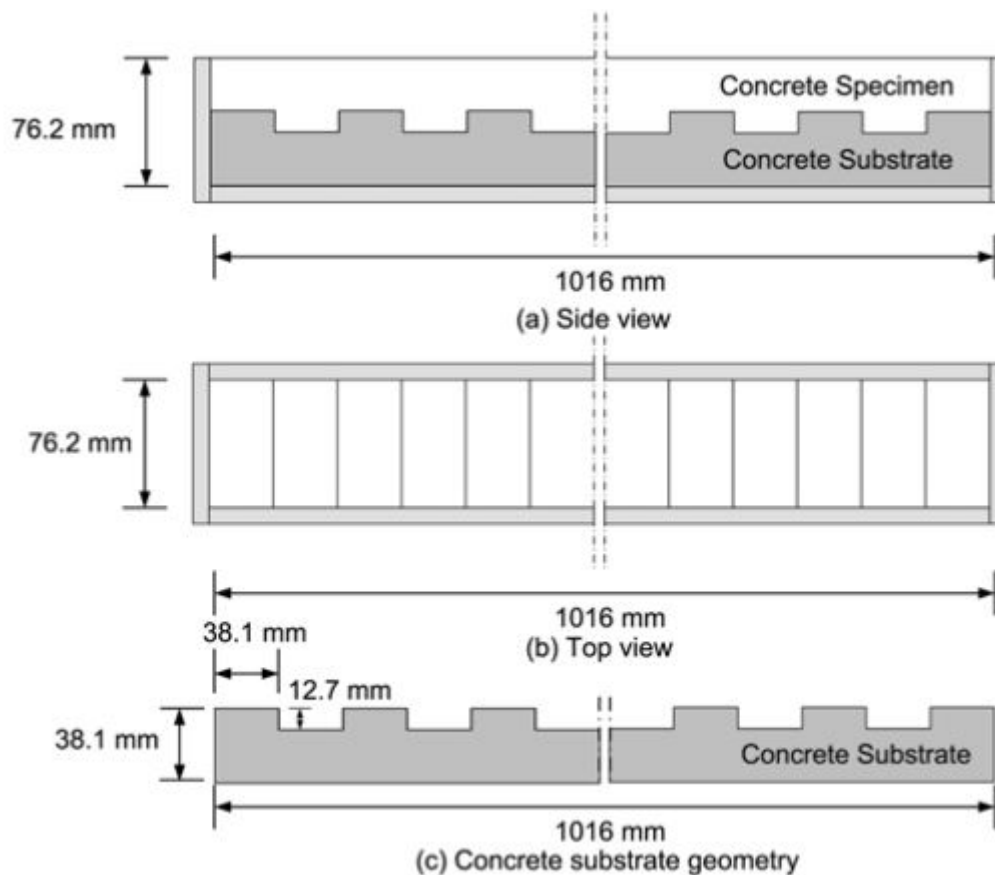


Figure 2.10: Schematic of plastic shrinkage cracking test setup: a) side view; b) top view; and c) concrete substrate geometry [50].

Another method of testing plastic shrinkage is based on ASTM C1579 [35], which suggested monitoring early-age concrete cracking or plastic shrinkage cracking during 6 hours after casting. This method had become popular in recent years [1,31,51–53]. With this method, most researchers found that plastic shrinkage cracks appeared in the second hour of testing which roughly corresponds to the initial concrete setting time. There is also a general agreement on the importance of controlling air and concrete temperature, wind speed, and relative humidity, which are the key factors governing the appearance of cracks. Therefore, in this research will used this method to restrain plastic shrinkage cracks with different parameters.

The plastic shrinkage tests were carried out based on ASTM C1579 [35], as shown in Figure 2.11, and Figure 2.12. A heater and relative humidity controller turned on for two hours before the test to achieve the desired environmental conditions. The test lasted for a total of six hours. Each half hour, the water loss recorded to calculate evaporation rate. The environmental conditions inside the rig recorded every hour to determine changes in air and concrete temperature, fan speed, and relative humidity over time. The environmental conditions of the



test to pre-heat and stabilise to the desired temperature ( $36\pm 3$  °C), relative humidity ( $30\pm 10\%$ ) and wind speed more than 4.7 m/s as recommended in ASTM C1579 [35].

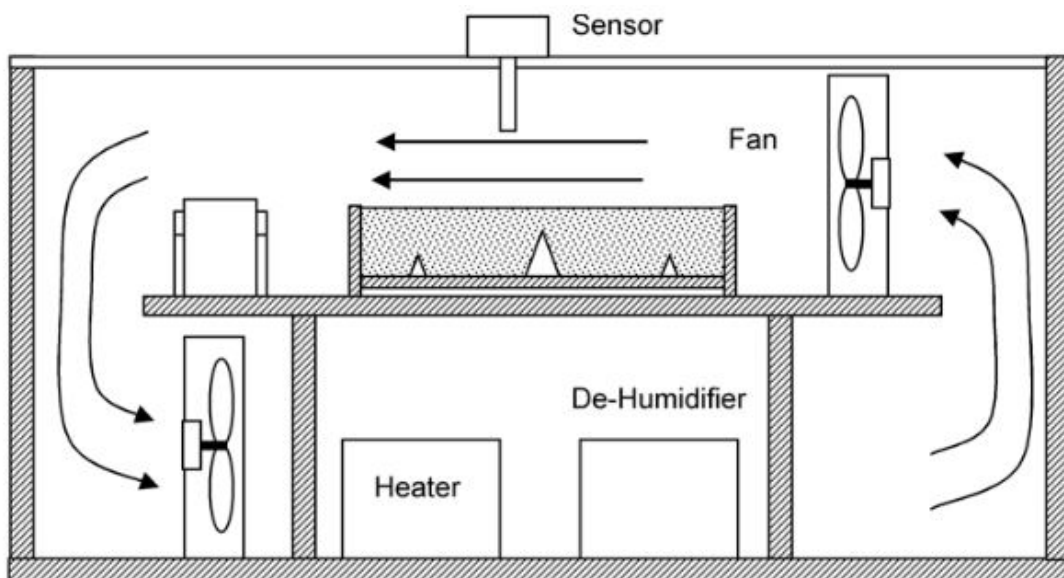


Figure 2.11: Schematic of the chamber as suggested by the [35].

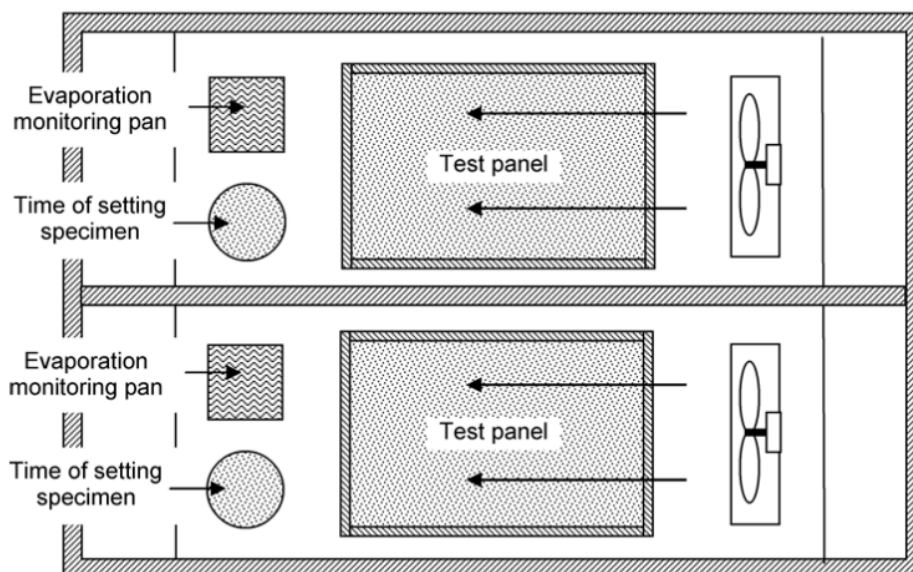


Figure 2.12: Left and right path in the chamber [35].

## 2.2. Materials properties

### 2.2.1. Cement

The cement that used in this study was a commercially available CEM II-42.5 which was used as binder. This types of cement contains around 10-15% of limestone in compliance with BS EN 197-1 [54] as shown in Table 2.1.

Table 2.1: Oxide and phase contents composition of CEM II-42.5 (% wt) [54].

Oxide formula	Weight content, %	Oxide formula	Weight content, %
SiO <sub>2</sub>	18.40	SO <sub>3</sub>	3.10
Al <sub>2</sub> O <sub>3</sub>	5.40	ZnO	0.19
Fe <sub>2</sub> O <sub>3</sub>	2.80	Rb <sub>2</sub> O	0.02
CaO	62.00	SrO	0.08
MgO	1.40	Nb <sub>2</sub> O <sub>5</sub>	0.01
TiO <sub>2</sub>	0.19	BaO	0.05
MnO	0.03	PbO	0.09
K <sub>2</sub> O	1.10	SiO <sub>2</sub>	2.73
Na <sub>2</sub> O	0.20	P <sub>2</sub> O <sub>5</sub>	0.29
Cr <sub>2</sub> O <sub>3</sub>	0.13	LOI	7.00

### 2.2.2. Water

The mixing water was from tap water in the lab. The temperature of the mixing water was controlled at 20 °C in a day before mixing concrete in normal lab temperature (20±2 °C) as recommended in [35,37].

### 2.2.3. Aggregates

#### 2.2.3.1. Fine aggregates

The fine aggregate that use in this study was a natural river sand and was tested in the lab in order of total evaporable moisture content of aggregate by drying as mentioned in ASTM C566 [55], and relative density (specific gravity oven dry (SG<sub>OD</sub>), specific gravity saturated surface dry (SG<sub>SSD</sub>), apparent specific gravity (ASG), and absorption) as recommended in ASTM C127-15 [56]. The fine aggregate are weighed and stored in standard laboratory conditions (20±2°C) a day before mixing concrete. According to BS EN 933-1 [57] and ASTM D6913 [58], a sieve analysis is made to calculate the particle size of fine aggregate as shown in Figure 2.13.

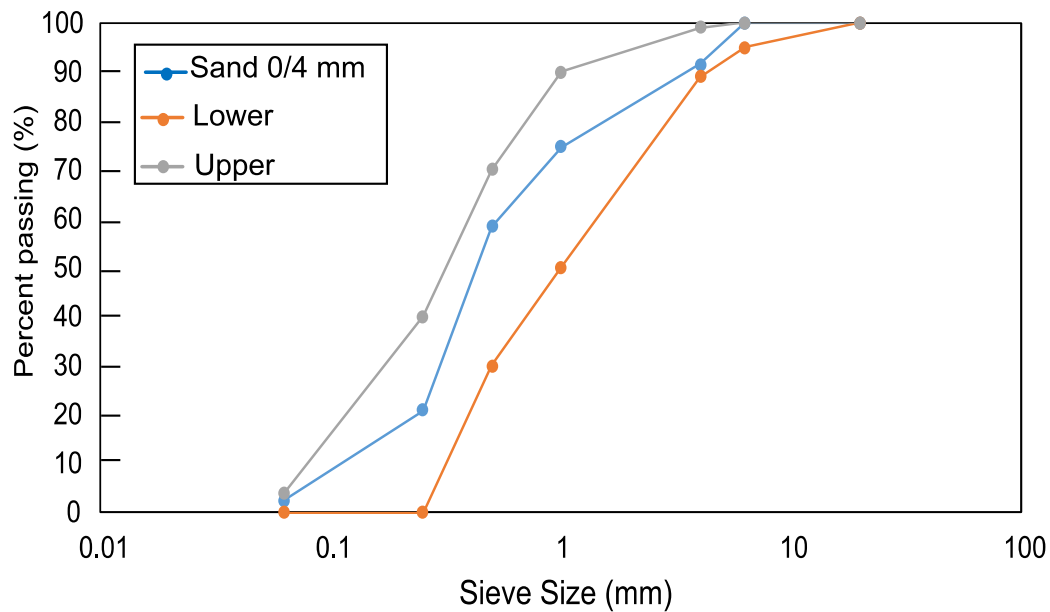


Figure 2.13: Particle size of fine aggregates with limitations

### 2.2.3.2. Coarse aggregates

Two types of coarse aggregate that were used in this study are 10 mm and 14 mm size. Both coarse aggregates are natural river round gravel. The 14 mm was sieved and washed in the lab from 20 mm coarse aggregate size. All of coarse aggregates properties were tested in the lab as recommended in [55,56]. Both of the coarse aggregates were weighed and stored in a standard laboratory conditions ( $20 \pm 2$  °C) a day before mixing concrete. According to BS EN 933-1 [57] and ASTM D6913 [58], a sieve analysis was made to calculate the particle size of 10 and 20 mm aggregates as shown in Figure 2.14, and Figure 2.15, respectively.

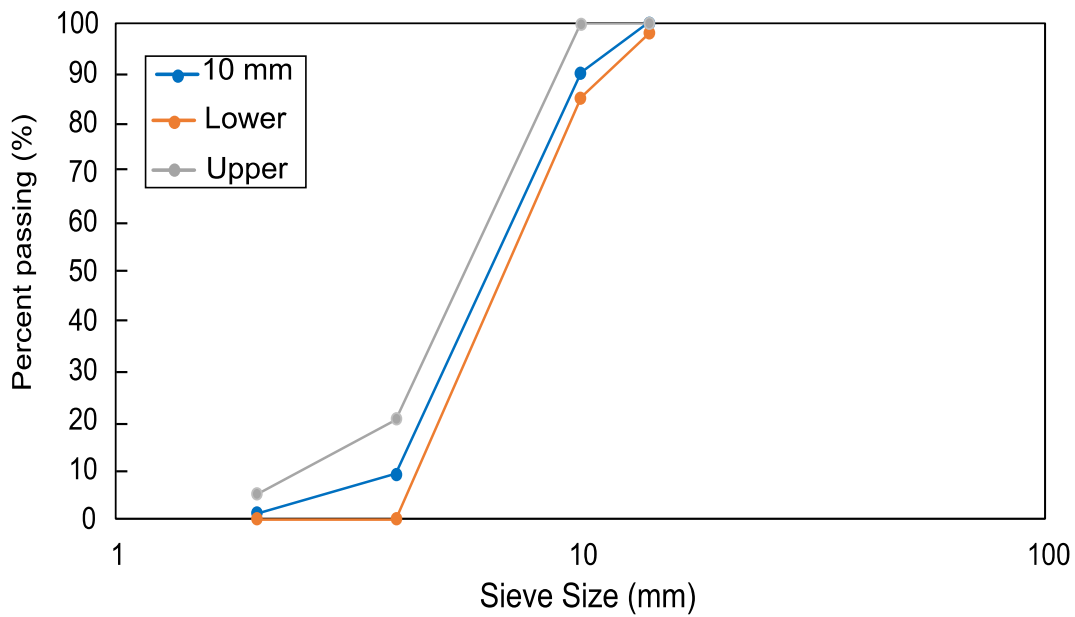


Figure 2.14: Particle size of 10 mm aggregates with limitations

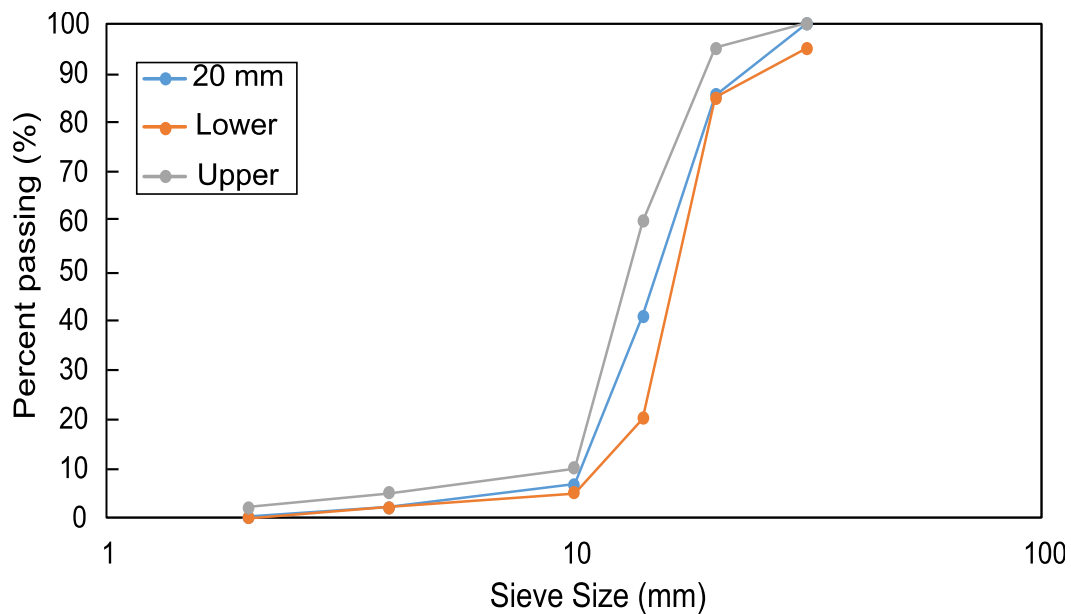


Figure 2.15: Particle size of 20 mm aggregates with limitations

### 2.2.3.3. Bulk density of aggregates

The type/source of aggregates was a river aggregates that were washed and supplied from the Trent Valley. All of the aggregates that were used in this study were tested to find the relative density. First, the aggregates were weighted to find (natural weight before test start ( $W_{ANT}$ ), and saturated in water for 24 hours as shown in Figure 2.16, and Figure 2.17. Then, the fine aggregate was dried by using a hairdryer and tested in the core test by tamping the fine aggregates until a successful failure core to find saturated surface dry weight ( $W_{SSD}$ ) of fine

aggregates as shown in Figure 2.18. On the other hand, the coarse aggregates were dried by towel many times and weighted to find saturated surface dry weight ( $W_{SSD}$ ) of coarse aggregates (see Figure 2.19, and Figure 2.20). After that the aggregates were stored in the water and found aggregates weight in the water ( $W_{IN\ WATER}$ ). Finally, the aggregates were stored in the oven for 24 hours to find the oven dry weight to find oven dry weight ( $W_{DRY}$ ) as shown in Figure 2.21.

After all the aggregates weight had taken, the equations (Eq.1-5), were used to find the moisture and relative density of the aggregates as shown in Table 2.2. The aggregates were tested in the lab in order of total evaporable moisture content of aggregate by drying as recommended in ASTM C566 [55], and relative density (specific gravity oven dry ( $SG_{OD}$ ), specific gravity saturated surface dry ( $SG_{SSD}$ ), apparent specific gravity ( $ASG$ )) and absorption were also determined, as recommended in ASTM C127-15 [56].

1. Total evaporable moisture content of aggregate by drying

$$Moisture\% = \frac{(W_{NAT} - W_{DRY})}{W_{DRY}} \times 100 \dots\dots\dots (Eq.1)$$

2. Relative density (specific gravity) oven dry

$$SG_{OD} = \frac{W_{DRY}}{(W_{SSD} - W_{IN\ WATER})} \dots\dots\dots (Eq.2)$$

3. Relative density (specific gravity) saturated surface dry

$$SG_{SSD} = \frac{W_{SSD}}{(W_{SSD} - W_{IN\ WATER})} \dots\dots\dots (Eq.3)$$

4. Apparent relative density (apparent specific gravity)

$$ASG = \frac{W_{DRY}}{(W_{DRY} - W_{IN\ WATER})} \dots\dots\dots (Eq.4)$$

5. Absorption percentage of aggregate

$$Absorption\% = \frac{(W_{SSD} - W_{DRY})}{W_{DRY}} \times 100 \dots\dots\dots (Eq.5)$$



Figure 2.16: Coarse aggregates weight in the water (10 mm, and 20 mm size)



Figure 2.17: Fine aggregates weight in the water



Figure 2.18: Tamping the aggregate into the mold (core test)



Figure 2.19: Dry the coarse aggregates 10 mm size by towel



Figure 2.20: Dry the coarse aggregates 20 mm size in the oven



Figure 2.21: Oven dry of the aggregates.



Table 2.2: Physical properties of fine and coarse aggregates.

<b>Bulk Density of Aggregate</b>	<b>Fine Aggregates</b>	<b>Coarse Aggregates Size 10 mm</b>	<b>Coarse Aggregates Size 20 mm</b>
Moisture %	2.58	0.83	0.24
SG <sub>OD</sub>	3.18	2.50	2.60
SG <sub>SSD</sub>	3.21	2.50	2.60
ASG	3.30	2.58	2.66
Absorption%	1.23	0.91	0.58

#### 2.2.4. Admixture

##### 2.2.4.1. High-range Water Reducing Admixture – Sika ViscoCrete Summary Data Sheet

A Superplasticiser that used in this study which is a Sika ViscoCrete 30HE and was provided by TWINCON Ltd that was supplied some of the materials of this research project. The aim of adding Superplasticiser is to maintain the workability of the concrete when the fibres were added. The product description, characteristics, and advantages are shown in the data sheet in Appendix A as received by the supplier.

### 2.3. References

- [1] P. Zhao, A.M. Zsaki, M.R. Nokken, Using digital image correlation to evaluate plastic shrinkage cracking in cement-based materials, *Constr. Build. Mater.* 182 (2018) 108–117. <https://doi.org/10.1016/j.conbuildmat.2018.05.239>.
- [2] M. Sahinagic-Isovic, G. Markovski, M. Čećez, Shrinkage strain of concrete - Causes and types, *Gradjevinar.* 64 (2012) 727–734. <https://doi.org/10.14256/jce.719.2012>.
- [3] L.A. Kuhlman, Cracks in LMC overlays; How do they get there; How serious are they; What to do about them, *Transp. Res. Rec.* 22 (1991) 17–21.
- [4] J.G. Cabrera, A.R. Cusens, Y. Brookes-Wang, Effect of superplasticizers on the plastic shrinkage of concrete, *Mag. Concr. Res.* 44 (1992) 149–155. <https://doi.org/10.1680/mac.1992.44.160.149>.
- [5] M.L. Kosmatka, Steven H.; WILSON, Design and Control of Concrete Mixtures – The Guide to Applications, Methods and Materials., 2011.
- [6] ACI 224R-01, Control of Cracking in Concrete Structures Reported by ACI Committee 224. ACI 224R-01, ACI Comm. 224R-01. (2001) 1–46.
- [7] A.A. Almusallam, M. Maslehuddin, M. Abdul-Waris, M.M. Khan, Effect of mix proportions on plastic shrinkage cracking of concrete in hot environments, *Constr. Build. Mater.* 12 (1998) 353–358. [https://doi.org/10.1016/S0950-0618\(98\)00019-1](https://doi.org/10.1016/S0950-0618(98)00019-1).
- [8] C. Qi, J. Weiss, J. Olek, Characterization of plastic shrinkage cracking in fiber reinforced concrete using image analysis and a modified Weibull function, *Mater. Struct. Constr.* 36 (2003) 386–395. <https://doi.org/10.1007/bf02481064>.
- [9] W. Hansen, Drying Shrinkage Mechanisms in Portland Cement Paste, *J. Am. Ceram. Soc.* 70 (1987) 323–328. <https://doi.org/10.1111/j.1151-2916.1987.tb05002.x>.
- [10] D. Wang, C. Shi, Z. Wu, J. Xiao, Z. Huang, Z. Fang, A review on ultra high performance concrete: Part II. Hydration, microstructure and properties, *Constr. Build. Mater.* 96 (2015) 368–377. <https://doi.org/10.1016/j.conbuildmat.2015.08.095>.
- [11] S. Em, N. Friburgo, Chemical shrinkage and autogenous shrinkage of hydrating cement paste, *Integr. Clim. Prot. Cult. Herit. Asp. Policy Dev. Plans. Free Hanseatic City Hambg.* 2 (1995) 1–37.
- [12] A.C.P. of C. at E.A. 231, Report on Early-Age Cracking: Causes, Measurement, and Mitigation., Am. Concr. Institute. (2010).
- [13] S.A. Altoubat, D.A. Lange, Tensile basic creep: Measurements and behavior at early

- age, *ACI Mater. J.* 98 (2001) 386–393. <https://doi.org/10.14359/10728>.
- [14] L. Yang, C. Shi, Z. Wu, Mitigation techniques for autogenous shrinkage of ultra-high-performance concrete – A review, *Compos. Part B Eng.* 178 (2019) 107456. <https://doi.org/10.1016/j.compositesb.2019.107456>.
- [15] Z. Wu, C. Shi, K.H. Khayat, Investigation of mechanical properties and shrinkage of ultra-high performance concrete: Influence of steel fiber content and shape, *Compos. Part B Eng.* 174 (2019) 107021. <https://doi.org/10.1016/j.compositesb.2019.107021>.
- [16] K. Hannawi, H. Bian, W. Prince-Agbodjan, B. Raghavan, Effect of different types of fibers on the microstructure and the mechanical behavior of Ultra-High Performance Fiber-Reinforced Concretes, *Compos. Part B Eng.* 86 (2016) 214–220. <https://doi.org/10.1016/j.compositesb.2015.09.059>.
- [17] W. Meng, K.H. Khayat, Effect of Hybrid Fibers on Fresh Properties, Mechanical Properties, and Autogenous Shrinkage of Cost-Effective UHPC, *J. Mater. Civ. Eng.* 30 (2018). [https://doi.org/10.1061/\(asce\)mt.1943-5533.0002212](https://doi.org/10.1061/(asce)mt.1943-5533.0002212).
- [18] Ma, R., Guo, L., Ye, S., Sun, W. and Liu, J., Influence of hybrid fiber reinforcement on mechanical properties and autogenous shrinkage of an ecological UHPFRCC., *J. Mater. Civ. Eng.* 31 (2019).
- [19] T. Zhang, P. Gao, R. Luo, Y. Guo, J. Wei, Q. Yu, Measurement of chemical shrinkage of cement paste: Comparison study of ASTM C 1608 and an improved method, *Constr. Build. Mater.* 48 (2013) 662–669. <https://doi.org/10.1016/j.conbuildmat.2013.07.086>.
- [20] P. Mounanga, A. Khelidj, A. Loukili, V. Baroghel-Bouny, Predicting Ca(OH)<sub>2</sub> content and chemical shrinkage of hydrating cement pastes using analytical approach, *Cem. Concr. Res.* 34 (2004) 255–265. <https://doi.org/10.1016/j.cemconres.2003.07.006>.
- [21] M. Bouasker, P. Mounanga, P. Turcry, A. Loukili, A. Khelidj, Chemical shrinkage of cement pastes and mortars at very early age: Effect of limestone filler and granular inclusions, *Cem. Concr. Compos.* 30 (2008) 13–22. <https://doi.org/10.1016/j.cemconcomp.2007.06.004>.
- [22] HARALD, J., Chemical shrinkage of cement pastes with plasticizing admixtures., *Nord. Concr. Res.* 24 (2000) 39–44.
- [23] ASTM C 1608., Standard test method for chemical shrinkage of hydraulic cement paste., *Am. Soc. Test. Mater.* West Conshohocken. (2007).
- [24] P. Rossi, P. Acker, A new approach to the basic creep and relaxation of concrete, *Cem. Concr. Res.* 18 (1988) 799–803. [https://doi.org/10.1016/0008-8846\(88\)90105-6](https://doi.org/10.1016/0008-8846(88)90105-6).

- [25] J. Saliba, E. Rozière, F. Grondin, A. Loukili, Influence of shrinkage-reducing admixtures on plastic and long-term shrinkage, *Cem. Concr. Compos.* 33 (2011) 209–217. <https://doi.org/10.1016/j.cemconcomp.2010.10.006>.
- [26] J. Jasiczak, P. Szymański, P. Nowotarski, Wider Perspective of Testing Early Shrinkage of Concrete Modified with Admixtures in Changeable W/C Ratio as Innovative Solution in Civil Engineering, *Procedia Eng.* 122 (2015) 310–319. <https://doi.org/10.1016/j.proeng.2015.10.041>.
- [27] G.W. Scherer, Drying, Shrinkage, and Cracking of Cementitious Materials, *Transp. Porous Media.* 110 (2015) 311–331. <https://doi.org/10.1007/s11242-015-0518-5>.
- [28] R.D. Toledo Filho, K. Ghavami, M.A. Sanjuán, G.L. England, Free, restrained and drying shrinkage of cement mortar composites reinforced with vegetable fibres, *Cem. Concr. Compos.* 27 (2005) 537–546. <https://doi.org/10.1016/j.cemconcomp.2004.09.005>.
- [29] K.H. Younis, F.S. Ahmed, K.B. Najim, Effect of recycled-steel fibers on compressive strength and shrinkage behavior of self-compacting concrete, *Proc. - Int. Conf. Dev. ESystems Eng. DeSE. 2018-Septe* (2019) 268–272. <https://doi.org/10.1109/DeSE.2018.00054>.
- [30] A. Sivakumar, M. Santhanam, A quantitative study on the plastic shrinkage cracking in high strength hybrid fibre reinforced concrete, *Cem. Concr. Compos.* 29 (2007) 575–581. <https://doi.org/10.1016/j.cemconcomp.2007.03.005>.
- [31] W.P. Boshoff, R. Combrinck, Modelling the severity of plastic shrinkage cracking in concrete, *Cem. Concr. Res.* (2013). <https://doi.org/10.1016/j.cemconres.2013.02.003>.
- [32] H. Sayahi, Faez and Hedlund, Plastic Shrinkage Cracking in Concrete: State of the Art, (2014) 146.
- [33] V. Slowik, M. Schmidt, R. Fritsch, Capillary pressure in fresh cement-based materials and identification of the air entry value, *Cem. Concr. Compos.* 30 (2008) 557–565. <https://doi.org/10.1016/j.cemconcomp.2008.03.002>.
- [34] H.G. Kwak, S.J. Ha, Plastic shrinkage cracking in concrete slabs. Part I: A numerical model, *Mag. Concr. Res.* 58 (2006) 505–516. <https://doi.org/10.1680/mac.2006.58.8.505>.
- [35] ASTM C1579, Standard Test Method for Evaluating Plastic Shrinkage Cracking of Restrained Fiber Reinforced Concrete, *Annu. B. ASTM Stand.* i (2006) 1–7. <https://doi.org/10.1520/C1579-06.2>.
- [36] P.J. Uno, Plastic shrinkage cracking and evaporation formulas, *ACI Mater. J.* 95

- (1998) 365–375. <https://doi.org/10.14359/379>.
- [37] ASTM C192/C192M, Standard Practice for Making and Curing Concrete Test Specimens in the Laboratory, Am. Soc. Test. Mater. (2016) 1–8. <https://doi.org/10.1520/C0192>.
- [38] P. Ghoddousi, A.M. Abbasi, E. Shahrokhinasab, M. Abedin, Prediction of Plastic Shrinkage Cracking of Self-Compacting Concrete, *Adv. Civ. Eng.* 2019 (2019). <https://doi.org/10.1155/2019/1296248>.
- [39] A.A. Almusallam, Effect of environmental conditions on the properties of fresh and hardened concrete, *Cem. Concr. Compos.* 23 (2001) 353–361. [https://doi.org/10.1016/S0958-9465\(01\)00007-5](https://doi.org/10.1016/S0958-9465(01)00007-5).
- [40] G.M. Moelich, J.E. van Zyl, N. Rabie, R. Combrinck, The influence of solar radiation on plastic shrinkage cracking in concrete, *Cem. Concr. Compos.* 123 (2021) 104182. <https://doi.org/10.1016/j.cemconcomp.2021.104182>.
- [41] S. Ghourchian, M. Wyrzykowski, P. Lura, The bleeding test: A simple method for obtaining the permeability and bulk modulus of fresh concrete, *Cem. Concr. Res.* 89 (2016) 249–256. <https://doi.org/10.1016/j.cemconres.2016.08.016>.
- [42] N. Banthia, R. Gupta, Plastic shrinkage cracking in cementitious repairs and overlays, *Mater. Struct. Constr.* 42 (2009) 567–579. <https://doi.org/10.1617/s11527-008-9403-9>.
- [43] O.S.B. Al-Amoudi, M. Maslehuddin, T.O. Abiola, Effect of type and dosage of silica fume on plastic shrinkage in concrete exposed to hot weather, *Constr. Build. Mater.* 18 (2004) 737–743. <https://doi.org/10.1016/j.conbuildmat.2004.04.031>.
- [44] M. Sirajuddin, R. Gettu, Plastic shrinkage cracking of concrete incorporating mineral admixtures and its mitigation, *Mater. Struct. Constr.* 51 (2018). <https://doi.org/10.1617/s11527-018-1173-4>.
- [45] CSA A23.1, Concrete Materials and Methods of Concrete Construction/Methods of Test and Standard Practices for Concrete., Can. Stand. Assoc. (2004).
- [46] A. C1581/C1581M, Standard Test Method for Determining Age at Cracking and Induced Tensile Stress Characteristics of Mortar and Concrete under Restrained Shrinkage, *ASTM Int.* (2016) 1–7. <https://doi.org/10.1520/C1581>.
- [47] Y. Ling, K. Wang, C. Fu, Shrinkage behavior of fly ash based geopolymers pastes with and without shrinkage reducing admixture, *Cem. Concr. Compos.* 98 (2019) 74–82. <https://doi.org/10.1016/j.cemconcomp.2019.02.007>.
- [48] Q. Cao, Q. Gao, J. Jia, R. Gao, Early-age cracking resistance of fiber-reinforced expansive self-consolidating concrete, *ACI Mater. J.* 116 (2019) 15–26.

- <https://doi.org/10.14359/51710957>.
- [49] N. Banthia, R. Gupta, Influence of polypropylene fiber geometry on plastic shrinkage cracking in concrete, *Cem. Concr. Res.* 36 (2006) 1263–1267.  
<https://doi.org/10.1016/j.cemconres.2006.01.010>.
- [50] A.E. Naaman, T. Wongtanakitcharoen, G. Hauser, Influence of different fibers on plastic shrinkage cracking of concrete, *ACI Mater. J.* 102 (2005) 49–58.  
<https://doi.org/10.14359/14249>.
- [51] G. Olivier, R. Combrinck, M. Kayondo, W.P. Boshoff, Combined effect of nano-silica, super absorbent polymers, and synthetic fibres on plastic shrinkage cracking in concrete, *Constr. Build. Mater.* 192 (2018) 85–98.  
<https://doi.org/10.1016/j.conbuildmat.2018.10.102>.
- [52] I.M.G. Bertelsen, L.M. Ottosen, G. Fischer, Quantitative analysis of the influence of synthetic fibres on plastic shrinkage cracking using digital image correlation, *Constr. Build. Mater.* 199 (2019) 124–137. <https://doi.org/10.1016/j.conbuildmat.2018.11.268>.
- [53] F. Matakah, Y. Jaradat, P. Soroushian, Plastic shrinkage cracking and bleeding of concrete prepared with alkali activated cement, *Heliyon.* 5 (2019) e01514.  
<https://doi.org/10.1016/j.heliyon.2019.e01514>.
- [54] BS EN 197-1, Methods of testing Composition, Specifications and Conformity Criteria for Common Cements, *Bs En 197-1.* (2011) 50.
- [55] A.C. C566, Standard Test Method for Total Evaporable Moisture Content of Aggregate by Drying, *ASTM C566-97, Annu. B. ASTM Stand.* 97 (1997) 5–7.
- [56] ASTM C127-15, ASTM C127-15: Standard Test Method for Density , Relative Density ( Specific Gravity ), and Absorption of Coarse Aggregate, *ASTM Stand. B.* (2013) 1–6.
- [57] BS EN 933-1, BS EN 933-1:1997 Tests for geometrical properties of aggregates Part 1: Determination of Particle Size Distribution - Sieving Method, *Br. Stand. Inst.* 3 (2005) 1–7. <https://bsol.bsigroup.com/en/Bsol-Item-Detail-Page/?pid=000000000030117183>.
- [58] Astm D6913-04R2009, Standard Test Methods for Particle-Size Distribution ( Gradation ) of Soils Using Sieve Analysis, *ASTM Int. West Conshohocken, PA.,* 04 (2004) 1–35. <https://doi.org/10.1520/D6913-17.1.6>.

**This page is intentionally left blank**

## Chapter 3 : Performance of Manufactured and Recycled Steel Fibres in Restraining Concrete Plastic Shrinkage Cracks

*Alshammari, T.O., Pilakoutas, K. and Guadagnini, M., 2023. Performance of Manufactured and Recycled Steel Fibres in Restraining Concrete Plastic Shrinkage Cracks. Materials, 16(2), p.713.*

### Author Contributions:

Conceptualization, software, data curation, investigation and writing—original draft, **T.O.A.**; methodology, writing—review and editing and supervision **K.P. and M.G.** All authors have read and agreed to the published version of the manuscript.

### Abstract:

Early-age plastic shrinkage cracks can reduce the durability of concrete slabs by creating direct paths for the ingress of aggressive agents and thus accelerating degradation due to environmental attack, in particular, in hot and windy environments. The elimination of such cracks is essential for durable and sustainable concrete structures. This paper parametrically investigates the effect of manufactured steel fibres (MSF) and recycled tyre steel fibres (RTSF) on restraining plastic shrinkage at different dosages (10, 20, and 30 kg/m<sup>3</sup>). The plastic shrinkage tests were carried out in a specially designed chamber, according to ASTM C1579. Various environmental conditions are examined, and their impact on compressive strength and crack potential is assessed. A digital image analysis technique is used to measure length, width, and the area of the crack on the exposed surface to gain additional insights into crack behaviour. The results show a slight early-age (one-day) increase in compressive strength of RTSF and MSF for the concrete exposed to the various environmental conditions, mostly as a result of higher temperatures. Through the use of the crack reduction ratio (CRR), both RTSF and MSF are shown to be successful in controlling plastic shrinkage, with the RTSF being superior due to the fact that they are better distributed in the concrete volume. The addition of 30 kg/m<sup>3</sup> of RTSF was effective in preventing crack development in most environments or restraining cracks in extremely harsh environments. The adoption of these results will lead to more sustainable concrete slabs in the harsher environmental conditions created by climate change. **Appendix B** has provided the relevant experimental data of this chapter.



**Keywords:**

Early-age concrete cracking; plastic shrinkage cracks; concrete shrinkage; recycled tyre steel fibre; manufactured steel fibres; steel-fibre-reinforced concrete

### 3.1. Introduction

Early-age cracking due to autogenous and plastic shrinkage is a key issue that affects concrete durability and reduces the lifespan of concrete structures. It is estimated that plastic shrinkage cracking is the source of roughly 80% of the early-age cracking in reinforced concrete structures [1,2]. Though plastic shrinkage cracks affect most structural members, they are more likely to occur in large surface area structures, such as slabs and pavements, and also walls [3].

Plastic shrinkage cracks are the result of volume changes that occur during the plastic stage, i.e., before the concrete hardens. These include air void expulsion and aggregate plastic settlement, as well as the bleeding and evaporation of water [4]. As the layer of bleeding water at the surface of concrete evaporates, water menisci develop between solid particles, causing the initiation of capillary pressure build-up. This capillary pressure has a limit and when this is reached, cracks develop [5]. Depending on the initial water content and the rate of evaporation, these cracks can be extensive and penetrate deep into the concrete surface. Cracks that initiate during the plastic state can progress until the final setting time and subsequently become drying shrinkage cracks [6–9]. Cracks facilitate the ingress of chemicals into concrete and accelerate concrete deterioration [10]. It is well accepted that such concrete cracks should be controlled and/or avoided.

Plastic shrinkage cracks occur due to rapid evaporation; hence, they are a direct consequence of environmental conditions, such as elevated temperature, low relative humidity, solar radiation, and exposure to high wind flows [11–14]. Such environments are encountered more often as a result of climate change and also as a result of population expansion and consequent exposure to more hostile environments, especially in dry/arid regions [15].

#### 3.1.1. Plastic Shrinkage Phenomenon

Plastic shrinkage cracking is expected to develop when the evaporation rate is greater than  $1.0 \text{ kg/m}^2/\text{h}$ , which is most likely to occur in hot weather concreting in arid climates [16]. Kwak and Ha [17] investigated the relationship between bleeding and evaporation rate. Figure 3.1 shows a typical evolution of evaporation and bleeding rate and the likely period of plastic shrinkage.

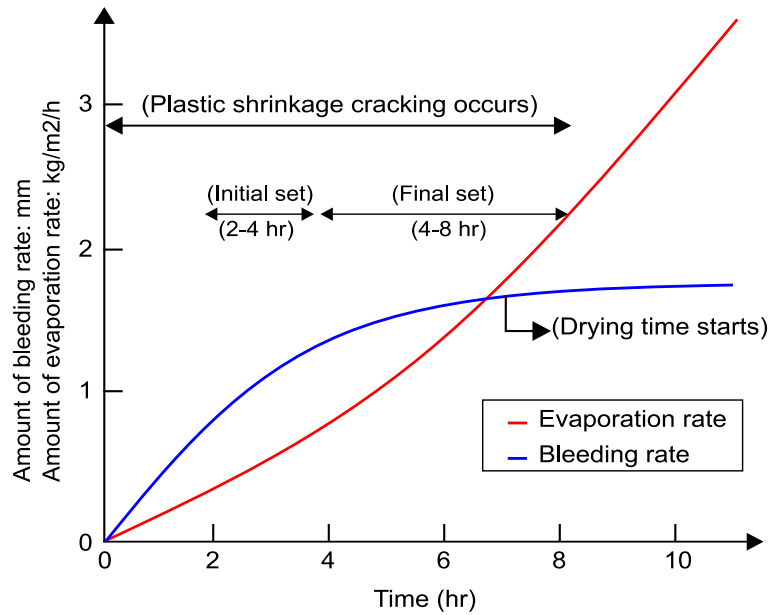


Figure 3.1: Evaporation and bleeding of concrete [17].

Soon after casting and during the initial setting time (2–4 h) (see Figure 3.1), the denser solid constituent materials tend to sink and can become unable to hold onto excess mixing water. This water migrates towards the surface and some bleeds out of the mix onto the surface [18]. The rate of bleeding depends on the water content, particle size distribution, viscosity, and rate of hydration of cement.

After the initial setting time, the rate of bleeding water stabilises and then ceases. During the final set (4–8 h), the hydration of cement causes the surface temperature to increase, and, as a result, the evaporation rate can exceed the bleeding rate. A high rate of evaporation, also aggravated by dry conditions and wind, can lead to plastic shrinkage cracking before the final set ends [19].

Boshoff and Combrinck [20] and Sayahi et al. [21] studied the behaviour of plastic shrinkage cracks and found that the capillary pressure develops rapidly once drying begins but reduces suddenly when air enters into the pores, before the initial setting time begins. The development of capillary pressure is shown schematically in Figure 3.2 together with the typical phenomenological behaviour of plastic shrinkage [20]. When initial setting time ( $T_{IS}$ ) starts, bleeding is slowed down and can be considered to end by the final setting time ( $T_{FS}$ ). Soon after the initial setting time, the onset of cracking ( $T_{CO}$ ) begins, and the crack width increases up to the final setting time. When the final setting time is reached, the crack growth reduces. This subsequent crack growth is the result of temperature, autogenous shrinkage, and drying shrinkage.

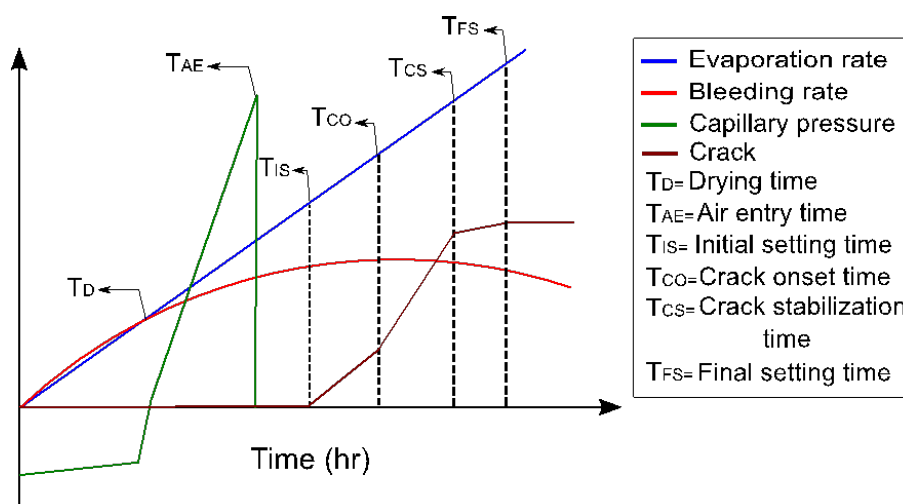


Figure 3.2: Typical behaviour of plastic shrinkage cracking [20].

### 3.1.2. Use of Fibres to Mitigate Shrinkage-Induced Cracking

Most recent research on plastic shrinkage cracks focuses on performance and durability enhancement of concrete as a material [22–24] and attempts to find solutions to avoid cracks or at least reduce their appearance. One of the most effective solutions to mitigate the shrinkage phenomenon is the use of different types of fibres in concrete, including steel, glass, polymer, and natural fibres.

Lee and Won [25] evaluated the effect of adding nano-synthetic fibres and hooked-end-type steel fibres (MSF) to concrete at volume fractions of 0.26%. The results showed that nano-synthetic fibres performed better than MSF to reduce crack width by about 36% but were not able to prevent the development of surface cracking. Mazzoli et al. [26] compared the ability of four types of fibres, including polypropylene (with three different lengths), polyvinyl alcohol, polyethylene, and steel (hooked ended), to control early-age shrinkage cracking (plastic and autogenous). The study concluded that polypropylene and polyethylene macro fibres were more effective at reducing the total crack area than MSF. Sivakumar and Santhanam [27] examined different combinations of fibres, such as MSF, polyester, polypropylene, and glass, and concluded that the combinations of MSF and polyester fibres had the best performance in controlling concrete plastic shrinkage cracking. This can be attributed to the fact that polymer fibres tend to have a smaller diameter and, as such, are better distributed.

Booya et al. [2] examined the effects of Kraft pulp fibres on plastic shrinkage cracking and found that these fibres are highly effective in controlling plastic shrinkage cracks. The use of natural fibres, such as flax and hemp, to restrain plastic shrinkage cracks in concrete and mortar

also compared well with polypropylene fibres [28]. Many other studies investigated different types of natural fibres to reduce plastic shrinkage cracks in concrete. Wang et al. [4], Balaguru [29], Soroushian and Ravanbakhsh [30], and Booya et al. [2] used natural cellulose fibres and found that they can reduce plastic crack widths but do not prevent concrete from cracking due to the high water absorption of the fibres compared to other types of fibres. Other studies examined the effects of sisal and coconut fibres to restrain plastic shrinkage cracks, and the results showed that sisal and coconut fibres can positively help reduce crack widths, but high volume fractions are needed to control plastic shrinkage cracks [31–33]. Nevertheless, natural fibres tend to reduce concrete strength, as well as increase permeability, and hence have limited general practical use in structural concrete. Hence, more robust and sustainable solutions are required.

For example, Karalar et al. [34] conducted a study that investigated the use of waste lathe scraps in reinforced concrete beams. The results showed that the addition of steel waste lathe scraps increased the compressive strength of the resulting concrete by up to 32.5% when a fibre volume of 3% was used and improved the beam's mechanical performance. Moreover, Ali et al. [35] examined the effects of lathe waste scrap on both fresh and hardened properties of fibre-reinforced concrete and observed that while an increase in compressive and tensile strength can be observed at increasing fibre volume, workability is negatively affected.

With around 1.5 billion tyres worldwide being discarded every year, each containing about 10% of highly engineered steel cord as reinforcement [36], various research groups have focused on examining the suitability of recycled tyre steel fibres (RTSF) as a more sustainable alternative to manufactured steel fibres (MSF) [37,38]. Recent findings have shown that when steel cords are extracted from tyres, mainly via mechanical shredding, they can be further processed to remove impurities and long lengths, which can cause balling, and turned into effective fibre reinforcement [39–43].

RTSF are typically characterised by a range of lengths and a smaller diameter than conventional MSF and may offer a more holistic shrinkage crack control (from plastic to drying shrinkage cracking), as well as structural reinforcement benefits. Su et al. [44] tested the mechanical and drying shrinkage properties of mortars, including plastic rubber (PR) (2%, 5%, 7.5%, and 10% by volume) and RTSF at a constant volume fraction of 0.2%. The results showed that the addition of RTSF and PR had increased the compressive strength up to 14–27% and reduced the drying shrinkage crack lengths by about 25% at 7 days curing. Jafarifar

et al. [45] studied the impact of adding RTSF (around 2.5% by weight) on the drying shrinkage of concrete pavements and found that the RTSF had the ability to control drying shrinkage compared to plain concrete. Graeff et al. [46] also found that the RTSF help in freeze–thaw, corrosion, and fatigue resistance. Al-musawi et al. [47] examined the effects of clean RTSF on the drying shrinkage of concrete made with different types of cement (CSA—calcium sulfoaluminate cement and RSC—calcium aluminate cement). The study showed that the inclusion of RTSF reduced the drying shrinkage strains by approximately 12%. Zhong and Zhang [48] examined the properties of concrete reinforced with three types of fibre, (i) manufactured steel fibre (MSF), (ii) recycled tyre steel fibre (RTSF), and (iii) polypropylene fibre (PPF). Surprisingly, the results showed that the fibres used did not significantly improve the mechanical properties in terms of compressive, splitting tensile, and flexural strengths compared to plain concrete. Nonetheless, the addition of RTSF had less impact on the workability of concrete than MSF and PPF and controlled drying shrinkage to a higher degree. Hence, although there is some uncertainty as to the effect of fibres on the overall performance of concrete, RTSF show real promise in enhancing shrinkage performance and thus warrants further studies.

### 3.1.3. Restrained Plastic Shrinkage Testing Techniques

As for all shrinkage cracks, plastic shrinkage cracks appear on the surface of the concrete as a result of external restraint. Hence, in plastic shrinkage tests, there is an attempt to amplify restraint, so as to accelerate cracking. Four main plastic shrinkage test techniques are used to evaluate plastic shrinkage cracks: ring, longitudinal, slab, and substrate restraint.

Bjøntegaard and Sellevold [49] adopted the ring test to restrain plastic shrinkage cracks in concrete. Concrete was placed between two concentric steel rings to a depth of 45–50 mm. The rings rest on a rigid plate and have 12 rigid ribs to restrain plastic shrinkage. The wind speed was controlled above the concrete specimens to achieve faster than normal drying time. The plastic shrinkage cracks occurred around the ribs. Ling et al. [50] used this arrangement in a more recent study and found that the ring test achieved high levels of plastic shrinkage cracks.

A test method relying on prisms with a size of  $40 \times 40 \times 500$  mm (longitudinal test) was first proposed in [51]. The arrangement utilises two bars at the two ends of the beams to restrain plastic shrinkage cracks. The test was further developed by Mora-Ruacho et al. [52] using larger specimens ( $150 \times 150 \times 600$  mm) and including a riser in the centre of the specimen to increase plastic shrinkage cracking potential and localise the cracks above the riser. These types

of arrangements eventually led to slab tests and substrate restraint tests that are more representative of real slabs, such as the test adopted here, as recommended in ASTM C1579 [53] and described in detail in the following section. The careful control of environmental conditions is also key for such tests [54,55].

### **3.1.4. Measurements**

Tracking plastic shrinkage cracks is challenging due to the random initiation time, location of crack, and irregular crack shape, which renders conventional strain measurements inadequate. Therefore, dynamic manual and image-based techniques are necessary. Manual methods include the use of microscopes and crack magnifiers to measure the crack width and length. It is accepted that it is necessary to obtain the measurements at more than one point and utilise the average of the measurements [3,55–57]. The advantages of these methods are that they are relatively simple and can be applied easily on site. On the other hand, these methods have been criticised due to the need for human judgement and are more prone to errors compared to other measurement techniques.

Image-based techniques include digital image correlation (DIC) and digital image processing (DIP). Those methods utilise high-resolution cameras that capture images of the entire concrete surface and these images are subsequently processed by specially developed algorithms. These methods can track the crack width, length, and area at the surface of the concrete from the time of casting to the end of the test. Recently, DIC has been used extensively in studies monitoring cracks on hardened concrete surfaces [36,58]. In this study, a digital image processing method will be used to measure the crack width, length, and area.

### **3.1.5. Significance of Research**

This paper aims to examine the impact of RTSF on plastic shrinkage cracking of concrete. A direct comparison is made with MSF and the impact of fibre distribution on crack initiation and development is investigated. Crack measurements are obtained through the implementation of a digital image processing method, in an attempt to have a more in-depth understanding of crack development and remove subjectivity. The use of finer structural fibres may lead to more sustainable and durable steel-fibre-reinforced concrete (SFRC) structures.

## 3.2. Experimental Program

### 3.2.1. Materials

#### 3.2.1.1. Manufactured Steel Fibre (MSF)

In this study, hooked-end fibres (Figure 3.3) were selected as they are cost-effective and are commonly used in large flat-slab construction. The fibres have a length of 50 mm and a diameter of 1.0 mm, and a nominal tensile strength of 1150 MPa.

#### 3.2.1.2. Recycled Tyre Steel Fibres (RTSF)

In this study, specially processed recycled tyre steel fibres (RTSF), as shown in Figure 3.3, were used in different amounts to assess their performance in controlling plastic shrinkage. The mechanical and physical characteristics of these fibres were obtained by testing more than 100 samples of individual RTSF (see Figure 3.4). The fibres were tested in tension according to ISO 6892-1 [59] using an electromechanical universal testing machine and specially modified capstan grips, as shown in Figure 3.5. The average value of the mechanical strength was determined, considering the mechanical performance of the samples that failed within the free length only. Results from samples that failed prematurely at the grips were rejected. The range of fibre lengths used in the experiment was determined by an automated optical method [60] and is shown in Figure 3.6.

The diameter was measured at 3 points along the fibre length. The average diameter was found to be 0.35 mm (SD = 0.036 mm), with measurements ranging between 0.32 and 0.41 mm (see Figure 3.4b). The average tensile strength was 2380 MPa (SD = 166 MPa), as shown in Figure 3.4c. Some fibres exceeded 3000 MPa, which shows that the original cord is of extremely high quality. Nonetheless, the mechanical shredding process used to extract the fibres causes damage, and some fibres fall below 1000 MPa. However, this loss of strength is unlikely to have any impact on plastic shrinkage cracking control as very little stress develops in the fibres at that stage.



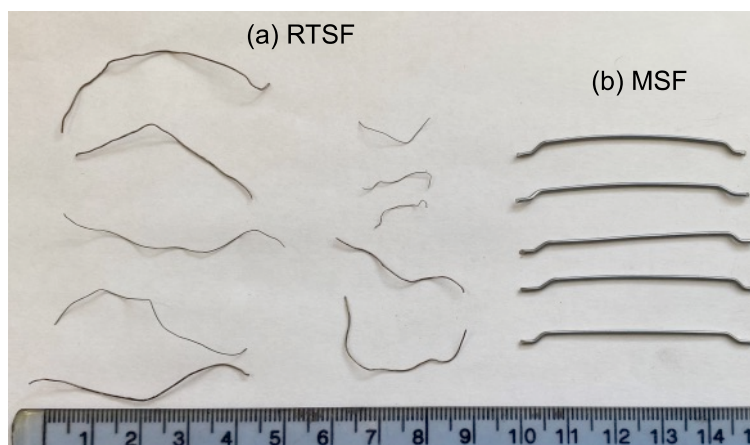


Figure 3.3 : Appearance of (a) RTSF and (b) MSF.

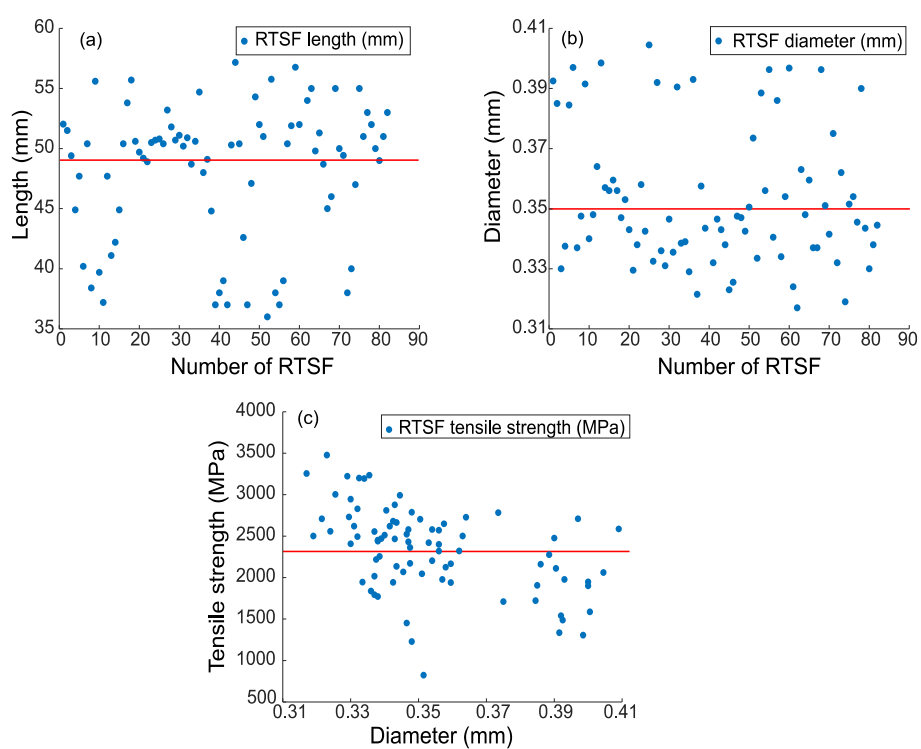


Figure 3.4: Average (a) length, (b) diameter, and (c) tensile strength of the RTSF.

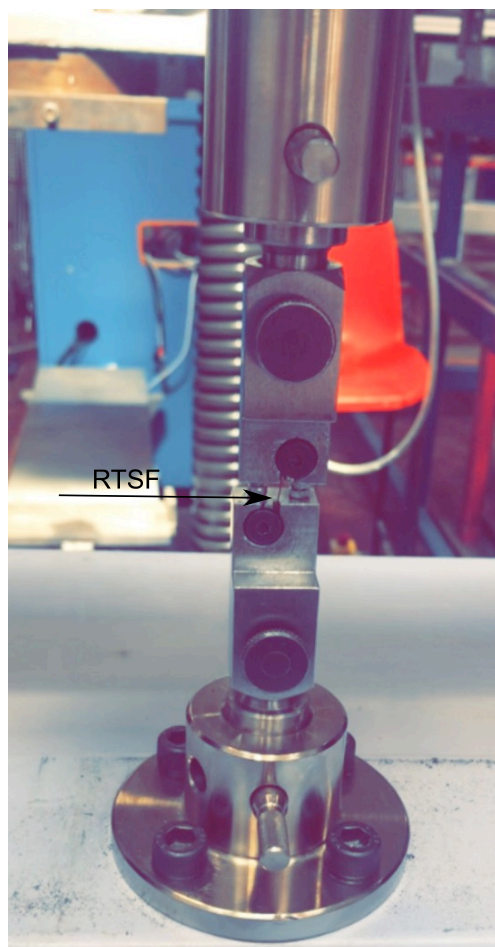


Figure 3.5: Set-up for tensile testing of RTSF.

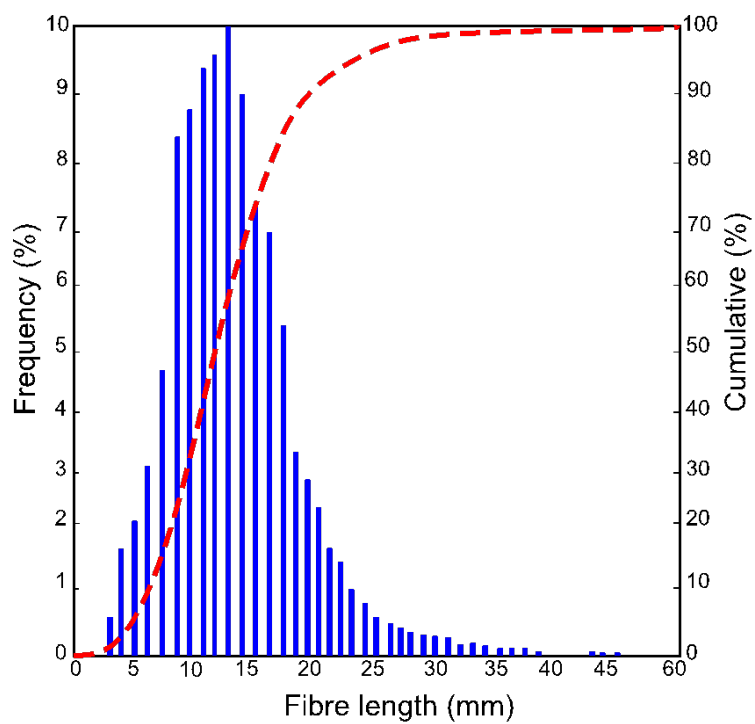


Figure 3.6: RTSF length distribution.

### 3.2.2. Mix Design

The mix design used in this experimental study is shown in Table 3.1 and was similar to that used in previous research projects [61]. A cement content of 335 kg/m<sup>3</sup> was selected, as this increases the likelihood of plastic shrinkage cracking.

Natural river sand and gravel were used as fine and coarse aggregates, and their total evaporable moisture content was determined by drying, as per [62]. The relative density (specific gravity oven dry (SG<sub>OD</sub>), specific gravity saturated surface dry (SG<sub>SSD</sub>), apparent specific gravity (ASG)) and absorption were also determined, as recommended in ASTM C127-15 [63]. All the properties of fine and coarse aggregates are shown in Table 3.2. The fine and coarse aggregates were weighed and stored in standard laboratory conditions at 20 ± 2 °C a day before mixing the concrete.

MSF and RTSF were used in different amounts, 0 kg ( $V_f = 0\%$ —control samples), 10 kg ( $V_f = 0.13\%$ ), 20 kg ( $V_f = 0.26\%$ ), and 30 kg ( $V_f = 0.38\%$ —typical for slabs on grade) per m<sup>3</sup> of concrete, to examine their impact on plastic shrinkage cracks.

Table 3.1 Concrete mix proportions.

<b>Material</b>	<b>Quantity</b>
Cement (CEMII 42.5)	335 kg/m <sup>3</sup>
Fine Aggregate (dry) (river round sand)	847 kg/m <sup>3</sup>
Gravel 10 mm (dry) (river round gravel)	491 kg/m <sup>3</sup>
Gravel 14 mm (dry) (river round gravel)	532 kg/m <sup>3</sup>
Water	185 kg/m <sup>3</sup>
Superplasticiser (Sika ViscoCrete 30HE)	1.5 lt/m <sup>3</sup>
MSF	10 kg/m <sup>3</sup> , 20 kg/m <sup>3</sup> , and 30 kg/m <sup>3</sup>
RTSF	10 kg/m <sup>3</sup> , 20 kg/m <sup>3</sup> , and 30 kg/m <sup>3</sup>

Table 3.2 Physical properties of fine and coarse aggregates.

<b>Bulk Density Aggregate</b>	<b>Fine of Aggregates</b>	<b>Coarse Aggregates Size 10 mm</b>	<b>Coarse Aggregates Size 20 mm</b>
Moisture %	2.58	0.83	0.24
SG <sub>OD</sub>	3.18	2.50	2.60
SG <sub>SSD</sub>	3.21	2.50	2.60
ASG	3.30	2.58	2.66
Absorption%	1.23	0.91	0.58

Note: SG<sub>OD</sub> = specific gravity oven dry; SG<sub>SSD</sub> = specific gravity saturated surface dry, ASG = apparent specific gravity.

### 3.2.3. Mixing and Casting Procedure

A pan mixer was used for all mixes and the following mixing/casting procedure was adopted:

1. Materials were weighted according to ASTM C192/C192M [64].
2. Cement and aggregates were dry mixed for 1 min, after which water was added.
3. Mixing continued for 3 min, after which half of the mix was removed to cast the first plastic shrinkage mould (according to ASTM C1579 [53], see next section) and four 100 mm cubes (to measure compressive strength).
4. The MSF and RTSF were then added and mixing continued for an additional 3 min.
5. The second plastic shrinkage mould was then filled, and four 100 mm cubes were cast.

According to ASTM C1579 [53], the concrete was cast in one layer, followed by a 30 s vibration on a vibrating table. The top surface of the specimen was then screeded three times in the direction perpendicular to the stress riser.

## 3.3. Methodology

### 3.3.1. Workability

A slump test was carried out in accordance with ASTM C143/C143M [65] to ensure adequate workability after the addition of fibre, with a target of slump of  $100 \pm 10$  mm.

### 3.3.2. Compressive Strength

The compressive strength of the mixes was obtained in accordance with BS EN, 12390-3 [66] from tests on 100 mm cubes in a servo hydraulic universal testing machine. Two cubes were tested on day 1 to observe the effects of the environmental conditions (air temperature, relative humidity, and airflow) on early-age strength, whilst the other two cubes after exposed to environmental conditions inside and outside the chamber for six hours, it were stored under standard laboratory conditions ( $20 \pm 2^\circ\text{C}$ ) and tested after 28 days of curing.

### 3.3.3. Evaporation Rate

To quantify the base water evaporation rate in the chamber, two aluminium pans were filled with water and were placed next to each slab specimen. The exposed water surface area of each pan was  $0.019 \text{ m}^2$ . The evaporation rate at each time interval was determined by (Equation (1)) ASTM C1579 [53]; the mass loss was divided by the surface area of the water

and the time interval between successive weighings. The average evaporation rate should exceed  $1.0 \text{ kg/m}^2/\text{h}$ ; otherwise, the test is rejected [53].

$$E = \frac{M_2 - M_1}{\text{water surface area of the pan} \times (T_2 - T_1)} \quad (1)$$

Where  $E$ : Evaporation rate,  $\text{kg/m}^2/\text{h}$ ;  $M_2 - M_1$ : the mass loss between successive weighings, g; and  $T_2 - T_1$ : the time interval between successive weighings, h.

### 3.3.4. Plastic Shrinkage Test

Figure 3.7 and Figure 3.8 diagrammatically show the chamber ASTM C1579 [53] used to evaluate the performance of different types of fibres in controlling plastic shrinkage cracking. According to ASTM C1579 [53], two comparative specimens were placed in an environmental chamber immediately after casting. The chamber was controlled in terms of air temperature, relative humidity, and airflow. In addition to the specimens, two water pans and two concrete cubes (100 mm) were placed inside the chamber to measure water evaporation and compressive strength of concrete, respectively.

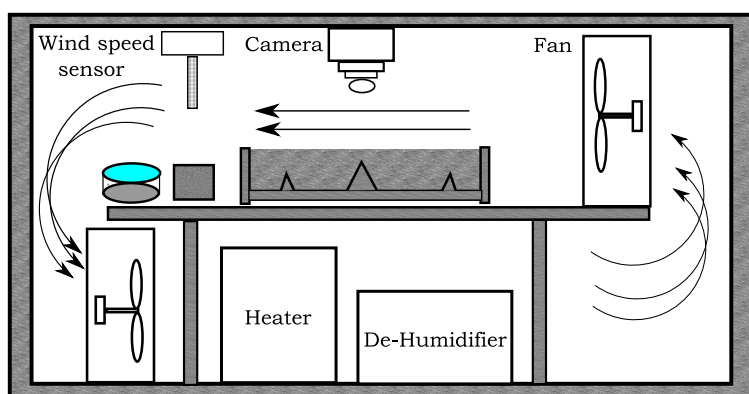


Figure 3.7: Schematic section of the chamber.

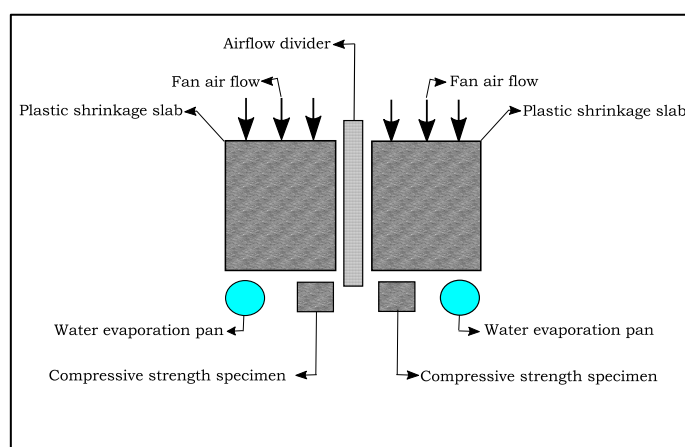


Figure 3.8: Schematic plan of the contents of the chamber.

The plastic shrinkage tests were designed to give a comparative analysis of crack behaviour (width, length, and area) between two slabs in the same environmental conditions. The specimens were rectangular with dimensions of 560 mm in length, 355 mm in width, and 100 mm in depth. A tall triangular stress riser was fixed at the middle of the mould's steel base to induce cracking, and two shorter triangular internal restraints were fixed close to the sides of the mould (Figure 3.9) on either side. Both stress risers and internal restraints were made of solid steel. The side and the base of the moulds were made from 20 mm thick steel plates (Figure 3.10).

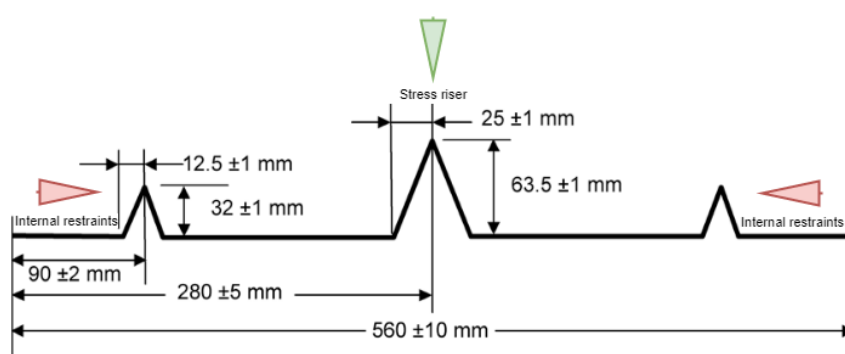


Figure 3.9: Geometry of the stress riser and internal restraints [53].



Figure 3.10: The complete mould.

The chamber was turned on two hours prior to the start of the test to pre-heat and stabilise the environment to the desired temperature ( $36 \pm 3$  °C) and relative humidity ( $30 \pm 10\%$ ), as recommended by [53]. Immediately after casting, the moulds and cubes were placed inside the chamber.

Records of the water mass loss and water evaporation rate were taken every 30 min, according to ASTM C1579 [53]. The evaporation rate was recorded by removing the monitoring pan from the air stream, weighing it, and returning it to the air stream within 15 s,

as recommended in [53]. In addition, the air temperature and relative humidity were recorded every hour, as recommended in [53]. These should be in the range of  $36 \pm 3$  °C and  $30 \pm 10\%$ , respectively. It should be noted that the wind velocity must be sufficient to maintain the minimum evaporation rate during the test. The wind speed, as recommended in ASTM C1579 [53], should be more than 4.7 m/s over the entire test panel's surface area. A typical test lasts six hours, after which the fans, heater, and dehumidifier are turned off, the samples covered with plastic sheeting, and the doors of the environmental chamber left open to stabilise to normal lab environmental conditions. Figure 3.11 shows a photo of specimens in the chamber.

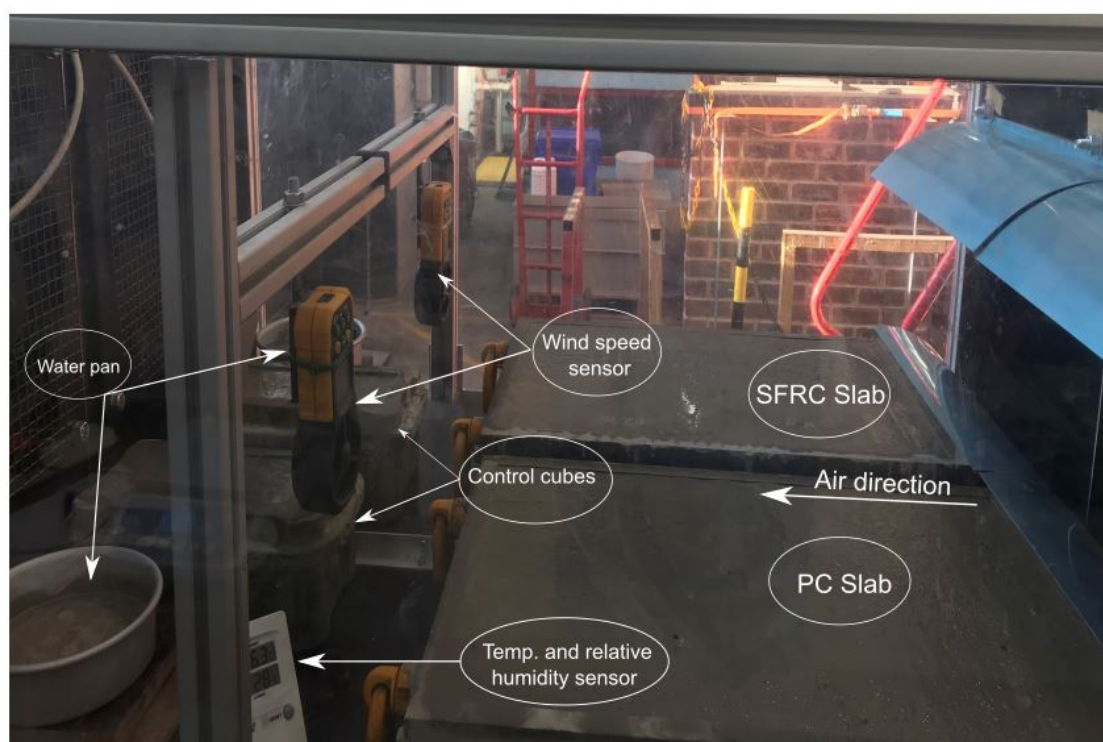


Figure 3.11: Set-up for plastic shrinkage test.

#### 3.3.4.1. Measurements

Measurements of the plastic shrinkage cracks (length, width, and area) were carried out using a digital image processing method, whereby a camera is placed above the samples during the test to capture images of the samples at different times. The images were then analysed using a digital imaging processing script written in MATLAB. The MATLAB script was written and developed by [67]. The script converts the original images to greyscale (see Figure 3.12a, b). The greyscale image is then converted to a binary image (see Figure 3.12c) and cleaned of spurious black pixels (see Figure 3.12d). This allows the pixels forming the crack to be counted and the average crack width to be determined.

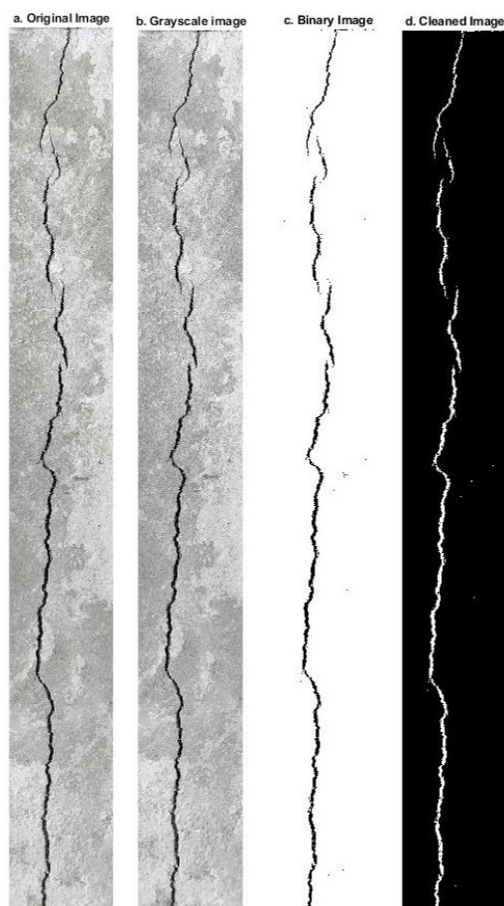


Figure 3.12: Image processing steps.

At 24 h, measurements of crack width were obtained by using both digital image analysis, as explained above, and an optical micrometre at more than 25 locations along the crack length to calculate the average of crack width. These measurements were made for comparison purposes between the two methods.

The average plastic shrinkage crack width is used to calculate the crack reduction ratio (CRR) at 6 and 24 h from the start of the test and uses the following equation, as recommended in [53]:

$$\text{CRR} = \left[ 1 - \frac{\text{Average Crack Width of Fibre Reinforced Concrete Mixture}}{\text{Average Crack Width of Fibre Control Concrete Mixture}} \right] \times 100\% \quad (2)$$

## 3.4. Experimental Results and Discussion

### 3.4.1. Workability

The concrete workability is affected by various factors. It was observed that the addition of RTSF and MSF lead to a reduction in the slump of concrete compared with plain concrete, as shown in Figure 3.13. This reduction increases with increasing fibre dosage. The RTSF



reduced the workability by 20%, 32%, and 45% for doses of 10 kg/m<sup>3</sup>, 20 kg/m<sup>3</sup>, and 30 kg/m<sup>3</sup>, respectively. The corresponding reductions in workability were less when using MSF and were equal to 13%, 25%, and 36%. This is because the number of RTSF fibres is much higher for a single fibre volume compared to MSF, and this also increases the shear resistance of fresh concrete making it harder to flow [68]. These results agree well with published research on RTSF by [26,69].

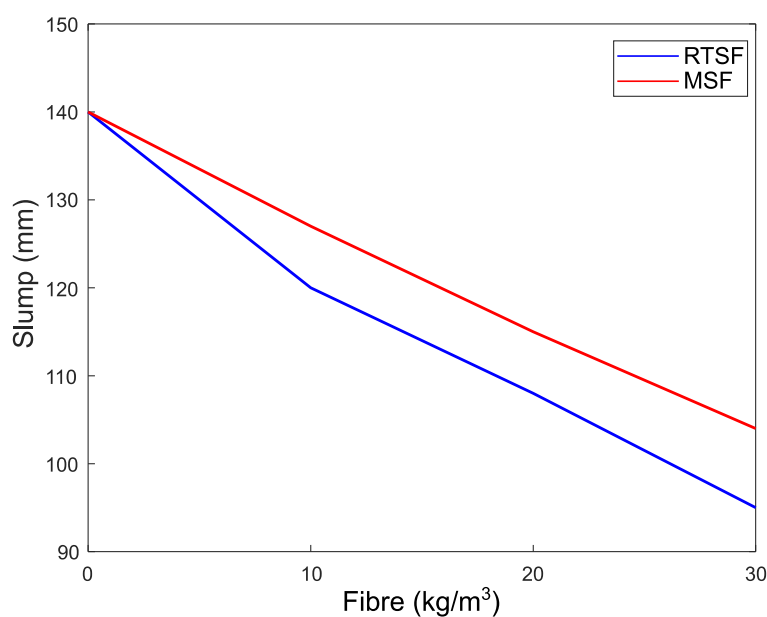


Figure 3.13: Effect of fibre type and dosage on slump of concrete.

### 3.4.2. Compressive Strength

The compressive strength of control specimens (plain concrete-PC) and steel-fibre-reinforced concrete (RTSF and MSF) at 1 day and 28 days, measured on cubes that were conditioned inside and outside the chamber, are shown in Figure 3.14, along with the corresponding normalized ratios.

As expected, given the work of [70–72], the addition of MSF and RTSF results in only marginal increases in compressive strength, which is seen to increase with fibre content in line with other studies [73–75]. Zeybek et al. [76] examined the influence of steel fibres extracted from waste tyres on concrete performance and observed an increase in compressive strength between 17%, 30%, and 46% when adding a volume of fibres from 1%, 2%, and 3%, respectively.

However, the one-day compressive strength after exposure in the chamber for 6 h is around 10% higher than for cubes that were kept outside the chamber (see Figure 3.14a, c). Dzayeb et

al. [77] attributes this increase to the higher temperature inside the chamber, which speeds up the hydration reaction. The impact of this early increase in strength is no longer significant after 28 days (see Figure 3.14b, d).

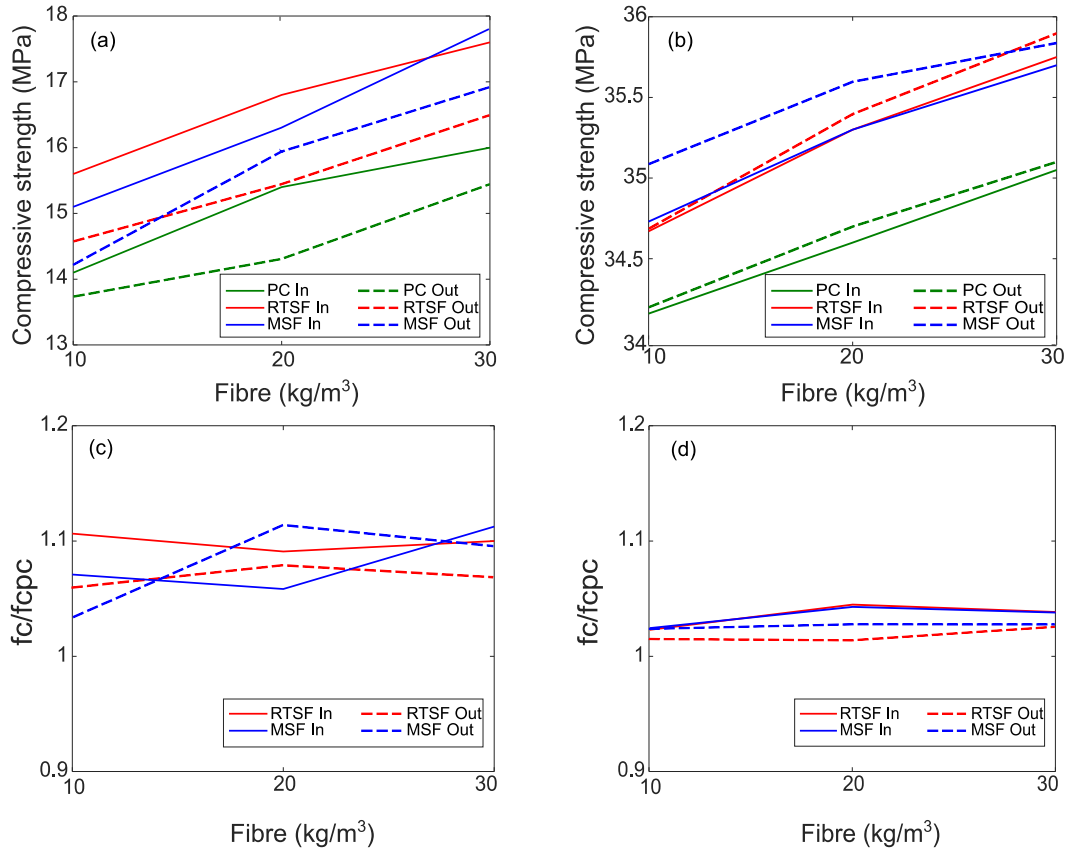


Figure 3.14: Compressive strength and normalized ratio of PC and FRC at 1 day (a, c) and 28 days (b, d) for cubes inside (In) and outside (Out) the chamber.

### 3.4.3. Evaporation Rate

#### 3.4.3.1. Environmental Conditions

The evaporation rate is accepted as one of the main factors that influence the likelihood of plastic shrinkage cracking. When the evaporation rate increases, the crack area and width increases [50,78]. In this study, an attempt was made to expose all test specimens to identical environmental conditions, but the initial temperature is hard to control precisely due to daily variations in temperatures ( $15 \pm 2$  °C). Wind speed and relative humidity were controlled, as recommended in ASTM C1579 [53] at  $30 \pm 10\%$ , and 5 m/s, respectively, as shown in Figure 3.15. The high drop of relative humidity from 40% to 20% during the test was due to the increase in the air temperature from  $28 \pm 2$  °C to the end of the test at  $36 \pm 2$  °C.

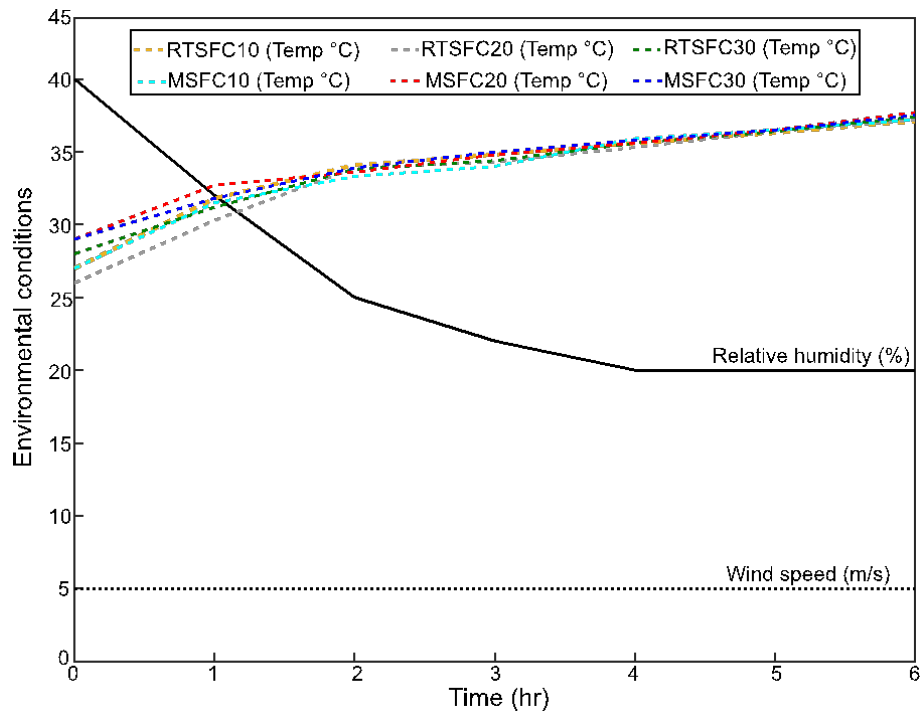


Figure 3.15: Environmental conditions for all mixes.

### 3.4.3.2. Bleeding and Evaporation Rates

Figure 3.16 a–f show the effect of environmental conditions on the evaporation rate of bleed water. All water pan evaporation rates exceed the minimum of  $1.0 \text{ kg/m}^2/\text{h}$  required by ASTM C1579 [53].

The evaporation rate of all mixes increases roughly in a similar manner, irrespective of fibre amount and type. The increase in the evaporation rate is consistent with the increase in temperature during the test. Initially, the evaporation rate is more or less constant, but after two to three hours of the test, the evaporation rate increases slightly. This could indicate an increase in bleed water, but this is unlikely as cracks also appear at this stage, which means that this is likely due to increased surface temperature due to hydration. The development of cracks means that by now the bleeding rate has slowed down or stopped, which is in agreement with other works [79,80].

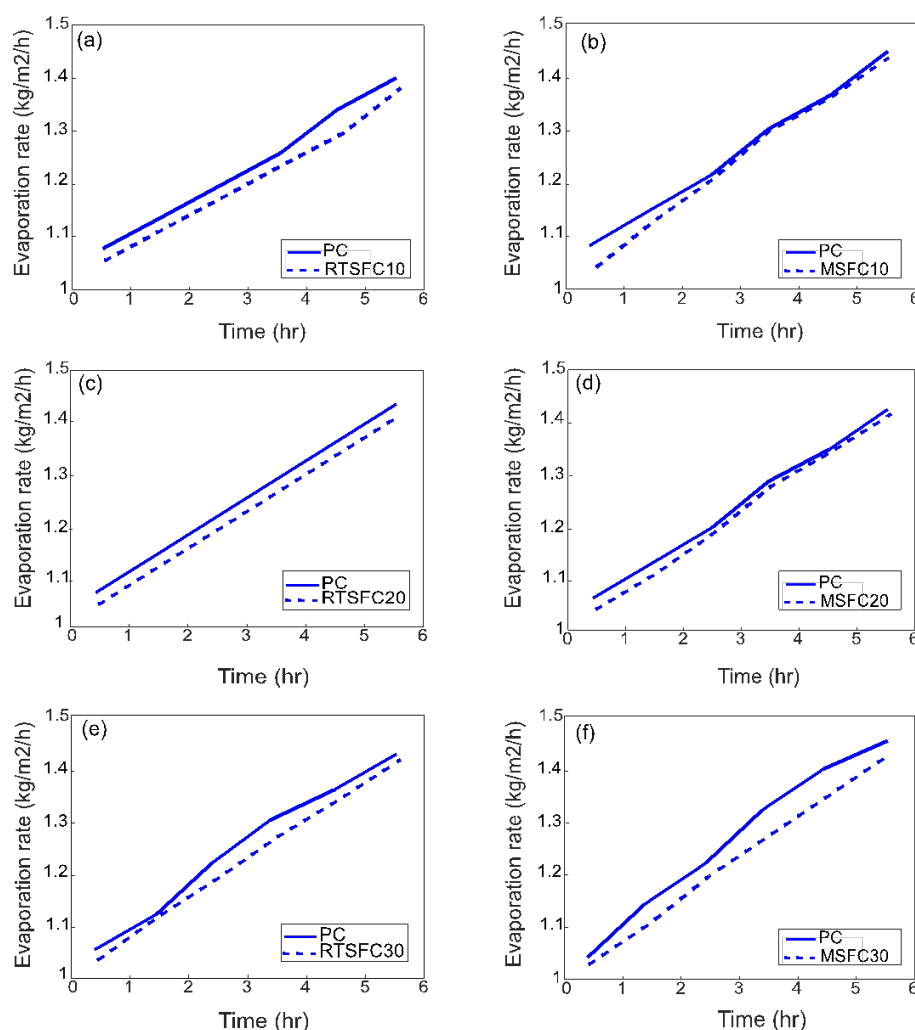


Figure 3.16: Evaporation rate of the various mixes compared to PC: (a) RTSFC10; (b) MSFC10; (c) RTSFC20; (d) MSFC20; (e) RTSFC30; (f) MSFC30.

### 3.4.4. Plastic Shrinkage Test Results

#### 3.4.4.1. Study of Cracks on Concrete Surface Using Digital Image Analysis

A digital image analysis technique was used to evaluate the evolution of plastic shrinkage cracking during the test. Photos of the concrete surface were taken every 10 min until the cracks first appeared (about two to three hours), and every 30 min thereafter until the end of the test (six hours). Photos were also taken at 24 h, as recommended in [53]. All photos were processed to determine the cracks, as described in Section 3.3.4.1. The evolution of crack width for all specimens is shown in Figure 3.17.

Most cracks appear after 2 h, corresponding to the initial setting time, while they show a fast evolution (width) during the first two to three hours after initiation and tend to stabilise towards the end of the test when the concrete is reaching or has reached its final setting time.

As expected, after the end of the test and up to 24 h, none of the cracks showed any significant increase in width. These results are in agreement with other similar studies [18,81,82].

The rapid increase in crack width immediately after cracking is attributed to the evaporation rate being equal to or higher than the bleeding rate, which indicates the stage that the concrete surface begins to dry and a negative pore pressure is created [83–85]. This negative pore pressure is one of the main causes of surface crack development.

Measurements at 24 h were made using digital image analysis and optical methods for comparison purposes and are also shown in Figure 3.17. The measurements from the two methods are practically identical, confirming the ability of digital image analysis methods to be used in this application.

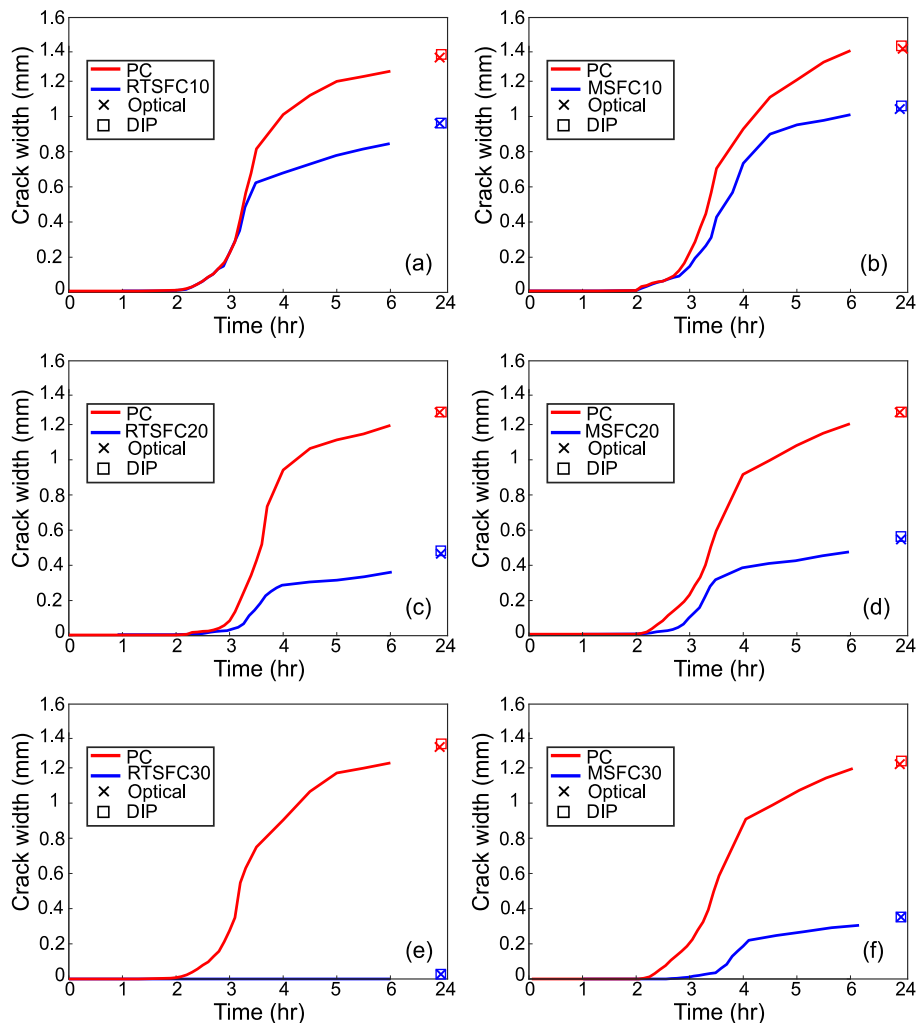


Figure 3.17: Crack width evolution for all specimens compared to their PC counterpart: (a) RTSFC10; (b) MSFC10; (c) RTSFC20; (d) MSFC20; (e) RTSFC30; (f) MSFC30.

### 3.4.4.2. Influence of Fibres

Overall, the addition of fibres has a beneficial effect in delaying and preventing plastic cracks, as also reported in [31,86], likely due to their ability to bridge micro-cracks, thus preventing them from joining and propagating.

All of the crack reduction ratios (CRR) of this study were determined at the end of the tests, according to Equation (2), and are shown in Figure 3.18, whilst Figure 3.19 shows the evolution of CRR with time.

Both fibre types (RTSF and MSF) show a good performance in controlling plastic shrinkage cracking. Better crack control is achieved at increasing fibre dosages, and cracking is avoided completely when using 30 kg/m<sup>3</sup> of RTSF. This was also observed in [87].

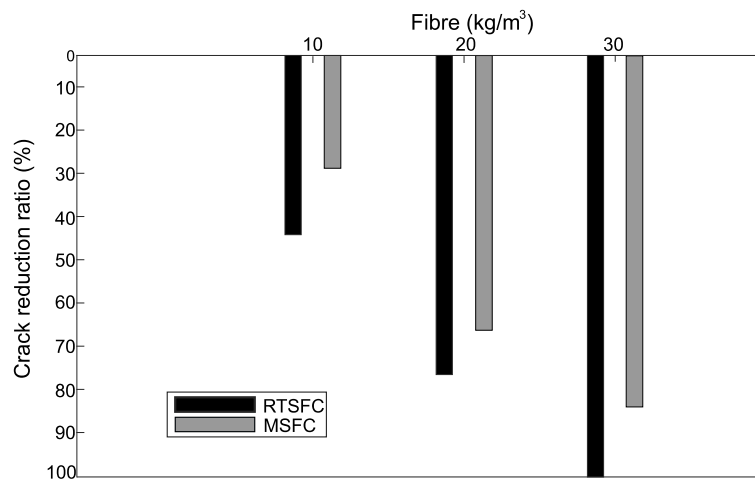


Figure 3.18: Crack reduction ratio (CRR) in specimens containing RTSF and MSF at 24 h.

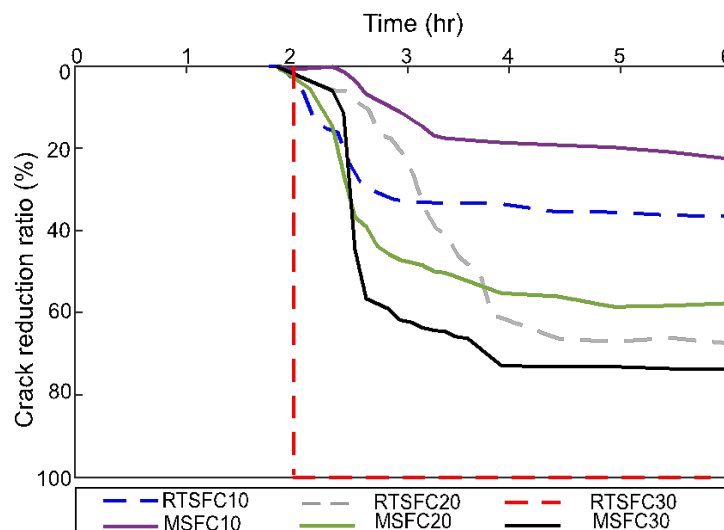


Figure 3.19: Evolution of crack reduction ratio (CRR) for specimens containing RTSF and MSF at 6 h.

### 3.4.4.3. MSF vs. RTSF

The impact of RTSF on plastic shrinkage cracking has not been discussed in previous studies. Overall, the results show that RTSF outperforms MSF at all dosages, and the qualitative image analysis presented below seems to confirm that the number of fibres, their weight, and their overall rigidity play a role in their performance. Cross-sections of the RTSF and MSF slabs were cut in the proximity of the stress riser, as shown in Figure 3.20. These sections are examined for fibre distribution, as shown in Figure 3.21a–d. Overall, RTSF appear to be better distributed within the mix (Figure 3.21c) than the MSF (Figure 3.21d). This can be attributed to the smaller diameter of the RTSF, which results, for the same dosage, in a much larger number of fibres that are available to reinforce the matrix and to intersect possible cracks. Furthermore, their larger surface area relative to their weight means that they are less likely to sink to the bottom than MSF (see Figure 3.21d). Finally, the irregular shape and flexibility of RTSF means that they can more easily move around aggregates and fill gaps, rather than control and restrain the distribution of the aggregates via their rigidity.

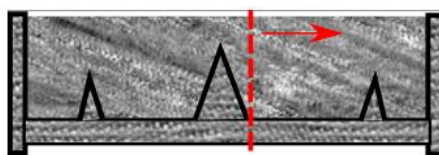


Figure 3.20: Location of the cross-section of RTSF and MSF slabs (red dashed line).

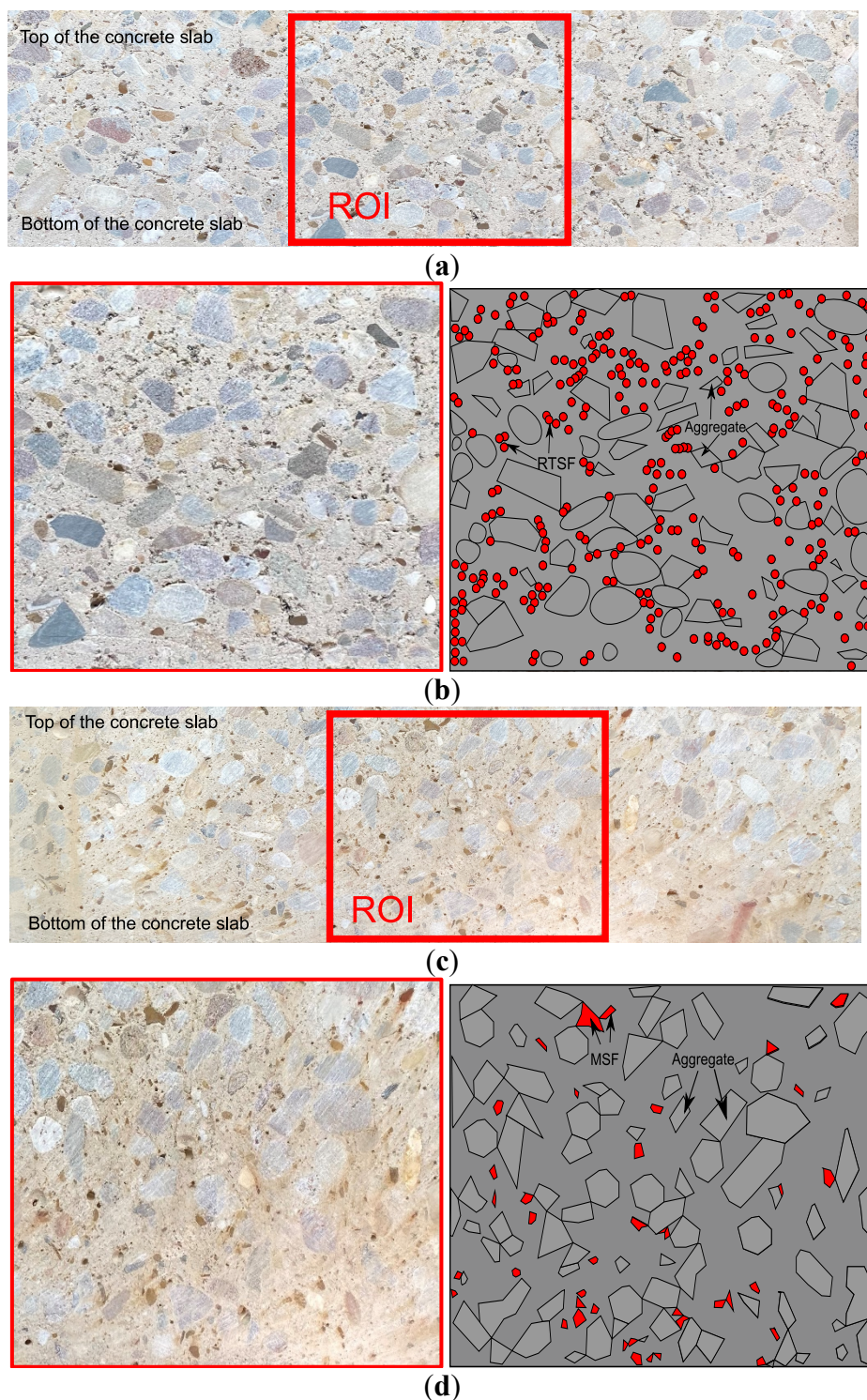


Figure 3.21: (a) Cross-section of specimen RTSFC30 and selected region of interest (ROI). (b). Magnified ROI of cross-section of specimen RTSFC30 (left) and distribution of aggregates and fibres (right). (c). Cross-section of specimen MSFC30 and selected region of interest (ROI). (d). Magnified ROI of cross-section of specimen MSFC30 (left) and distribution of aggregates and fibres (right).



### 3.5. Conclusions

This paper investigates the effect of different dosages of RTSF and MSF on restraining concrete plastic shrinkage at the fresh stage. Plain concrete and fibre-reinforced concrete slab specimens are tested according to the test method recommended in ASTM C1579 under controlled environmental conditions, and their crack initiation and development is examined, along with other physical parameters. From the analysis of the results presented in this paper, the following conclusions can be drawn:

- The evaporation rates are similar for all specimens and increase with increasing temperature.
- Cracking initiates after approximately 2 h from casting, indicating the initial setting time, and substantially stopped after 6 h, which can be considered as the final setting time.
- Exposure to the higher temperature in the chamber increases the hydration rate and 24 h strength of the concrete, although this had no major impact on the 28-day strength. The fibres only have a minor enhancing effect on compressive strength.
- RTSF outperform MSF in mitigating plastic shrinkage cracking at all dosages, with CRR values of 42%, 75%, and 100% for fibre dosages of 10 kg/m<sup>3</sup> ( $V_f = 0.13\%$ ), 20 kg/m<sup>3</sup> ( $V_f = 0.26\%$ ), and 30 kg/m<sup>3</sup> ( $V_f = 0.38\%$ ), respectively. The better performance of RTSF is attributed to their larger number and better distribution within the concrete volume when compared to MSF.

Although an appropriate fibre volume should be selected depending on mix design and target overall performance, a fibre dosage of 30 kg/m<sup>3</sup> ( $V_f = 0.38\%$ ) can be used to prevent plastic shrinkage cracking completely in most typical applications and environmental conditions.

This study provides compelling experimental evidence that RTSF are a sustainable and effective alternative to MSF in preventing plastic shrinkage cracks, in the same way as they are effective against drying shrinkage. The use of finer fibres has a beneficial effect in controlling plastic shrinkage cracks and their use (or the use of blends of MSF and RTSF) is expected to provide structural, durability, and sustainability benefits, particularly in the harsher environmental conditions created by climate change.

Future studies should examine the synergistic effects of using sustainable fibre alternatives, such as the RTSF used in the work presented in this paper, with different cement and aggregate replacements, as well as different curing methods to reduce or prevent plastic shrinkage cracking in concrete.

**Acknowledgments:** The first author would like to thank Jouf University and the Ministry of Education in the Kingdom of Saudi Arabia for sponsoring his Ph.D. studies. The authors would also like to thank TWINCON Ltd. for supplying materials for this project.

### 3.6. References

- [1] S. Ghourchian, M. Wyrzykowski, L. Baquerizo, P. Lura, Performance of passive methods in plastic shrinkage cracking mitigation, *Cem. Concr. Compos.* 91 (2018) 148–155. <https://doi.org/10.1016/j.cemconcomp.2018.05.008>.
- [2] E. Booya, K. Gorospe, H. Ghaednia, S. Das, Free and restrained plastic shrinkage of cementitious materials made of engineered kraft pulp fibres, *Constr. Build. Mater.* 212 (2019) 236–246. <https://doi.org/10.1016/j.conbuildmat.2019.03.296>.
- [3] J. Branston, S. Das, S.Y. Kenno, C. Taylor, Influence of basalt fibres on free and restrained plastic shrinkage, *Cem. Concr. Compos.* 74 (2016) 182–190. <https://doi.org/10.1016/j.cemconcomp.2016.10.004>.
- [4] P. Wang, K., Shah, S.P. and Phuaksuk, Plastic shrinkage cracking in concrete materials—influence of fly ash and fibers, *Mater. J.* 98 (2001) 458–464.
- [5] Mehta, P.K.; Monteiro, P.J. *Concrete: Microstructure, Properties, and Materials*; McGraw-Hill Education: New York, NY, USA, 2014; Volume 7, ISBN 9772081415.
- [6] U. Aktan, H.M., Fu, G., Dekelbab, W. and Attanayaka, Investigate causes & develop methods to minimize early-age deck cracking on Michigan bridge decks, (No. Res. Rep. RC-1437). (2003).
- [7] J.B. K. Folliard, C. Smith, G. Sellers, M. Brown, Evaluation of Alternative Materials to Control Drying-shrinkage Cracking in Concrete Bridge Decks, (No. FHWA/TX-04/0-4098-4,). (2003).
- [8] L.D. Linford, M. S., & Reaveley, A Study of the I-15 Reconstruction Project to Investigate Variables Affecting Bridge Deck Cracking, (No. UT-04.04,). (2004).
- [9] Saadeghvaziri, M.A.; Hadidi, R. Cause and Control of Transverse Cracking in Concrete Bridge Decks; FHWA-NJ-2002-019, Final Report; The National Academies of Sciences, Engineering, and Medicine: Washington, DC, USA, 2002.
- [10] I.M.G. Bertelsen, L.M. Ottosen, G. Fischer, Quantitative analysis of the influence of synthetic fibres on plastic shrinkage cracking using digital image correlation, *Constr. Build. Mater.* 199 (2019) 124–137. <https://doi.org/10.1016/j.conbuildmat.2018.11.268>.
- [11] T. Seerangurayar, A.M. Al-Ismaili, L.H. Janitha Jeewantha, A. Al-Nabhani, Experimental investigation of shrinkage and microstructural properties of date fruits at three solar drying methods, *Sol. Energy.* 180 (2019) 445–455. <https://doi.org/10.1016/j.solener.2019.01.047>.
- [12] S. Swaddiwudhipong, H.R. Lu, T.H. Wee, Direct tension test and tensile strain capacity of concrete at early age, *Cem. Concr. Res.* 33 (2003) 2077–2084. [https://doi.org/10.1016/S0008-8846\(03\)00231-X](https://doi.org/10.1016/S0008-8846(03)00231-X).
- [13] Q. Liu, J. Xiao, A. Singh, Quantification of plastic shrinkage and cracking in mortars containing different recycled powders using digital image correlation technique, *Constr. Build. Mater.* 293 (2021) 123509. <https://doi.org/10.1016/j.conbuildmat.2021.123509>.

- [14] P.J. Uno, Plastic shrinkage cracking and evaporation formulas, *ACI Mater. J.* 95 (1998) 365–375. <https://doi.org/10.14359/379>.
- [15] G.M. Moelich, J.E. van Zyl, N. Rabie, R. Combrinck, The influence of solar radiation on plastic shrinkage cracking in concrete, *Cem. Concr. Compos.* 123 (2021) 104182. <https://doi.org/10.1016/j.cemconcomp.2021.104182>.
- [16] ACI Committee 305. Hot-Weather Concreting; American Concrete Institute: Farmington Hills, MI, USA, 1999; Volume 17.
- [17] H.G. Kwak, S.J. Ha, Plastic shrinkage cracking in concrete slabs. Part II: A numerical model, *Mag. Concr. Res.* 58 (2006) 505–516. <https://doi.org/10.1680/mac.2006.58.8.505>.
- [18] T. Rahmani, B. Kiani, M. Bakhshi, M. Shekarchizadeh, Application of different fibers to reduce plastic shrinkage cracking of concrete, *RILEM Bookseries.* 4 (2012). <https://doi.org/10.1007/978-94-007-4566-7>.
- [19] A. Radocea, A model of plastic shrinkage, *Mag. Concr. Res.* 46 (1994) 125–132. <https://doi.org/10.1680/mac.1994.46.167.125>.
- [20] W.P. Boshoff, R. Combrinck, Modelling the severity of plastic shrinkage cracking in concrete, *Cem. Concr. Res.* (2013). <https://doi.org/10.1016/j.cemconres.2013.02.003>.
- [21] Sayahi, F.; Hedlund, H. Plastic Shrinkage Cracking in Concrete: State of the Art. *Nord. Concr. Res.* 2014, 51, 146.
- [22] G. Olivier, R. Combrinck, M. Kayondo, W.P. Boshoff, Combined effect of nano-silica, super absorbent polymers, and synthetic fibres on plastic shrinkage cracking in concrete, *Constr. Build. Mater.* 192 (2018) 85–98. <https://doi.org/10.1016/j.conbuildmat.2018.10.102>.
- [23] Z. Wu, C. Shi, K.H. Khayat, Investigation of mechanical properties and shrinkage of ultra-high performance concrete: Influence of steel fiber content and shape, *Compos. Part B Eng.* 174 (2019) 107021. <https://doi.org/10.1016/j.compositesb.2019.107021>.
- [24] S. Ghourchian, M. Wyrzykowski, L. Baquerizo, P. Lura, Susceptibility of Portland cement and blended cement concretes to plastic shrinkage cracking, *Cem. Concr. Compos.* 85 (2018) 44–55. <https://doi.org/10.1016/j.cemconcomp.2017.10.002>.
- [25] S.J. Lee, J.P. Won, Shrinkage characteristics of structural nano-synthetic fibre-reinforced cementitious composites, *Compos. Struct.* 157 (2016) 236–243. <https://doi.org/10.1016/j.compstruct.2016.09.001>.
- [26] A. Mazzoli, S. Monosi, E.S. Plescia, Evaluation of the early-age-shrinkage of Fiber Reinforced Concrete (FRC) using image analysis methods, *Constr. Build. Mater.* 101 (2015) 596–601. <https://doi.org/10.1016/j.conbuildmat.2015.10.090>.
- [27] A. Sivakumar, M. Santhanam, A quantitative study on the plastic shrinkage cracking in high strength hybrid fibre reinforced concrete, *Cem. Concr. Compos.* 29 (2007) 575–581. <https://doi.org/10.1016/j.cemconcomp.2007.03.005>.

- [28] M. Saad, V. Sabathier, A. Turatsinze, S. Geoffroy, Effect of Natural and Polypropylene Fibers on early Age Cracking of Mortars, *Bio-Based Build. Mater.* 1 (2022) 103–112. <https://doi.org/10.4028/www.scientific.net/cta.1.103>.
- [29] P. Balaguru, Contribution of fibers to Crack Reduction of Cement Composites During the Initial and Final Setting Period, *Mater. J.* 91 (1994) 280–288.
- [30] S. Soroushian, P. and Ravanbakhsh, Control of plastic shrinkage cracking with specialty cellulose fibers., *Mater. J.* 4 (1998) 429–435.
- [31] E. Boghossian, L.D. Wegner, Use of flax fibres to reduce plastic shrinkage cracking in concrete, *Cem. Concr. Compos.* 30 (2008) 929–937. <https://doi.org/10.1016/j.cemconcomp.2008.09.003>.
- [32] C.A. Juarez, G. Fajardo, S. Monroy, A. Duran-Herrera, P. Valdez, C. Magniont, Comparative study between natural and PVA fibers to reduce plastic shrinkage cracking in cement-based composite, *Constr. Build. Mater.* 91 (2015) 164–170. <https://doi.org/10.1016/j.conbuildmat.2015.05.028>.
- [33] G. Araya-Letelier, F.C. Antico, M. Carrasco, P. Rojas, C.M. García-Herrera, Effectiveness of new natural fibers on damage-mechanical performance of mortar, *Constr. Build. Mater.* 152 (2017) 672–682. <https://doi.org/10.1016/j.conbuildmat.2017.07.072>.
- [34] M. Karalar, Y.O. Özkılıç, A.F. Deifalla, C. Aksoylu, M.H. Arslan, M. Ahmad, M.M.S. Sabri, Improvement in Bending Performance of Reinforced Concrete Beams Produced with Waste Lathe Scraps, *Sustain.* 14 (2022) 1–17. <https://doi.org/10.3390/su141912660>.
- [35] A.İ. Çelik, Y.O. Özkılıç, Ö. Zeybek, N. Özdöner, B.A. Tayeh, Performance Assessment of Fiber-Reinforced Concrete Produced with Waste Lathe Fibers, *Sustain.* 14 (2022). <https://doi.org/10.3390/su141911817>.
- [36] The European Tyre Recycling Association. 2018. Available online: [http:// www.etra-eu.org](http://www.etra-eu.org) (accessed on 10 June 2018.).
- [37] K. Piotrowska, W. Kruszelnicka, P. Bałdowska-Witos, R. Kasner, J. Rudnicki, A. Tomporowski, J. Flizikowski, M. Opielak, Assessment of the environmental impact of a car tire throughout its lifecycle using the LCA method, *Materials (Basel)*. 12 (2019) 1–25. <https://doi.org/10.3390/MA12244177>.
- [38] M. Mastali, A. Dalvand, A.R. Sattarifard, M. Illikainen, Development of eco-efficient and cost-effective reinforced self- consolidation concretes with hybrid industrial / recycled steel fibers, *Constr. Build. Mater.* 166 (2018) 214–226. <https://doi.org/10.1016/j.conbuildmat.2018.01.147>.
- [39] M. Leone, G. Centonze, D. Colonna, F. Micelli, M.A. Aiello, Fiber-reinforced concrete with low content of recycled steel fiber : Shear behaviour, *Constr. Build. Mater.* 161 (2018) 141–155. <https://doi.org/10.1016/j.conbuildmat.2017.11.101>.
- [40] Z. Zamanzadeh, L. Lourenço, J. Barros, Recycled Steel Fibre Reinforced Concrete failing in bending and in shear, *Constr. Build. Mater.* 85 (2015) 195–207.

- <https://doi.org/10.1016/j.conbuildmat.2015.03.070>.
- [41] Z. Al-Kamyani, M. Guadagnini, K. Pilakoutas, Predicting shrinkage induced curvature in plain and reinforced concrete, *Eng. Struct.* 176 (2018) 468–480. <https://doi.org/10.1016/j.engstruct.2018.09.034>.
- [42] M.N. Isa, K. Pilakoutas, M. Guadagnini, Shear behaviour of E-UHPC containing recycled steel fibres and design of E-UHPC screw piles, *Constr. Build. Mater.* 304 (2021) 124555. <https://doi.org/10.1016/j.conbuildmat.2021.124555>.
- [43] A. Alsaif, Y.R. Alharbi, Strength, durability and shrinkage behaviours of steel fiber reinforced rubberized concrete, *Constr. Build. Mater.* 345 (2022) 128295. <https://doi.org/10.1016/j.conbuildmat.2022.128295>.
- [44] P. Su, Q. Dai, M. Li, Y. Ma, J. Wang, Investigation of the mechanical and shrinkage properties of plastic-rubber compound modified cement mortar with recycled tire steel fiber, *Constr. Build. Mater.* 334 (2022) 127391. <https://doi.org/10.1016/j.conbuildmat.2022.127391>.
- [45] N. Jafarifar, K. Pilakoutas, T. Bennett, Moisture transport and drying shrinkage properties of steel-fibre-reinforced-concrete, *Constr. Build. Mater.* 73 (2014) 41–50. <https://doi.org/10.1016/j.conbuildmat.2014.09.039>.
- [46] A.G. Graeff, K. Pilakoutas, K. Neocleous, M.V.N.N. Peres, Fatigue resistance and cracking mechanism of concrete pavements reinforced with recycled steel fibres recovered from post-consumer tyres, *Eng. Struct.* 45 (2012) 385–395. <https://doi.org/10.1016/j.engstruct.2012.06.030>.
- [47] H. Al-musawi, F.P. Figueiredo, M. Guadagnini, K. Pilakoutas, Shrinkage properties of plain and recycled steel–fibre-reinforced rapid hardening mortars for repairs, *Constr. Build. Mater.* 197 (2019) 369–384. <https://doi.org/10.1016/j.conbuildmat.2018.11.099>.
- [48] H. Zhong, M. Zhang, Experimental study on engineering properties of concrete reinforced with hybrid recycled tyre steel and polypropylene fibres, *J. Clean. Prod.* 259 (2020) 120914. <https://doi.org/10.1016/j.jclepro.2020.120914>.
- [49] E.J. Bjøntegaard, Ø. and Sellevold, THERMAL DILATION.—AUTOGENOUS SHRINKAGE: HOW TO SEPARATE, *Autogenous Shrinkage Concr.* (1999) 245.
- [50] Y. Ling, K. Wang, C. Fu, Shrinkage behavior of fly ash based geopolymer pastes with and without shrinkage reducing admixture, *Cem. Concr. Compos.* 98 (2019) 74–82. <https://doi.org/10.1016/j.cemconcomp.2019.02.007>.
- [51] C. Bantia, N. and Yan, Shrinkage cracking in polyolefin fiber-reinforced concrete., *Mater. J.* 97 (2000) 432–437.
- [52] A. Mora-Ruacho, J., Gettu, R., & Aguado, Influence of shrinkage-reducing admixtures on the reduction of plastic shrinkage cracking in concrete., *Cem. Concr. Res.* 39 (2009) 141–146.
- [53] ASTM C1579; Standard Test Method for Evaluating Plastic Shrinkage Cracking of Restrained Fiber Reinforced Concrete. ASTM International: West Conshohocken, PA,

- USA, 2006. <https://doi.org/10.1520/C1579-06.2>. <https://doi.org/10.1520/C1579-06.2>.
- [54] R.D. Toledo Filho, K. Ghavami, M.A. Sanjuán, G.L. England, Free, restrained and drying shrinkage of cement mortar composites reinforced with vegetable fibres, *Cem. Concr. Compos.* 27 (2005) 537–546.  
<https://doi.org/10.1016/j.cemconcomp.2004.09.005>.
- [55] A.E. Naaman, T. Wongtanakitcharoen, G. Hauser, Influence of different fibers on plastic shrinkage cracking of concrete, *ACI Mater. J.* 102 (2005) 49–58.  
<https://doi.org/10.14359/14249>.
- [56] Soroushian, P., Mirza, F. and Alhozajiny, A., Plastic shrinkage cracking of polypropylene fiber reinforced concrete., *Mater. J.* 92 (1993) 553–560.
- [57] S.J. Choi, B.T. Hong, S.J. Lee, J.P. Won, Shrinkage and corrosion resistance of amorphous metallic-fiber-reinforced cement composites, *Compos. Struct.* 107 (2014) 537–543. <https://doi.org/10.1016/j.compstruct.2013.08.010>.
- [58] C.G. Berrocal, I. Löfgren, K. Lundgren, N. Görander, C. Halldén, Characterisation of bending cracks in R/FRC using image analysis, *Cem. Concr. Res.* 90 (2016) 104–116.  
<https://doi.org/10.1016/j.cemconres.2016.09.016>.
- [59] ISO EN 6892-1; Metallic materials—Tensile testing—Part 1: Method of test at room temperature. ISO: Geneva, Switzerland, 2019.
- [60] M.N. Isa, K. Pilakoutas, M. Guadagnini, Determination of tensile characteristics and design of eco-efficient UHPC, *Structures.* 32 (2021) 2174–2194.  
<https://doi.org/10.1016/j.istruc.2021.03.114>.
- [61] H. Hu, P. Papastergiou, H. Angelakopoulos, M. Guadagnini, K. Pilakoutas, Mechanical properties of SFRC using blended Recycled Tyre Steel Cords (RTSC) and Recycled Tyre Steel Fibres (RTSF), *Constr. Build. Mater.* 187 (2018) 553–564.  
<https://doi.org/10.1016/j.conbuildmat.2018.07.206>.
- [62] ASTM C566-97; Standard Test Method for Total Evaporable Moisture Content of Aggregate by Drying. ASTM International: West Conshohocken, PA, USA, 1997.
- [63] ASTM C127-15; Standard Test Method for Density, Relative Density( Specific Gravity), and Absorption of Coarse Aggregate. ASTM International: West Conshohocken, PA, USA, 2013.
- [64] ASTM C192/C192M; Standard Practice for Making and Curing Concrete Test Specimens in the Laboratory. ASTM International: West Conshohocken, PA, USA, 2016.
- [65] ASTM C 143/C 143M–03; Standard Test Method for Slump of Hydraulic-Cement Concrete. ASTM International: West Conshohocken, PA, USA, 2003.
- [66] BS EN 12390-3; Testing hardened concrete. Compressive strength of test specimens. British Standards Institution: London, UK, 2009.
- [67] P. Zhao, A.M. Zsaki, M.R. Nokken, Using digital image correlation to evaluate plastic

- shrinkage cracking in cement-based materials, *Constr. Build. Mater.* 182 (2018) 108–117. <https://doi.org/10.1016/j.conbuildmat.2018.05.239>.
- [68] S. Grünewald, *Fibre reinforcement and the rheology of concrete*, Woodhead Publishing Limited, 2012. <https://doi.org/10.1533/9780857095282.2.229>.
- [69] A. Baricevic, D. Bjegovic, M. Skazlic, Hybrid Fiber–Reinforced Concrete with Unsorted Recycled-Tire Steel Fibers, *J. Mater. Civ. Eng.* 29 (2017). [https://doi.org/10.1061/\(asce\)mt.1943-5533.0001906](https://doi.org/10.1061/(asce)mt.1943-5533.0001906).
- [70] Ö. Eren, K. Marar, Effect of steel fibers on plastic shrinkage cracking of normal and high strength concretes, *Mater. Res.* 13 (2010) 135–141. <https://doi.org/10.1590/S1516-14392010000200004>.
- [71] J.A. Carneiro, P.R.L. Lima, M.B. Leite, R.D. Toledo Filho, Compressive stress-strain behavior of steel fiber reinforced-recycled aggregate concrete, *Cem. Concr. Compos.* 46 (2014) 65–72. <https://doi.org/10.1016/j.cemconcomp.2013.11.006>.
- [72] K.H. Younis, F.S. Ahmed, K.B. Najim, Effect of recycled-steel fibers on compressive strength and shrinkage behavior of self-compacting concrete, *Proc. - Int. Conf. Dev. ESystems Eng. DeSE. 2018-Septe (2019)* 268–272. <https://doi.org/10.1109/DeSE.2018.00054>.
- [73] M.A. Aiello, F. Leuzzi, G. Centonze, A. Maffezzoli, Use of steel fibres recovered from waste tyres as reinforcement in concrete: Pull-out behaviour, compressive and flexural strength, *Waste Manag.* (2009). <https://doi.org/10.1016/j.wasman.2008.12.002>.
- [74] Y. Mohammadi, S.P. Singh, S.K. Kaushik, Properties of steel fibrous concrete containing mixed fibres in fresh and hardened state, *Constr. Build. Mater.* 22 (2008) 956–965. <https://doi.org/10.1016/j.conbuildmat.2006.12.004>.
- [75] Ş. Yazici, G. Inan, V. Tabak, Effect of aspect ratio and volume fraction of steel fiber on the mechanical properties of SFRC, *Constr. Build. Mater.* 21 (2007) 1250–1253. <https://doi.org/10.1016/j.conbuildmat.2006.05.025>.
- [76] Y.O. Özkılıç, Ö. Zeybek, A.İ. ÇELİK, A. Deifalla, M. Ahmad, M. Sabri, Performance evaluation of fiber-reinforced concretes produced with steel fibers extracted from waste tire, *Front. Mater.* (2022) 692. <https://doi.org/10.3389/fmats.2022.1057128>.
- [77] E.D. Dzaye, E. Tsangouri, K. Spiessens, G. De Schutter, D.G. Aggelis, Digital image correlation (DIC) on fresh cement mortar to quantify settlement and shrinkage, *Arch. Civ. Mech. Eng.* 19 (2019) 205–214. <https://doi.org/10.1016/j.acme.2018.10.003>.
- [78] P.S. Deb, P. Nath, P.K. Sarker, Drying shrinkage of slag blended fly ash geopolymer concrete cured at room temperature, *Procedia Eng.* 125 (2015) 594–600. <https://doi.org/10.1016/j.proeng.2015.11.066>.
- [79] S. Ghourchian, M. Wyrzykowski, M. Plamondon, P. Lura, On the mechanism of plastic shrinkage cracking in fresh cementitious materials, *Cem. Concr. Res.* (2019). <https://doi.org/10.1016/j.cemconres.2018.10.015>.
- [80] I.M.G. Bertelsen, L.M. Ottosen, G. Fischer, Influence of fibre characteristics on plastic



- shrinkage cracking in cement-based materials: A review, *Constr. Build. Mater.* (2020).  
<https://doi.org/10.1016/j.conbuildmat.2019.116769>.
- [81] Q. Cao, Q. Gao, J. Jia, R. Gao, Early-age cracking resistance of fiber-reinforced expansive self-consolidating concrete, *ACI Mater. J.* 116 (2019) 15–26.  
<https://doi.org/10.14359/51710957>.
- [82] M. Wyrzykowski, P. Trtik, B. Münch, J. Weiss, P. Vontobel, P. Lura, Plastic shrinkage of mortars with shrinkage reducing admixture and lightweight aggregates studied by neutron tomography, *Cem. Concr. Res.* (2015).  
<https://doi.org/10.1016/j.cemconres.2015.03.013>.
- [83] P. Turcry, A. Loukili., Evaluation of Plastic shrinkage Cracking of self compacting concrete., *Am. Concr. Inst.* 103 (2006) 272–280.
- [84] M. Aldalinsi, C. Ferregut, C. Carrasco, V. Tandon, M. Alderette, A method to reduce plastic shrinkage cracking of concrete using the re-vibration technique, *Struct. Congr. 2014 - Proc. 2014 Struct. Congr.* (2014) 1942–1954.  
<https://doi.org/10.1061/9780784413357.171>.
- [85] M. Sirajuddin, R. Gettu, Plastic shrinkage cracking of concrete incorporating mineral admixtures and its mitigation, *Mater. Struct. Constr.* 51 (2018).  
<https://doi.org/10.1617/s11527-018-1173-4>.
- [86] J.H.J. Kim, C.G. Park, S.W. Lee, S.W. Lee, J.P. Won, Effects of the geometry of recycled PET fiber reinforcement on shrinkage cracking of cement-based composites, *Compos. Part B Eng.* 39 (2008) 442–450.  
<https://doi.org/10.1016/j.compositesb.2007.05.001>.
- [87] Z. Al-Kamyani, F.P. Figueiredo, H. Hu, M. Guadagnini, K. Pilakoutas, Shrinkage and flexural behaviour of free and restrained hybrid steel fibre reinforced concrete, *Constr. Build. Mater.* 189 (2018) 1007–1018.  
<https://doi.org/10.1016/j.conbuildmat.2018.09.052>.

**This page is intentionally left blank**

## **Chapter 4 : The Effect of Harsh Environmental Conditions on Concrete Plastic Shrinkage Cracks: Case Study Saudi Arabia**

*Alshammari, T.O., Guadagnini, M. and Pilakoutas, K., 2022. The Effect of Harsh Environmental Conditions on Concrete Plastic Shrinkage Cracks: Case Study Saudi Arabia. Materials, 15(23), p.8622.*

### **Author Contributions:**

Conceptualization, software, data curation, investigation and writing—original draft, **T.O.A.**; methodology, writing—review and editing and supervision **K.P. and M.G.** All authors have read and agreed to the published version of the manuscript.

### **Abstract:**

Due to climate change and population expansion, concrete structures are progressively being subjected to more extreme environments. As the environment affects plastic shrinkage directly, there is a need to understand the effect of environmental changes on plastic shrinkage cracking. This paper examines the plastic shrinkage crack development parametrically at low, mid, and high drying environmental conditions, corresponding to different environments in three Saudi cities. The effects of water-cement ratios and quantities of recycled tire steel fibers (RTSF) in concrete are also investigated. The different environmental conditions for the plastic shrinkage tests were simulated in a specially designed chamber as per ASTM C1579, 2006. A digital image processing (DIP) technique was used to monitor crack initiation and development. Through the use of the crack reduction ratio (CRR), it was found that 30 kg/m<sup>3</sup> of RTSF can control plastic shrinkage cracks at low and mid conditions. For the more extreme (high) conditions, the use of 40 kg/m<sup>3</sup> of RTSF fiber was sufficient to completely eliminate surface plastic shrinkage cracks. This work can help develop more sustainable concrete structures in a wider set of environmental conditions and help mitigate the impact of climate change on concrete infrastructure.

**Appendix C** has provided the relevant experimental data of this chapter.

**Keywords:**

Early age concrete cracking; plastic shrinkage concrete cracks; concrete shrinkage; digital image processing; recycled tire steel fiber; hot weather concreting; Saudi Arabia environmental conditions

## **4.1. Introduction**

Climate change is creating more extreme environments around the world and is impacting concrete durability. Population expansion is also pushing development in more extreme environments. CO<sub>2</sub> emissions and high energy consumption (including for cement production) are some of the reasons for extreme heat waves in Middle East countries such as Saudi Arabia as well as Europe, Asia, and North America [1,2]. Many countries, such as Saudi Arabia, where in some parts, air temperature can exceed 50 °C in the summer, are struggling to produce quality concrete in hot weather conditions. Early-age environmental conditions, including air temperature, wind speed, and relative humidity, can affect concrete in its plastic stage adversely by accelerating early-age plastic shrinkage cracks [3].

Long-term concrete cracking is unavoidable, and large openings impact concrete durability [4,5]. In hot and dry areas of the world, high air temperature, wind, and low relative humidity are also known to impact durability [6], as they can cause high plastic and drying shrinkage strains in concrete [7–9]. ACI 224R-01 [10] attributes early-age concrete cracks to excessive evaporation due to environmental conditions prior to concrete setting. The earlier concrete cracks develop, the shorter the serviceable life of concrete is expected [11,12]. Plastic shrinkage cracks are the earliest to appear, as they occur two-three hours after casting, prior to setting. Subsequent propagation of plastic shrinkage cracks will allow ingress of water and offensive agents such as chlorides and increase the possibility of concrete deterioration and corrosion of steel rebars [13,14]. Plastic shrinkage cracks not only reduce concrete durability but are also aesthetically undesirable [15].

Volume changes in concrete before the hardening of cement-based materials are the main cause of plastic shrinkage strain and cracking [16,17]. Volume loss at the plastic stage is caused by the consolidation of aggregates, bleeding, and evaporation of water. In its plastic state, when undisturbed, the denser solid particles settle and tend to sink down, whilst the lighter-weight materials, such as air and free water, begin to rise to the surface. Air escapes faster, but the escaping water, called bleeding water, escapes slower, and when it reaches the surface, it starts evaporating [18]. When the evaporation rate exceeds the bleeding rate, the concrete surface dries, and at this stage, the possibility of plastic shrinkage cracking increases [19–21]. Both environmental conditions and concrete mix composition affect plastic shrinkage, as seen in Figure 4.1 [22].

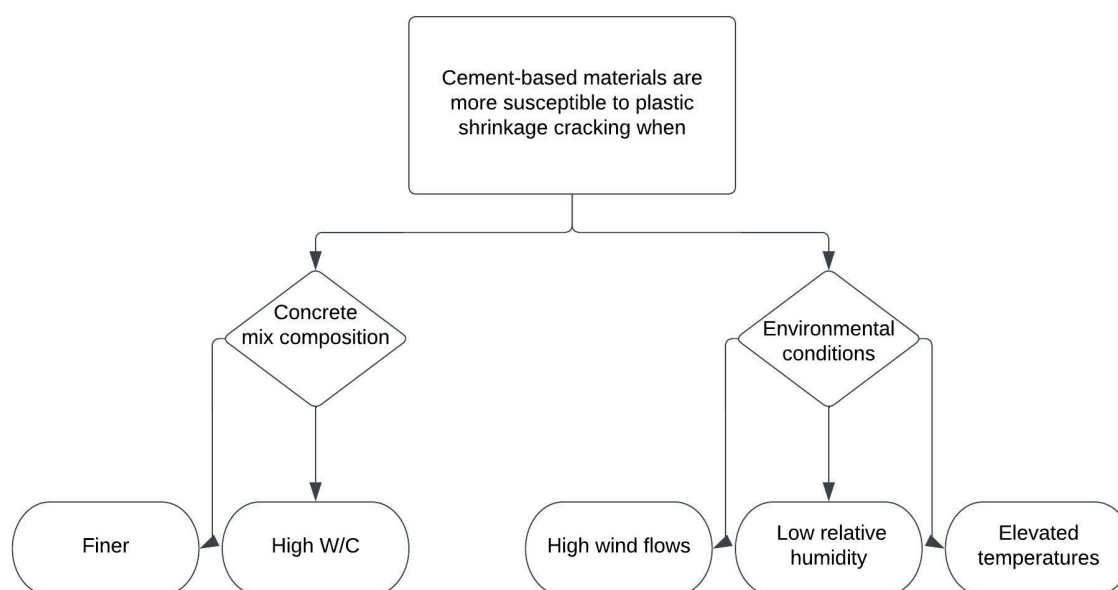


Figure 4.1: Factors affecting plastic shrinkage cracking.

Hot weather casting is known to increase plastic shrinkage cracking [23]. It is widely accepted that plastic shrinkage starts when the evaporation rate exceeds the bleeding rate. Several studies reported that environmental conditions such as high air temperature, high wind speed, and low relative humidity have a direct effect on fresh and hardened concrete, as they also accelerate the final set time [24,25].

Ambient conditions influence the water evaporation rate. As air temperature increases, relative humidity sees a corresponding decrease, and thus evaporation rate increases. Higher wind speeds also increase the evaporation rate. When the evaporation rate is less than the bleeding rate, a thin layer of water covers the surface of the concrete, which helps increase the evaporation rate due to the increased exposed area [26].

Eventual drying of the surface leads to a rise in capillary pressure converting it from a mildly compressive to a tensile pressure [27]. When capillary pressure inside the concrete builds up, plastic shrinkage cracking will occur.

According to ASTM C1579 [28], plastic shrinkage cracks occur when the water evaporation rate is equal, or more than,  $1.0 \text{ kg/m}^2/\text{h}$ . However, Sayahi and Hedlund [26] found that most existing researchers conclude that this value is too high and plastic shrinkage cracks might appear when the evaporation rate is less than  $1.0 \text{ kg/m}^2/\text{h}$ , especially in hot weather conditions. For example, Almusallam et al. [29] concluded from observations in two studies

that the beginning of plastic shrinkage cracking could occur at an evaporation rate between 0.2–0.7 kg/m<sup>2</sup>/h.

To examine the possibility of plastic shrinkage cracking in concrete, ASTM C1579 [28] recommends a set of environmental conditions to be applied: air temperature  $36 \pm 3$  °C, wind speed more than 4.7 m/s, and relative humidity around  $30 \pm 10\%$ . These environmental conditions were selected based on past experimental work [28]. However, Al-Gahtani et al. [30], working in the eastern part of Saudi Arabia, known for high temperature and humidity, found that concrete is more likely to crack with and without the environmental conditions proposed by [28,31].

Nabil et al. [32] examined substrate bases of concrete (50 × 95 × 365 mm) for plastic shrinkage cracking in an environmental chamber by covering concrete with plastic sheets. The concrete mixes were exposed to a temperature of 55 °C during the first 8 h after casting and 50 °C until the end of the test (24 h). The relative humidity (RH) was about 10%, and the wind speed was 10 km/h during the duration of the test. As expected, it was found that covering concrete with plastic sheets was more efficient in minimizing plastic shrinkage cracking and reducing loss of water compared with non-covering. Almutairi et al. [33] did a survey to determine the causes of all early-age cracking in concrete structures in Kuwait city and concluded that the environmental conditions were the main reason for most the concrete cracking, but also high concrete temperature. It was recommended to prevent early-age cracking, the concrete temperature should be controlled by adding ice to the mixing water [33].

Almusallam et al. [29] and Safiuddin et al. [34] found that plastic shrinkage cracks increase with an increase in the water/cement ratio and content of fine aggregate. Sayahi and Hedlund et al. [26] reported that micro-settlement cracks also occur on the surface of the concrete. Sulakshna et al. [35] examined a Poly Carboxylate Ether (PCE) as superplasticizer to self-compacting concrete of w/c ratio of about 0.45, with encouraging results.

Zhang and Xiao [36] investigated the effect of recycled sand as fine aggregate for 3D-printed mortar on plastic shrinkage cracks. The replacement ratios tested were at 25%, 50%, 75%, and 100% of natural sand, and the w/c ratio was (0.6) due to the high-water absorption of the recycled sand. The results showed that increased replacement ratios of recycled sand mortar resulted in increased plastic shrinkage cracking. Cohen et al. [37] found that the increase in fine content in concrete (such as fly ash, silica fume, slag, etc.) is not favorable in relation

to plastic shrinkage cracking. Lofgren and Esping et al. [38] came to the same conclusion when using silica fume. Zhao et al. [39] examined the influence of clay minerals in manufactured sand and found that as clay lowers the permeability, it also reduces the plastic tensile strength, which leads to an increase in plastic shrinkage cracking.

In conclusion, plastic shrinkage cracking is likely to worsen with climate change, and further work is needed to understand both how the environment and mitigation measures affect its development.

#### **4.1.1. Problem Statement**

The increase in harsh environmental conditions created by climate change can significantly affect concrete durability, in particular, due to their impact on plastic shrinkage. Hence, there is a need to investigate such conditions and their impact on concrete with various compositions, as well as possible mitigation measures.

#### **4.1.2. Selection of Environmental Conditions**

Saudi Arabia has been selected as a case study region in this investigation as it typifies extremely hot environments, with a drier climate in the northern and central areas and a wetter climate in the southern, western, and eastern areas. Despite the significant variation in humidity, most of the countries in the Middle East share the same high air temperatures [33].

Hasanain et al. [40] tested the effects of hot weather on the evaporation rate of concrete slabs in external daytime environmental conditions in Jeddah, the biggest western city in Saudi Arabia, known for its hot-wet weather due to its location next to the Red Sea. The results showed that casting at noon or afternoon had a higher evaporation rate compared to casting early in the morning. The minimum evaporation rate was recorded when casting in the morning and occurred 3–5 h after casting when the concrete had partly been set.

##### **4.1.2.1. Selected Environments**

Three cities in Saudi Arabia were chosen to evaluate the effect of concreting under severe hot and dry weather conditions as shown in Figure 4.2. Figure 4.3 shows the “Climate Graphs” for Saudi Arabia and the three case study cities, including average, minimum and maximum air temperature; relative humidity; and wind speed [41]. While the overall conditions for Saudi Arabia reflect well the ASTM C1579 [28] conditions, the specific environments of each city depart from these climatic settings.



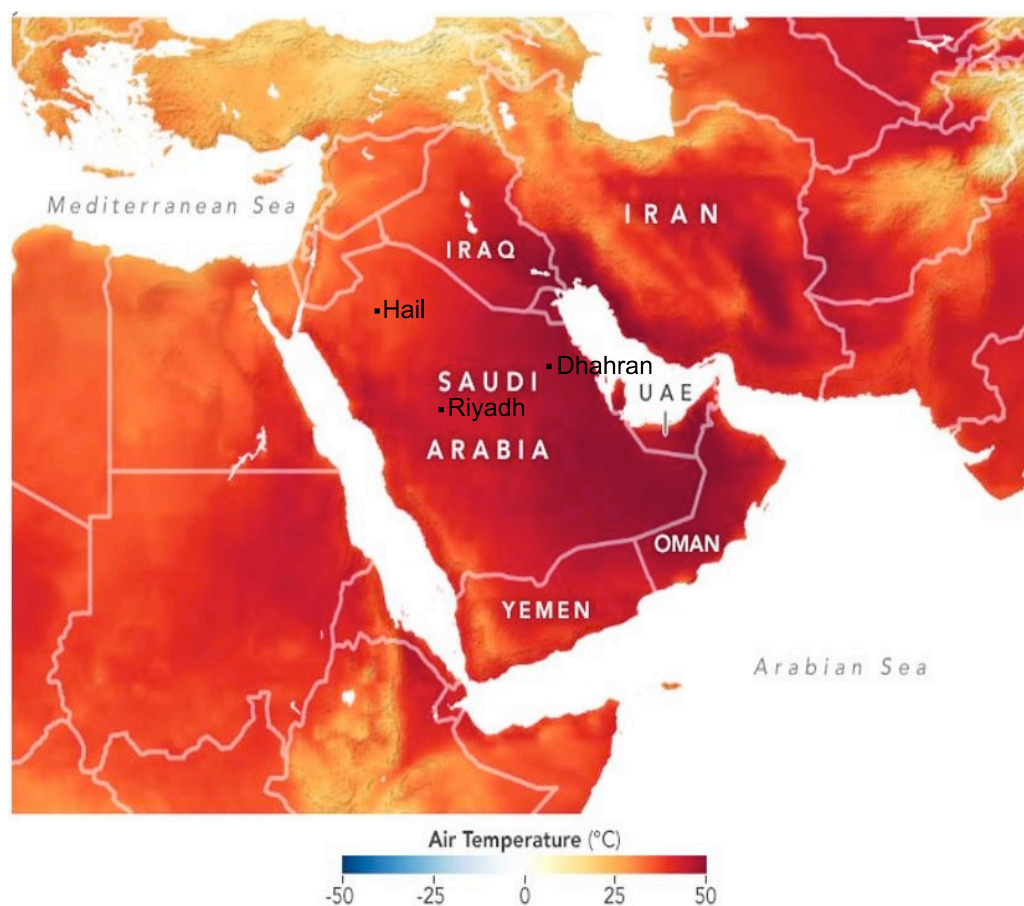


Figure 4.2: Map of the three selected cities of Saudi Arabia

(a) Riyadh

The capital of Saudi Arabia, Riyadh city, is located in the middle of Saudi Arabia. Temperatures are high in the summer, and the relative humidity is very low in both winter and summer (see Figure 4.3b). During the months of June to September, the air temperature, relative humidity, and wind speed are at the levels that increase the possibility of plastic shrinkage cracks, as anticipated by ASTM C1579 [28], and concreting at temperatures around 45 °C is not uncommon. This (high) temperature level will be examined in this study, as well as the effect of a lower average wind speed of 3 m/s.

Arafah et al. [42] investigated the effects of hot weather on the strength of concrete cast in Riyadh during summer, with target temperatures of 45–48 °C. The high temperature caused high bleeding. Concrete cubes, covered with burlap and cured by water sprinkling two times a day, resulted in concrete strength lower than the ACI 305 [43] general requirement. Khan and Abbas et al. [44] reported the influence of hot weather conditions in Riyadh city on concrete made with cement and cement replacements silica fume (SF) and fly ash (FA). It was observed

that the initial concrete strength tends to increase with moist curing, but that had insignificant effects on long-term strength. In addition, shrinkage cracks were observed on the surface even though moist curing was applied.

(b) Dhahran

Dhahran city, on the eastern side of Saudi Arabia, is one of the hottest cities in Saudi Arabia and the Middle East region, and its climate is characterized by high humidity levels in both winter and summer (see Figure 4.3c) as it is located by the Gulf Sea. Although high humidity is not expected to affect plastic shrinkage adversely, the high wind speed of 7 m/s typical of this region is, and this wind speed is considered as “high” in this study.

Al-Gahtani [45] conducted a study in Dhahran examining the impact of curing methods on concrete specimens made with cement and cement replacements (SF and FA). The specimens were cured by covering them with wet burlaps or applying curing compounds. The results showed that specimens cured under wet burlap showed better strength development than those treated with curing compounds. The impact of hot temperature on plastic and drying shrinkage, however, was very significant for both curing methods. Nasir and Syed [46] also studied the influence of the water-cement ratio (in the range of 0.3 to 0.45) at different air temperatures (25 to 45 °C) and different curing methods such as concrete covering ponding, and use of curing compounds. All curing methods showed a positive impact on the concrete strength parameters at all w/c ratios and temperatures used in the study. A high evaporation rate was observed for the plain concrete (without special curing), and this was attributed to the high heat evolution, which in turn had a negative impact on the overall shrinkage behavior.

(c) Hail

Known as one of the coolest cities in winter in the country, Hail is one of the northern cities in Saudi Arabia. Few studies have examined concreting in this region, but while the relative humidity in this part of the country is relatively low during the months of June to September, the combination of environmental conditions experienced in this area is likely to affect plastic shrinkage [28,31,43] recommendations. The lower temperature of 28 °C will be included in the study (Figure 4.3d).

Due to the different levels of relative humidity in the selected case study regions, the relative humidity was kept around 20%, which is close to the minimum over the summer for Saudi Arabia (see Figure 4.3a).

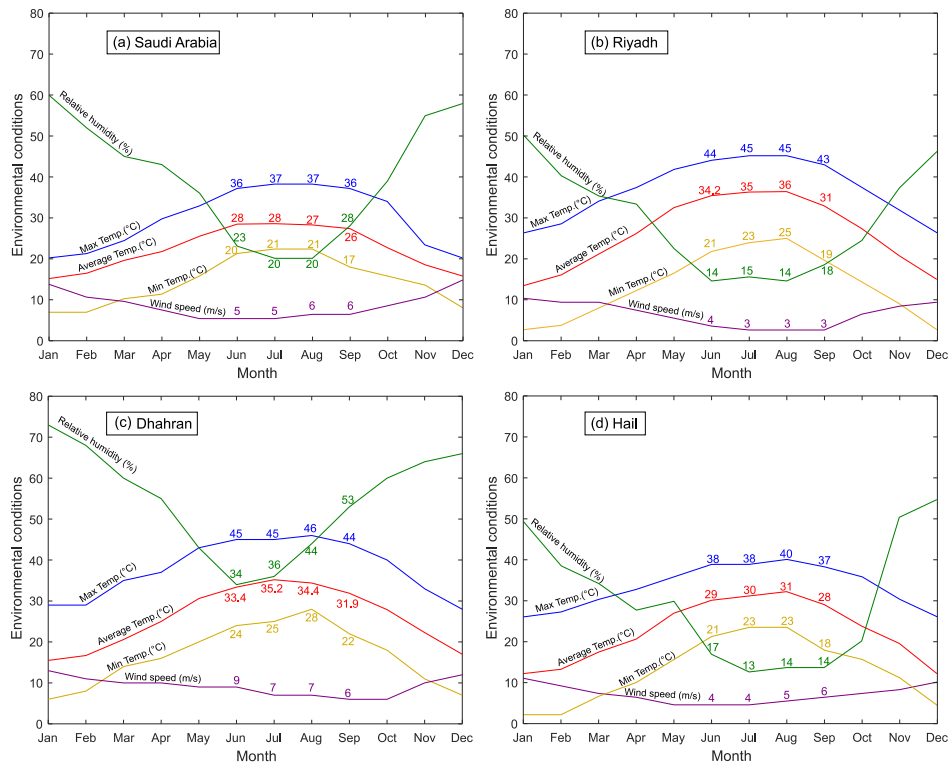


Figure 4.3: Selected environments climate graphs [41].

### 4.1.3. Significance of Research

This paper examines the impact of various environmental conditions (high, mid, and low wind speed, air temperature, and relative humidity) on the plastic shrinkage performance of concrete made with different w/c ratios. The addition of different dosages of recycled tire steel fiber (RTSF) is also examined as a plastic shrinkage mitigation measure. The results will help improve concrete performance in hot regions such as the Middle East and in more extreme environments created by climate change and will reduce the use of natural and virgin materials by reusing tire steel fiber to control early-age cracking in concrete structures.

## 4.2. Materials

### 4.2.1. Concrete and Specimen Preparations

As the likelihood of plastic shrinkage cracking increases with high cement content, a relatively cement content was selected [47]. The cement (CEMII 42.5) content was  $335 \text{ kg/m}^3$  with a w/c of 0.55 for the control environmental mix (CM) superplasticizer (Sika ViscoCrete 30HE) was used at a dosage of  $1.5 \text{ lt/m}^3$ . Two sizes of gravel (river round gravel) were used,  $491 \text{ kg/m}^3$  of 5–10 mm, and  $532 \text{ kg/m}^3$  of 10–14 mm. The fine aggregate (river-round sand) was  $847 \text{ kg/m}^3$ . RTSF was used at different proportions ( $0$ ,  $30 \text{ kg/m}^3$ , and  $40 \text{ kg/m}^3$ ).

The water-cement ratios that were used in this study include 0.5, 0.55, and 0.6 as Low, Mid, and High ratios, respectively. The superplasticizer (Sika ViscoCrete 30HE) dosages were adjusted in accordance of the water cement ratio used.

Concrete mixing and specimen casting were carried out according to [28,48]. The mixes used with the various parameters are shown in Table 4.1. A slump test was made to control the workability of all mixes (RTSFC and PC) to reach the target of the slump test results, which is more than  $100 \pm 10$  mm.

Table 4.1: Parameters of the study.

Parameters	Temp. (C°)	Wind Speed (m/s)	RH (%)	W/C
Low	28	3.0	$30 \pm 10$	0.50
Mid (CM)	36	4.7	$30 \pm 10$	0.55
High	45	7.0	$30 \pm 10$	0.60

#### 4.2.2. Recycled Tire Steel Fibre (RTSF)

Waste disposal is becoming a critical environmental pollution issue worldwide. According to Mohajerani et al. [49], billions of tires are replaced every year around the world, while half of them are disposed of by burning or landfilling. Nowadays, there is an increasing interest in the use of secondary raw materials in the construction field of civil engineering [50,51]. Recycled tire steel fibers (RTSF), produced from waste tires, have been used as a substitute for manufactured steel fibers (MSF) and were shown to improve the performance of concrete and enhance its cracking resistance due to shrinkage and structural loads [52–55].

Hu et al. [56] showed that RTSF could improve the splitting and flexural strength of concrete and result in comparable (or better) performance to MSF. Baricevic et al. [57] examined the effect of using blends of recycled tire steel and manufactured steel fibers, and the results showed a positive impact in delaying the development of drying shrinkage cracks. Graeff et al. [14] examined the performance of RTSF concrete under cyclic loading and showed that the addition of RTSF can improve the fatigue behavior of concrete and help restrain micro-cracks.

The advantages of using RTSF instead of MSF in concrete are not just in terms of overall performance but also in terms of economic and environmental benefits, as RTSF has lower greenhouse gas emissions and cost compared to MSF [58–60]. Moreover, Mastali et al. [61] estimated that the use of 1.5% (by volume) of RTSF can make up about 35% of the total

cost, while this increase to more than 50% when using MSF. According to the same study, the use of RTSF also contributed to lower carbon emissions from 40% (for 1.5% of MSF) to 15% (for 1.5% of RTSF).

The authors showed in previous work by Alshammari et al. [62] that RTSF of  $30 \text{ kg/m}^3$  by volume can stop plastic shrinkage cracks. That same amount is used in high, mid, and low environmental conditions and increased to  $40 \text{ kg/m}^3$  if cracks develop. RTSF (see Figure 4.4) has different lengths and diameters with an average tensile strength of 2380 MPa (SD = 166 MPa), as shown in Figure 4.5a as tested in the lab for more than 100 samples of RTSF. The tensile strength test was carried out according to ISO 6892-1 [63]. The length distribution of RTSF, which was determined by an automated optical method [64], is shown in Figure 4.5b.



Figure 4.4: RTSF.

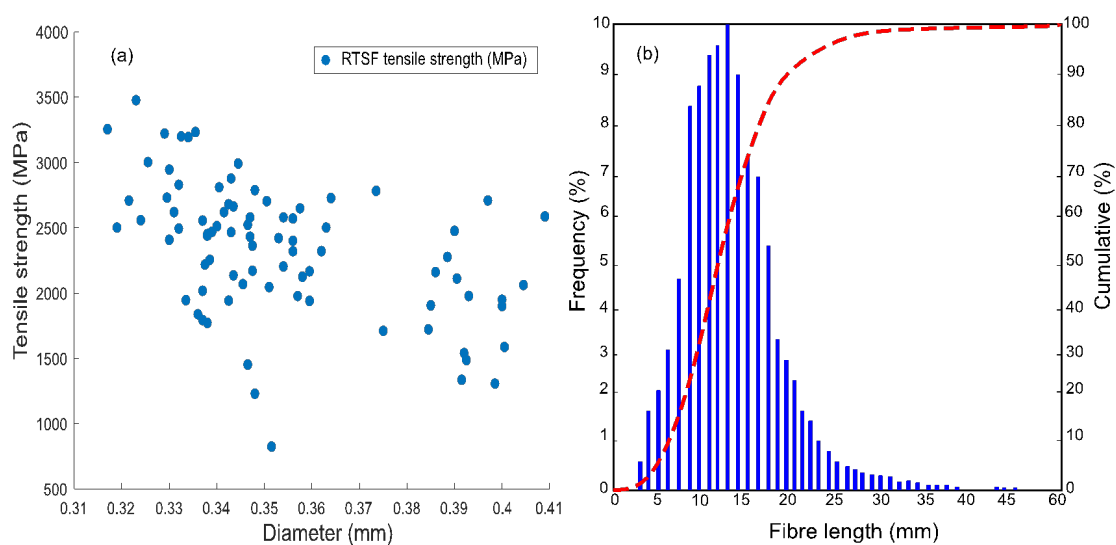


Figure 4.5: (a) Tensile strength; and (b) RTSF length distributions.

### 4.3. Methodology

#### 4.3.1. Compressive Strength

The 28-day compressive strength of all mixes were determined from 100 mm cubes tested using a servo-hydraulic universal testing machine according to [65]. For each mix, four cubes were casted which two of the cubes were initially stored in the environmental chamber under the different environmental conditions applied during the plastic shrinkage test. The other half was stored in normal lab conditions  $20 \pm 2$  °C.

#### 4.3.2. Evaporation Rate

Two aluminum pans filled with water were placed inside the chamber. Each water pan rested on a scale to quantify the evaporation rate at time intervals of 30 min, as recommended by [28]. The evaporation rate at each time interval was determined by (Equation (1)), and if the average evaporation rate was less than 1.0 kg/m<sup>2</sup>/h, the test was rejected [28].

$$E = \frac{M2-M1}{\text{water surface area of the pan} \times (T2-T1)} \quad (1)$$

Where, E: Evaporation rate, kg/m<sup>2</sup>/h, M2-M1: the mass loss between successive weighings, g. and T2-T1: the time interval between successive weighings, h.

#### 4.3.3. Plastic Shrinkage Test

The test was carried out on fresh/plastic concrete in accordance with ASTM C1579 [28] and ACI Committee 305 [31] and typically lasted 6 h. Two concrete slabs were tested in parallel in the chamber (see Figure 4.6).

At the end of the test (after 6 h), the doors of the chamber were left open, and the slabs were covered with a plastic sheet and left undisturbed for an additional 18 h. The cracks were then measured 24 h again after casting.

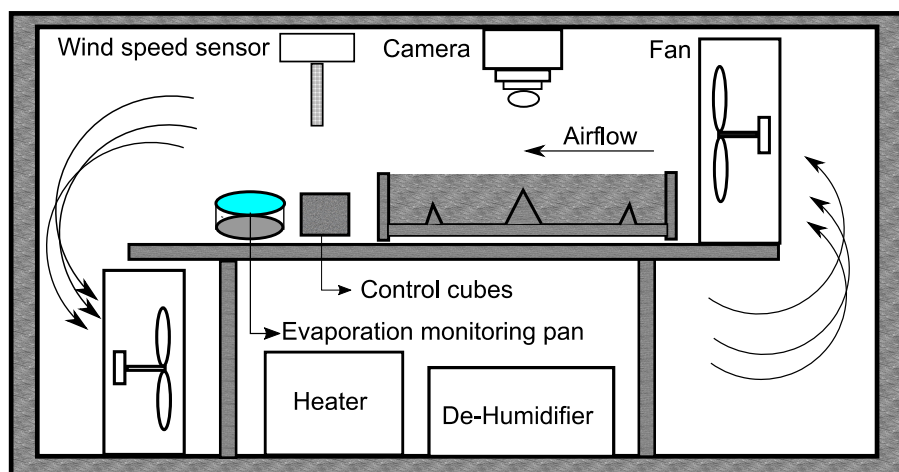


Figure 4.6: Schematic section of the chamber.

#### 4.3.4. Measurement of the Cracks

The method used to measure the cracks followed the recommendations of ASTM C1579 [28], coupled with digital image processing (DIP). Digital photographs of the surface of the specimens were taken at regular intervals during the test and at 24 h from casting and subsequently processed in MATLAB to determine the length, width, and area of the plastic shrinkage cracks [5]. Moreover, at 24 h after the concrete was cracked, a conventional manual optical method was used to measure the average crack width at more than 25 points of the crack by using a millimeter steel ruler and compared to the DIP. The crack reduction ratio (CRR) was determined by using Equation (2), as recommended in [28].

$$\text{CRR} = \left[ 1 - \frac{\text{Average Crack Width of Fibre Reinforced Concrete Mixture}}{\text{Average Crack Width of Fibre Control Concrete Mixture}} \right] \times 100\% \quad (2)$$

#### 4.3.5. Examined Environmental Conditions

Figure 4.7 shows all the environmental conditions examined in this study in terms of temperature and wind speed values. The mid values correspond to those also recommended in ASTM C1579 [28] and include a wind speed of 4.7 m/s, a temperature of  $36 \pm 3$  °C, and relative humidity of  $30 \pm 10\%$ . The low temperature of 28 °C was selected as it corresponds to the minimum temperature during the day in the three case study areas (Riyadh, Dhahran, and Hail), while the high temperature of 45 °C corresponds to the higher temperature experienced in the region during the hot months.

The low wind speed of 3 m/s and the high wind speed of 7 m/s corresponds to the average wind speeds experienced in the summer in Riyadh and Dhahran, respectively.

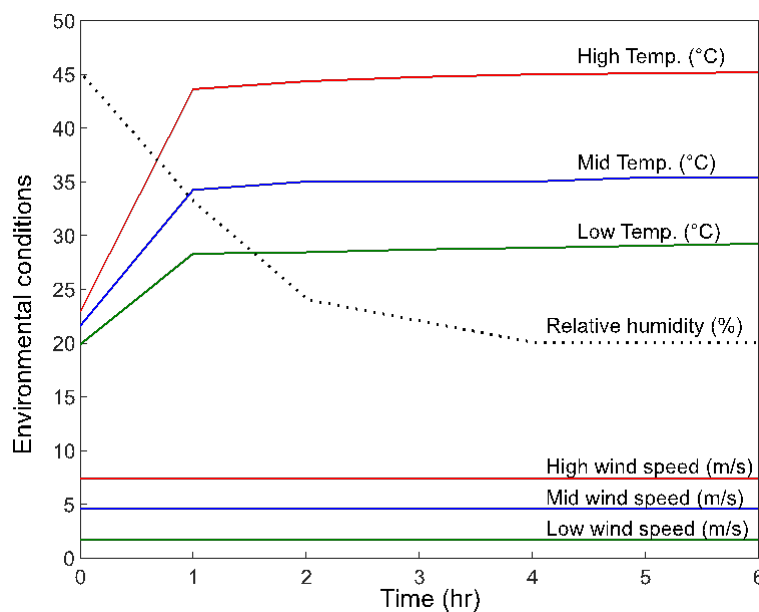


Figure 4.7: Examined sets of environmental conditions.

## 4.4. Experimental Results and Discussion

### 4.4.1. Compressive Strength

The 28-day compressive strength of the control specimens (PC) and SFRC reinforced specimens was determined on cubes that were kept both inside (In) and outside (Out) the chamber during the plastic shrinkage tests, and the corresponding values are summarized in Figure 4.8.

The results do not show any significant influence of temperature and wind speed on the compressive strength of the cubes that were kept inside the chamber (see Figure 4.8a). As expected, a slight increase in compressive strength can be seen with increased fiber content [66–68].

Naturally, concrete strength increases with the reduction in the water-cement ratio (see Figure 4.8b) in line with other works [69–71]. This can be attributed to the closer spacing between the cement particles, which results in a denser and stronger cement paste [72].



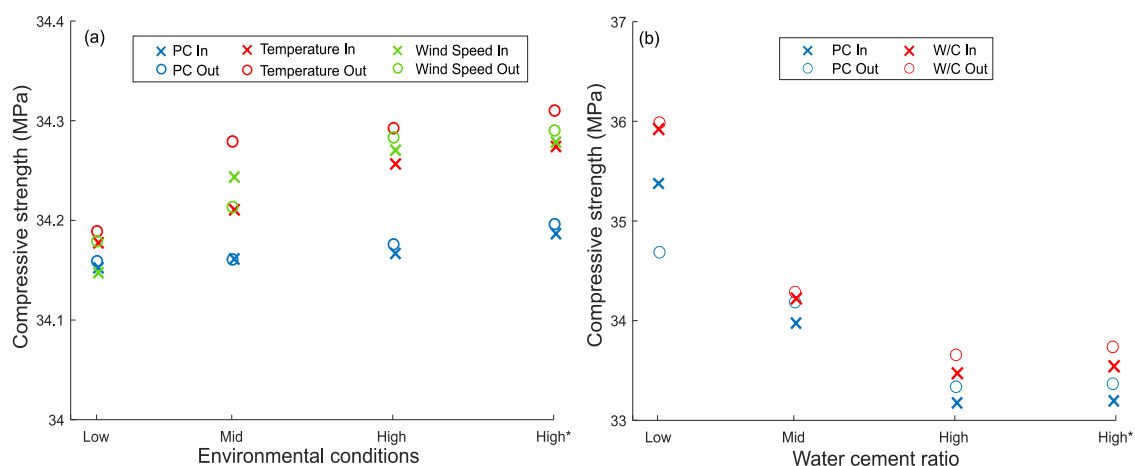


Figure 4.8: Compressive strength of PC and FRC at 28 days of curing for cubes inside and outside the chamber. \* higher content of RTSF ( $40 \text{ kg/m}^3$ ).

#### 4.4.2. Evaporation Rate

Figure 4.9, Figure 4.10, and Figure 4.11 show the evaporation rates determined for the different environmental conditions. As recommended in ASTM C1579 [28], the evaporation rate should be more than  $1 \text{ kg/m}^2/\text{h}$ , or the test should be rejected. It can be seen that all the environmental conditions exceeded that rate and achieved the minimum value even in the low environmental conditions. As expected, in general, the evaporation rates increase with time, as bleeding gathers momentum and concrete temperature increases with the heat of hydration and then slows down towards the end of the test as bleeding slows down with setting.

The evaporation rate increases with wind speed and temperature and nearly doubles from Low to High conditions. This can be attributed to the higher bleeding induced by temperature and wind, as also reported by others [25,27,73–78].

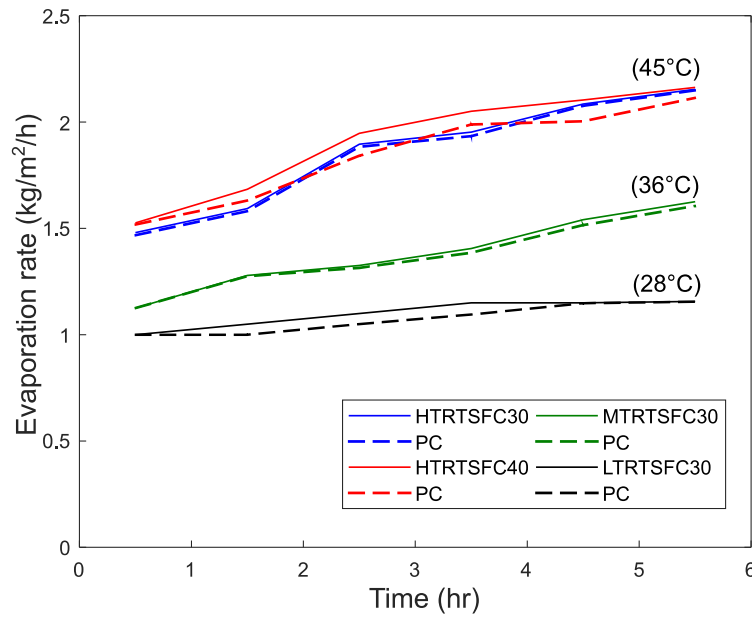


Figure 4.9: Effect of temperature on evaporation rates (wind speed = 4.7 m/s).

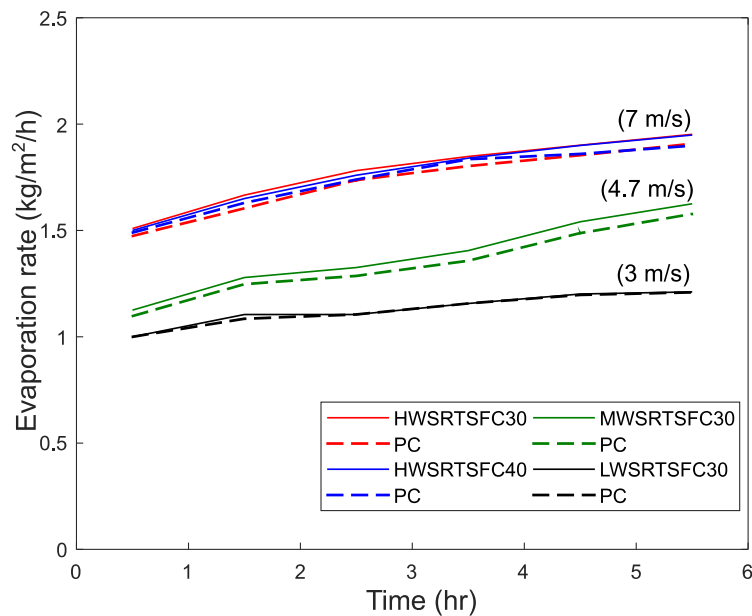


Figure 4.10: Effect of wind speed on evaporation rates ( $T = 36\text{ }^{\circ}\text{C}$ ).

The evaporation rates for low, mid, and high water-cement ratio mixtures are shown in Figure 4.11. It can be seen that higher water-cement ratio somewhat increases the evaporation rate, as more water is available to bleed. Holt and Leivo [79] and Kayondo et al. [26] had a similar finding which led to plastic shrinkage cracks appearing faster on the surface of the concrete.

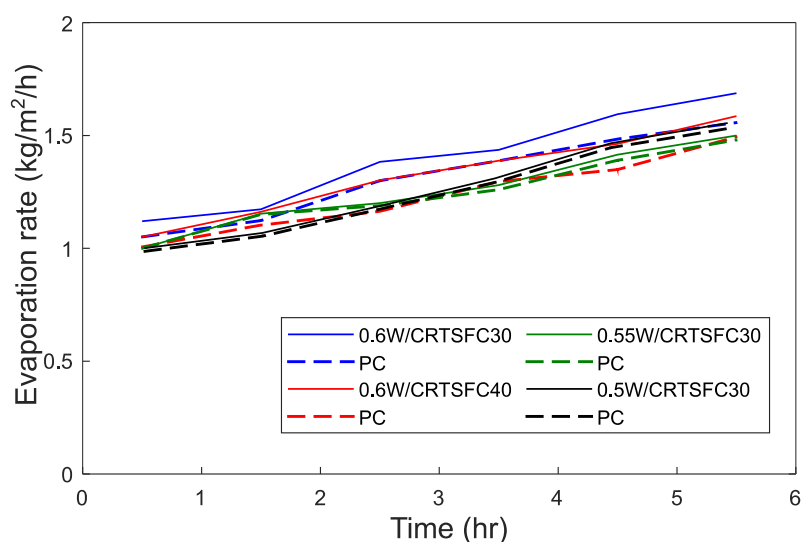


Figure 4.11: Effect of water cement ratio on evaporation rates ( $T = 36\text{ }^{\circ}\text{C}$ , Wind speed =  $4.7\text{ m/s}$ ).

#### 4.4.3. Crack Measurements and Results

For crack measurement, a DIP system was used in which two cameras were placed above the slabs, with each camera taking images every 10 min during the test. The images were subsequently analyzed using MATLAB to measure an average crack (width). A typical photo of the crack for the plain mix is shown below (Figure 4.12):



Figure 4.12: Typical crack pattern in plain concrete (PC) specimens of high temperature examined at 24 h.

Figure 4.13, Figure 4.14, and Figure 4.15 show the evolution of the cracks for the three variable parameters: temperature, wind speed, and w/c ratio, respectively. The graphs also show the crack widths at 24 h measured both with DIP and a conventional manual optical

device. The crack widths obtained for the two methods of measurement are almost identical, confirming that DIP works well. The mean difference between the two measurements was 0.113 mm.

Figure 4.13 shows that with a temperature increase, cracking starts earlier, and the eventual crack width is wider by almost 100% when comparing Low and High temperatures. The use of 30 kg/m<sup>3</sup> of RTSF seems to prevent cracking completely for the Low and Medium temperatures. However, though the addition of RTSF delays and helps control the crack, cracking still develops at High temperatures. For the more extreme temperature tested in this study, the increase in fiber dosage to 40 kg/m<sup>3</sup> seems to prevent plastic cracking.

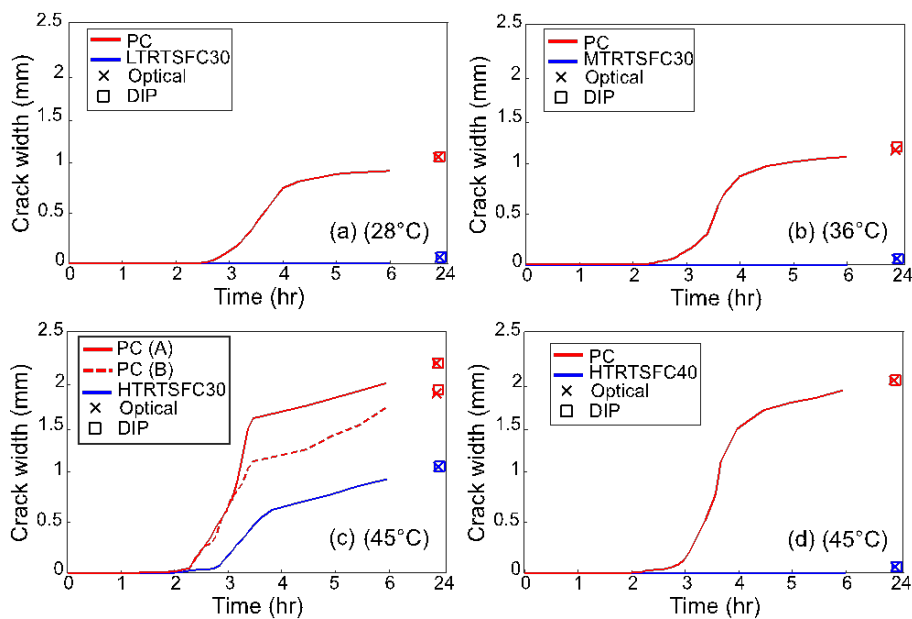


Figure 4.13: Crack evolution for the specimens subjected to the examined temperatures.

Similarly, to what was observed for increasing temperature values, increasing wind speed causes earlier cracking to develop and eventually leads to larger crack widths. Interestingly, both the Low wind speed and Low-temperature environments, which are below the ASTM C1579 [28] recommendations, led to cracks (see Figure 4.14).

Again, the use of RTSF at a dosage of 30 kg/m<sup>3</sup> prevented cracking in the specimens subjected to the Low and Medium wind speeds only, whilst 40 kg/m<sup>3</sup> of RTSF was effective in preventing cracking at High wind speeds.

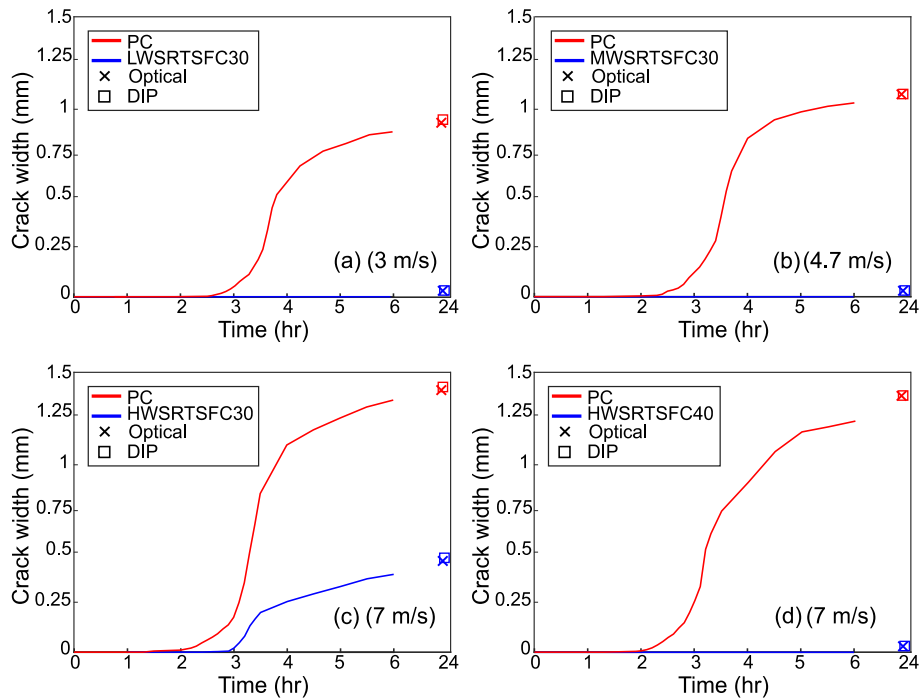


Figure 4.14: Crack evolution for the specimens subjected to the examined wind speeds.

Figure 4.15 shows the crack width evolution for different w/c ratios. As expected, the use of lower w/c ratios delayed the crack initiation and development. As with the previous results, the addition of 30 kg/m<sup>3</sup> of RTSF was not sufficient to prevent cracking in the specimens with a high water-cement ratio, but 40 kg/m<sup>3</sup> of RTSF prevented the formation of cracks completely.

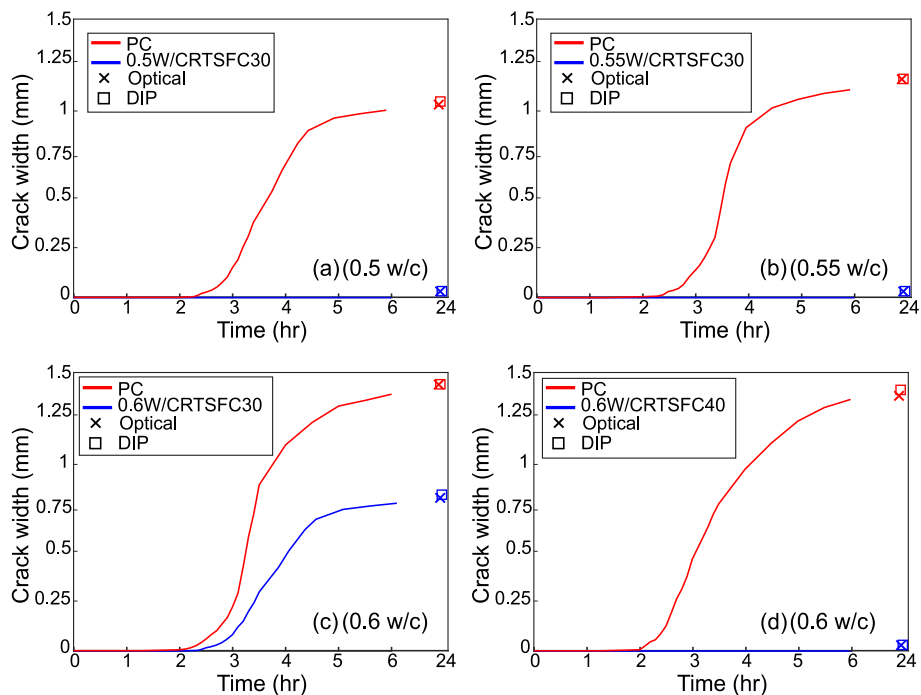


Figure 4.15: Crack evolution for the specimens manufactured using different w/c ratios.

#### 4.4.4. Influence of Environmental Conditions on Evaporation Rate and Cracking

The effect of the three parameters examined in this study on the evaporation rate at crack initiation and time of crack initiation is shown in Figure 4.16.

As expected, for all mixes, cracking starts earlier, and the evaporation rate is higher with increasing temperature, wind, and  $w/c$  ratio, and the final cracks are wider. The plain mid-temperature concrete cracked just before the second hour, as expected by [28].

Cracks develop even at the low temperature of 28 °C but crack initiation is delayed by about an hour when compared to specimens exposed to the highest examined temperature. Though surface temperature cannot be changed easily, to reduce plastic shrinkage cracking, the concrete temperature can be cooled down by using cooler materials, including iced water.

In the case of high air temperature (see Figure 4.12), it was noticed that the plain concrete developed two cracks on the surface, which could adversely impact the durability of the concrete.

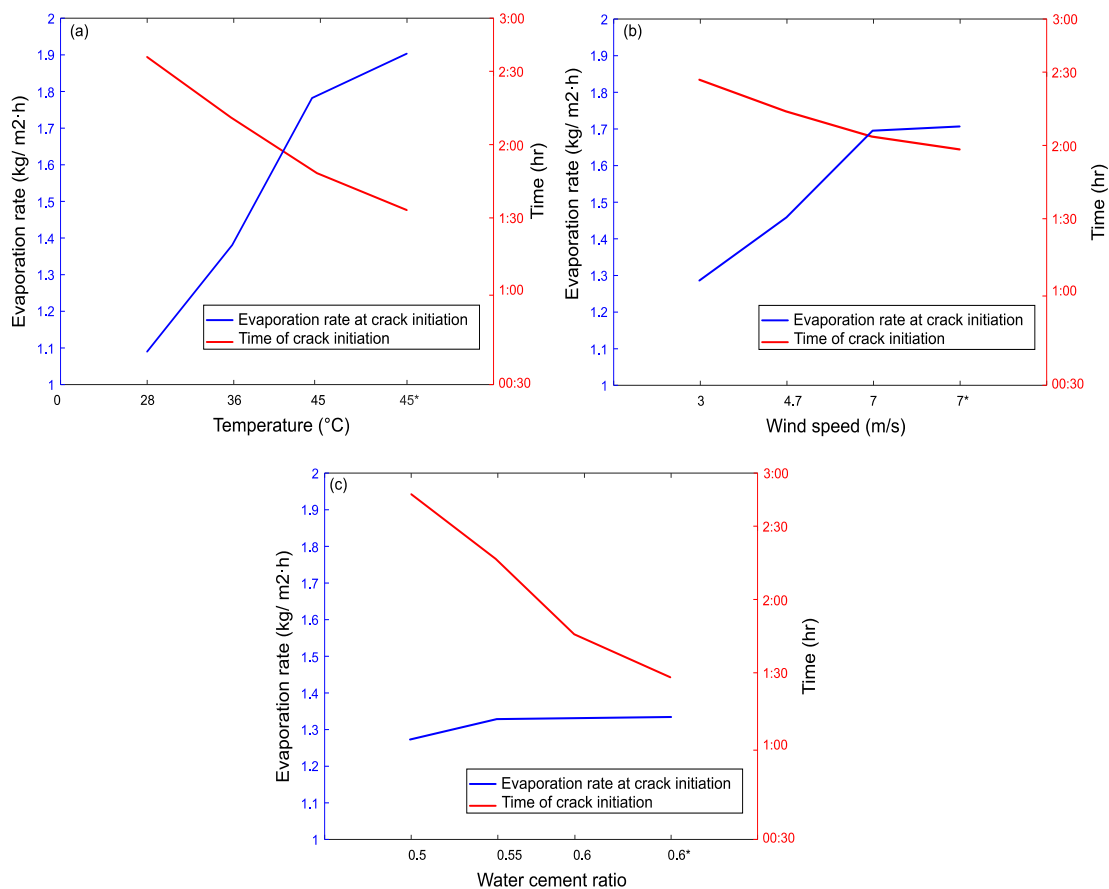


Figure 4.16: Effect of (a) temperature; (b) wind speed; and (c)  $w/c$  ratio on evaporation rate at crack initiation and time of crack initiation. \* higher content of RTSF (40 kg/m<sup>3</sup>).

At low wind speeds (3 m/s), the evaporation rate reduces but the plain concrete cracks only a bit later and a bit less wide. Hence, at the ranges used, wind speed seems to play a less important role than temperature.

The w/c ratio seems to influence the evaporation rate the least, compared to temperature and wind. However, the w/c ratio has a big influence on the time of crack initiation. This was attributed by Topçu, and Elgün [80] to a high bleed and evaporation rate, though the results contradict the higher evaporation rate. Hence, this study concludes that high w/c ratios only accelerate the initiation of high cracking due to the earlier and higher bleed rate.

#### 4.4.5. Crack Reduction Ratio (CRR)

Crack reduction ratios were determined in this study according to Equation (1). Figure 4.17 shows these ratios for the different temperatures examined in this study for concrete mixes with 30 kg/m<sup>3</sup> and 40 kg/m<sup>3</sup> of RTSF. It can be seen that the addition of 30 kg/m<sup>3</sup> of RTSF can eliminate the occurrence of plastic shrinkage cracks at low (28 °C) and mid (36 °C) temperatures.

In comparison, Borg et al. [81] examined the use of recycled PET fibers (polyethylene terephthalate) to control plastic shrinkage cracks and found that 1.5% of fiber (by volume) could reduce cracking by up to 57%. Pešić et al. [82] examined the effect of adding recycled high-density polyethylene (HDPE) plastic fibers and found that early-age concrete cracks can be reduced by up to 50% with a fiber volume of 1.25%. Hence, steel fibers appear to be a more robust solution for stopping plastic shrinkage cracks.

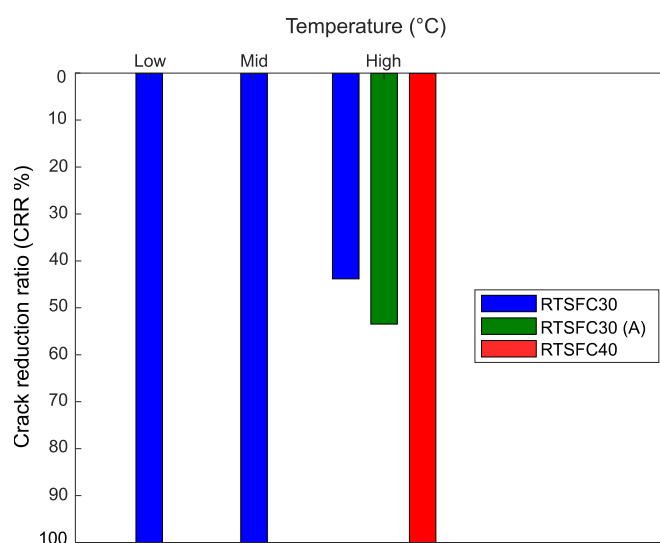


Figure 4.17: Crack reduction ratio for all temperatures.

At the highest examined temperature of 45 °C (High), the plain concrete developed two surface cracks, and the corresponding CRR ratios are represented in Figure 4.17 by a blue and green (A) bar, showing that the addition of 30 kg/m<sup>3</sup> of RTSF effectively reduced these cracks by up to 45%, and 55%, respectively. The addition of RTSF at a rate of 40 kg/m<sup>3</sup> eliminated the cracks completely, and this dosage is recommended for these high temperatures.

Al-Tulaian et al. [83] used recycled plastic fibers (RP) with two lengths (50 and 20 mm) to restrain plastic shrinkage in mortar concrete at high temperatures (45 °C) and found that RP reduced the plastic shrinkage cracks by up to 70% for a volume fraction of 1.5% and fiber length of 50 mm. Hence, steel fibers appear to be the only solution to stop cracks completely at these high temperatures.

The CRR for the examined values of wind speed is shown in Figure 4.18. Again, 30 kg/m<sup>3</sup> of RTSF eliminated cracks at low and mid-wind speeds, while 40 kg/m<sup>3</sup> of RTSF was necessary to eliminate plastic shrinkage cracking at high wind speeds.

Sirajuddin and Gettu [84] examined the plastic shrinkage behavior of specimens exposed to a wind speed of  $4.5 \pm 1$  m/s and made of concrete comprising cement and fly ash and granulated blast furnace slag and reinforced with different volume fractions of four types of fiber (polypropylene, polyester fibers, polyacrylonitrile and glass fibers). The results showed that increasing the volume fraction of the different types of fibers led to a reduction in cracking by up to 60%.

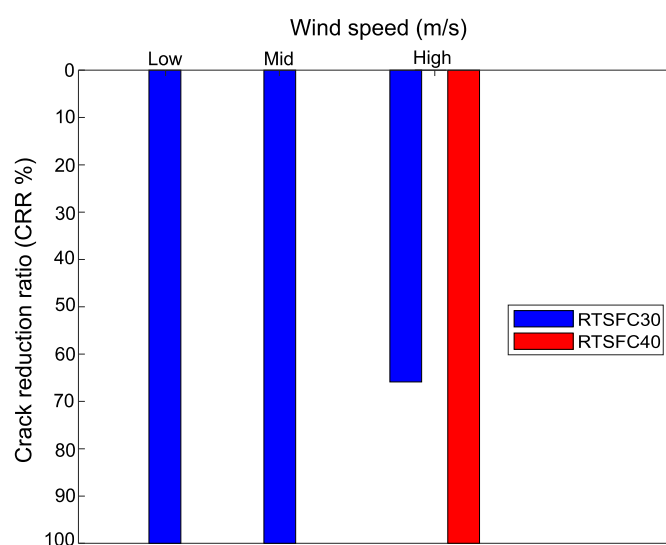


Figure 4.18: Crack reduction ratio for all wind speeds.



The CRR for various w/c ratios is shown in Figure 4.19. In this case, again, the 30 kg/m<sup>3</sup> of RTSF eliminated cracks at low and mid w/c ratios, while 40 kg/m<sup>3</sup> of RTSF eliminated the cracks at the high w/c ratio.

Mazzoli et al. [85] examined the impact of adding different types of fibres (polypropylene, polyvinyl alcohol, polyethylene, steel) to restrain plastic shrinkage cracks of concrete with a w/c ratio of 0.5 and observed that the fibres were effective in reducing the crack width, but the cracks were still visible at the surface of the concrete.

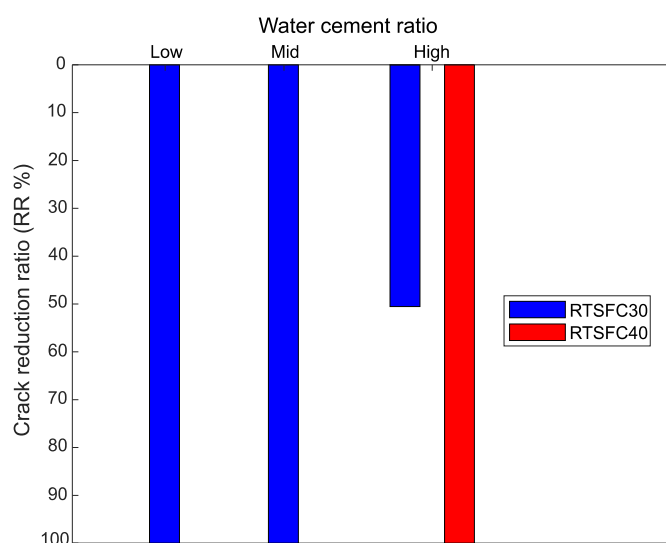


Figure 4.19: Crack reduction ratio for all water cement ratio.

## 4.5. Conclusions

This paper discusses the impact of low, mid, and high environmental conditions on the plastic shrinkage of concrete. Two w/c ratios and dosages of RTSF were used to assess their effect in restraining cracking in fresh concrete. From the results, the following conclusions can be drawn:

- Harsher environmental conditions result in earlier and more severe cracking (i.e., larger crack width, length, and area).
- Temperature is the most important parameter in accelerating cracking, whilst wind speed is the least significant.
- The use of higher water/cement ratios increases cracking, primarily as a result of earlier and heavier bleeding.

- The addition of RTSF fibers was found to be effective in controlling plastic shrinkage cracking, with 40 kg/m<sup>3</sup> eliminating the cracks completely in the harshest of the examined environments.

**Acknowledgments:** The first author would like to thank Jouf University and the Ministry of Education in the Kingdom of Saudi Arabia for sponsoring his Ph.D. studies. The authors would also like to thank TWINCON Ltd. for supplying materials for this project.

## 4.6. References

- [1] Alhozaimy, A.M.; Al-Negheimish, A.I. Plastic Shrinkage in Hot and Arid Environments. *Concr. Int.* 2009, 31, 26–32.
- [2] Heiskanen, J.; Brümmer, C.; Buchmann, N.; Calfapietra, C.; Chen, H.; Gielen, B.; Gkritzalis, T.; Hammer, S.; Hartman, S.; Herbst, M.; et al. The integrated carbon observation system in Europe. *Bull. Am. Meteorol. Soc.* 2022, 103, 855–872.
- [3] J.B. Copas, Regression, prediction and shrinkage, *J. R. Stat. Soc. Ser. B.* 45 (1983) 311–335.
- [4] C. Qi, J. Weiss, J. Olek, Statistical significance of the restrained slab test for quantifying plastic cracking in fiber reinforced concrete, *J. ASTM Int.* 2 (2005) 105–122. <https://doi.org/10.1520/jai12242>.
- [5] P. Zhao, A.M. Zsaki, M.R. Nokken, Using digital image correlation to evaluate plastic shrinkage cracking in cement-based materials, *Constr. Build. Mater.* 182 (2018) 108–117. <https://doi.org/10.1016/j.conbuildmat.2018.05.239>.
- [6] O.S.B. Al-Amoudi, M. Maslehuddin, M. Shameem, M. Ibrahim, Shrinkage of plain and silica fume cement concrete under hot weather, *Cem. Concr. Compos.* 29 (2007) 690–699. <https://doi.org/10.1016/j.cemconcomp.2007.05.006>.
- [7] S. Ghourchian, M. Wyrzykowski, P. Lura, The bleeding test: A simple method for obtaining the permeability and bulk modulus of fresh concrete, *Cem. Concr. Res.* 89 (2016) 249–256. <https://doi.org/10.1016/j.cemconres.2016.08.016>.
- [8] G.M. Moelich, J. Kruger, R. Combrinck, Plastic shrinkage cracking in 3D printed concrete, *Compos. Part B Eng.* 200 (2020) 108313. <https://doi.org/10.1016/j.compositesb.2020.108313>.
- [9] Kurian, J.; Sivan, S ; Mary, L; Payyappilly, L; John, E. Study on shrinkage properties of concrete with and without mineral admixtures. *IJARIT* 2019, 5, 1840–1850.
- [10] ACI 224R-01. Control of Cracking in Concrete Structures Reported by ACI Committee 224. ACI 224R-01 ACI Comm. 2001, 224R-01, 1–46.
- [11] A. Radocea, A model of plastic shrinkage, *Mag. Concr. Res.* 46 (1994) 125–132. <https://doi.org/10.1680/mac.1994.46.167.125>.
- [12] J.L. Granju, S.U. Balouch, Corrosion of steel fibre reinforced concrete from the cracks, *Cem. Concr. Res.* 35 (2005) 572–577. <https://doi.org/10.1016/j.cemconres.2004.06.032>.
- [13] A.E. Naaman, T. Wongtanakitcharoen, G. Hauser, Influence of different fibers on plastic shrinkage cracking of concrete, *ACI Mater. J.* 102 (2005) 49–58. <https://doi.org/10.14359/14249>.
- [14] A.G. Graeff, K. Pilakoutas, K. Neocleous, M.V.N.N. Peres, Fatigue resistance and cracking mechanism of concrete pavements reinforced with recycled steel fibres recovered from post-consumer tyres, *Eng. Struct.* 45 (2012) 385–395.

- <https://doi.org/10.1016/j.engstruct.2012.06.030>.
- [15] J. Branston, S. Das, S.Y. Kenno, C. Taylor, Influence of basalt fibres on free and restrained plastic shrinkage, *Cem. Concr. Compos.* 74 (2016) 182–190. <https://doi.org/10.1016/j.cemconcomp.2016.10.004>.
- [16] V. Slowik, M. Schmidt, R. Fritzsich, Capillary pressure in fresh cement-based materials and identification of the air entry value, *Cem. Concr. Compos.* 30 (2008) 557–565. <https://doi.org/10.1016/j.cemconcomp.2008.03.002>.
- [17] Mehta, P.K.; Monteiro, P.J. *Concrete: Microstructure, Properties, and Materials*; McGraw-Hill Education: New York City. 2014.
- [18] P. Lura, B. Pease, G. Mazzotta, F. Rajabipour, J. Weiss, Influence of shrinkage-reducing admixtures on development of plastic shrinkage cracks, *ACI Mater. J.* 104 (2007) 187–194. <https://doi.org/10.14359/18582>.
- [19] Á. García, D. Castro-fresno, J.A. Polanco, Maturity Approach Applied to Concrete by Means of Vicat Tests, *ACI Mater. J.* 105 (2008) 445.
- [20] S. Banthia, N., Yan, C. and Mindess, Restrained shrinkage cracking in fiber reinforced concrete: a novel test technique, *Cem. Concr. Res.* 26 (1996) 9–14.
- [21] N. Banthia, R. Gupta, Influence of polypropylene fiber geometry on plastic shrinkage cracking in concrete, *Cem. Concr. Res.* 36 (2006) 1263–1267. <https://doi.org/10.1016/j.cemconres.2006.01.010>.
- [22] I.M.G. Bertelsen, L.M. Ottosen, G. Fischer, Influence of fibre characteristics on plastic shrinkage cracking in cement-based materials: A review, *Constr. Build. Mater.* (2020). <https://doi.org/10.1016/j.conbuildmat.2019.116769>.
- [23] S. Chatterji, Probable mechanisms of crack formation at early ages of concretes: A literature survey, *Cem. Concr. Res.* 12 (1982) 371–376. [https://doi.org/10.1016/0008-8846\(82\)90085-0](https://doi.org/10.1016/0008-8846(82)90085-0).
- [24] T. M'hammed, K. Hamid, An experimental study on the influence of arid climate on early-age cracking of concrete—A case study of the city of Adrar in Algeria, *AIMS Mater. Sci.* 8 (2021) 200–220. <https://doi.org/10.3934/matersci.2021014>.
- [25] M. Nasir, O.S. Baghabra Al-Amoudi, M. Maslehuddin, Effect of placement temperature and curing method on plastic shrinkage of plain and pozzolanic cement concretes under hot weather, *Constr. Build. Mater.* 152 (2017) 943–953. <https://doi.org/10.1016/j.conbuildmat.2017.07.068>.
- [26] M. Kayondo, R. Combrinck, W.P. Boshoff, State-of-the-art review on plastic cracking of concrete, *Constr. Build. Mater.* 225 (2019) 886–899. <https://doi.org/10.1016/j.conbuildmat.2019.07.197>.
- [27] M. Al-Fadhala, K.C. Hover, Rapid evaporation from freshly cast concrete and the Gulf environment, *Constr. Build. Mater.* 15 (2001) 1–7. [https://doi.org/10.1016/S0950-0618\(00\)00064-7](https://doi.org/10.1016/S0950-0618(00)00064-7).

- [28] ASTM C1579; Standard Test Method for Evaluating Plastic Shrinkage Cracking of Restrained Fiber Reinforced Concrete. ASTM International: West Conshohocken, PA, USA, 2006. <https://doi.org/10.1520/C1579-06.2>. <https://doi.org/10.1520/C1579-06.2>.
- [29] A.A. Almusallam, M. Maslehuddin, M. Abdul-Waris, M.M. Khan, Effect of mix proportions on plastic shrinkage cracking of concrete in hot environments, *Constr. Build. Mater.* 12 (1998) 353–358. [https://doi.org/10.1016/S0950-0618\(98\)00019-1](https://doi.org/10.1016/S0950-0618(98)00019-1).
- [30] H.J. Al-Gahtani, A.G.F. Abbasi, O.S.B. Al-Amoudi, Concrete mixture design for hot weather: Experimental and statistical analyses, *Mag. Concr. Res.* 50 (1998) 95–105. <https://doi.org/10.1680/mac.1998.50.2.95>.
- [31] ACI Committee 305. Hot-Weather Concreting; American Concrete Institute: Farmington Hills, MI, USA, 1999; Volume 17.
- [32] B. Nabil, A. Aissa, B.I. Aguida, Use of a new approach (design of experiments method) to study different procedures to avoid plastic shrinkage cracking of concrete in hot climates, *J. Adv. Concr. Technol.* 9 (2011) 149–157. <https://doi.org/10.3151/jact.9.149>.
- [33] N.S. Almutairi, T.E. Almutairi, Preventing failures of concrete in regions of hot weather, *Int. J. Eng. Res. Appl.* 10 (2020) 47–53. <https://doi.org/10.9790/9622-1012034753>.
- [34] M. Safiuddin, A.B.M.A. Kaish, C.O. Woon, S.N. Raman, Early-age cracking in concrete: Causes, consequences, remedial measures, and recommendations, *Appl. Sci.* 8 (2018). <https://doi.org/10.3390/app8101730>.
- [35] S. Sulakshna, A. Pal, S. Kishor, H. Ali, Proceedings Reduction of shrinkage of self compacting concrete using polycarboxylate ether as shrinkage reducing admixture, *Mater. Today Proc.* 60 (2022) 448–451. <https://doi.org/10.1016/j.matpr.2022.01.316>.
- [36] H. Zhang, J. Xiao, Plastic shrinkage and cracking of 3D printed mortar with recycled sand, *Constr. Build. Mater.* 302 (2021) 124405. <https://doi.org/10.1016/j.conbuildmat.2021.124405>.
- [37] M.D. Cohen, J. Olek, W.L. Dolch, Mechanism of Plastic Shrinkage Cracking in Portland Cement and Portland Cement-Silica Fume Paste and Mortar, *Cem. Concr. Res.* 20 (1990) 3–19.
- [38] O.E. I. Löfgren, Early age cracking of self-compacting concrete, *Int. RILEM Conf. Vol. Chang. Hardening Concr. Test. Mitig.* 20-23 August 2006, Tech. Univ. Denmark, Lyngby, Denmark EARLY. C (2006) 251–260. <https://doi.org/10.1617/2351580052.027>.
- [39] H. Zhao, Y. Ma, J. Zhang, Z. Hu, H. Li, Y. Wang, J. Liu, Z. Li, Effect of clay content on plastic shrinkage cracking of cementitious materials, *Constr. Build. Mater.* 342 (2022) 127989. <https://doi.org/10.1016/j.conbuildmat.2022.127989>.
- [40] G.S. Hasanain and T.A. Khallaf and K. Mahmood, Water evaporation from freshly placed concrete surfaces in hot weather, *Cem. Concr. Res.* 19 (1989) 465–475. [https://doi.org/https://doi.org/10.1016/0008-8846\(89\)90035-5](https://doi.org/https://doi.org/10.1016/0008-8846(89)90035-5).

- [41] Climatemps.com. World Climate & Temperature. Available online: <http://www.climatemps.com/> (accessed on 1-11-2022).
- [42] G.H. Arafah, A.M., Al-Haddad, M.S., Al-Zaid, R.Z. and Siddiqi, EFFICIENCY OF CONCRETE CURING IN RIYADH AREA, Proceeding Int. Conf. Concr. under Sev. Cond. 95 (1995) 890–897.
- [43] ACI Committee 305. Building Code Requirements for Structural Concrete (ACI 318-05) and Commentary (ACI 318R-05); American Concrete Institute: USA, Miami, Florida; 2005.
- [44] M.I. Khan, Y.M. Abbas, Curing optimization for strength and durability of silica fume and fuel ash concretes under hot weather conditions, *Constr. Build. Mater.* 157 (2017) 1092–1105. <https://doi.org/10.1016/j.conbuildmat.2017.09.173>.
- [45] A.S. Al-Gahtani, Effect of curing methods on the properties of plain and blended cement concretes, *Constr. Build. Mater.* 24 (2010) 308–314. <https://doi.org/10.1016/j.conbuildmat.2009.08.036>.
- [46] M. Nasir, I.A. Syed, U. Gazder, M. Maslehuddin, O.S. Baghabra, Prediction of Properties of Concrete Cured Under Hot Weather Using Multivariate Regression and ANN Models, *Arab. J. Sci. Eng.* 45 (2020) 4111–4123. <https://doi.org/10.1007/s13369-020-04403-y>.
- [47] H. Hu, P. Papastergiou, H. Angelakopoulos, M. Guadagnini, K. Pilakoutas, Mechanical properties of SFRC using blended Recycled Tyre Steel Cords (RTSC) and Recycled Tyre Steel Fibres (RTSF), *Constr. Build. Mater.* 187 (2018) 553–564. <https://doi.org/10.1016/j.conbuildmat.2018.07.206>.
- [48] ASTM C192/C192M, Standard Practice for Making and Curing Concrete Test Specimens in the Laboratory, *Am. Soc. Test. Mater.* (2016) 1–8. <https://doi.org/10.1520/C0192>.
- [49] A. Mohajerani, L. Burnett, J. V Smith, S. Markovski, G. Rodwell, Resources , Conservation & Recycling Recycling waste rubber tyres in construction materials and associated environmental considerations : A review, *Resour. Conserv. Recycl.* 155 (2020) 104679. <https://doi.org/10.1016/j.resconrec.2020.104679>.
- [50] O. Benaïmeche, A. Carpinteri, M. Mellas, C. Ronchei, D. Scorza, S. Vantadori, The influence of date palm mesh fibre reinforcement on flexural and fracture behaviour of a cement-based mortar, *Compos. Part B.* 152 (2018) 292–299. <https://doi.org/10.1016/j.compositesb.2018.07.017>.
- [51] Vantadori, S.; Carpinteri, A.; Zanichelli, A. Lightweight construction materials : Mortar reinforced with date-palm mesh fibres. 2019, 100, 39–45. <https://doi.org/10.1016/j.tafmec.2018.12.011..>
- [52] A. Alsaif, L. Koutas, S.A. Bernal, M. Guadagnini, K. Pilakoutas, Mechanical performance of steel fibre reinforced rubberised concrete for flexible concrete pavements, *Constr. Build. Mater.* 172 (2018) 533–543. <https://doi.org/10.1016/j.conbuildmat.2018.04.010>.

- [53] Z. Al-Kamyani, F.P. Figueiredo, H. Hu, M. Guadagnini, K. Pilakoutas, Shrinkage and flexural behaviour of free and restrained hybrid steel fibre reinforced concrete, *Constr. Build. Mater.* 189 (2018) 1007–1018. <https://doi.org/10.1016/j.conbuildmat.2018.09.052>.
- [54] M. Leone, G. Centonze, D. Colonna, F. Micelli, M.A. Aiello, Fiber-reinforced concrete with low content of recycled steel fiber : Shear behaviour, *Constr. Build. Mater.* 161 (2018) 141–155. <https://doi.org/10.1016/j.conbuildmat.2017.11.101>.
- [55] G. Baghban, M. Farzam, S. Soleymani, Behavior of recycled steel fiber reinforced concrete under uniaxial cyclic compression and biaxial tests, *Constr. Build. Mater.* 263 (2020) 120664. <https://doi.org/10.1016/j.conbuildmat.2020.120664>.
- [56] H. Hu, P. Papastergiou, H. Angelakopoulos, M. Guadagnini, K. Pilakoutas, Mechanical properties of SFRC using blended manufactured and recycled tyre steel fibres, *Constr. Build. Mater.* 163 (2018) 376–389. <https://doi.org/10.1016/j.conbuildmat.2017.12.116>.
- [57] A. Baricevic, D. Bjegovic, M. Skazlic, Hybrid Fiber–Reinforced Concrete with Unsorted Recycled-Tire Steel Fibers, *J. Mater. Civ. Eng.* 29 (2017). [https://doi.org/10.1061/\(asce\)mt.1943-5533.0001906](https://doi.org/10.1061/(asce)mt.1943-5533.0001906).
- [58] M.N. Isa, K. Pilakoutas, M. Guadagnini, H. Angelakopoulos, Mechanical performance of affordable and eco-efficient ultra-high performance concrete ( UHPC ) containing recycled tyre steel fibres, *Constr. Build. Mater.* 255 (2020) 119272. <https://doi.org/10.1016/j.conbuildmat.2020.119272>.
- [59] K.M. Liew, A. Akbar, The recent progress of recycled steel fiber reinforced concrete, *Constr. Build. Mater.* 232 (2020) 117232. <https://doi.org/10.1016/j.conbuildmat.2019.117232>.
- [60] Ş Bianca-maria, D. Nastac, O. Vasile, M. Bratu, Sound absorbing materials made by embedding crumb rubber waste in a concrete matrix, 124 (2016) 755–763. <https://doi.org/10.1016/j.conbuildmat.2016.07.145>.
- [61] M. Mastali, A. Dalvand, A.R. Sattarifard, M. Illikainen, Development of eco-efficient and cost-effective reinforced self- consolidation concretes with hybrid industrial / recycled steel fibers, *Constr. Build. Mater.* 166 (2018) 214–226. <https://doi.org/10.1016/j.conbuildmat.2018.01.147>.
- [62] T. Alshammari, K. Pilakoutas, M. Guadagnini, Performance of Manufactured and Recycled Steel Fibres in Restraining Concrete Plastic Shrinkage Cracks, *Materials (Basel)*. 16 (2023) 713. <https://doi.org/10.2139/ssrn.4232808>.
- [63] ISO EN 6892-1; Metallic materials—Tensile testing—Part 1: Method of test at room temperature. ISO: Geneva, Switzerland, 2019.
- [64] M.N. Isa, K. Pilakoutas, M. Guadagnini, Determination of tensile characteristics and design of eco-efficient UHPC, *Structures*. 32 (2021) 2174–2194. <https://doi.org/10.1016/j.istruc.2021.03.114>.
- [65] BS EN 12390-3; Testing hardened concrete. Compressive strength of test specimens.

- British Standards Institution: London, UK, 2009.
- [66] M.A. Aiello, F. Leuzzi, G. Centonze, A. Maffezzoli, Use of steel fibres recovered from waste tyres as reinforcement in concrete: Pull-out behaviour, compressive and flexural strength, *Waste Manag.* (2009). <https://doi.org/10.1016/j.wasman.2008.12.002>.
- [67] O.J. Qi C., Weiss J., Characterization of plastic shrinkage cracking in fiber reinforced concrete using image analysis and a modified Weibull function, *Mater. Struct. Constr.* Volume 36 (2003) Pages 386-395.
- [68] N. Banthia, R. Gupta, C. Qi, J. Weiss, J. Olek, Statistical significance of the restrained slab test for quantifying plastic cracking in fiber reinforced concrete, *J. ASTM Int.* 42 (2009) 105–122. <https://doi.org/10.1617/s11527-008-9403-9>.
- [69] E. Yaşar, Y. Erdogan, A. Kiliç, Effect of limestone aggregate type and water-cement ratio on concrete strength, *Mater. Lett.* 58 (2004) 772–777. <https://doi.org/10.1016/j.matlet.2003.06.004>.
- [70] B. Felekoğlu, S. Türkel, B. Baradan, Effect of water/cement ratio on the fresh and hardened properties of self-compacting concrete, *Build. Environ.* 42 (2007) 1795–1802. <https://doi.org/10.1016/j.buildenv.2006.01.012>.
- [71] S.B. Singh, P. Munjal, N. Thammishetti, Role of water/cement ratio on strength development of cement mortar, *J. Build. Eng.* 4 (2015) 94–100. <https://doi.org/10.1016/j.jobbe.2015.09.003>.
- [72] S. Popovics, Analysis of concrete strength versus water-cement ratio relationship., *Mater. J.* 5 (1990) 517–529.
- [73] H. Xu, J.S.J. Van Deventer, The geopolymerisation of alumino-silicate minerals, *Int. J. Miner. Process.* 59 (2000) 247–266. [https://doi.org/10.1016/S0301-7516\(99\)00074-5](https://doi.org/10.1016/S0301-7516(99)00074-5).
- [74] S. Ghourchian, M. Wyrzykowski, L. Baquerizo, P. Lura, Performance of passive methods in plastic shrinkage cracking mitigation, *Cem. Concr. Compos.* 91 (2018) 148–155. <https://doi.org/10.1016/j.cemconcomp.2018.05.008>.
- [75] A.K. Schindler, J.M. Ruiz, R.O. Rasmussen, G.K. Chang, L.G. Wathne, Concrete pavement temperature prediction and case studies with the FHWA HIPERPAV models, *Cem. Concr. Compos.* 26 (2004) 463–471. [https://doi.org/10.1016/S0958-9465\(03\)00075-1](https://doi.org/10.1016/S0958-9465(03)00075-1).
- [76] R. Combrinck, M. Kayondo, B.D. le Roux, W.I. de Villiers, W.P. Boshoff, Effect of various liquid admixtures on cracking of plastic concrete, *Constr. Build. Mater.* 202 (2019) 139–153. <https://doi.org/10.1016/j.conbuildmat.2018.12.060>.
- [77] H.G. Kwak, S.J. Ha, Plastic shrinkage cracking in concrete slabs. Part I: A numerical model, *Mag. Concr. Res.* 58 (2006) 505–516. <https://doi.org/10.1680/macr.2006.58.8.505>.
- [78] A.A. Almusallam, Effect of environmental conditions on the properties of fresh and hardened concrete, *Cem. Concr. Compos.* 23 (2001) 353–361. [https://doi.org/10.1016/S0958-9465\(01\)00007-5](https://doi.org/10.1016/S0958-9465(01)00007-5).



- [79] E. Holt, M. Leivo, Cracking risks associated with early age shrinkage, *Cem. Concr. Compos.* 26 (2004) 521–530. [https://doi.org/10.1016/S0958-9465\(03\)00068-4](https://doi.org/10.1016/S0958-9465(03)00068-4).
- [80] I.B. Topçu, V.B. Elgün, Influence of concrete properties on bleeding and evaporation, *Cem. Concr. Res.* 34 (2004) 275–281. <https://doi.org/10.1016/j.cemconres.2003.07.004>.
- [81] R.P. Borg, O. Baldacchino, L. Ferrara, Early age performance and mechanical characteristics of recycled PET fibre reinforced concrete, *Constr. Build. Mater.* 108 (2016) 29–47. <https://doi.org/10.1016/j.conbuildmat.2016.01.029>.
- [82] N. Pešić, S. Živanović, R. Garcia, P. Papastergiou, Mechanical properties of concrete reinforced with recycled HDPE plastic fibres, *Constr. Build. Mater.* 115 (2016) 362–370. <https://doi.org/10.1016/j.conbuildmat.2016.04.050>.
- [83] B.S. Al-Tulaian, M.J. Al-Shannag, A.R. Al-Hozaimy, Recycled plastic waste fibers for reinforcing Portland cement mortar, *Constr. Build. Mater.* 127 (2016) 102–110. <https://doi.org/10.1016/j.conbuildmat.2016.09.131>.
- [84] M. Sirajuddin, R. Gettu, Plastic shrinkage cracking of concrete incorporating mineral admixtures and its mitigation, *Mater. Struct. Constr.* 51 (2018). <https://doi.org/10.1617/s11527-018-1173-4>.
- [85] A. Mazzoli, S. Monosi, E.S. Plescia, Evaluation of the early-age-shrinkage of Fiber Reinforced Concrete (FRC) using image analysis methods, *Constr. Build. Mater.* 101 (2015) 596–601. <https://doi.org/10.1016/j.conbuildmat.2015.10.090>.

**This page is intentionally left blank**

## Chapter 5 : Effect of Curing Methods on Plastic Shrinkage Cracking

*Alshammari, T.O., Pilakoutas, K. and Guadagnini, M., 2023. Effect of Curing Methods on Plastic Shrinkage Cracking. Construction Materials, 3(2), pp.244-258.*

### Author Contributions:

Conceptualization, software, data curation, investigation and writing—original draft, **T.O.A.**; methodology, writing—review and editing and supervision **K.P. and M.G.** All authors have read and agreed to the published version of the manuscript.

### Abstract

Early age cracking occurring during the plastic stage is unsightly and a cause of future durability problems. This paper investigates the effect of various simple curing methods used in practice to enhance early age concrete cracking performance, including: covering concrete with plastic sheet and wet hessian fabric, surface power floating and use of cold water in the mix. The benefits offered from the use of two standard curing methods (Safecure super concrete, and Safecure super 90w-10%). With and without a superplasticizer (Sika ViscoCrete 30HE) is tested for a comparison purpose to see the effect of it on the plastic shrinkage cracking and as well as recycled tire steel fibres at 40 kg/m<sup>3</sup> are also examined. A digital image processing (DIP) technique is used to measure crack widths, whilst temperature in the concrete is measured via a thermocouple. The results show that all concrete curing methods are successful in restraining plastic shrinkage cracks, but the use of recycled tire steel fibre (RTSFC40) was the most effective at eliminating plastic shrinkage surface cracks. All of the examined methods are compared in terms of speed and cost of application, quality of the surface finish and environmental credentials. This study will inform best practice on enhancing durability and sustainability of concrete structures, in particular for slab on grade applications.

**Appendix D** has provided the relevant experimental data of this chapter.

**Keywords:**

Early-age concrete cracking; plastic shrinkage cracks; concrete curing; curing admixtures; power float concrete; steel-fibre-reinforced concrete

## **5.1. Introduction**

Fast drying of concrete in its plastic stage before final set can affect concrete durability due to the development of plastic shrinkage cracks [1]. Such early age cracks are known to impact concrete performance (mainly in slabs, and pavements) as they can lead to potential large cracks, physical and chemical deterioration of concrete as well as reinforcement corrosion [2,3]. Therefore, in practice concrete curing is necessary to improve not only the mechanical characteristics, but also to mitigate the occurrence of plastic shrinkage induced cracks and enhance durability [4]. ASTM C192/C192M [5] provides good practice guidance on material mixing and curing to avoid concrete durability issues.

Plastic shrinkage cracks commonly occur during the first-six hours whilst concrete is in the plastic state and before final set [6]. Research confirms that the main parameters that increase the possibility of plastic shrinkage cracking are: 1) environmental conditions (temperature, wind speed, and relative humidity); 2) materials and mix proportions, and 3) construction procedures [7–9]. These parameters affect the evaporation rate and the rate at which concrete water bleeds to the surface [10].

### **5.1.1. Concrete curing methods**

Many practical and proprietary methods exist to avoid plastic shrinkage cracking, including various curing methods, power floating, the use of cold water, curing admixtures and fibres.

Covering concrete with plastic sheets or a wet burlap are the most common practical concrete curing methods. Nasir et al. [11] conducted a study on specimens made of concretes including different cementitious materials (OPC, fly ash, very fine fly ash, silica fume, blast furnace slag and natural pozzolan concrete) and cured under a plastic sheet and found that plastic shrinkage cracks were reduced by up to 25% compared with non-covered specimens. Al-Amoudi et al. [12] studied the drying shrinkage of specimen made of plain concrete and concrete containing silica fume and covered with wet-burlap. It was found that there was no discernible improvement in drying shrinkage performance. Nevertheless, there is no published research on the effect of wet-burlap on plastic shrinkage cracks.

Power floating is also used to eliminate plastic cracks in slabs and to polish the surface. This method, which is applied once all the surface bleed water rises and starts to evaporate, involves the use of a power floating machine to polish the surface of the concrete (with or without the application of a dry shake), while also sealing any plastic shrinkage cracks [13]. Combrinck et al. [1] found out that power floating can close the plastic shrinkage cracks on the surface, but deep in the concrete the cracks may reappear depending on the time of power floating application. In general, power floating is not recommended earlier than two hours from casting, as, if applied too early, the bleed water can be trapped under the sealed surface and cause subsequent delamination.

In hot environmental conditions, the use of cold water is another possible solution as it is expected to delay the evaporation of the bleed water and reduce the temperature rise due to hydration. Surprisingly, Jacobsen et al. [14] found that ice water can propagate and enhance the damage due to micro cracks on the surface of the concrete. On the contrary, Xie et al. [15] showed that replacing 50% of water with crushed ice in ultra-high performance concrete reduced drying shrinkage cracking.

Proprietary curing methods are widely used and some are specifically designed to delay the evaporation of bleed water [16]. Shah et al. [17] conducted a study on the use of curing method (Propylene glycol derivatives) in volumes of 1%, and 2% of total water and found a reduction in plastic shrinkage cracks up to 32%, and 45%, respectively. Pease et al. [18] examined the effects of using another curing method (Tetraguard AS20) in volume of 2.5% of total water and found that the total crack area was reduced by up to 60%.

The use of superplasticizers in concrete is widespread as they increase the workability of concrete and reduce water demand. However increased workability may increase the bleed water and promote plastic shrinkage cracks [19]. Combrinck et al. [20] confirmed experimentally that an increase in superplasticizer dosage resulted in larger plastic crack widths.

The addition of fibres in concrete can improve the stability of wet concrete and reduce bleed water, and in turn stop plastic shrinkage cracking, also due to crack bridging effect of the fibres. Many different types of fibres are currently being used to control cracking in concrete, such as: polymeric fibres, natural fibres, metallic fibres (including recycled fibres [21,22]), as well as other non-metallic high-modulus fibres such as glass, carbon and basalt [23]. Banthia et al. [24] investigated the effects of using different dosages of polypropylene fibres (0.1% to

0.3% by volume) with two different lengths to control early-age cracking. The results showed that the polypropylene fibres had a positive effect on reducing early-age concrete cracks, with the longer fibre performing best. Al-Tulaian et al. [25] examined the use of recycled plastic fibres (1.5% by volume) with different lengths and also found that the longer fibres resulted in a better performance. Sivakumar et al. [26] examined the effect of different types of fibres (steel and polyester, polypropylene and glass) on plastic shrinkage cracking and found that the steel fibres were the best performing and reduced cracking up to 99% compared with the plain concrete.

From the various methods used to control plastic shrinkage, it is difficult to discern which are the most effective, as there is a lack of empirical evidence to compare the effect of the various methods.

### 5.1.2. Significance of research

This paper presents a comparative study on the effect of using different concrete curing methods and mitigation strategies on the plastic shrinkage cracking behaviour of concrete. A multi-parameter (time, cost, and quality) analysis is carried out to compare the examined methods and recommendations are made.

## 5.2. Materials and experimental methods

### 5.2.1. Mixture proportioning

The mix design used in this experimental study was adopted from [27] as shown in Table 5.1, [27] as this was used in previous research work by the authors and the results from this study can provide useful complementary data on the material behaviour during the plastic stage. All aggregates were sieved and weighted a day before casting to control moisture content and temperature as recommended in [6,28].

Table 5.1: Concrete mix proportions.

Material	Quantity
Cement (CEMII 42.5)	335 kg/m <sup>3</sup>
Fine Aggregate (river round sand)	847 kg/m <sup>3</sup>
Gravel 10mm (river round gravel)	491 kg/m <sup>3</sup>
Gravel 14mm (river round gravel)	532 kg/m <sup>3</sup>
Water	185 kg/m <sup>3</sup>
Superplasticizer (Sika ViscoCrete 30HE)	1.5 lt/m <sup>3</sup>

### 5.2.2. Mixing and placing

Concrete was mixed in a pan mixer of 60 L capacity. The dry materials were added first and mixed with some of the mixing water before starting the mixer. After starting the mixer, the rest of the mixing water was added along with the superplasticizer and mixing continued for 3 minutes followed by a 3 minutes rest, and a 2 minutes final mixing, as recommended by [5].

### 5.2.3. Experimental methods

#### 5.2.3.1. Plastic shrinkage test

A plastic shrinkage test was performed as recommended in ASTM C1579 [6] to evaluate the restrained early-age cracking of concrete. The plastic shrinkage test set up is shown in Figure 5.1, and Figure 5.2, and involves a controlled environmental chamber divided into two compartments with the same environmental conditions. Two slabs, one reference slab and one using a special admixture or curing method, are placed in the two compartments and their behaviour is compared over the same amount of time from casting. Each of the slabs is equipped with a thermocouple (TC) placed at a depth of 20 mm to monitor continuously the concrete temperature during the test. Each compartment had an exposed water pan to determine the hourly evaporation rate during the test. The test duration since the slabs were placed inside the chambers was 6 hours. At the end of the test, the doors of the chamber were opened for 24 hours to allow the specimen to return to standard laboratory environmental conditions. During the test the environment conditions were controlled as recommended in ASTM C1579 [6] as follows: temperature ( $36\pm 3$  °C), relative humidity ( $30\pm 10\%$ ) and wind speed greater than 4.7 m/s.

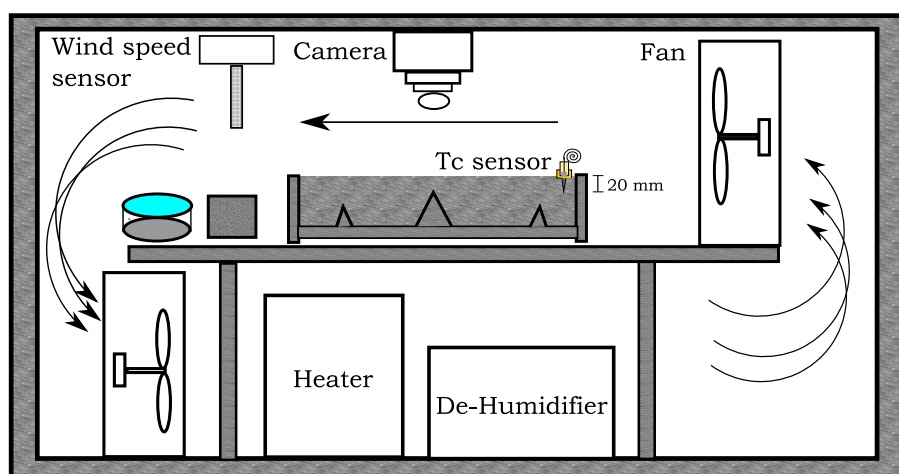


Figure 5.1: Plastic shrinkage test chamber



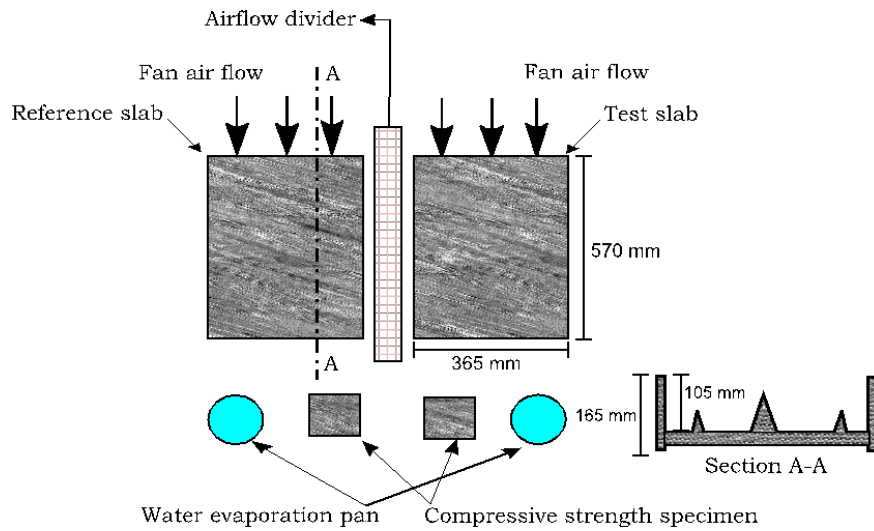


Figure 5.2: Schematic of inside the chamber

The measurements of the plastic shrinkage crack (length, width, and area) were carried out using a 2D digital image processing (DIP) method, whereby a camera was placed above the samples during the test to capture images of the samples at specified times. The images were then analysed by using a DIP software (in MATLAB). In addition, after 24 h from the start of the test, a millimetre steel ruler was used to measure the crack at more than 25 points of the crack and these measurements were compared to the results obtained from DIP. The average plastic shrinkage crack width for each specimen was used to calculate the crack reduction ratio (CRR) by using the following equation (Eq.1) as recommended in ASTM C1579 [6]:

$$CRR = \left[ 1 - \frac{\text{Average Crack Width of Fibre Reinforced Concrete Mixture}}{\text{Average Crack Width of Fibre Control Concrete Mixture}} \right] \times 100\% \dots \dots \dots \text{(Eq.1)}$$

**5.2.3.2. Evaporation rate**

To find the evaporation rate two methods were used as recommended in [6,29]. Firstly, as seen in Figure 5.2, two water pans (left and right) inside the chamber were filled with water at the beginning of the test. According to ASTM C1579 [6] to determine the evaporation rate during each time interval as shown in (Eq.2), If the average evaporation rate was less than 1.0 kg/m<sup>2</sup>/h, the test was to be rejected [6].

$$E = \frac{M2 - M1}{\text{water surface area of the pan} \times (T2 - T1)} \dots \dots \dots \text{(Eq.2)}$$

where:

E: Evaporation rate, kg/m<sup>2</sup>/h,

M<sub>2</sub>-M<sub>1</sub>: The mass loss between successive weighings, g.

T<sub>2</sub>-T<sub>1</sub>: The time interval between successive weighings, hr.

Secondly, the “single operation” equation (Eq.3) (based upon Menzel’s formula) was used to find the evaporation rate [29] based on the temperature in the concrete and the external environmental parameters. This method is also suitable for on-site quick checks to assess whether evaporation will affect plastic shrinkage cracking.

$$E = 5([T_c+18]^{2.5} - r \times [T_a + 18]^{2.5}) (V + 4) \times 10^{-6} \dots\dots\dots (Eq.3)$$

where:

E= Evaporation rate, kg/m<sup>2</sup>/h.

T<sub>c</sub>= Concrete (water surface) temperature, °C,

T<sub>a</sub>= Air temperature, °C,

r= (RH percent)/100,

and V= Wind velocity, kph.

### 5.2.3.3. Parameters of the study

The concrete curing methods compared in this study are listed below. A specimen made with a plain concrete (PC) mix, with no additional admixtures or subjected to special curing methods, is used for direct comparisons. PC contained a normal plasticiser (Sika ViscoCrete 30HE) at (1.5 lt/m<sup>3</sup>) / (335 kg/m<sup>3</sup>).

**PSC:** Plastic sheet concrete. Covering concrete with a plastic sheet is common as it prevents direct water evaporation

**HFC:** Hessian fabric concrete. Concrete is covered with a wet hessian concrete, to keep the moisture and provide additional water for curing. This is often applied in smaller structures and laboratory specimens

**PFC:** Power float concrete. Power floating concrete is normally applied on slabs-on-grade (SoG) or slabs for which a polished surface is required. The power floating concrete method was examined in the laboratory as well as in a site application. In the laboratory, due to the small dimensions, the concrete slab was hand trowelled under the controlled environmental

conditions. A larger scale trial was conducted at a site in Saudi Arabia under ambient environmental conditions.

**CWC:** Cold water concrete. To mitigate the effects of extreme environments, the initial concrete temperature may be modified to reduce issues at the plastic stage [30]. The normal water temperature used for PC was at room temperature (around 20 °C), whilst the cold water used for CWC was at 7 °C

**SSC:** Safecure Super concrete & **SS90WC:** Safecure Super 90W-10% concrete. Two curing methods were selected (Safecure Super, and Safecure Super 90w-10%). Both were supplied by Adomast Manufacturing Ltd and approved by the Water Regulations Approval Scheme (WRAS) and tested in [31,32]. The two curing methods were applied in the specimen as recommended in the data sheet at 4-6 m<sup>2</sup> per litre.

**PC-S:** A PC devoid of superplasticizer was used for comparison purposes.

**RTSFC40:** Recycled tire steel fibre 40 kg/m<sup>3</sup> concrete: As steel fibres are commonly used in SoG, a recycled tire steel fibre (RTSF) mix was examined at 40 kg/m<sup>3</sup>. The use of 40 kg/m<sup>3</sup> was found in an earlier in a study by Alshammari et al. [33] to provide the best performance in eliminating plastic shrinkage concrete cracks at the surface. The average tensile strength of RTSF was measured from individual fibres and was found to be 2380 MPa. The RTSF length distribution was determined by an automated optical method as by [34] (see Figure 5.3).

The time of application of the concrete curing methods and strategies depends on when it needs to apply to the concrete. For example, some of the concrete curing methods and strategies had been used during mixing such as adding RTSF, PC-S, and CWC. The covering concrete curing methods and strategies (PSC, and HFC) were applied after casting immediately to the concrete. The other concrete curing methods and strategies were cured after a period of time of casting when the concrete is reaching the drying time as found and suggested in the literature like curing methods (SSC, and SS90WC) , and PFC.

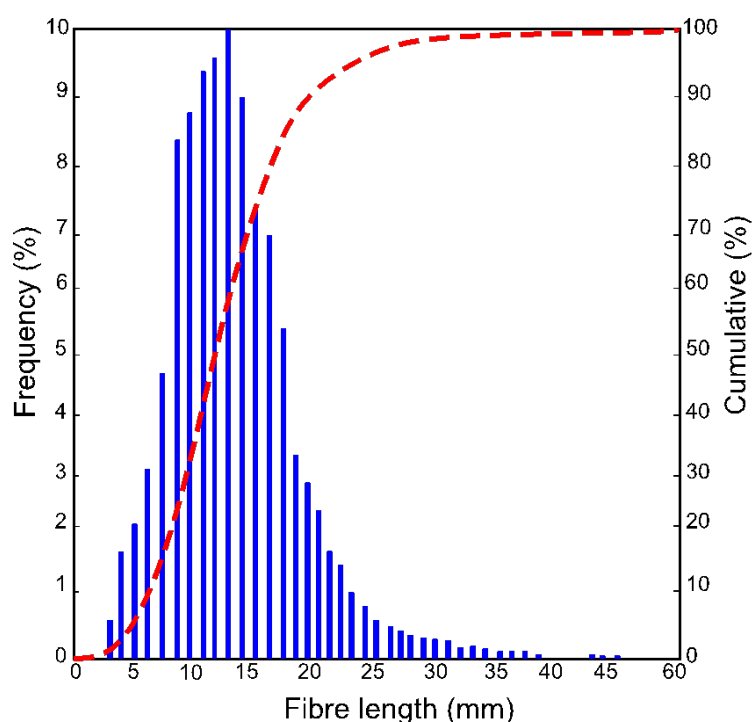


Figure 5.3: RTSF length distribution.

### 5.3. Experimental results and discussion

In accordance to ASTM C1579 [6], and as shown in Figure 5.4, during the test timescale (6 hours) the environmental conditions in the chamber were kept within the limits of air temperature  $36 \pm 3$  °C, relative humidity  $30 \pm 10\%$  and a wind speed of 5 m/s,. These conditions are necessary to achieve a similar evaporation environment for all specimens.

The temperature recorded inside the concrete is shown in Figure 5.5. In general, the temperature starts from room temperature and increases to about 30 °C after 6 hours, mainly due to the heat of hydration. The PSC temperature increases faster than the other specimens and reaches 37 °C at the end of the test. This is expected as the plastic sheet provided some insulation and prevented heat loss due to water evaporation. The CWC showed the overall lower temperatures as it started at a lower temperature than the other specimens.

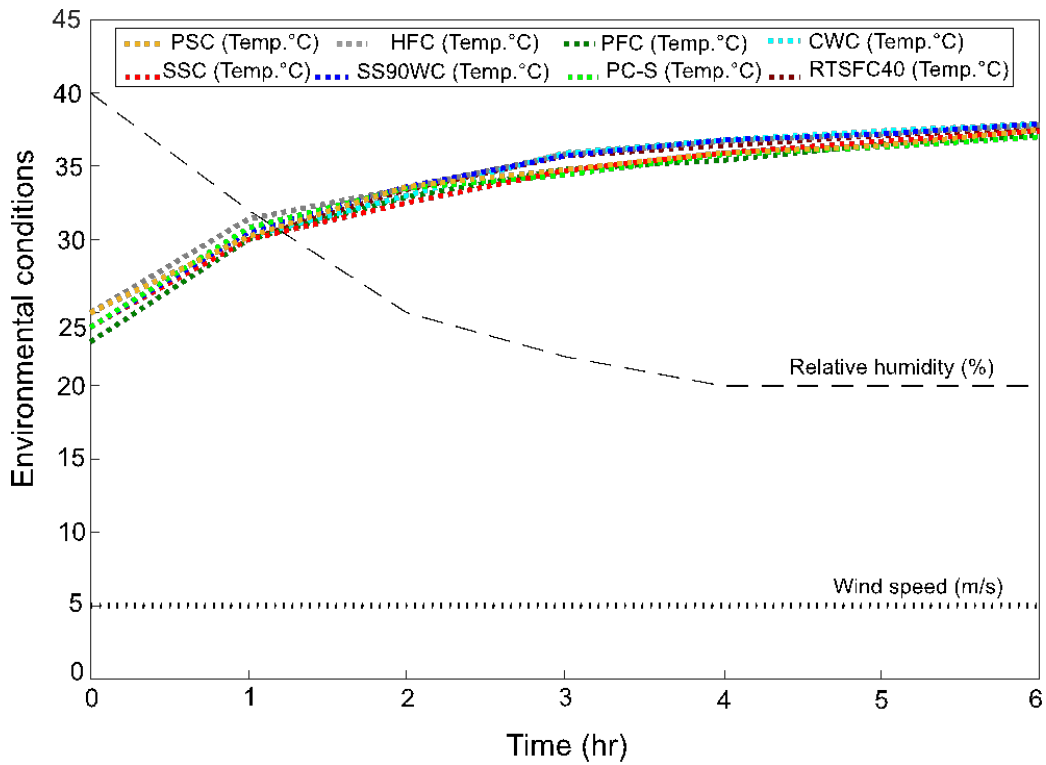


Figure 5.4: Environmental conditions of all concrete curing methods.

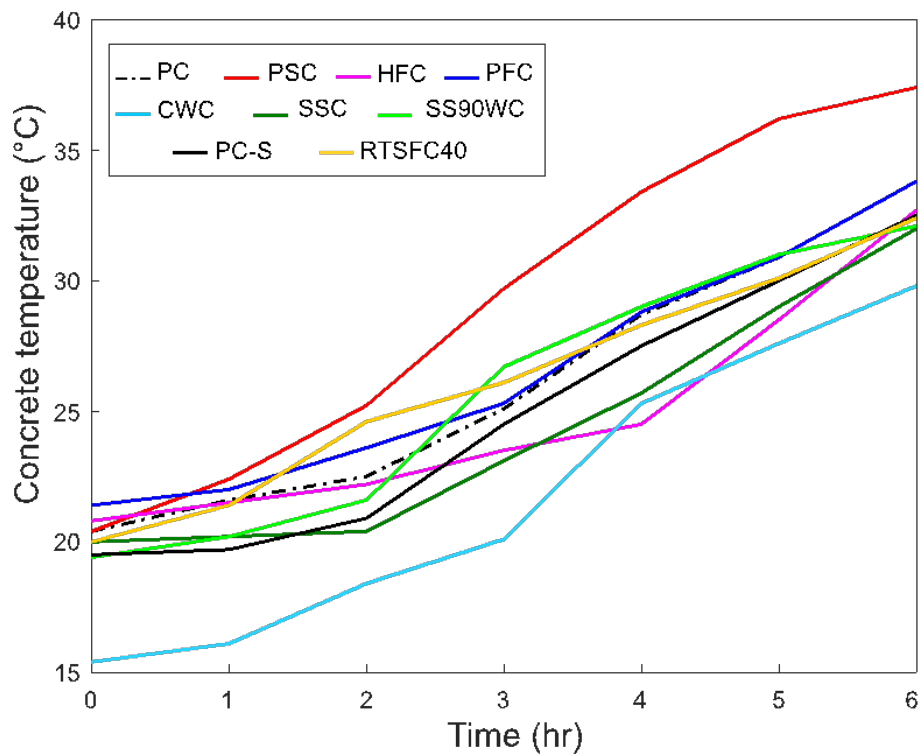


Figure 5.5: Concrete temperature of all concrete curing methods.

### 5.3.1. Evaporation rate

The evaporation rate is determined by two methods as described earlier: a) ASTM C1579 [6] and b) Menzel's formula [29]. As shown in Figure 5.6 (a-h) the evaporation rates are almost identical for the water pan evaporation rate method (blue lines) with the average water pan evaporation rate method (black line). This is expected, as the specimens themselves cannot change the local environment by much. The initial water pan temperatures were about  $15\pm 3$  °C. However, there is a significant difference in the predicted evaporation rate by Menzel's formula and the water pan method, due to differences in the concrete temperatures developed as a result of the curing methods applied.

In PSC, Menzel's formula predicts a higher evaporation rate (see Figure 5.6 (a)). This is a natural consequence of the higher concrete temperature recorded. Nonetheless, as the surface is shielded from the wind, the actual concrete surface evaporation rate is not correct by either method, as bleed water cannot evaporate freely.

The HFC evaporation rate is shown in Figure 5.6 (b). The hessian seems to keep the temperature of the concrete slightly lower than that of the PC specimen, hence the Menzel's predicted evaporation rate is lower than for PC. The hessian fabric was weighed before wetting (97g), after wetting (364g), and at the end of the test (at 24 hours, 109g). As the hessian was not completely dry, it shows that the hessian retained some moisture and kept the concrete wet by delaying the evaporation of bleed water. Hence, HFC provides a barrier to water evaporation without trapping the heat of hydration. Other studies such as McCarter and Ben-Saleh [35] found similar results. Maslehuddin et al. [36] also examined curing compounds (acrylic, bitumen-based and coal tar epoxy) on plain and silica fume concrete and found that wetted hessian fabric gave the best results as reduce the shrinkage strain and increase the corrosion resistance.

The PFC evaporation rate is shown in Figure 5.6 (c). The rate found by both methods is similar for both specimen (PC and PFC), due to similar temperature rises, as also found by others [6,29].

In the case of cold-water concrete curing method, the temperature of the water in both pans before the test started was 15 °C. The pan evaporation rate is similar to the other tests as it is only influenced by the external environmental conditions (see Figure 5.6 (d)). At the beginning of the test, the CWC temperature was 15.4 °C while for PC it was 20.4 °C, a

difference of 5 °C. This difference remained more or less the same throughout the test, with the specimens ending at 34.4 °C for CWC and 29.8 °C for PC. As the initial concrete temperatures are affected by the temperature of the water, Menzel's formula predicts lower evaporation rate for the CWC and in this case this evaporation rate is likely to be more accurate than the pan method. Shen et al. [37] also found that cooling concrete in hot environmental conditions improves concrete hydration, and delays evaporation of bleed water.

The evaporation rates of the two curing methods are similar and are shown in Figure 5.6 (e), and (f). As they affect the concrete temperature slightly differently, slightly different evaporation rates are predicted by Menzel's formula. Safecure Super method appeared to create a thin membrane on the surface of the concrete, which should have retarded the evaporation, and also resulted in a slightly lower concrete temperature. Safecure Super 90W-10% method is a wax emulsion that also formed a thin layer on the surface of the concrete. However, this thin layer seems to have increased slightly the concrete temperature acting a bit like the plastic sheet. Hence, it appears that different curing methods have different effects on evaporation and temperature.

The predicted evaporation rate of PC-S and PC was almost equal in both methods as shown in Figure 5.6 (g). During the experiment it was noticed that its bleeding rate was lower than plain concrete due to the low flowability of the concrete. This was also reported by Combrinck et al [20] when examining different doses of superplasticizer. The superplasticizer also seems to have slowed down the temperature rise, probably by retarding the hydration reaction.

The addition of 40 kg/m<sup>3</sup> of recycled tire steel fibre (RTSF) does not seem to affect the evaporation rates as shown in Figure 5.6 (h).

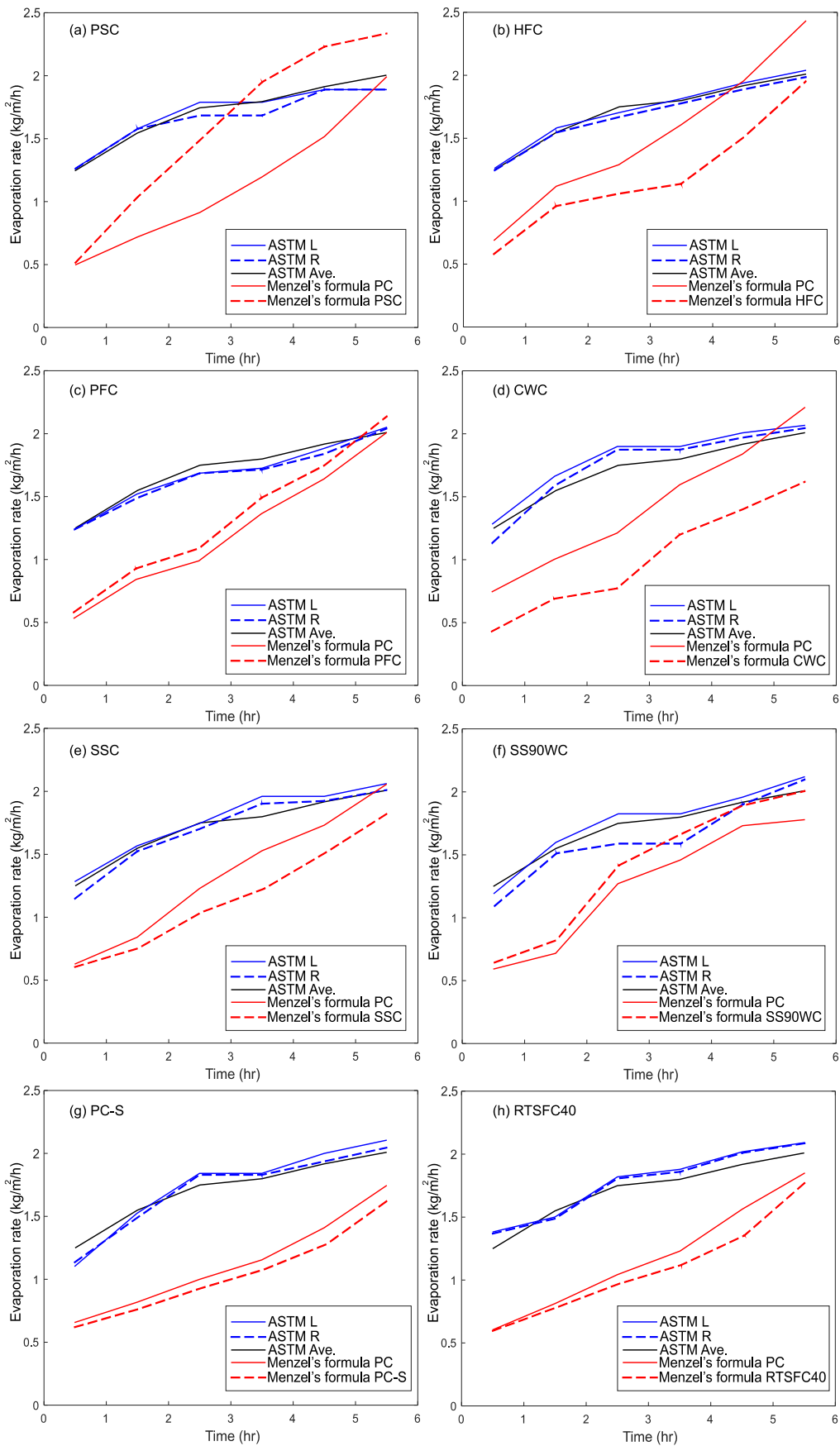


Figure 5.6: Evaporation rate of the various curing methods compared to PC.



### 5.3.2. Crack width development

The surface crack width development over time is shown in Figure 5.7 (a-h) for all tests. The graphs also show the concrete surface temperature and identify the temperature at the initiation of the first crack. All the PC specimens cracked at around 2 hours, when the surface temperature was around 24 °C and reached a width of just above 1 mm after 6 hours. This consistency shows that the environmental chamber controlled the environment very well, and that the concrete PC mixes were consistent with each other, enabling fair comparisons.

In PSC no plastic cracks were recorded as shown in Figure 5.7 (a), hence, the crack reduction ratio was 100% (see Figure 5.8). This was also found by other authors. For example, Nabil et al. [38] examined concrete in hot environmental conditions by covering concrete with plastic sheet, curing membrane, adding ice to the concrete, and polypropylene fibres. The results showed that the curing compound followed by plastic sheet covering was most efficient in controlling plastic shrinkage cracks on the surface of the concrete.

During the wet-hessian test, the crack development could not be observed during the test, as the surface was covered. However, after 24h when the hessian was removed a crack of around 0.6 mm was found (Figure 5.7 (b)), a reduction of 49% compared to plain concrete (see Figure 5.8). Nassif et al. [39] who study silica fume and fly ash cement replacements also found that none of the applied concrete curing methods (air-dry curing, wet-burlap, and moist curing) totally controlled early age cracks despite early-age strength enhancement.

The crack development for power floated concrete is shown in Figure 5.7 (c). PFC cracked at the edges only. As the floating was done by hand, it is possible that the crack developed at edges that could not be floated properly. Therefore, the CRR of PFC at the centre was 100% reduction of crack width compared to PC as shown in Figure 5.8. Similarly, for the in-situ application where half the slab was power floated, no cracks appeared the PFC, whilst cracks appear on the boundary of the PC half of the slab (see Figure 5.9). Kori et al. [40] also studied power floating concrete and found an improvement in durability and reduction in the total crack area at the surface of the concrete.

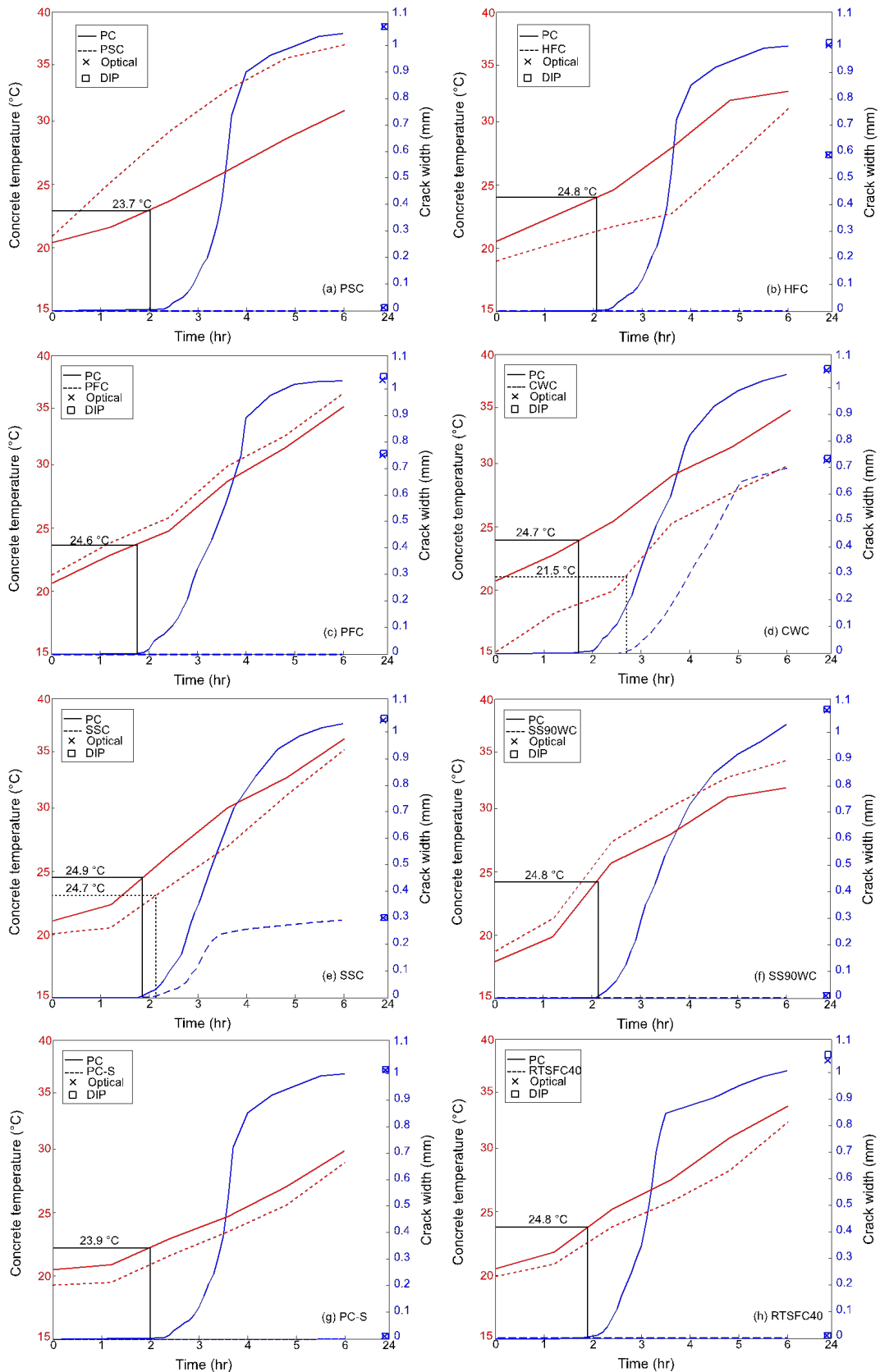


Figure 5.7: Temperature (red curves) and crack width (blue curves) evolution for all curing methods compared to their PC counterpart.

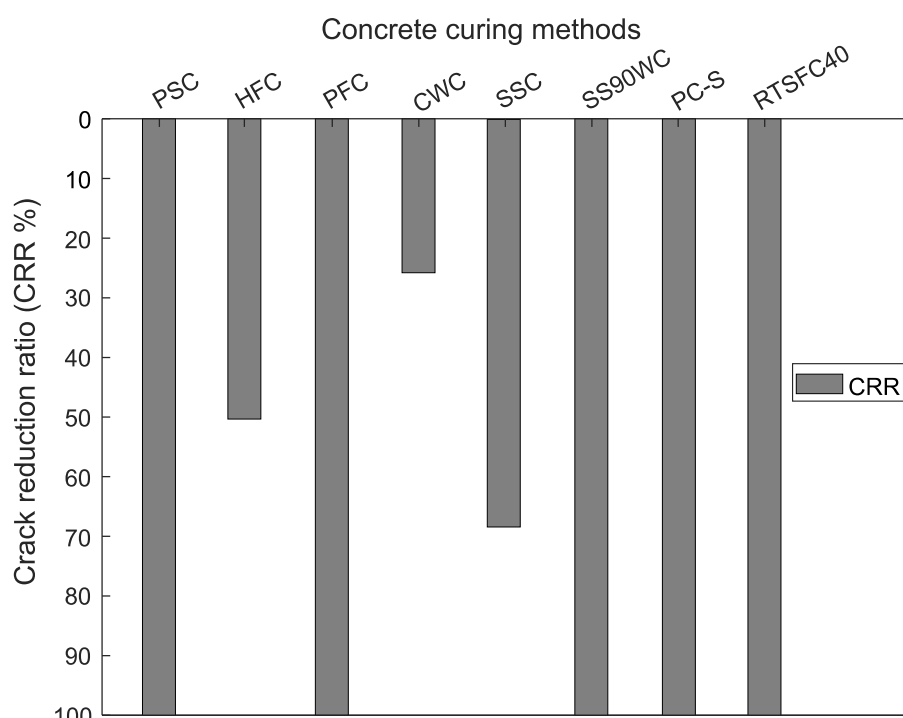


Figure 5.8: Crack reduction ratio of all concrete curing methods



Figure 5.9: Power floating concrete of big scale.

CWC delayed the crack initiation by about one hour compared to PC as shown in Figure 5.7 (d). The concrete also appears to crack at the lower temperature of 21.5 °C compared to 24 °C for all other specimens that cracked. The crack reduction ratio of CWC (see Figure 5.8) was 25%.

SS90WC was found to offer the best crack control width of the three curing methods used, with a crack reduction of 100% (Figure 5.8). SSC also helped offering a 70% crack reduction. Saliba et al. [41] also reported that curing methods can control early-age cracking in normal lab environmental conditions. The study reported that the curing methods reduced the

micro and plastic shrinkage crack up to 25% compared to plain concrete. Leemann et al. [42] investigated self-compacting concrete with an organic hydroxyl-compound as curing method in environmental conditions of  $T = (30 \pm 1) ^\circ\text{C}$ ,  $\text{RH} = (60 \pm 5) \%$ , and wind speed of  $(7 \pm 0.5)$  m/s. The results showed that with increasing doses of curing method, the crack width was reduced but still seen at the surface of the concrete.

On the other hand, PC cracked faster than PC-S, which had no visible cracks on the surface of the concrete (see Figure 5.7 (g)). The reason for the PC-S having no cracks was because of the low workability of the concrete, which failed to reach the target of the slump test of  $100 \pm 10$  mm. Combrinck et al. [43] also found that super-plasticized concrete (PC) results in larger micro and plastic shrinkage cracks compared to concrete devoid of admixtures (PC-S).

RTSFC40 eliminated completely concrete cracks on the surface of the concrete as shown in Figure 5.7 (h). Eren et al. [44] also found that steel fibres (hooked end) of different length and aspect ratios can reduced cracks by up to 70% when using high fibre volumes (1.5%) and longer fibre lengths (80 mm).

### 5.3.3. Comparison of the concrete curing methods

All concrete curing methods are compared in terms of cost, time of application, sustainability, quality, crack initiation and concrete temperature in Table 5.3 and Figure 5.10. Eq.4 was used to find the total cost of power floating a slab with a surface area of  $360 \text{ m}^2$  in Saudi Arabia, which was used as a reference site.

The time of application was determined from the start to finish of the curing method as if it had been applied on the reference slab. The minimum efficiency index is given for the application that took the longest.

The sustainability index was based on whether the material was recycled, reusable, and ECO friendly. Such as, if the used material was recycled and can be reused on the next concrete curing, then the material has advantages in improving the sustainability of the concrete. Also, when the material has a low  $\text{CO}_2$  emissions during production and application, it is considered as an ECO friendly material. The sustainability efficiency that shown in Table 5.2, it means when the used material was recycled will has (33.3), reusable (33.3), and ECO friendly (33.3) of total of 100%.

The quality index is proportional to the CRR%. The crack initiation index is 1 for methods that did not crack, and the worse score is attributed to slabs that cracked between 2 and 3 hours. The concrete temperature index is linear between 20 and 30 °C.

$$\text{Total cost} = C_M + C_L \dots \dots \dots \text{(Eq.4)}$$

where:

$C_M$  = Materials cost, £/m<sup>2</sup>.

$C_L$  = Labourer cost per hour, £/m<sup>2</sup>.

Table 5.3: Comparison of concrete curing methods (in brackets the efficiency index used in Figure 5.10)

Method	Range	PSC	HFC	PFC	CW C	SSC	SS90W C	RTSFC4 0
Cost	4-0 (£/m <sup>2</sup> )	0.18 (0.8)	0.21 (0.8)	0.30 (0.6)	0.10 (1)	0.33 (0.6)	0.33 (0.6)	4 (0)
Time of application	0-30 (s/m <sup>2</sup> )	13 (0.6)	20 (0.4)	20 (0.4)	0 (1)	5 (0.8)	5 (0.8)	30 (0)
Sustainability	0-100 (%)	66.6 6 (0.6)	100 (1)	33.3 3 (0.3)	100 (1)	0 (0)	0 (0)	33.33 (0.3)
Quality	0-100 (CRR %)	100 (1)	48 (0.5)	100 (1)	22 (0.2)	78 (0.78)	100 (1)	100 (1)
Crack initiation	2-3 (hr)	No crack (1)	02:20 (0.3)	No crack (1)	02:30 (0.5)	02:30 (0.5)	No crack (1)	No crack (1)
Concrete temp.	20-30 (°C)	29.7 (0)	23.5 (0.6)	25.3 (0.5)	20.1 (1)	23.1 (0.7)	26.7 (0.3)	24 (0.6)
Overall relative score	0-6	4	3.6	3.8	4.5	3.3	3.6	2.9

In PSC, the plastic sheets can be reused many times up to 5 times and the method is cheap and fast, taking only 13 s/m<sup>2</sup> to prepare and apply. PSC avoided early age cracking during the test, but it has increased the concrete temperature, which could result in drying shrinkage cracks in the future.

In HFC, hessian fabric can also be reused up to 10 times, but cost, drying and storing is probably a bit more of an issue than plastic sheets, though with less environmental impact. The

preparation and speed of application of HFC was around 20 s/m<sup>2</sup>. HFC delayed the crack initiation and reduced the overall crack width without increasing the concrete temperature.

PFC was applied directly on site and accurate values were available. Power floating machines can be used hundreds of times but need fuel to run. Hence, they produce some gas emissions that can affect air quality and are also noisy. The large-scale application of PFC was found to increase the concrete surface temperature in outdoor environmental conditions slab, possibly due to the work done by the machine. The cost of PFC depends on the area of the concrete, but it is still higher compared to other concrete curing methods used in this study. PFC can help control surface cracks, but it is time consuming and possibly only viable when a polished surface is required.

The need for cold mixing water in CWC adds only a small amount of time in the construction process. The cost of cold water or ice depends on the total volume of concrete, but in general it is low compared to other curing methods. In this study, only the direct refrigeration costs were considered. CWC can delay and reduce plastic shrinkage cracks and can also have longer term benefits due to the reduced temperature of the concrete at the early age.

The curing methods used are both non-toxic and non-flammable. The cost of SSC and SS90WC was 0.33 £/m<sup>2</sup> which is higher compared to most curing methods used in this study. Applying them is relatively easy by spraying the concrete surface and it just takes 5 s/m<sup>2</sup>, but it should be applied to the concrete surface when all the bleeding water has evaporated. SS90WC eliminated crack completely, but led to a slight increase in temperature, whilst SSC helped delay and reduce plastic shrinkage cracks.

The PC-S is not acceptable as a concrete curing method as it results in low workability concrete, hence it is not evaluated for efficiency.

RTSFC40 eliminated the cracks completely and it is relatively time consuming to apply at 30 s/m<sup>2</sup>. However, it can also help with long-term cracks and it is often used as structural reinforcement. Its relative cost was found to be higher compared to other curing methods, hence, it may not be the ideal solution if only needed for plastic shrinkage.

The overall relative score shows that the CWC was the best concrete curing method even though it cannot eliminate plastic shrinkage cracking completely. Therefore, combining two

concrete curing methods may be necessary to get the best performance of concrete curing methods like CWC with PSS or RTSFC40.

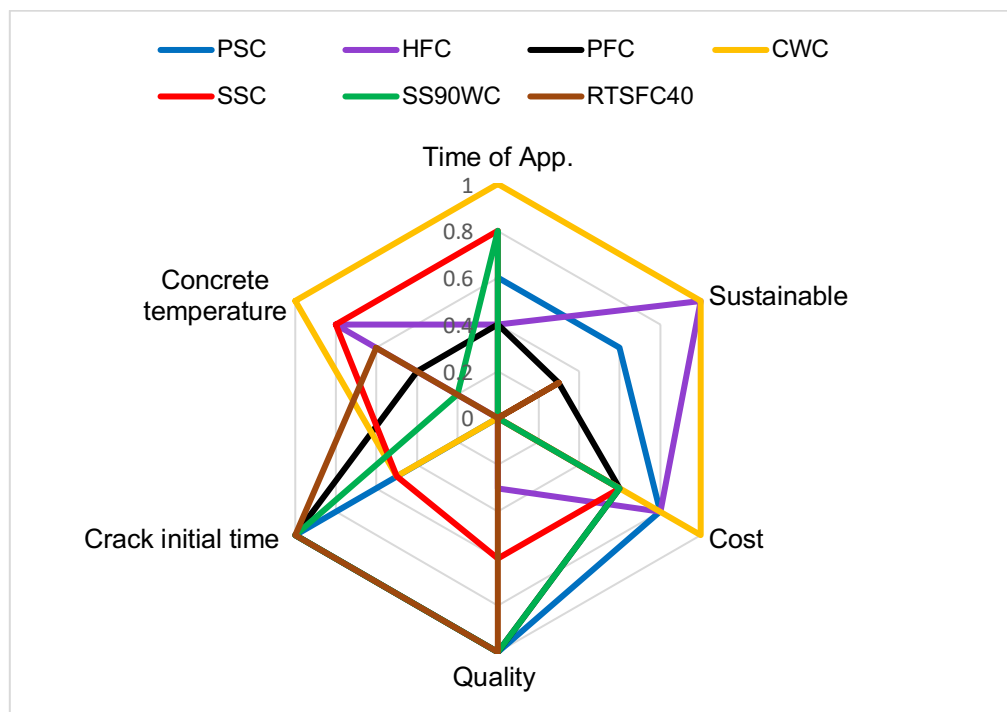


Figure 5.10: Comparison between concrete curing methods

## 5.4. Conclusion

This paper presents an experimental work on various concrete curing methods to restrain plastic shrinkage cracking, and it compares them in terms of the cost, time of application, sustainability, quality, crack initiation and temperature. Plastic shrinkage is determined according to ASTM C1579 under controlled environmental conditions. From the findings, the following conclusions can be drawn:

- The ASTM evaporation rates are similar for all the specimens and are affected by the initial water pan temperature, while the Menzel's formula evaporation rates increase with an increase in the concrete temperature.
- All the concrete curing methods are successful to some extent in restraining plastic shrinkage cracking.
- Covering concrete with plastic sheets (PSC) prevents the evaporation of the bleed water and eliminates plastic shrinkage cracks, albeit at the expense of increased temperatures,

while covering concrete with wet hessian fabric (HFC) decreases plastic shrinkage cracks and keeps the concrete temperature down.

- The power floating concrete curing method (PFC) reduces or eliminates cracks, although it takes time to apply and increases the concrete temperature.
- Cold water concrete (CWC) gives the best overall relative efficiency score but does not eliminate cracking, so it is recommended as a supplementary method in hot climates.
- Both curing methods (SSC and SS90WC) used in this study prevent and reduce plastic shrinkage cracks but affect the concrete temperature negatively.
- Recycled tire steel fibres (RTSFC40) eliminate plastic shrinkage cracking, but due to their cost, they are not recommended just for plastic shrinkage control, but it can also control the long-term cracks and it is often used as structural reinforcement.

The use of CWC shows a reduction in the concrete temperature but does not prevent plastic shrinkage cracks. On the other hand, PSC and RTSFC40 eliminate completely concrete cracks on the surface of the concrete, although they increase the concrete temperature. Therefore, combining two concrete curing methods may be necessary to obtain the best performance of the concrete curing methods, for example, CWC with PSC or RTSFC40.

Future work on real-scale applications could provide more representative data in terms of the cost, quality and time of application. The synergistic effect of two or more curing methods should be explored to optimize the structural performance and environmental impact.



## 5.5. References

- [1] R. Combrinck, L. Steyl, W.P. Boshoff, Influence of concrete depth and surface finishing on the cracking of plastic concrete, *Constr. Build. Mater.* 175 (2018) 621–628. <https://doi.org/10.1016/j.conbuildmat.2018.04.225>.
- [2] F. Matakah, Y. Jaradat, P. Soroushian, Plastic shrinkage cracking and bleeding of concrete prepared with alkali activated cement, *Heliyon.* 5 (2019) e01514. <https://doi.org/10.1016/j.heliyon.2019.e01514>.
- [3] F.U.A. Shaikh, Effect of Cracking on Corrosion of Steel in Concrete, *Int. J. Concr. Struct. Mater.* 12 (2018). <https://doi.org/10.1186/s40069-018-0234-y>.
- [4] M. Nasir, I.A. Syed, U. Gazder, M. Maslehuddin, O.S. Baghabra, Prediction of Properties of Concrete Cured Under Hot Weather Using Multivariate Regression and ANN Models, *Arab. J. Sci. Eng.* 45 (2020) 4111–4123. <https://doi.org/10.1007/s13369-020-04403-y>.
- [5] ASTM C192/C192M, Standard Practice for Making and Curing Concrete Test Specimens in the Laboratory, *Am. Soc. Test. Mater.* (2016) 1–8. <https://doi.org/10.1520/C0192>.
- [6] ASTM C1579, Standard Test Method for Evaluating Plastic Shrinkage Cracking of Restrained Fiber Reinforced Concrete, *Annu. B. ASTM Stand.* i (2006) 1–7. <https://doi.org/10.1520/C1579-06.2>.
- [7] M. Safiuddin, A.B.M.A. Kaish, C.O. Woon, S.N. Raman, Early-age cracking in concrete: Causes, consequences, remedial measures, and recommendations, *Appl. Sci.* 8 (2018). <https://doi.org/10.3390/app8101730>.
- [8] G. De Schutter, L. Taerwe, Specific heat and thermal diffusivity of hardening concrete, *Mag. Concr. Res.* 47 (1995) 203–208.
- [9] G.M. Moelich, J.E. van Zyl, N. Rabie, R. Combrinck, The influence of solar radiation on plastic shrinkage cracking in concrete, *Cem. Concr. Compos.* 123 (2021) 104182. <https://doi.org/10.1016/j.cemconcomp.2021.104182>.
- [10] G. Naaman, A.E., Wongtanakitcharoen, T. and Hauser, Influence of different fibers on plastic shrinkage cracking of concrete, *ACI Mater. J.* 102 (2005) 49.
- [11] M. Nasir, O.S. Baghabra Al-Amoudi, M. Maslehuddin, Effect of placement temperature and curing method on plastic shrinkage of plain and pozzolanic cement concretes under hot weather, *Constr. Build. Mater.* 152 (2017) 943–953. <https://doi.org/10.1016/j.conbuildmat.2017.07.068>.

- [12] O.S.B. Al-Amoudi, M. Maslehuddin, M. Shameem, M. Ibrahim, Shrinkage of plain and silica fume cement concrete under hot weather, *Cem. Concr. Compos.* 29 (2007) 690–699. <https://doi.org/10.1016/j.cemconcomp.2007.05.006>.
- [13] ACI 224R-01, Control of Cracking in Concrete Structures Reported by ACI Committee 224. ACI 224R-01, *ACI Comm.* 224R-01. (2001) 1–46.
- [14] S. Jacobsen, G.W. Scherer, E.M. Schulson, Concrete-ice abrasion mechanics, *Cem. Concr. Res.* 73 (2015) 79–95. <https://doi.org/10.1016/j.cemconres.2015.01.001>.
- [15] T. Xie, C. Fang, M.S. Mohamad Ali, P. Visintin, Characterizations of autogenous and drying shrinkage of ultra-high performance concrete (UHPC): An experimental study, *Cem. Concr. Compos.* 91 (2018) 156–173. <https://doi.org/10.1016/j.cemconcomp.2018.05.009>.
- [16] P. min Zhan, Z. hai He, Application of shrinkage reducing admixture in concrete: A review, *Constr. Build. Mater.* 201 (2019) 676–690. <https://doi.org/10.1016/j.conbuildmat.2018.12.209>.
- [17] C. Shah, S. P., Marikunte, S., Yang, W., & Aldea, Control of Cracking with Shrinkage-Reducing Admixtures, *Transp. Res. Rec.* 1574 (1997) 25–36.
- [18] B. Pease, H. Shah, J. Weiss, Shrinkage behavior and residual stress development in mortar containing Shrinkage Reducing Admixtures (SRAs), *Am. Concr. Institute, ACI Spec. Publ. SP-227* (2005) 285–302. <https://doi.org/10.14359/14435>.
- [19] J.G. Cabrera, A.R. Cusens, Y. Brookes-Wang, Effect of superplasticizers on the plastic shrinkage of concrete, *Mag. Concr. Res.* 44 (1992) 149–155. <https://doi.org/10.1680/mac.1992.44.160.149>.
- [20] R. Combrinck, M. Kayondo, B.D. le Roux, W.I. de Villiers, W.P. Boshoff, Effect of various liquid admixtures on cracking of plastic concrete, *Constr. Build. Mater.* 202 (2019) 139–153. <https://doi.org/10.1016/j.conbuildmat.2018.12.060>.
- [21] T. Alshammari, K. Pilakoutas, M. Guadagnini, Performance of Manufactured and Recycled Steel Fibres in Restraining Concrete Plastic Shrinkage Cracks, *Materials (Basel)*. 16 (2023) 713. <https://doi.org/10.2139/ssrn.4232808>.
- [22] C. Banthia, N. and Yan, Shrinkage cracking in polyolefin fiber-reinforced concrete., *Mater. J.* 97 (2000) 432–437.
- [23] I.M.G. Bertelsen, L.M. Ottosen, G. Fischer, Influence of fibre characteristics on plastic shrinkage cracking in cement-based materials: A review, *Constr. Build. Mater.* (2020). <https://doi.org/10.1016/j.conbuildmat.2019.116769>.
- [24] N. Banthia, R. Gupta, Influence of polypropylene fiber geometry on plastic shrinkage

- cracking in concrete, *Cem. Concr. Res.* 36 (2006) 1263–1267.  
<https://doi.org/10.1016/j.cemconres.2006.01.010>.
- [25] B.S. Al-Tulaian, M.J. Al-Shannag, A.R. Al-Hozaimy, Recycled plastic waste fibers for reinforcing Portland cement mortar, *Constr. Build. Mater.* 127 (2016) 102–110.  
<https://doi.org/10.1016/j.conbuildmat.2016.09.131>.
- [26] A. Sivakumar, M. Santhanam, A quantitative study on the plastic shrinkage cracking in high strength hybrid fibre reinforced concrete, *Cem. Concr. Compos.* 29 (2007) 575–581. <https://doi.org/10.1016/j.cemconcomp.2007.03.005>.
- [27] H. Hu, P. Papastergiou, H. Angelakopoulos, M. Guadagnini, K. Pilakoutas, Mechanical properties of SFRC using blended Recycled Tyre Steel Cords (RTSC) and Recycled Tyre Steel Fibres (RTSF), *Constr. Build. Mater.* 187 (2018) 553–564.  
<https://doi.org/10.1016/j.conbuildmat.2018.07.206>.
- [28] ASTM C136-01, ASTM C136-01 Standard Test Method for Sieve Analysis of Fine and Coarse Aggregates, *Annu. B. ASTM Stand.* 13 (2005) 85–86.
- [29] P.J. Uno, Plastic shrinkage cracking and evaporation formulas, *ACI Mater. J.* 95 (1998) 365–375. <https://doi.org/10.14359/379>.
- [30] L. Liu, C. Zhu, C. Qi, M. Wang, C. Huan, B. Zhang, K.I.I.L. Song, Effects of curing time and ice-to-water ratio on performance of cemented paste backfill containing ice slag, *Constr. Build. Mater.* 228 (2019) 116639.  
<https://doi.org/10.1016/j.conbuildmat.2019.08.020>.
- [31] ASTM C 309, Standard Specification for Liquid Membrane-Forming Compounds for Curing Concrete 1, *Astm.* 06 (2015) 8–10.
- [32] BS 7542, Method of test for Curing compounds for concrete, *Br. Stand. Inst.* (1992).
- [33] T.O. Alshammari, M. Guadagnini, K. Pilakoutas, The Effect of Harsh Environmental Conditions on Concrete Plastic Shrinkage Cracks: Case Study Saudi Arabia, *Materials (Basel)*. 15 (2022). <https://doi.org/10.3390/ma15238622>.
- [34] M.N. Isa, K. Pilakoutas, M. Guadagnini, Determination of tensile characteristics and design of eco-efficient UHPC, *Structures.* 32 (2021) 2174–2194.  
<https://doi.org/10.1016/j.istruc.2021.03.114>.
- [35] W.J. McCarter, A.M. Ben-Saleh, Influence of practical curing methods on evaporation of water from freshly placed concrete in hot climates, *Build. Environ.* 36 (2001) 919–924. [https://doi.org/10.1016/S0360-1323\(00\)00048-2](https://doi.org/10.1016/S0360-1323(00)00048-2).
- [36] M. Maslehuddin, M. Ibrahim, M. Shameem, M.R. Ali, M.H. Al-Mehthel, Effect of curing methods on shrinkage and corrosion resistance of concrete, *Constr. Build.*

- Mater. 41 (2013) 634–641. <https://doi.org/10.1016/j.conbuildmat.2012.12.064>.
- [37] Y. Shen, Y. Lv, H. Yang, W. Ma, L. Zhang, J. Pan, Effect of different ice contents on heat transfer and mechanical properties of concrete, *Cold Reg. Sci. Technol.* 199 (2022) 103570. <https://doi.org/10.1016/j.coldregions.2022.103570>.
- [38] B. Nabil, A. Aissa, B.I. Aguida, Use of a new approach (design of experiments method) to study different procedures to avoid plastic shrinkage cracking of concrete in hot climates, *J. Adv. Concr. Technol.* 9 (2011) 149–157. <https://doi.org/10.3151/jact.9.149>.
- [39] H. Nassif, N. Suksawang, M. Mohammed, Effect of Curing Methods on Early-Age and Drying Shrinkage of High-Performance Concrete, *Transp. Res. Rec.* (2003) 48–58. <https://doi.org/10.3141/1834-07>.
- [40] K. Kori, S.S. Goliya, Use of Discrete fiber in road pavement, *Mater. Today Proc.* (2022) 1–5. <https://doi.org/10.1016/j.matpr.2022.05.042>.
- [41] J. Saliba, E. Rozière, F. Grondin, A. Loukili, Influence of shrinkage-reducing admixtures on plastic and long-term shrinkage, *Cem. Concr. Compos.* 33 (2011) 209–217. <https://doi.org/10.1016/j.cemconcomp.2010.10.006>.
- [42] A. Leemann, P. Nygaard, P. Lura, Impact of admixtures on the plastic shrinkage cracking of self-compacting concrete, *Cem. Concr. Compos.* 46 (2014) 1–7. <https://doi.org/10.1016/j.cemconcomp.2013.11.002>.
- [43] R. Combrinck, W.P. Boshoff, Typical plastic shrinkage cracking behaviour of concrete, *Mag. Concr. Res.* 65 (2013) 486–493. <https://doi.org/10.1680/mac.12.00139>.
- [44] Ö. Eren, K. Marar, Effect of steel fibers on plastic shrinkage cracking of normal and high strength concretes, *Mater. Res.* 13 (2010) 135–141. <https://doi.org/10.1590/S1516-14392010000200004>.

**This page is intentionally left blank**

## **Chapter 6 : Conclusions and Recommendations for Future Work**

This chapter introduces the main conclusions of each chapter of this thesis and recommendations for future work.

## 6.1. Conclusions

The aim of this research was to investigate the plastic shrinkage behaviour of concrete exposed to different environmental conditions and examine the impact of steel fibre, different curing methods and other mitigation strategies on restraining plastic shrinkage cracking. Based on the results reported in previous work, the main conclusions of the various phases of the project are summarised in the following sections.

### 6.1.1. Performance of RTSF and MSF in restraining plastic shrinkage cracking (Chapter 3).

The potential of different dosages of RTSF, and MSF (0, 10, 20, 30 kg/m<sup>3</sup>) in concrete to restrain plastic shrinkage cracking was examined under different environmental conditions (temperature 36±3 °C, relative humidity 30±10% and a wind speed of 5 m/s).

- Both RTSF and MSF were effective in reducing plastic shrinkage cracking at all tested dosages, but overall RTSF outperformed MSF. The better performance of RTSF is attributed to their larger number and better distribution within the concrete volume.
- RTSF led to substantial reductions in plastic shrinkage crack width, with measured CRR values of 42%, 75%, and 100% for fibre dosages of 10 kg/m<sup>3</sup> ( $V_f = 0.13\%$ ), 20 kg/m<sup>3</sup> ( $V_f = 0.26\%$ ), and 30 kg/m<sup>3</sup> ( $V_f = 0.38\%$ ), respectively.
- The use of 30 kg/m<sup>3</sup> of RTSF showed the best performance and eliminated cracking completely under the examined environmental conditions.

### 6.1.2. The Effect of Harsh Environmental Conditions on Concrete Plastic Shrinkage Cracks: Case Study Saudi Arabia (Chapter 4).

The effect of different environmental conditions of temperature (28, 36, and 45 °C) and wind speed (3, 4.7, and 7 m/s), typical of Saudi Arabia, water to cement ratios (0.5, 0.55, and 0.6), and RTSF fibre dosages (30, and 40 kg/m<sup>3</sup>) on plastic shrinkage were examined.

- Harsher environmental conditions (temperature, and wind speed), and high water to cement ratios were found a result of earlier and more severe cracking (i.e., larger crack width, length, and area).
- Temperature is the most important parameter of the environmental conditions in accelerating cracking as found with increasing temperature, the cracking starts earlier, and the eventual crack width is wider whilst wind speed is the least significant.

- The use of higher water/cement ratios increases cracking, primarily as a result of earlier and heavier bleeding.
- The addition of RTSF fibres (30 kg/m<sup>3</sup>) was found to be effective in controlling plastic shrinkage cracking to the low and medium of different environmental conditions, with (40 kg/m<sup>3</sup>) eliminating the cracks completely in the harshest of the examined environments.

### 6.1.3. Effect of various curing methods on plastic shrinkage cracking (Chapter 5).

The effect of different curing methods and other strategies to control plastic shrinkage cracking was investigated. Typical curing methods were assessed such as covering concrete (plastic sheets, and wet-hessian fabric), power floating concrete, curing admixtures, and along with the use of cold water in the mix and recycled tyre steel fibre (RTSF) at 40 kg/m<sup>3</sup>.

- Based on the analysis of different criteria, including cost, time of application, sustainability, quality, crack initiation, and concrete temperature, the examined curing methods can be ranked as following (from the most effective to the least), (1- Cold water, 2- Plastic sheets, 3- Power floating, 4- Wet-hessian fabric, and Safecure Super 90w-10%, 5- Safecure Super, 6- Recycled tyre steel fibres)
- Covering concrete with plastic sheets (PSC) prevents evaporation of the bleed water, and eliminates plastic shrinkage cracks, but at the expense of increased concrete temperature.
- Covering concrete with wet-hessian fabric (HFC) can effectively decreases plastic shrinkage cracks, while also keeping concrete temperature down.
- Power floating concrete (PFC) can reduce or eliminate cracks, but it requires a considerable amount of time for the application and increases concrete temperature slightly.
- Cold water concrete (CWC) gives the best overall relative efficiency score but does not eliminate cracking, so it is recommended as a supplementary method in hot climates.
- Both shrinkage reducing methods (SSC and SS90WC) used in this study reduced or prevented plastic shrinkage cracks but affected concrete temperature negatively.
- The use of 40 kg/m<sup>3</sup> of recycled tyre steel fibres (RTSFC40) was found to eliminate plastic shrinkage cracking. The high cost of fibres, compared to the other commonly used mitigation techniques, makes RTSF less attractive for plastic shrinkage control only applications. However, the use of RTSF can lead to cost effective solutions when



used as structural reinforcement, also in combination with reinforcing bars, as it can effectively improve long-term performance and control structural and non- structural cracks.

## **6.2. Recommendations for Future Work**

This section provides recommendations for future research to examine the problems that have not been addressed during this research due to limited time and resources.

### **6.2.1. Fibre length distribution and hybrid blends**

- Different RTSF lengths distributions should be examined to optimize the performance of the RTSFC at both plastic and hardened state.
- The use of fibre blends including RTSF and polymeric synthetic fibres could further improve the resistance to plastic shrinkage cracking. Polymeric synthetic fibre can reduce bleeding water at the concrete surface, while RTSF can reduce the width of plastic shrinkage cracks.
- The effect of natural fibres to restrain plastic shrinkage cracking (e.g.) jute, sugarcane, vegetables, and banana fibre, could be examined.

### **6.2.2. Modifications to the plastic shrinkage cracking test**

- The evaporation rates could be measured directly from the concrete slab during the test, by placing the specimens directly on a suitable scale or load cell and monitoring their weight loss.
- The evolution of capillary pressure could be monitored through the use of sensors (e.g. electric pressure sensors).
- Examine the effect of top steel reinforcement on plastic shrinkage cracks.
- Examine plastic shrinkage behaviour in cold environmental conditions in terms of high wind speed with low temperature.

### **6.2.3. Concrete curing methods**

- The effect of the various curing methods on concrete performance (i.e. compressive and tensile strength) could be investigated.
- The synergistic effect of two or more curing methods could be explored to optimize structural performance and environmental impact.
- The effect of different curing methods for cold weather concreting could be assessed.

- A more detailed assessment of curing methods could be carried out on real scale applications so as to yield to more representative data in terms of cost, quality and time of application.

**This page is intentionally left blank**

## **Appendix A**

### **Chapter 2: Literature review**

This appendix presents additional information, images on the plastic shrinkage testing techniques, and the materials properties and tests of chapter 2.

**A.1 Particle size****A.1.1 Fine aggregate****Table A.1** Fine aggregate sieve analysis.

<b>Sieve Size</b>	<b>Sample retained</b>	<b>% Retained</b>	<b>% Cumulative retained</b>	<b>% Finer</b>
<b>10 mm</b>	0	0	0	100
<b>8 mm</b>	0	0	0	100
<b>6.3 mm</b>	0	0	0	100
<b>4 mm</b>	175.3	7	7	93
<b>2.8 mm</b>	548.9	21.95	28.95	71
<b>2 mm</b>	500	20	48.95	51.41
<b>1 mm</b>	665	26.6	56	75.55
<b>0.5 mm</b>	562	22.5	95.48	27
<b>0.25</b>	37	1.48	96.96	3
<b>0.125</b>	4	0.16	97.12	2.9
<b>Pan</b>	2	0.08	97.2	0.10%
			<b>Fineness Modulus = 5.28</b>	

### A.1.2 Coarse aggregate 10 mm size

**Table A.2** Coarse aggregate 10 mm size sieve analysis.

<b>Sieve Size</b>	<b>Sample retained</b>	<b>% Retained</b>	<b>% Cumulative retained</b>	<b>% Finer</b>
<b>40 mm</b>	0	0	0	100
<b>31.5 mm</b>	0	0	0	100
<b>20 mm</b>	0	0	0	100
<b>14 mm</b>	0	0	0	100
<b>10 mm</b>	300	12	12	88
<b>4 mm</b>	2187	87.48	99.48	1
<b>2 mm</b>	13	0.52	100	0
<b>Pan</b>	0	0	100	0.10%
			<b>Fineness Modulus = 2.12</b>	

### A.1.3 Coarse aggregate 20 mm size

**Table A.3** Coarse aggregate 20 mm size sieve analysis.

<b>Sieve Size</b>	<b>Sample retained</b>	<b>% Retained</b>	<b>% Cumulative retained</b>	<b>% Finer</b>
<b>31.5 mm</b>	0	0	0	100
<b>20 mm</b>	359.7	14.388	14.388	85.612
<b>14 mm</b>	1119.8	44.792	59.18	40.82
<b>10 mm</b>	853.3	34.132	93.312	6.688
<b>4 mm</b>	160.2	6.408	99.72	0.28
<b>2 mm</b>	2.7	0.108	99.828	0.172
<b>Pan</b>	1.9	0.076	99.904	0.10%
			<b>Fineness Modulus = 3.66</b>	

## **A.2 Admixture**

### **A.2.1 High-range Water Reducing Admixture – Sika ViscoCrete Summary Data Sheet**



Construction

**Product Data Sheet**  
Edition 12/07/2016  
Identification no:  
02 13 01 01 100 0 000409  
Sika® ViscoCrete® 30HE (UK)


CE

## Sika® ViscoCrete® 30HE (UK)

### Accelerating High Range Water Reducing/Superplasticising Concrete Admixture

---

<b>Product Description</b>	Sika® ViscoCrete® 30HE (UK) is a liquid admixture for concrete which is used as an accelerating high range water reducer or superplasticiser. It meets the requirements of BS EN 934-2.
<b>Uses</b>	<p>Sika® ViscoCrete® 30HE (UK) has been specifically formulated for the production of concrete mixes which require high early strength development, powerful water reduction and excellent flowability.</p> <ul style="list-style-type: none"> <li>■ Precast concrete</li> <li>■ Fast track concrete</li> <li>■ Self compacting concrete</li> </ul>
<b>Characteristics / Advantages</b>	<ul style="list-style-type: none"> <li>■ Significantly increased early age strength</li> <li>■ Excellent water reduction</li> <li>■ Excellent flowability</li> <li>■ Reduced drying shrinkage</li> <li>■ Improved surface finish</li> </ul>
<b>Tests</b>	
<b>Approvals / Standards</b>	Conforms to the requirements of BS EN 934-2 Tables 3.1 & 3.2 DoP 02 13 01 01 100 0 000422 1088, certified by Factory Production Control Body 0086, Certificate 541325, and provided with the CE mark
<b>Product Data</b>	
<b>Form</b>	
<b>Appearance / Colour</b>	Light Brown Liquid
<b>Packaging</b>	25 litre drum and 1000 litre IBC
<b>Storage</b>	
<b>Storage Conditions / Shelf-Life</b>	12 months from date of production if stored in unopened and undamaged original sealed containers protected from moisture at temperatures between +5°C and +25°C.



1/3

Sika® ViscoCrete® 30HE (UK)

<b>Technical Data</b>	
Chemical Base	Modified Polycarboxylate
Density	1.06 kg/litre
pH Value	4.4 ± 1.0
Water Soluble Chloride Content	<0.1% w/w (chloride free)
Alkali Content	< 0.40%
<b>System Information</b>	
<b>Application Details</b>	
Consumption / Dosage	<ul style="list-style-type: none"> <li>■ 0.2 - 0.8% by weight of cement (medium workability)</li> <li>■ 1.0 – 2.0% by weight of cement (high workability/SCC)</li> </ul>
Dispensing	<ul style="list-style-type: none"> <li>■ Sika®ViscoCrete® 30HE (UK) should be dispensed through suitable calibrated equipment</li> </ul>
Application Conditions / Limitations	<ul style="list-style-type: none"> <li>■ Sika®ViscoCrete® 30HE (UK) should not be added to dry cement</li> <li>■ Sika®ViscoCrete® 30HE (UK) should be added with the mixing water</li> </ul>
Compatibility	<p>Sika®Admixtures:</p> <ul style="list-style-type: none"> <li>■ Compatibility information available on request</li> </ul> <p>Cements:</p> <ul style="list-style-type: none"> <li>■ All cement combinations</li> </ul>
Notes on Application / Limitations	Support from our Technical Service Department is recommended.
Value Base	All technical data stated in this Product Data Sheet are based on laboratory tests. Actual measured data may vary due to circumstances beyond our control.
Local Restrictions	Please note that as a result of specific local regulations the performance of this product may vary from country to country. Please consult the local Product Data Sheet for the exact description of the application fields.
Health and Safety Information	For information and advice on the safe handling, storage and disposal of chemical products, users shall refer to the most recent Material Safety Data Sheet containing physical, ecological, toxicological and other safety-related data.
Legal Notes	The information, and, in particular, the recommendations relating to the application and end-use of Sika products, are given in good faith based on Sika's current knowledge and experience of the products when properly stored, handled and applied under normal conditions in accordance with Sika's recommendations. In practice, the differences in materials, substrates and actual site conditions are such that no warranty in respect of merchantability or of fitness for a particular purpose, nor any liability arising out of any legal relationship whatsoever, can be inferred either from this information, or from any written recommendations, or from any other advice offered. The user of the product must test the product's suitability for the intended application and purpose. Sika reserves the right to change the properties of its products. The proprietary rights of third parties must be observed. All orders are accepted subject to our current terms of sale and delivery. Users must always refer to the most recent issue of the local Product Data Sheet for the product concerned, copies of which will be supplied on request.

### A.3 The MATLAB script developed to determine the crack area is presented in this section.

```
%% read image
I = imread('RTSFPC.jpeg');
figure, imshow(I);
title('a. Original Image');


---


%% convert RGB image to grayscale image
Igray = rgb2gray(I);
figure, imshow(Igray);
title('b. Grayscale image');


---


%% convert grayscale image to binary image
level = 0.3;
Ithres = im2bw(Igray, level);
figure, imshow(Ithres);
title('c. Binary Image');


---


%% image morphological operation
Icomp = imcomplement(Ithres);
Iclean = bwareaopen(Icomp, 8);
figure, imshow(Iclean);
title('d. Cleaned Image');


---


%% calculate crack area
CrackPixels = bwarea(Iclean);
CalibrationArea = 50; % mm2
CalibrationPixels = 14613;
CrackArea = CrackPixels*CalibrationArea/CalibrationPixels; % mm2
```

**This page is intentionally left blank**

## **Appendix B:**

### **Chapter 3: Performance of Manufactured and Recycled Steel Fibres in Restraining Concrete Plastic Shrinkage.**

This appendix presents additional information regarding the results found in Chapter 3.

**B.1 Environmental conditions and evaporation rate****B.1.1 RTSFC10****Table B.1** RTSFC10 environmental conditions and evaporation rate.

<b>Time (hr)</b>	<b>Temp. (°C)</b>	<b>Wind speed (m/s)</b>	<b>RH (%)</b>	<b>PC water pan (g)</b>	<b>PC Eva. rate (kg/m<sup>2</sup>/h)</b>	<b>RTSFC10 water pan (g)</b>	<b>RTSFC10 Eva. rate (kg/m<sup>2</sup>/h)</b>
<b>0</b>	22.2	0	45	501	-	506	-
<b>1</b>	32	5	21	481	1.11	485	1.10
<b>2</b>	34.1	5	20	460	1.16	463	1.11
<b>3</b>	34.8	5	20	438	1.21	440	1.16
<b>4</b>	35	5	20	415	1.26	416	1.21
<b>5</b>	36.3	5	20	391	1.37	390	1.26
<b>6</b>	36.9	5	20	365	1.42	363	1.40

**B.1.2 RTSFC20****Table B.2** RTSFC20 environmental conditions and evaporation rate.

<b>Time (hr)</b>	<b>Temp. (°C)</b>	<b>Wind speed (m/s)</b>	<b>RH (%)</b>	<b>PC water pan (g)</b>	<b>PC Eva. rate (kg/m<sup>2</sup>/h)</b>	<b>RTSFC20 water pan (g)</b>	<b>RTSFC20 Eva. rate (kg/m<sup>2</sup>/h)</b>
<b>0</b>	21.8	0	46	504	-	506	-
<b>1</b>	30.3	5	28	483	1.10	484	1.10
<b>2</b>	33.9	5	22	461	1.16	461	1.14
<b>3</b>	34	5	20	438	1.30	437	1.21
<b>4</b>	35.3	5	20	414	1.40	412	1.30
<b>5</b>	36.3	5	20	389	1.40	386	1.40
<b>6</b>	37	5	20	363	1.45	359	1.42

**B.1.3 RTSFC30****Table B.3** RTSFC30 environmental conditions and evaporation rate.

<b>Time (hr)</b>	<b>Temp. (°C)</b>	<b>Wind speed (m/s)</b>	<b>RH (%)</b>	<b>PC water pan (g)</b>	<b>PC Eva. rate (kg/m<sup>2</sup>/h)</b>	<b>RTSFC30 water pan (g)</b>	<b>RTSFC30 Eva. rate (kg/m<sup>2</sup>/h)</b>
<b>0</b>	24.9	0	41	500	-	508	-
<b>1</b>	33.8	5	20	479	1.21	485	1.11
<b>2</b>	35.8	5	20	456	1.37	459	1.21
<b>3</b>	36.4	5	20	430	1.53	430	1.37
<b>4</b>	37.4	5	20	402	1.68	398	1.48
<b>5</b>	38.6	5	20	371	1.74	365	1.63
<b>6</b>	39.4	5	20	338	1.84	330	1.74

**B.1.4 MSFC10****Table B.4** MSFC10 environmental conditions and evaporation rate.

<b>Time (hr)</b>	<b>Temp. (°C)</b>	<b>Wind speed (m/s)</b>	<b>RH (%)</b>	<b>PC water pan (g)</b>	<b>PC Eva. rate (kg/m<sup>2</sup>/h)</b>	<b>MSFC10 water pan (g)</b>	<b>MSFC10 Eva. rate (kg/m<sup>2</sup>/h)</b>
<b>0</b>	21.2	0	44	508	-	509	-
<b>1</b>	31.5	5	21	489	1.11	488	1.0
<b>2</b>	34.3	5	20	468	1.16	466	1.11
<b>3</b>	35	5	20	445	1.21	443	1.19
<b>4</b>	35.9	5	20	420	1.32	418	1.31
<b>5</b>	36.5	5	20	393	1.36	391	1.35
<b>6</b>	37.2	5	20	363	1.46	360	1.43

**B.1.5 MSFC20****Table B.5** MSFC20 environmental conditions and evaporation rate.

<b>Time (hr)</b>	<b>Temp. (°C)</b>	<b>Wind speed (m/s)</b>	<b>RH (%)</b>	<b>PC water pan (g)</b>	<b>PC Eva. rate (kg/m<sup>2</sup>/h)</b>	<b>MSFC20 water pan (g)</b>	<b>MSFC20 Eva. rate (kg/m<sup>2</sup>/h)</b>
0	21.4	0	43	505	-	503	-
1	31.2	5	21	484	1.16	481	1.11
2	34.3	5	20	462	1.21	458	1.16
3	35.1	5	20	439	1.26	434	1.24
4	35.8	5	20	413	1.37	408	1.34
5	36.4	5	20	385	1.40	380	1.39
6	37.7	5	20	355	1.48	350	1.45

**B.1.5 MSFC30****Table B.6** MSFC30 environmental conditions and evaporation rate.

<b>Time (hr)</b>	<b>Temp. (°C)</b>	<b>Wind speed (m/s)</b>	<b>RH (%)</b>	<b>PC water pan (g)</b>	<b>PC Eva. rate (kg/m<sup>2</sup>/h)</b>	<b>MSFC30 water pan (g)</b>	<b>MSFC30 Eva. rate (kg/m<sup>2</sup>/h)</b>
0	24.3	0	41	507	-	500	-
1	32.1	5	21	488	1.10	480	1.10
2	34.6	5	20	467	1.16	458	1.10
3	35.9	5	20	445	1.21	435	1.16
4	36.6	5	20	422	1.32	410	1.21
5	37.1	5	20	398	1.37	384	1.26
6	37.4	5	20	373	1.37	358	1.32



**B.2 Workability****Table B.7** Slump test of all mixes.

<b>Mix ID</b>	<b>PC</b>	<b>Fibre</b>
<b>RTSFC10</b>	140	120
<b>RTSFC20</b>	140	108
<b>RTSFC30</b>	140	95
<b>MSFC10</b>	140	127
<b>MSFC20</b>	140	115
<b>MSFC30</b>	140	104

**B.3 Compressive strength****B.3.1 RTSFC10****Table B.8** RTSFC10 compressive strength at one day.

<b>Batch</b>	<b>Compressive strength (MPa)</b>	<b>Weight of the cube (kg)</b>	<b>Volume of the cube (m<sup>3</sup>)</b>	<b>Density of the cube (kg/m<sup>3</sup>)</b>	<b>Age of curing</b>
RTSFC10 Out	14.56	2.38	100× 100×100	2380	1
RTSFC10 In	15.60	2.24	100× 100×100	2240	1
PC Out	13.74	2.25	100× 100×100	2250	1
PC In	14.01	2.25	100× 100×100	2250	1

**Table B.9** RTSFC10 compressive strength at 28 days curing.

<b>Batch</b>	<b>Compressive strength (MPa)</b>	<b>Weight of the cube (kg)</b>	<b>Volume of the cube (m<sup>3</sup>)</b>	<b>Density of the cube (kg/m<sup>3</sup>)</b>	<b>Age of curing</b>
RTSFC10 Out	34.67	2.24	100× 100×100	2240	28
RTSFC10 In	34.69	2.27	100× 100×100	2270	28
PC Out	34.16	2.26	100× 100×100	2260	28
PC In	34.20	2.25	100× 100×100	2250	28

**B.3.2 RTSFC20****Table B.10** RTSFC20 compressive strength at one day.

<b>Batch</b>	<b>Compressive strength (MPa)</b>	<b>Weight of the cube (kg)</b>	<b>Volume of the cube (m<sup>3</sup>)</b>	<b>Density of the cube (kg/m<sup>3</sup>)</b>	<b>Age of curing</b>
RTSFC20 Out	15.44	2.33	100× 100×100	2330	1
RTSFC20 In	16.80	2.33	100× 100×100	2330	1
PC Out	13.62	2.27	100× 100×100	2270	1
PC In	14.50	2.24	100× 100×100	2240	1

**Table B.11** RTSFC20 compressive strength at 28 days curing.

<b>Batch</b>	<b>Compressive strength (MPa)</b>	<b>Weight of the cube (kg)</b>	<b>Volume of the cube (m<sup>3</sup>)</b>	<b>Density of the cube (kg/m<sup>3</sup>)</b>	<b>Age of curing</b>
RTSFC20 Out	35.40	2.29	100× 100×100	2290	28
RTSFC20 In	35.30	2.31	100× 100×100	2310	28
PC Out	35.18	2.27	100× 100×100	2270	28
PC In	35.08	2.22	100× 100×100	2220	28

**B.3.3 RTSFC30****Table B.12** RTSFC30 compressive strength at one day.

<b>Batch</b>	<b>Compressive strength (MPa)</b>	<b>Weight of the cube (kg)</b>	<b>Volume of the cube (m<sup>3</sup>)</b>	<b>Density of the cube (kg/m<sup>3</sup>)</b>	<b>Age of curing</b>
RTSFC30 Out	16.50	2.38	100× 100×100	2380	1
RTSFC30 In	17.60	2.39	100× 100×100	2390	1
PC Out	15.62	2.21	100× 100×100	2210	1
PC In	14.55	2.20	100× 100×100	2200	1

**Table B.13** RTSFC30 compressive strength at 28 days curing.

<b>Batch</b>	<b>Compressive strength (MPa)</b>	<b>Weight of the cube (kg)</b>	<b>Volume of the cube (m<sup>3</sup>)</b>	<b>Density of the cube (kg/m<sup>3</sup>)</b>	<b>Age of curing</b>
RTSFC30 Out	35.90	2.30	100× 100×100	2230	28
RTSFC30 In	35.75	2.30	100× 100×100	2230	28
PC Out	35.16	2.22	100× 100×100	2200	28
PC In	35.06	2.24	100× 100×100	2240	28

**B.3.4 MSFC10****Table B.14** MSFC10 compressive strength at one day.

<b>Batch</b>	<b>Compressive strength (MPa)</b>	<b>Weight of the cube (kg)</b>	<b>Volume of the cube (m<sup>3</sup>)</b>	<b>Density of the cube (kg/m<sup>3</sup>)</b>	<b>Age of curing</b>
MSFC10 Out	14.22	2.29	100× 100×100	2290	1
MSFC10 In	15.10	2.31	100× 100×100	2310	1
PC Out	13.22	2.25	100× 100×100	2250	1
PC In	13.65	2.25	100× 100×100	2250	1

**Table B.15** MSFC10 compressive strength at 28 days curing.

<b>Batch</b>	<b>Compressive strength (MPa)</b>	<b>Weight of the cube (kg)</b>	<b>Volume of the cube (m<sup>3</sup>)</b>	<b>Density of the cube (kg/m<sup>3</sup>)</b>	<b>Age of curing</b>
MSFC10 Out	35.09	2.27	100× 100×100	2270	28
MSFC10 In	34.73	2.27	100× 100×100	2270	28
PC Out	34.15	2.25	100× 100×100	2250	28
PC In	34.08	2.25	100× 100×100	2250	28

**B.3.5 MSFC20****Table B.16** MSFC20 compressive strength at one day.

<b>Batch</b>	<b>Compressive strength (MPa)</b>	<b>Weight of the cube (kg)</b>	<b>Volume of the cube (m<sup>3</sup>)</b>	<b>Density of the cube (kg/m<sup>3</sup>)</b>	<b>Age of curing</b>
MSFC20 Out	14.22	2.32	100× 100×100	2320	1
MSFC20 In	15.1	2.33	100× 100×100	2330	1
PC Out	13.83	2.25	100× 100×100	2250	1
PC In	14.07	2.29	100× 100×100	2290	1

**Table B.17** MSFC20 compressive strength at 28 days curing.

<b>Batch</b>	<b>Compressive strength (MPa)</b>	<b>Weight of the cube (kg)</b>	<b>Volume of the cube (m<sup>3</sup>)</b>	<b>Density of the cube (kg/m<sup>3</sup>)</b>	<b>Age of curing</b>
MSFC20 Out	35.60	2.29	100× 100×100	2290	28
MSFC20 In	35.30	2.30	100× 100×100	2300	28
PC Out	34.86	2.28	100× 100×100	2280	28
PC In	34.13	2.25	100× 100×100	2500	28

**B.3.6 MSFC30****Table B.18** MSFC30 compressive strength at one day.

<b>Batch</b>	<b>Compressive strength (MPa)</b>	<b>Weight of the cube (kg)</b>	<b>Volume of the cube (m<sup>3</sup>)</b>	<b>Density of the cube (kg/m<sup>3</sup>)</b>	<b>Age of curing</b>
MSFC30 Out	16.50	2.28	100× 100×100	2280	1
MSFC30 In	17.60	2.33	100× 100×100	2330	1
PC Out	13.62	2.23	100× 100×100	2230	1
PC In	14.50	2.24	100× 100×100	2240	1

**Table B.19** MSFC30 compressive strength at 28 days curing.

Batch	Compressive strength (MPa)	Weight of the cube (kg)	Volume of the cube (m <sup>3</sup> )	Density of the cube (kg/m <sup>3</sup> )	Age of curing
MSFC30 Out	35.84	2.24	100× 100×100	2240	28
MSFC30 In	35.70	2.30	100× 100×100	2300	28
PC Out	34.18	2.23	100× 100×100	2230	28
PC In	34.15	2.24	100× 100×100	2240	28

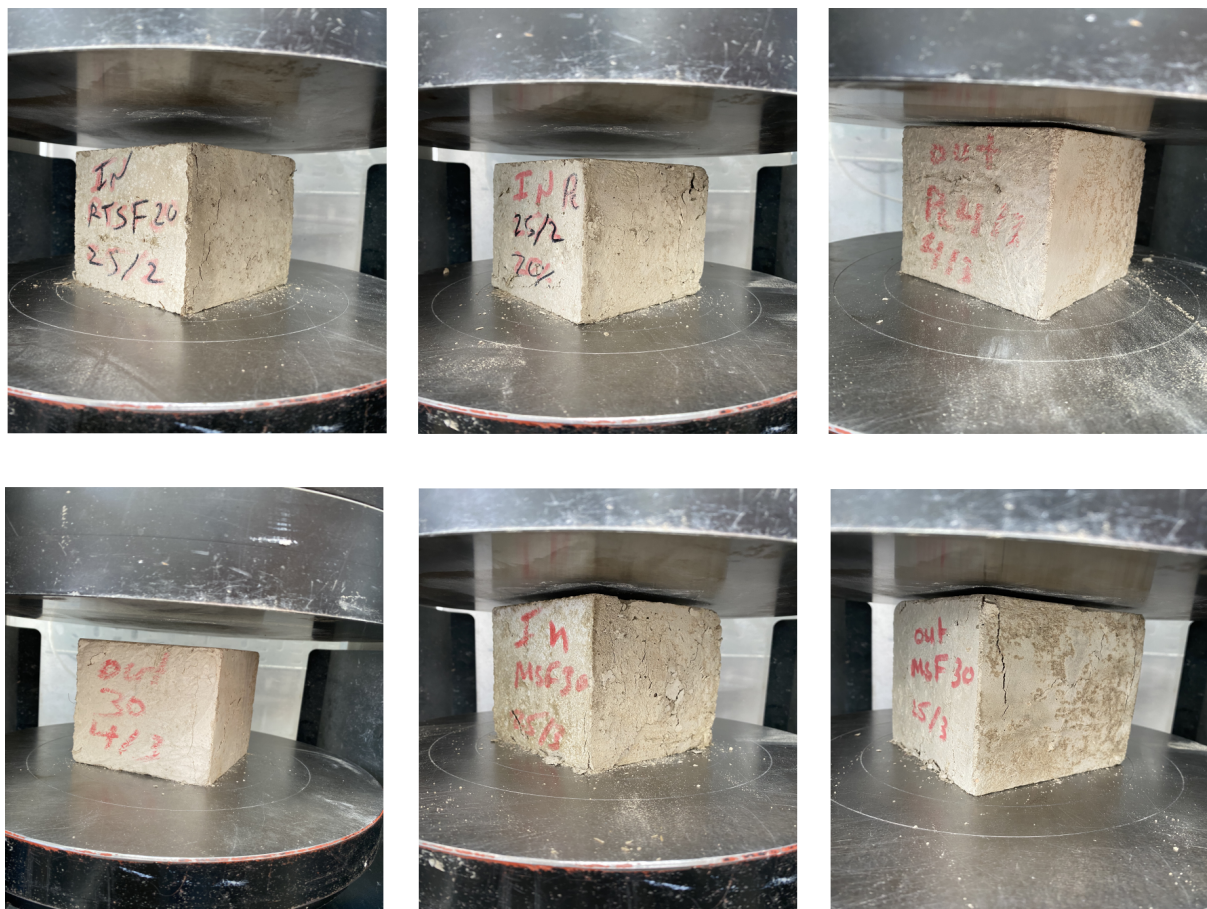


Figure B.1: RTSF and MSF concrete cubes compressive strength test.

## B.4 Crack measurements

### B.4.1 RTSFC10

#### B.4.1.1 MATLAB and IC measure software



Figure B.2: IC crack length at 24 hours of plain concrete.

<input type="checkbox"/>	CrackArea	520.0472
<input type="checkbox"/>	CrackPixels	1.8999e+04
<input type="checkbox"/>	I	3075x1457x3 uint8
<input checked="" type="checkbox"/>	Iclean	3075x1457 logical
<input checked="" type="checkbox"/>	Icomp	3075x1457 logical
<input type="checkbox"/>	Igray	3075x1457 uint8
<input checked="" type="checkbox"/>	Ithres	3075x1457 logical

Figure B.3: MATLAB crack area at 24 hours of plain concrete.

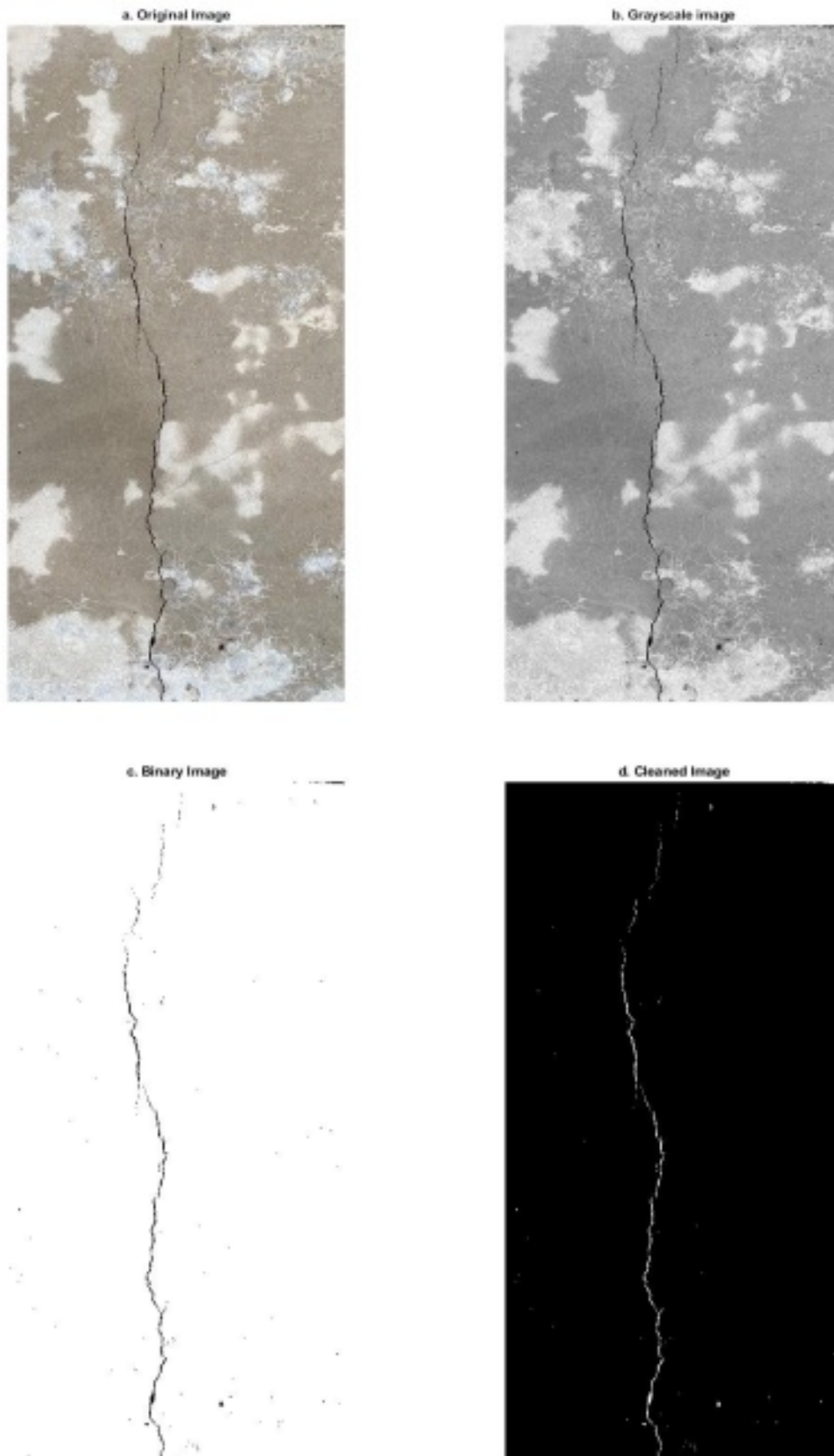


Figure B.4: MATLAB image processing steps for plain concrete.

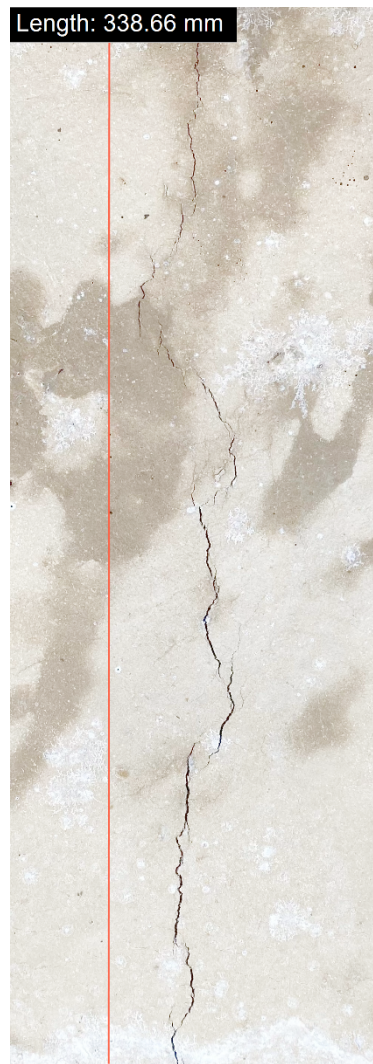


Figure B.5: IC crack length at 24 hours of RTSFC10.

<input type="checkbox"/>	CrackArea	317.2719
<input type="checkbox"/>	CrackPixels	8.4296e+03
<input type="checkbox"/>	I	2851x1002x3 uint8
<input checked="" type="checkbox"/>	Iclean	2851x1002 logical
<input checked="" type="checkbox"/>	Icomp	2851x1002 logical
<input type="checkbox"/>	Igray	2851x1002 uint8
<input checked="" type="checkbox"/>	Ithres	2851x1002 logical

Figure B.6: MATLAB crack area at 24 hours of RTSFC10.



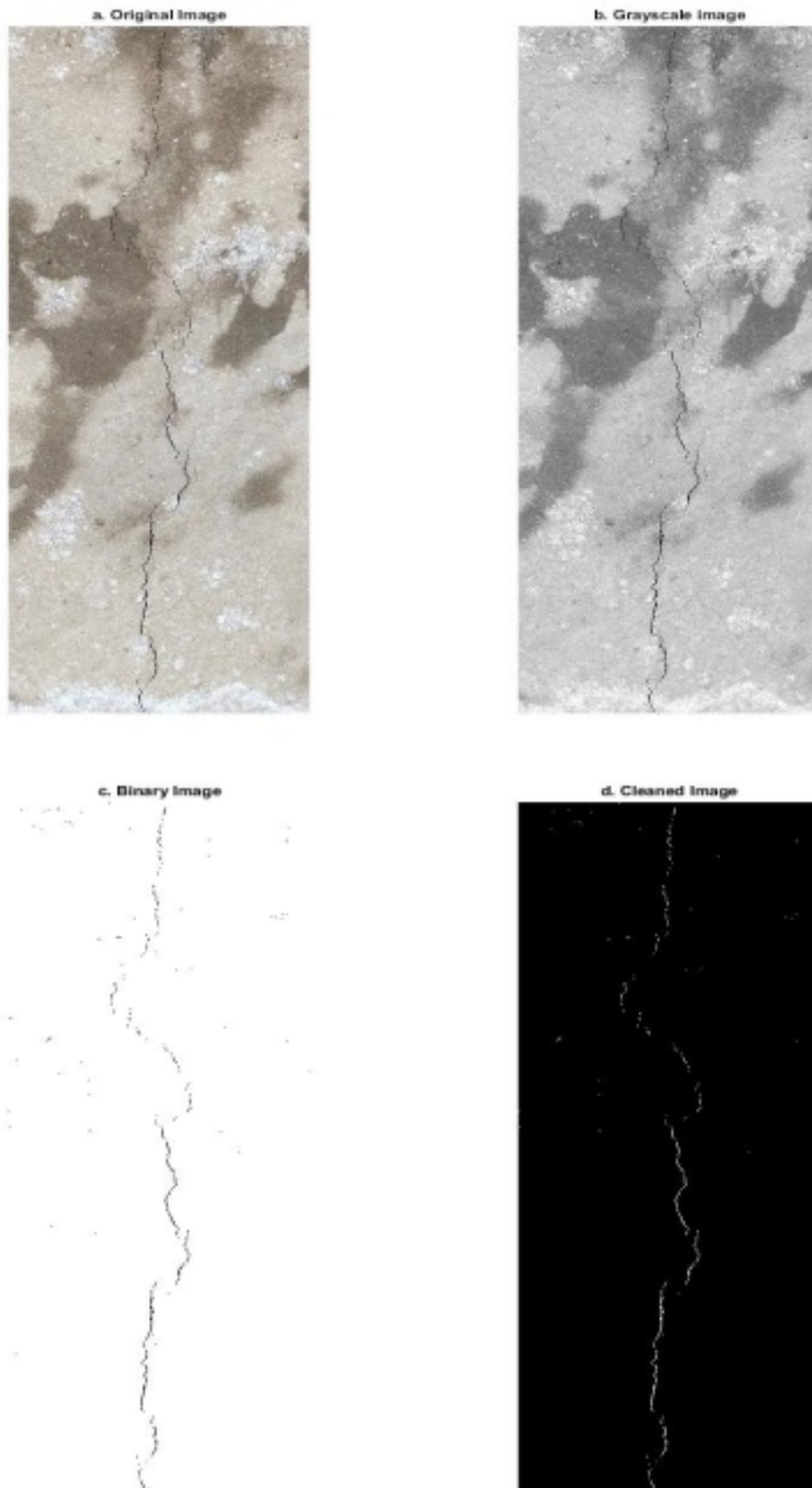


Figure B.7: MATLAB image processing steps for RTSFC10.

**B.4.1.2 Optical methods measure****Table B.20** RTSFC10 optical measurement.

<b>Point</b>	<b>PC (mm)</b>	<b>RTSFC10 (mm)</b>
1	1	0.5
2	1	0.7
3	1.2	0.7
4	1.2	0.7
5	1.2	0.8
6	1.4	0.8
7	1.4	0.8
8	1.4	0.7
9	1.4	0.9
10	1.4	0.9
11	1.4	0.9
12	1.4	0.9
13	1.5	0.9
14	1.4	0.9
15	1.4	1
16	1.3	1
17	1.4	1
18	1.6	1
19	1.4	1
20	1.4	1
21	1.4	1
22	1.4	1
23	1.4	1
24	1.3	0.9
25	1.3	0.9
26	1.5	0.8
<b>Ave</b>	1.40	0.80

**B.4.1.3 Crack width methods measure**

<b>Concrete</b>	<b>MATLAB (mm)</b>	<b>Optical (mm)</b>
PC	1.43	1.40
RTSFC10	0.94	0.86

## B.4.2 RTSFC20

### B.4.2.1 MATLAB and IC measure software



Figure B.8: IC crack length at 24 hours of plain concrete.

<input type="checkbox"/>	CrackArea	489.6244
<input type="checkbox"/>	CrackPixels	1.1826e+04
<input type="checkbox"/>	I	2686x1015x3 uint8
<input checked="" type="checkbox"/>	Iclean	2686x1015 logical
<input checked="" type="checkbox"/>	Icomp	2686x1015 logical
<input type="checkbox"/>	Igray	2686x1015 uint8
<input checked="" type="checkbox"/>	Ithres	2686x1015 logical

Figure B.9: MATLAB crack area at 24 hours of plain concrete.

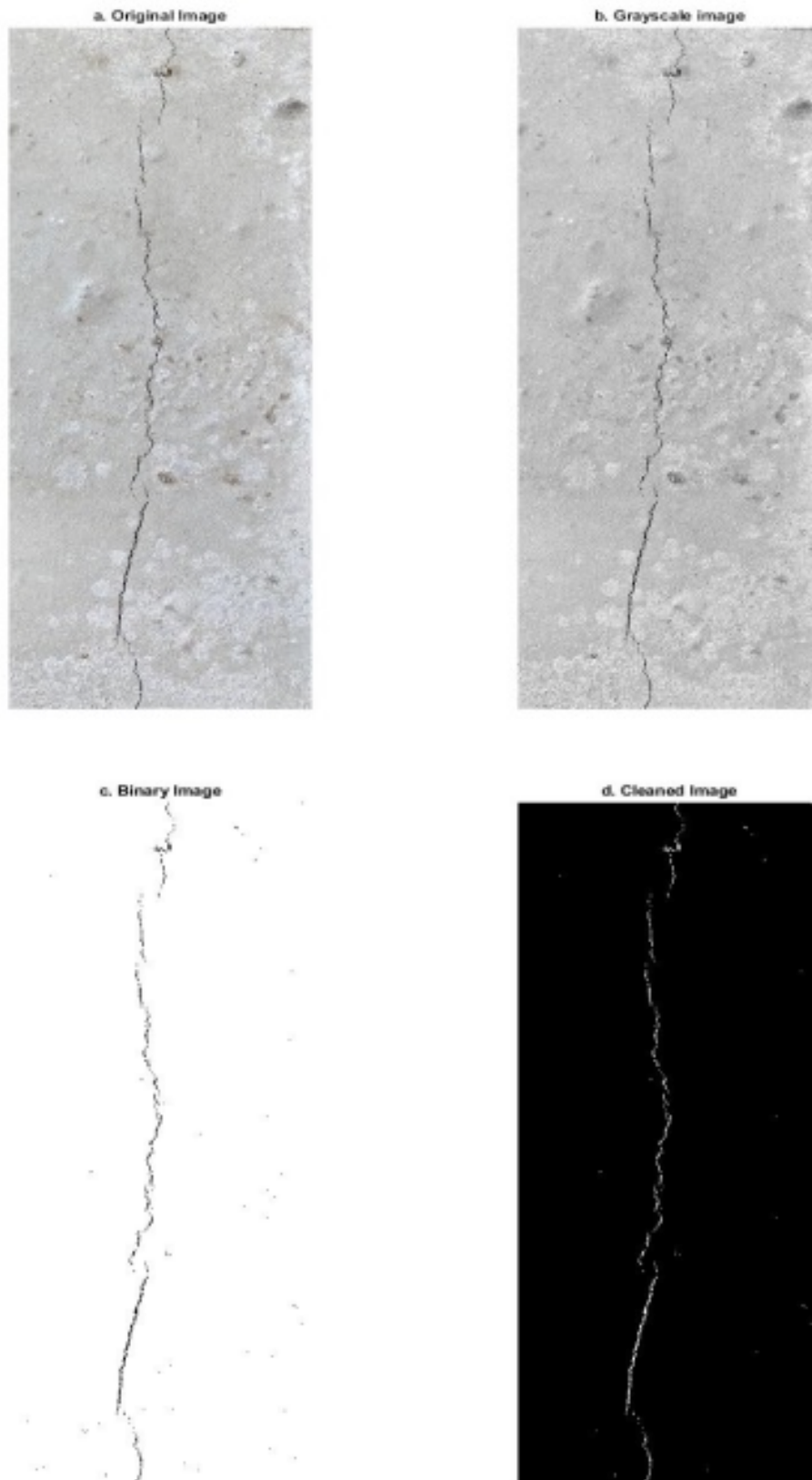


Figure B.10: MATLAB image processing steps for plain concrete.



Figure B.11: IC crack length at 24 hours of RTSFC20.

<input type="checkbox"/>	CrackArea	156.9878
<input type="checkbox"/>	CrackPixels	7.6469e+03
<input type="checkbox"/>	I	2781x609x3 uint8
<input checked="" type="checkbox"/>	Iclean	2781x609 logical
<input checked="" type="checkbox"/>	Icomp	2781x609 logical
<input type="checkbox"/>	Igray	2781x609 uint8
<input checked="" type="checkbox"/>	Ithres	2781x609 logical

Figure B.12: MATLAB crack area at 24 hours of RTSFC20.

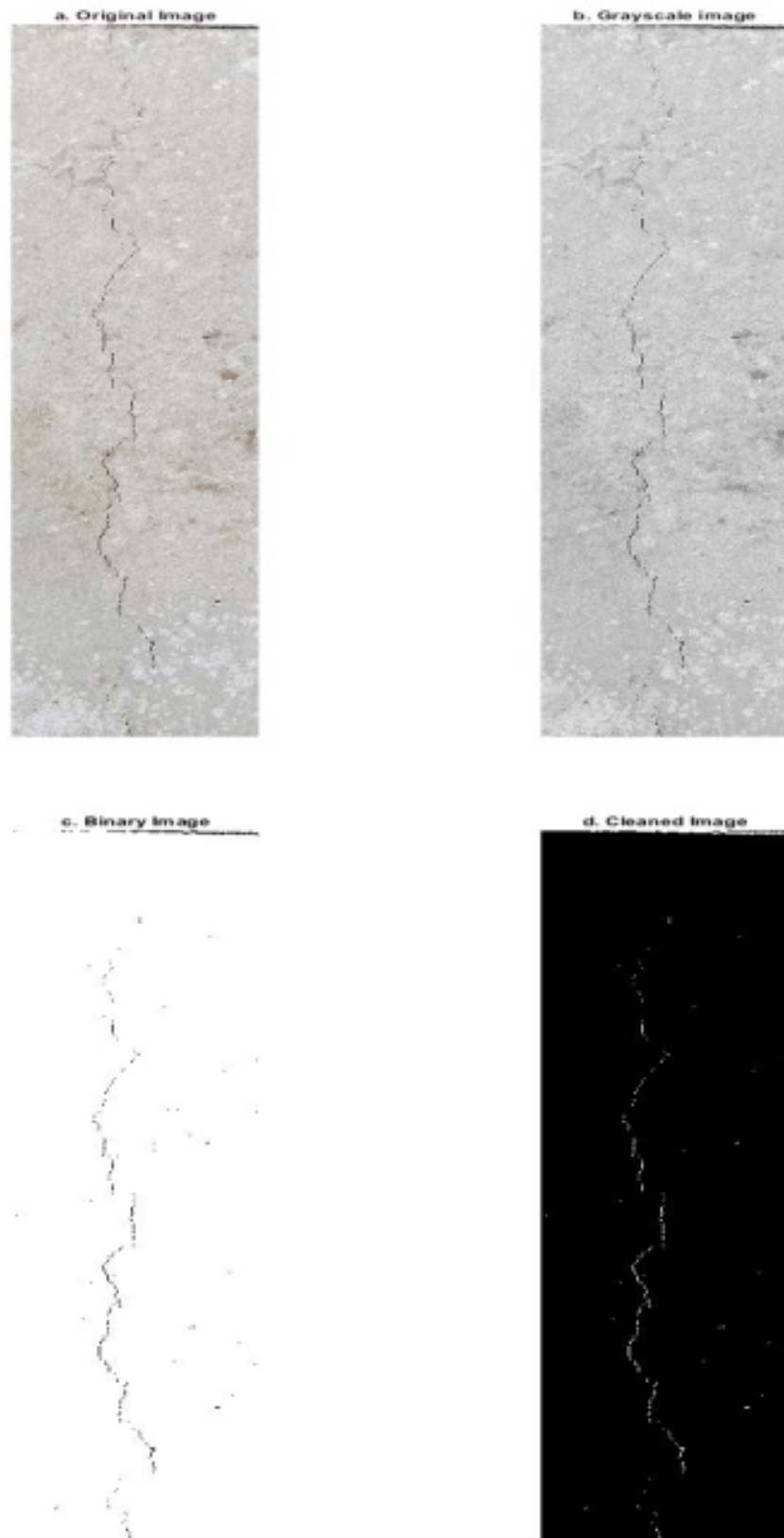


Figure B.13: MATLAB image processing steps for RTSFC20.

**B.4.2.2 Optical methods measure****Table B.21** RTSFC20 optical measurement.

<b>Point</b>	<b>PC (mm)</b>	<b>RTSFC20 (mm)</b>
1	1	0.3
2	1	0.3
3	1.2	0.3
4	1.2	0.3
5	1.2	0.3
6	1.2	0.4
7	1.3	0.4
8	1.3	0.4
9	1.3	0.4
10	1.3	0.4
11	1.3	0.5
12	1.3	0.5
13	1.3	0.5
14	1.4	0.5
15	1.4	0.5
16	1.4	0.5
17	1.4	0.5
18	1.3	0.5
19	1.3	0.5
20	1.3	0.4
21	1.3	0.4
22	1.3	0.4
23	1.3	0.4
24	1.3	0.4
25	1.3	0.3
26	1.3	0.3
<b>Ave</b>	1.30	0.41

**B.4.2.3 Crack width methods measure**

<b>Concrete</b>	<b>MATLAB (mm)</b>	<b>Optical (mm)</b>
PC	1.35	1.30
RTSFC20	0.48	0.41

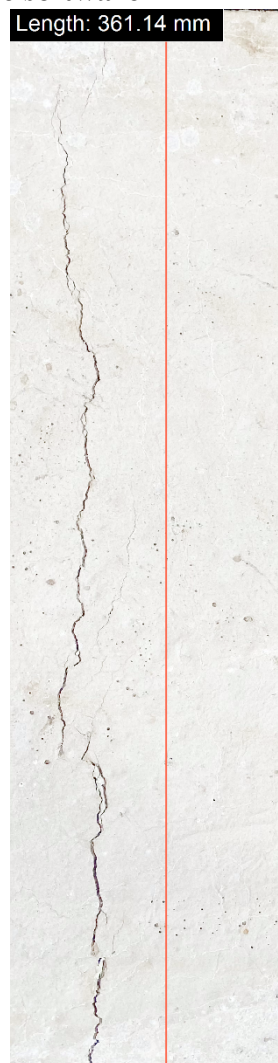
**B.4.3 RTSFC30****B.4.3.1 MATLAB and IC measure software**

Figure B.14: IC crack length at 24 hours of plain concrete.

<input type="checkbox"/>	CrackArea	493.5139
<input type="checkbox"/>	CrackPixels	9.6156e+03
<input type="checkbox"/>	I	3031x712x3 uint8
<input checked="" type="checkbox"/>	Iclean	3031x712 logical
<input checked="" type="checkbox"/>	Icomp	3031x712 logical
<input type="checkbox"/>	Igray	3031x712 uint8
<input checked="" type="checkbox"/>	Ithres	3031x712 logical

Figure B.15: MATLAB crack area at 24 hours of plain concrete.



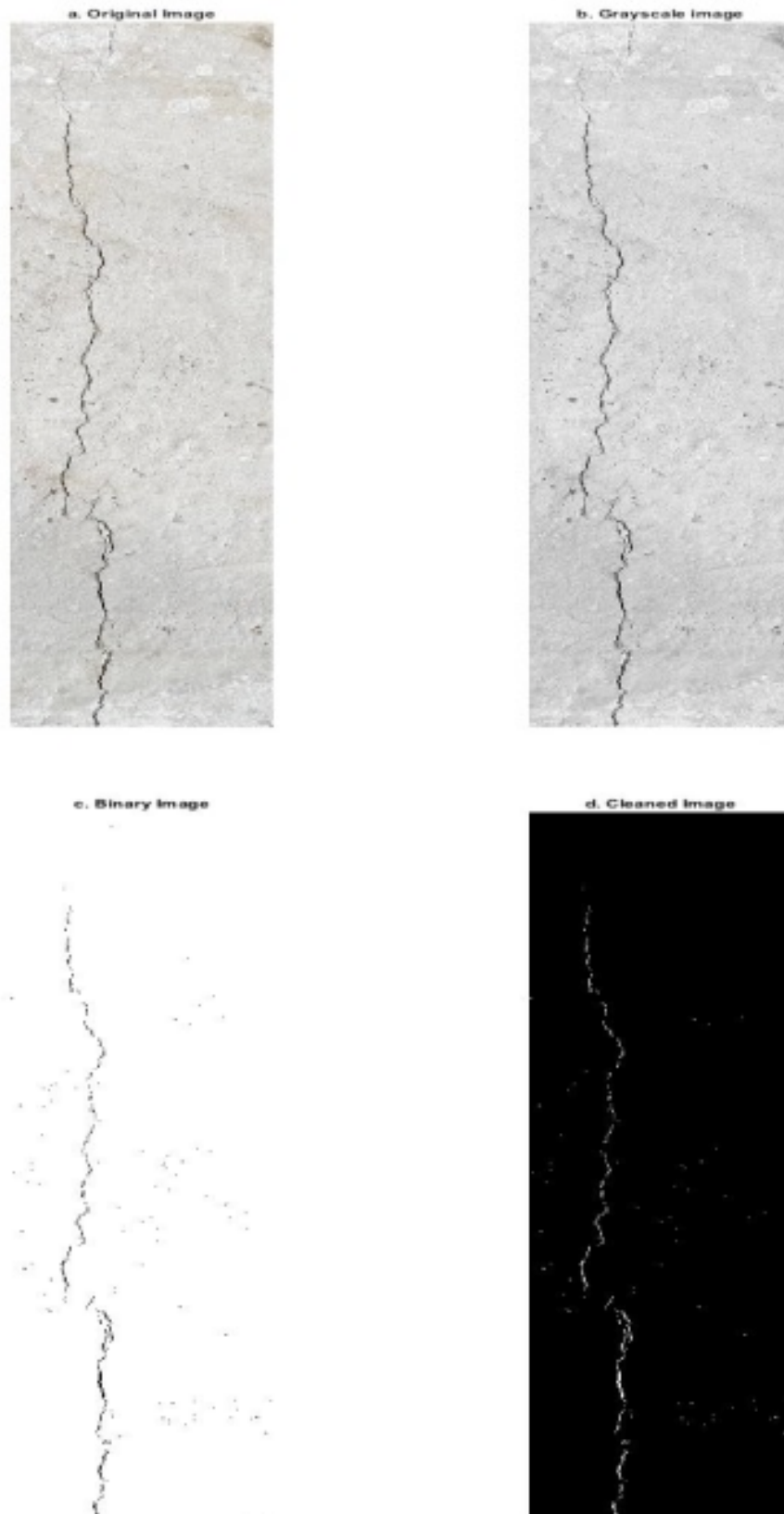


Figure B.16: MATLAB image processing steps for plain concrete.

**B.4.3.2 Optical methods measure****Table B.22** RTSFC30 optical measurement.

<b>Point</b>	<b>PC (mm)</b>	<b>RTSFC30 (mm)</b>
1	1.3	0
2	1.3	0
3	1.3	0
4	1.3	0
5	1.3	0
6	1.4	0
7	1.4	0
8	1.4	0
9	1.4	0
10	1.3	0
11	1.3	0
12	1.3	0
13	1.3	0
14	1.3	0
15	1.3	0
16	1.3	0
17	1.3	0
18	1.3	0
19	1.3	0
20	1.3	0
21	1.3	0
22	1.3	0
23	1.3	0
24	1.3	0
25	1.3	0
26	1.3	0
<b>Ave</b>	1.30	0

**B.4.3.3 Crack width methods measure**

<b>Concrete</b>	<b>MATLAB (mm)</b>	<b>Optical (mm)</b>
PC	1.37	1.30
RTSFC30	0	0

### B.4.4 MSFC10

#### B.4.4.1 MATLAB and IC measure software



Figure B.17: IC crack length at 24 hours of plain concrete.

	CrackArea	517.8546
	CrackPixels	1.2206e+04
	I	2654x947x3 uint8
	Iclean	2654x947 logical
	Icomp	2654x947 logical
	Igray	2654x947 uint8
	Ithres	2654x947 logical

Figure B.18: MATLAB crack area at 24 hours of plain concrete.

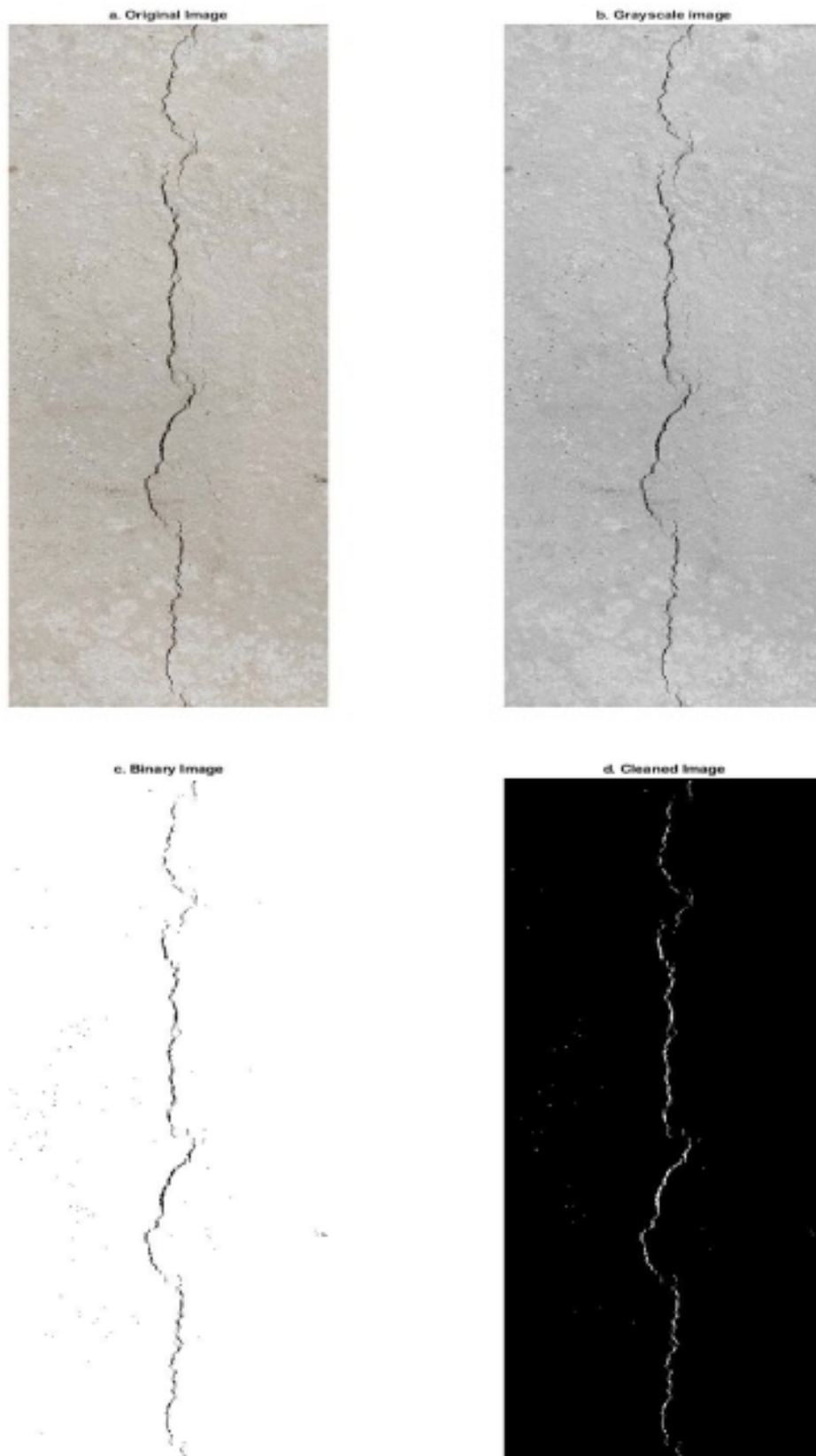


Figure B.19: MATLAB image processing steps for plain concrete.



Figure B.20: IC crack length at 24 hours of MSFC10.

<input type="checkbox"/>	CrackArea	397.8228
<input type="checkbox"/>	CrackPixels	1.3520e+04
<input type="checkbox"/>	I	2613x801x3 uint8
<input checked="" type="checkbox"/>	Iclean	2613x801 logical
<input checked="" type="checkbox"/>	Icomp	2613x801 logical
<input type="checkbox"/>	Igray	2613x801 uint8
<input checked="" type="checkbox"/>	Ithres	2613x801 logical

Figure B.21: MATLAB crack area at 24 hours of MSFC10.

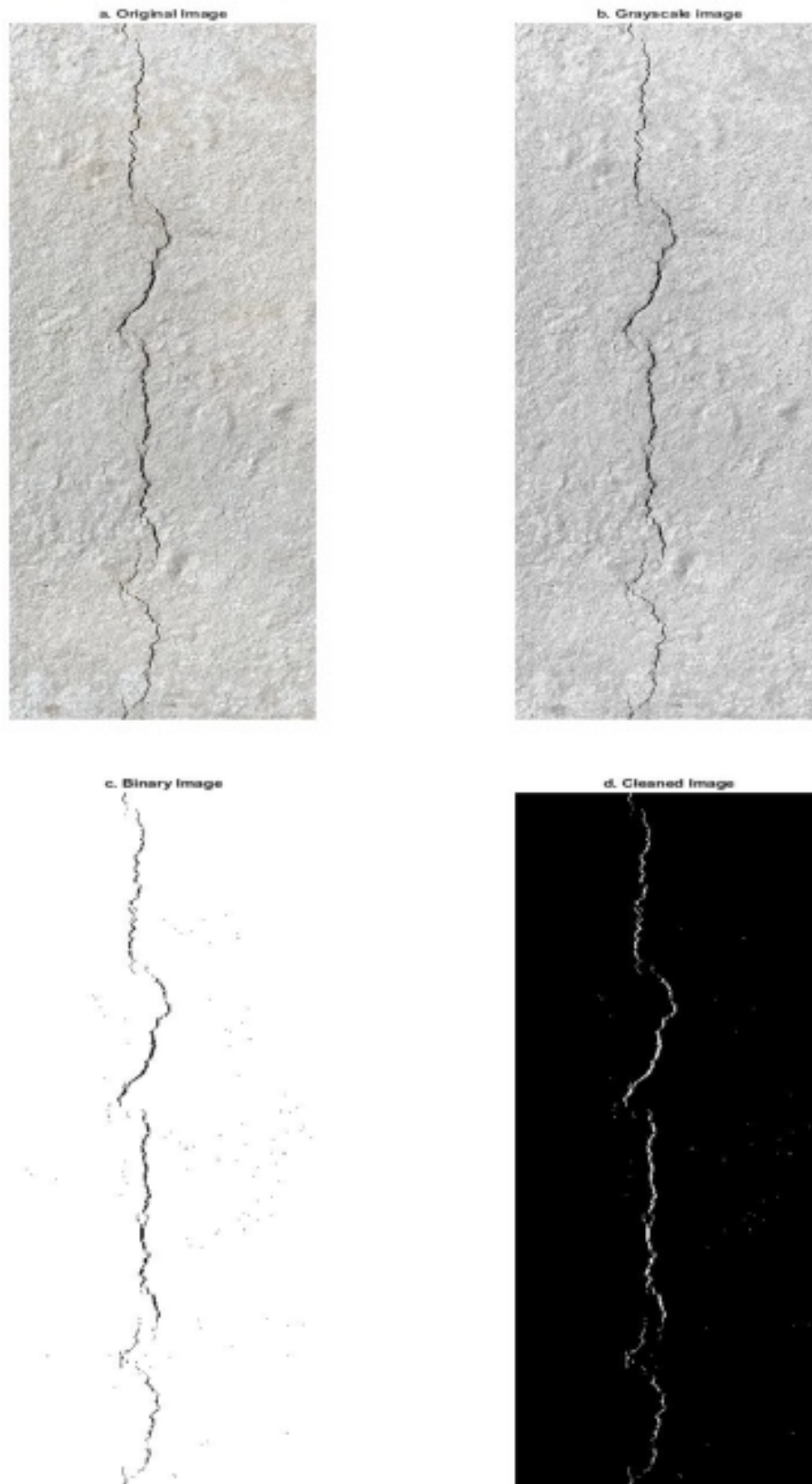


Figure B.22: MATLAB image processing steps for MSFC10.

**B.4.4.2 Optical methods measure****Table B.23** MSFC10 optical measurement.

<b>Point</b>	<b>PC (mm)</b>	<b>MSFC10 (mm)</b>
<b>1</b>	1.3	1
<b>2</b>	1.3	1
<b>3</b>	1.3	1
<b>4</b>	1.3	1
<b>5</b>	1.3	1
<b>6</b>	1.3	1.1
<b>7</b>	1.3	1.1
<b>8</b>	1.4	1.1
<b>9</b>	1.4	1.1
<b>10</b>	1.4	1.1
<b>11</b>	1.4	1.1
<b>12</b>	1.4	1.1
<b>13</b>	1.5	1.2
<b>14</b>	1.5	1.2
<b>15</b>	1.5	1.2
<b>16</b>	1.5	1.2
<b>17</b>	1.5	1.2
<b>18</b>	1.5	1.2
<b>19</b>	1.4	1.2
<b>20</b>	1.4	1.1
<b>21</b>	1.4	1.1
<b>22</b>	1.4	1.1
<b>23</b>	1.4	1.1
<b>24</b>	1.3	1.1
<b>25</b>	1.3	1.1
<b>26</b>	1.3	1.1
<b>Ave</b>	1.4	1.11

**B.4.4.3 Crack width methods measure**

<b>Concrete</b>	<b>MATLAB (mm)</b>	<b>Optical (mm)</b>
<b>PC</b>	1.44	1.40
<b>MSFC10</b>	1.13	1.11

**B.4.5 MSFC20****B.4.5.1 MATLAB and IC measure software**

Figure B.23: IC crack length at 24 hours of plain concrete.

<input type="checkbox"/>	CrackArea	435.4671
<input type="checkbox"/>	CrackPixels	4.9521e+03
<input type="checkbox"/>	I	2252x870x3 uint8
<input checked="" type="checkbox"/>	Iclean	2252x870 logical
<input checked="" type="checkbox"/>	Icomp	2252x870 logical
<input type="checkbox"/>	Igray	2252x870 uint8
<input checked="" type="checkbox"/>	Ithres	2252x870 logical

Figure B.24: MATLAB crack area at 24 hours of plain concrete.



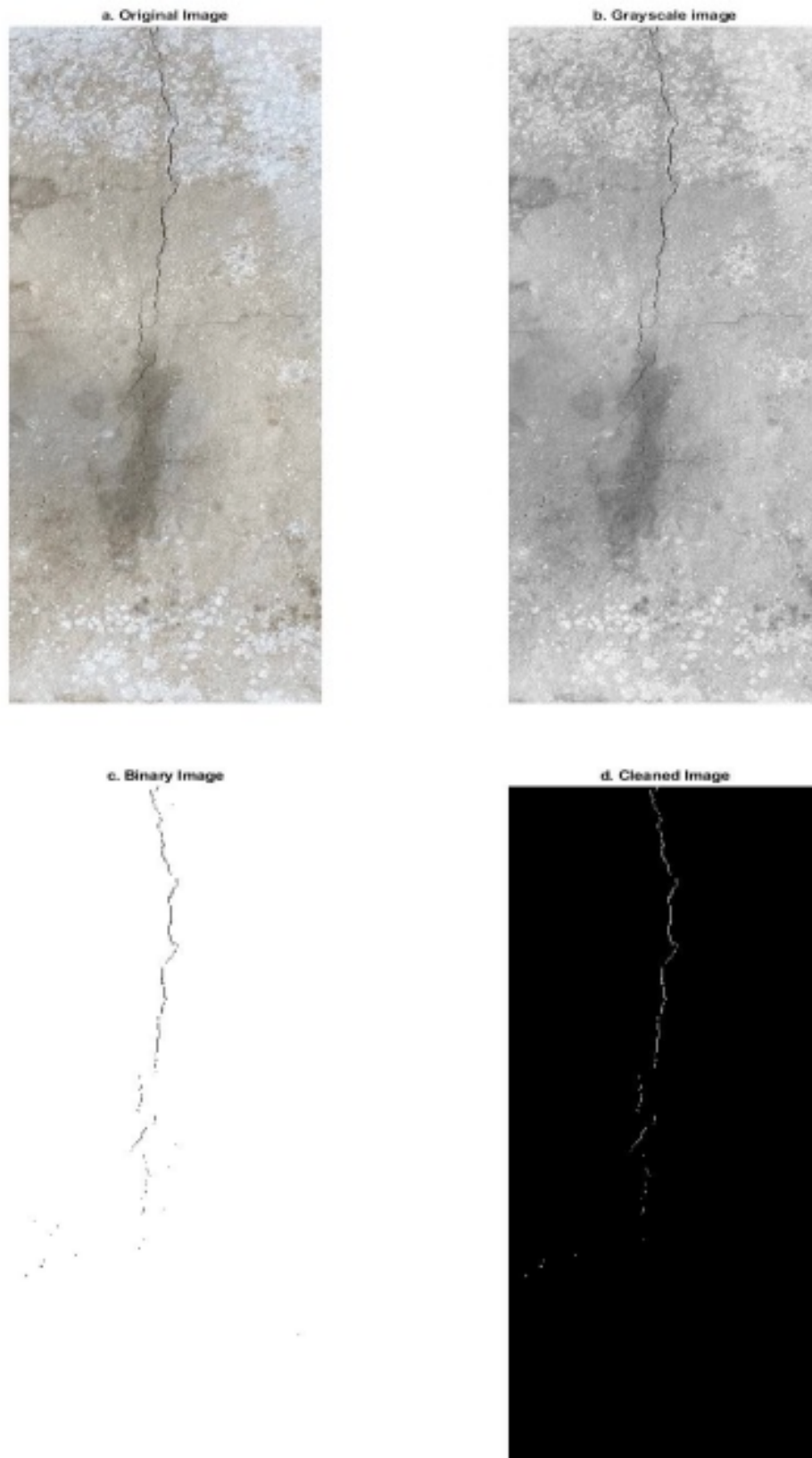


Figure B.25: MATLAB image processing steps for plain concrete.



Figure B.26: IC crack length at 24 hours of MSFC20.

	CrackArea	200.1719
	CrackPixels	4.3335e+03
	I	2884x622x3 uint8
	Iclean	2884x622 logical
	Icomp	2884x622 logical
	Igray	2884x622 uint8
	Ithres	2884x622 logical

Figure B.27: MATLAB crack area at 24 hours of MSFC20.

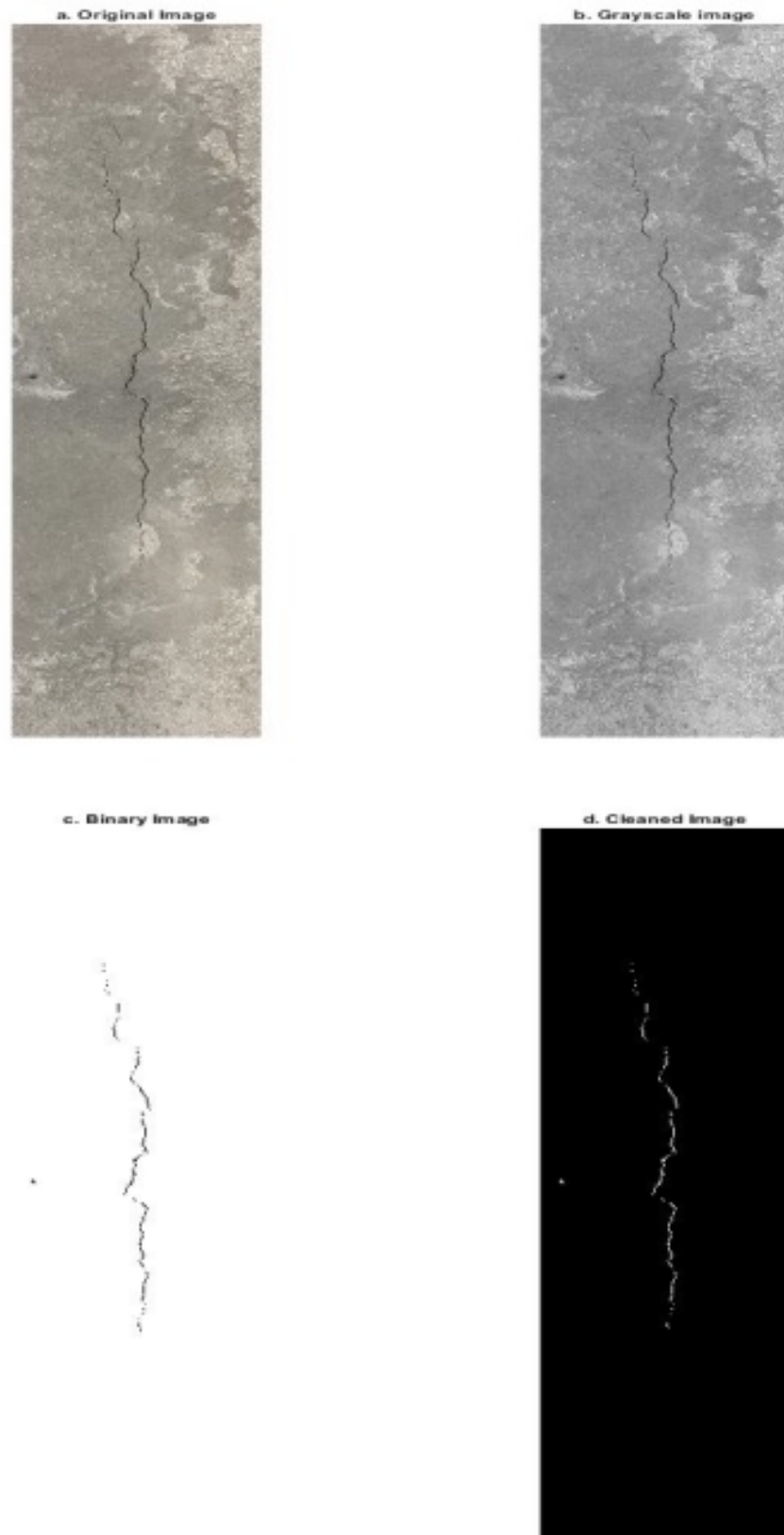


Figure B.28: MATLAB image processing steps for MSFC20.

**B.4.5.2 Optical methods measure****Table B.24** MSFC20 optical measurement.

<b>Point</b>	<b>PC (mm)</b>	<b>MSFC20 (mm)</b>
1	1	0.4
2	1	0.4
3	1.2	0.4
4	1.2	0.4
5	1.2	0.5
6	1.2	0.5
7	1.3	0.5
8	1.3	0.5
9	1.3	0.6
10	1.3	0.6
11	1.3	0.6
12	1.3	0.6
13	1.3	0.6
14	1.4	0.6
15	1.4	0.6
16	1.4	0.6
17	1.4	0.6
18	1.3	0.6
19	1.3	0.5
20	1.3	0.5
21	1.3	0.6
22	1.3	0.6
23	1.3	0.6
24	1.3	0.5
25	1.3	0.5
26	1.3	0.5
<b>Ave</b>	1.30	0.53

**B.4.5.3 Crack width methods measure**

<b>Concrete</b>	<b>MATLAB (mm)</b>	<b>Optical (mm)</b>
<b>PC</b>	1.33	1.30
<b>MSFC20</b>	0.68	0.53

### B.4.6 MSFC30

#### B.4.6.1 MATLAB and IC measure software



Figure B.29: IC crack length at 24 hours of plain concrete.

<input type="checkbox"/>	CrackArea	483.2529
<input type="checkbox"/>	CrackPixels	1.1770e+04
<input type="checkbox"/>	I	2712x854x3 uint8
<input checked="" type="checkbox"/>	Iclean	2712x854 logical
<input checked="" type="checkbox"/>	Icomp	2712x854 logical
<input type="checkbox"/>	Igray	2712x854 uint8
<input checked="" type="checkbox"/>	Ithres	2712x854 logical

Figure B.30: MATLAB crack area at 24 hours of plain concrete.

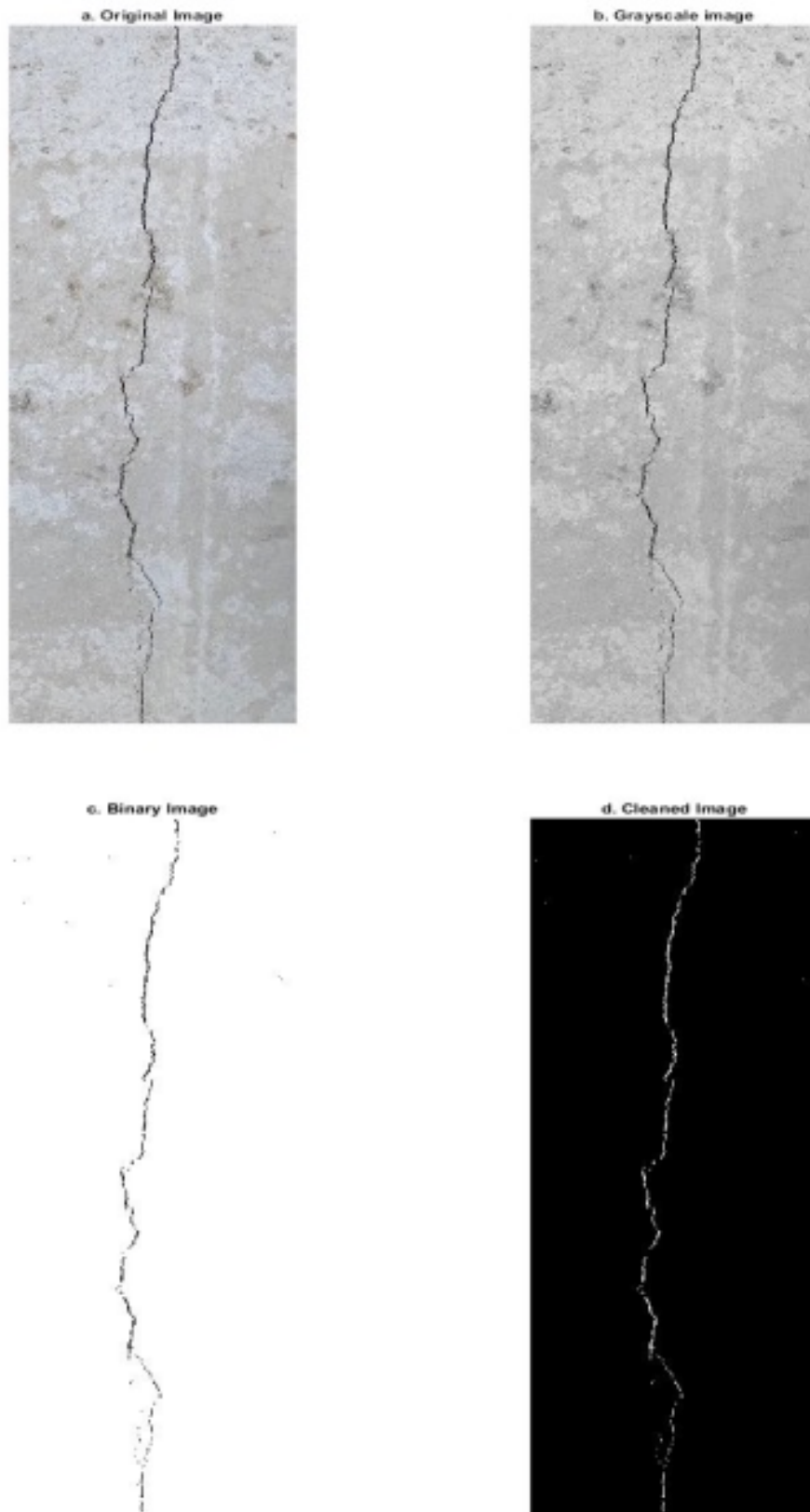


Figure B.31: MATLAB image processing steps for plain concrete.



Figure B.32: IC crack length at 24 hours of MSFC30.

<input type="checkbox"/>	CrackArea	121.1500
<input type="checkbox"/>	CrackPixels	3.3721e+03
<input type="checkbox"/>	I	2859x798x3 uint8
<input checked="" type="checkbox"/>	Iclean	2859x798 logical
<input checked="" type="checkbox"/>	Icomp	2859x798 logical
<input type="checkbox"/>	Igray	2859x798 uint8
<input checked="" type="checkbox"/>	Ithres	2859x798 logical

Figure B.33: MATLAB crack area at 24 hours of MSFC30.

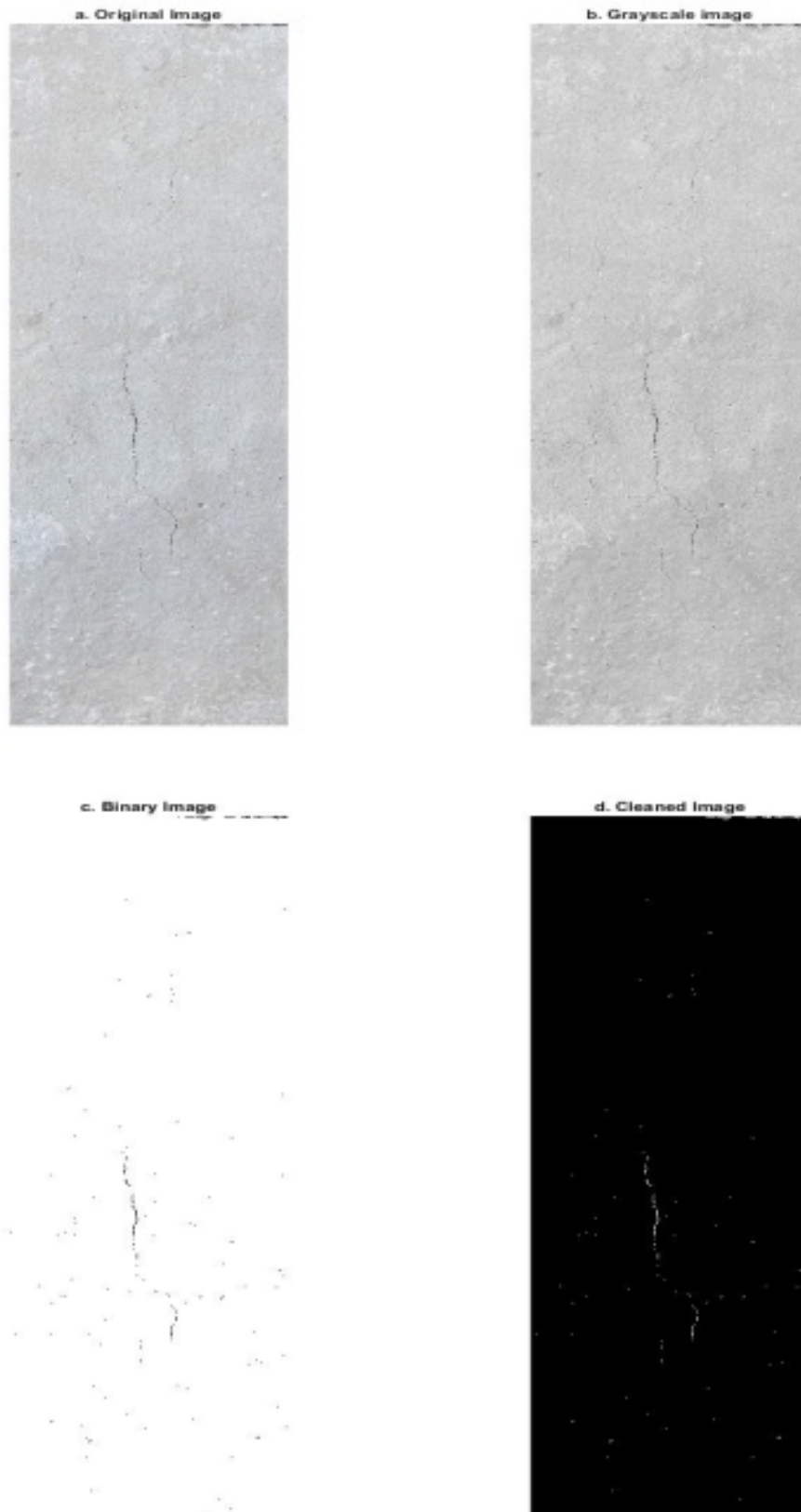


Figure B.34: MATLAB image processing steps for MSFC30.



**B.4.6.2 Optical methods measure****Table B.25** MSFC30 optical measurement.

<b>Point</b>	<b>PC (mm)</b>	<b>MSFC30 (mm)</b>
<b>1</b>	1.2	0.2
<b>2</b>	1.2	0.2
<b>3</b>	1.3	0.2
<b>4</b>	1.3	0.3
<b>5</b>	1.3	0.3
<b>6</b>	1.3	0.3
<b>7</b>	1.3	0.3
<b>8</b>	1.3	0.3
<b>9</b>	1.3	0.4
<b>10</b>	1.3	0.4
<b>11</b>	1.3	0.4
<b>12</b>	1.3	0.4
<b>13</b>	1.3	0.4
<b>14</b>	1.3	0.4
<b>15</b>	1.3	0.4
<b>16</b>	1.3	0.4
<b>17</b>	1.3	0.4
<b>18</b>	1.3	0.4
<b>19</b>	1.2	0.4
<b>20</b>	1.2	0.3
<b>21</b>	1.2	0.3
<b>22</b>	1.2	0.3
<b>23</b>	1.2	0.3
<b>24</b>	1.2	0.3
<b>25</b>	1.2	0.3
<b>26</b>	1.2	0.2
<b>Ave</b>	1.30	0.30

**B.4.6.3 Crack width methods measure**

<b>Concrete</b>	<b>MATLAB (mm)</b>	<b>Optical (mm)</b>
<b>PC</b>	1.32	1.30
<b>MSFC30</b>	0.39	0.30

**This page is intentionally left blank**

## **Appendix C:**

### **Chapter 4: The Effect of Harsh Environmental Conditions on Concrete Plastic Shrinkage Cracks: Case Study Saudi Arabia.**

This appendix presents additional information regarding the results found in Chapter 4.

**C.1 Environmental conditions and evaporation rate****C.1.1 LTRTSFC30****Table C.1** LTRTSFC30 environmental conditions and evaporation rate.

<b>Time (hr)</b>	<b>Temp. (°C)</b>	<b>Wind speed (m/s)</b>	<b>RH (%)</b>	<b>PC water pan (g)</b>	<b>PC Eva. rate (kg/m<sup>2</sup>/h)</b>	<b>LTRTSFC30 water pan (g)</b>	<b>LTRTSFC30 Eva. rate (kg/m<sup>2</sup>/h)</b>
<b>0</b>	22	-	45	510	-	502	-
<b>1</b>	26.6	4.7	35	484	1	483	1
<b>2</b>	27	4.7	25	462	1	464	1.05
<b>3</b>	27.8	4.7	23	442	1.05	444	1.05
<b>4</b>	28.3	4.7	20	422	1.05	424	1.15
<b>5</b>	28.9	4.7	20	402	1.15	402	1.15
<b>6</b>	29.5	4.7	20	382	1.15	382	1.15

**C.1.2 MTRTSFC30****Table C.2** MTRTSFC30 environmental conditions and evaporation rate.

<b>Time (hr)</b>	<b>Temp. (°C)</b>	<b>Wind speed (m/s)</b>	<b>RH (%)</b>	<b>PC water pan (g)</b>	<b>PC Eva. rate (kg/m<sup>2</sup>/h)</b>	<b>MTRTSFC30 water pan (g)</b>	<b>MTRTSFC30 Eva. rate (kg/m<sup>2</sup>/h)</b>
<b>0</b>	23	-	45	502	-	501	-
<b>1</b>	33	4.7	36	483	1.11	480	1
<b>2</b>	35	4.7	24	463	1.16	458	1.17
<b>3</b>	35	4.7	20	441	1.16	432	1.18
<b>4</b>	35	4.7	20	420	1.16	412	1.16
<b>5</b>	36	4.7	20	400	1.16	392	1.17
<b>6</b>	36	4.7	20	379	1.16	370	1.17

**C.1.3 HTRTSFC30****Table C.3** HTRTSFC30 environmental conditions and evaporation rate.

<b>Time (hr)</b>	<b>Temp. (°C)</b>	<b>Wind speed (m/s)</b>	<b>RH (%)</b>	<b>PC water pan (g)</b>	<b>PC Eva. rate (kg/m<sup>2</sup>/h)</b>	<b>HTRTSFC30 water pan (g)</b>	<b>HTRTSFC30 Eva. rate (kg/m<sup>2</sup>/h)</b>
0	33	-	45	500	-	500	-
1	42	4.7	28	471	1.53	471	1.52
2	44.5	4.7	20	439	1.68	440	1.63
3	44.8	4.7	15	402	1.95	405	1.84
4	45	4.7	15	370	2.05	374	1.99
5	45	4.7	15	341	2.10	345	2.00
6	45.2	4.7	15	314	2.16	318	2.11

**C.1.4 HTRTSFC40****Table C.4** HTRTSFC40 environmental conditions and evaporation rate.

<b>Time (hr)</b>	<b>Temp. (°C)</b>	<b>Wind speed (m/s)</b>	<b>RH (%)</b>	<b>PC water pan (g)</b>	<b>PC Eva. rate (kg/m<sup>2</sup>/h)</b>	<b>HTRTSFC40 water pan (g)</b>	<b>HTRTSFC40 Eva. rate (kg/m<sup>2</sup>/h)</b>
0	30	-	45	500	-	500	-
1	40	4.7	30	472	1.48	472	1.48
2	44.3	4.7	22	442	1.59	440	1.59
3	44.8	4.7	20	405	1.90	405	1.90
4	44.5	4.7	15	368	1.95	370	1.90
5	45	4.7	15	328	2.10	330	2.10
6	45	4.7	15	287	2.15	289	2.10

**C.1.5 LWSRTSFC30****Table C.5** LWSRTSFC30 environmental conditions and evaporation rate.

<b>Time (hr)</b>	<b>Temp. (°C)</b>	<b>Wind speed (m/s)</b>	<b>RH (%)</b>	<b>PC water pan (g)</b>	<b>PC Eva. rate (kg/m<sup>2</sup>/h)</b>	<b>LWSRTSFC30 water pan (g)</b>	<b>LWSRTSFC30 Eva. rate (kg/m<sup>2</sup>/h)</b>
<b>0</b>	28.8	-	45	510	-	514	-
<b>1</b>	32.1	3	28	489	1	493	1
<b>2</b>	34.2	3	20	464	1	468	1.10
<b>3</b>	35.4	3	19	442	1.10	446	1.10
<b>4</b>	36	3	19	417	1.16	424	1.16
<b>5</b>	36	3	19	395	1.16	401	1.20
<b>6</b>	36	3	19	370	1.20	381	1.21

**C.1.6 MWSRTSFC30****Table C.6** MWSRTSFC30 environmental conditions and evaporation rate.

<b>Time (hr)</b>	<b>Temp. (°C)</b>	<b>Wind speed (m/s)</b>	<b>RH (%)</b>	<b>PC water pan (g)</b>	<b>PC Eva. rate (kg/m<sup>2</sup>/h)</b>	<b>MWSRTSFC30 water pan (g)</b>	<b>MWSRTSFC30 Eva. rate (kg/m<sup>2</sup>/h)</b>
<b>0</b>	25	-	45	502	-	501	-
<b>1</b>	33	4.7	36	483	1.11	480	1
<b>2</b>	35	4.7	24	463	1.16	458	1.17
<b>3</b>	35	4.7	20	441	1.16	432	1.18
<b>4</b>	35	4.7	20	420	1.16	412	1.16
<b>5</b>	36	4.7	20	400	1.16	392	1.17
<b>6</b>	36	4.7	20	379	1.16	370	1.17

**C.1.7 HWSRTSFC30****Table C.7** HWSRTSFC30 environmental conditions and evaporation rate.

<b>Time (hr)</b>	<b>Temp. (°C)</b>	<b>Wind speed (m/s)</b>	<b>RH (%)</b>	<b>PC water pan (g)</b>	<b>PC Eva. rate (kg/m<sup>2</sup>/h)</b>	<b>HWSRTSFC30 water pan (g)</b>	<b>HWSRTSFC30 Eva. rate (kg/m<sup>2</sup>/h)</b>
0	22.5	-	45	501	-	501	-
1	34	7	36	473	1.47	473	1.51
2	35.5	7	24	440	1.60	437	1.67
3	36	7	20	407	1.74	404	1.78
4	36	7	20	376	1.80	373	1.85
5	36	7	20	343	1.85	340	1.90
6	36	7	20	301	1.91	297	1.95

**C.1.8 HWSRTSFC40****Table C.8** HWSRTSFC40 environmental conditions and evaporation rate.

<b>Time (hr)</b>	<b>Temp. (°C)</b>	<b>Wind speed (m/s)</b>	<b>RH (%)</b>	<b>PC water pan (g)</b>	<b>PC Eva. rate (kg/m<sup>2</sup>/h)</b>	<b>HWSRTSFC40 water pan (g)</b>	<b>HWSRTSFC40 Eva. rate (kg/m<sup>2</sup>/h)</b>
0	24	-	45	501	-	501	-
1	34.4	7	34	476	1.30	474	1.42
2	36	7	20	447	1.59	444	1.60
3	36	7	20	414	1.72	411	1.75
4	36	7	20	379	1.80	376	1.82
5	36	7	20	344	1.85	341	1.90
6	36	7	20	308	1.90	305	1.95

**C.1.9 0.5W/CRTSFC30****Table C.9** 0.5W/CRTSFC30 environmental conditions and evaporation rate.

<b>Time (hr)</b>	<b>Temp. (°C)</b>	<b>Wind speed (m/s)</b>	<b>RH (%)</b>	<b>PC water pan (g)</b>	<b>PC Eva. rate (kg/m<sup>2</sup>/h)</b>	<b>0.5W/CRTSFC30 water pan (g)</b>	<b>0.5W/CRTSFC30 Eva. Rate (kg/m<sup>2</sup>/h)</b>
0	23.2	-	45	500	-	501	-
1	33.5	4.7	35	478	1.15	478	1.20
2	35.8	4.7	20	459	1	458	1.05
3	36	4.7	20	439	1.05	438	1.52
4	36	4.7	20	416	1.11	415	1.11
5	36	4.7	20	394	1.12	392	1.12
6	36	4.7	20	357	1.21	355	1.22

**C.1.10 0.55W/CRTSFC30****Table C.10** 0.55W/CRTSFC30 environmental conditions and evaporation rate.

<b>Time (hr)</b>	<b>Temp. (°C)</b>	<b>Wind speed (m/s)</b>	<b>RH (%)</b>	<b>PC water pan (g)</b>	<b>PC Eva. rate (kg/m<sup>2</sup>/h)</b>	<b>0.55W/CRTSFC30 water pan (g)</b>	<b>0.55W/CRTSFC30 Eva. rate (kg/m<sup>2</sup>/h)</b>
0	25	-	45	502	-	501	-
1	33	4.7	36	483	1.11	480	1
2	35	4.7	22	463	1.16	458	1.17
3	35	4.7	20	441	1.16	432	1.18
4	35	4.7	20	420	1.16	412	1.16
5	36	4.7	20	400	1.16	392	1.17
6	36	4.7	20	379	1.16	370	1.17



**C.1.11 0.6W/CRTSFC30****Table C.11** 0.6W/CRTSFC30 environmental conditions and evaporation rate.

<b>Time (hr)</b>	<b>Temp. (°C)</b>	<b>Wind speed (m/s)</b>	<b>RH (%)</b>	<b>PC water pan (g)</b>	<b>PC Eva. rate (kg/m<sup>2</sup>/h)</b>	<b>0.6W/CRTSFC30 water pan (g)</b>	<b>0.6W/CRTSFC30 Eva. rate (kg/m<sup>2</sup>/h)</b>
<b>0</b>	25.4	-	45	500	-	500	-
<b>1</b>	34.4	4.7	34	475	1.31	471	1.25
<b>2</b>	36	4.7	20	449	1.37	444	1.32
<b>3</b>	36	4.7	20	425	1.56	418	1.50
<b>4</b>	36	4.7	20	395	1.63	388	1.59
<b>5</b>	36	4.7	20	364	1.80	355	1.68
<b>6</b>	36	4.7	20	330	1.88	320	1.75

**C.1.12 0.6W/CRTSFC40****Table C.12** 0.6W/CRTSFC40 environmental conditions and evaporation rate.

<b>Time (hr)</b>	<b>Temp. (°C)</b>	<b>Wind speed (m/s)</b>	<b>RH (%)</b>	<b>PC water pan (g)</b>	<b>PC Eva. rate (kg/m<sup>2</sup>/h)</b>	<b>0.6W/CRTSFC40 water pan (g)</b>	<b>0.6W/CRTSFC40 Eva. rate (kg/m<sup>2</sup>/h)</b>
<b>0</b>	26	-	45	500	-	500	-
<b>1</b>	35	4.7	32	476	1.25	477	1.20
<b>2</b>	36	4.7	20	450	1.36	452	1.30
<b>3</b>	36	4.7	20	421	1.50	427	1.34
<b>4</b>	36	4.7	20	391	1.58	399	1.49
<b>5</b>	36	4.7	20	361	1.66	370	1.54
<b>6</b>	36	4.7	20	327	1.78	338	1.67

**C.2 Compressive strength****Table C.13** LTRTSFC30 compressive strength at 28 days curing.

<b>Batch</b>	<b>Compressive strength (MPa)</b>	<b>Weight of the cube (kg)</b>	<b>Volume of the cube (m<sup>3</sup>)</b>	<b>Density of the cube (kg/m<sup>3</sup>)</b>
LTRTSFC30 Out	34.20	2.28	100 × 100 × 100	2280
LTRTSFC30 In	34.18	2.25	100 × 100 × 100	2250
PC Out	34.16	2.25	100 × 100 × 100	2250
PC In	34.14	2.25	100 × 100 × 100	2250

**Table C.14** MTRTSFC30 compressive strength at 28 days curing.

<b>Batch</b>	<b>Compressive strength (MPa)</b>	<b>Weight of the cube (kg)</b>	<b>Volume of the cube (m<sup>3</sup>)</b>	<b>Density of the cube (kg/m<sup>3</sup>)</b>
MTRTSFC30 Out	34.26	2.30	100 × 100 × 100	2300
MTRTSFC30 In	34.20	2.28	100 × 100 × 100	2280
PC Out	34.15	2.22	100 × 100 × 100	2220
PC In	34.17	2.25	100 × 100 × 100	2250

**Table C.15** HTRTSFC30 compressive strength at 28 days curing.

<b>Batch</b>	<b>Compressive strength (MPa)</b>	<b>Weight of the cube (kg)</b>	<b>Volume of the cube (m<sup>3</sup>)</b>	<b>Density of the cube (kg/m<sup>3</sup>)</b>
HTRTSFC30 Out	34.30	2.28	100 × 100 × 100	2280
HTRTSFC30 In	34.28	2.25	100 × 100 × 100	2250
PC Out	34.18	2.20	100 × 100 × 100	2200
PC In	34.15	2.20	100 × 100 × 100	2200

**Table C.16** HTRTSFC40 compressive strength at 28 days curing.

<b>Batch</b>	<b>Compressive strength (MPa)</b>	<b>Weight of the cube (kg)</b>	<b>Volume of the cube (m<sup>3</sup>)</b>	<b>Density of the cube (kg/m<sup>3</sup>)</b>
HTRTSFC40 Out	34.40	2.32	100 ×100×100	2320
HTRTSFC40 In	34.38	2.30	100 ×100×100	2300
PC Out	34.16	2.22	100 ×100×100	2220
PC In	34.12	2.25	100 ×100×100	2250

**Table C.17** LWSRTSFC30 compressive strength at 28 days curing.

<b>Batch</b>	<b>Compressive strength (MPa)</b>	<b>Weight of the cube (kg)</b>	<b>Volume of the cube (m<sup>3</sup>)</b>	<b>Density of the cube (kg/m<sup>3</sup>)</b>
LWSRTSFC30 Out	34.18	2.25	100 ×100×100	2250
LWSRTSFC30 In	34.15	2.25	100 ×100×100	2250
PC Out	34.11	2.22	100 ×100×100	2220
PC In	34.13	2.25	100 ×100×100	2250

**Table C.18** MWSRTSFC30 compressive strength at 28 days curing.

<b>Batch</b>	<b>Compressive strength (MPa)</b>	<b>Weight of the cube (kg)</b>	<b>Volume of the cube (m<sup>3</sup>)</b>	<b>Density of the cube (kg/m<sup>3</sup>)</b>
MWSRTSFC30 Out	34.26	2.30	100 ×100×100	2300
MWSRTSFC30 In	34.20	2.28	100 ×100×100	2280
PC Out	34.15	2.22	100 ×100×100	2220
PC In	34.17	2.25	100 ×100×100	2250

**Table C.19** HWSRTSFC30 compressive strength at 28 days curing.

<b>Batch</b>	<b>Compressive strength (MPa)</b>	<b>Weight of the cube (kg)</b>	<b>Volume of the cube (m<sup>3</sup>)</b>	<b>Density of the cube (kg/m<sup>3</sup>)</b>
HWSRTSFC30 Out	34.26	2.32	100 ×100×100	2320
HWSRTSFC30 In	34.24	2.30	100 ×100×100	2300
PC Out	34.22	2.28	100 ×100×100	2280
PC In	34.13	2.20	100 ×100×100	2200

**Table C.20** HWSRTSFC40 compressive strength at 28 days curing.

<b>Batch</b>	<b>Compressive strength (MPa)</b>	<b>Weight of the cube (kg)</b>	<b>Volume of the cube (m<sup>3</sup>)</b>	<b>Density of the cube (kg/m<sup>3</sup>)</b>
HWSRTSFC40 Out	34.30	2.35	100 ×100×100	2350
HWSRTSFC40 In	34.29	2.35	100 ×100×100	2350
PC Out	34.18	2.25	100 ×100×100	2250
PC In	34.17	2.22	100 ×100×100	2220

**Table C.21** 0.5W/SRTSFC30 compressive strength at 28 days curing.

<b>Batch</b>	<b>Compressive strength (MPa)</b>	<b>Weight of the cube (kg)</b>	<b>Volume of the cube (m<sup>3</sup>)</b>	<b>Density of the cube (kg/m<sup>3</sup>)</b>
0.5W/SRTSFC30 Out	36.0	2.25	100 ×100×100	2250
0.5W/SRTSFC30 In	35.95	2.20	100 ×100×100	2200
PC Out	35.40	2.20	100 ×100×100	2200
PC In	35.30	2.20	100 ×100×100	2200

**Table C.22** 0.55W/SRTSFC30 compressive strength at 28 days curing.

<b>Batch</b>	<b>Compressive strength (MPa)</b>	<b>Weight of the cube (kg)</b>	<b>Volume of the cube (m<sup>3</sup>)</b>	<b>Density of the cube (kg/m<sup>3</sup>)</b>
0.55W/SRTSFC30 Out	34.30	2.28	100 × 100 × 100	2280
0.55W/SRTSFC30 In	34.25	2.25	100 × 100 × 100	2250
PC Out	34.15	2.20	100 × 100 × 100	2200
PC In	34.0	2.20	100 × 100 × 100	2200

**Table C.23** 0.6W/SRTSFC30 compressive strength at 28 days curing.

<b>Batch</b>	<b>Compressive strength (MPa)</b>	<b>Weight of the cube (kg)</b>	<b>Volume of the cube (m<sup>3</sup>)</b>	<b>Density of the cube (kg/m<sup>3</sup>)</b>
0.6W/SRTSFC30 Out	34.67	2.30	100 × 100 × 100	2300
0.6W/SRTSFC30 In	34.50	2.23	100 × 100 × 100	2230
PC Out	33.35	2.22	100 × 100 × 100	2220
PC In	33.20	2.20	100 × 100 × 100	2200

**Table C.24** 0.6W/SRTSFC40 compressive strength at 28 days curing.

<b>Batch</b>	<b>Compressive strength (MPa)</b>	<b>Weight of the cube (kg)</b>	<b>Volume of the cube (m<sup>3</sup>)</b>	<b>Density of the cube (kg/m<sup>3</sup>)</b>
0.6W/SRTSFC40 Out	33.33	2.20	100 × 100 × 100	2200
0.6W/SRTSFC40 In	33.80	2.22	100 × 100 × 100	2200
PC Out	33.22	2.20	100 × 100 × 100	2200
PC In	33.38	2.25	100 × 100 × 100	2250

### C.3 Crack measurements

#### C.3.1 LTRTSFC30

##### C.3.1.1 MATLAB and IC measure software



Figure C.1: IC crack length at 24 hours of plain concrete.

<input type="checkbox"/>	CrackArea	401.6449
<input type="checkbox"/>	CrackPixels	4.0478e+03
<input type="checkbox"/>	I	1641x931x3 uint8
<input checked="" type="checkbox"/>	Iclean	1641x931 logical
<input checked="" type="checkbox"/>	Icomp	1641x931 logical
<input type="checkbox"/>	Igray	1641x931 uint8
<input checked="" type="checkbox"/>	Ithres	1641x931 logical

Figure C.2: MATLAB crack area at 24 hours of plain concrete.

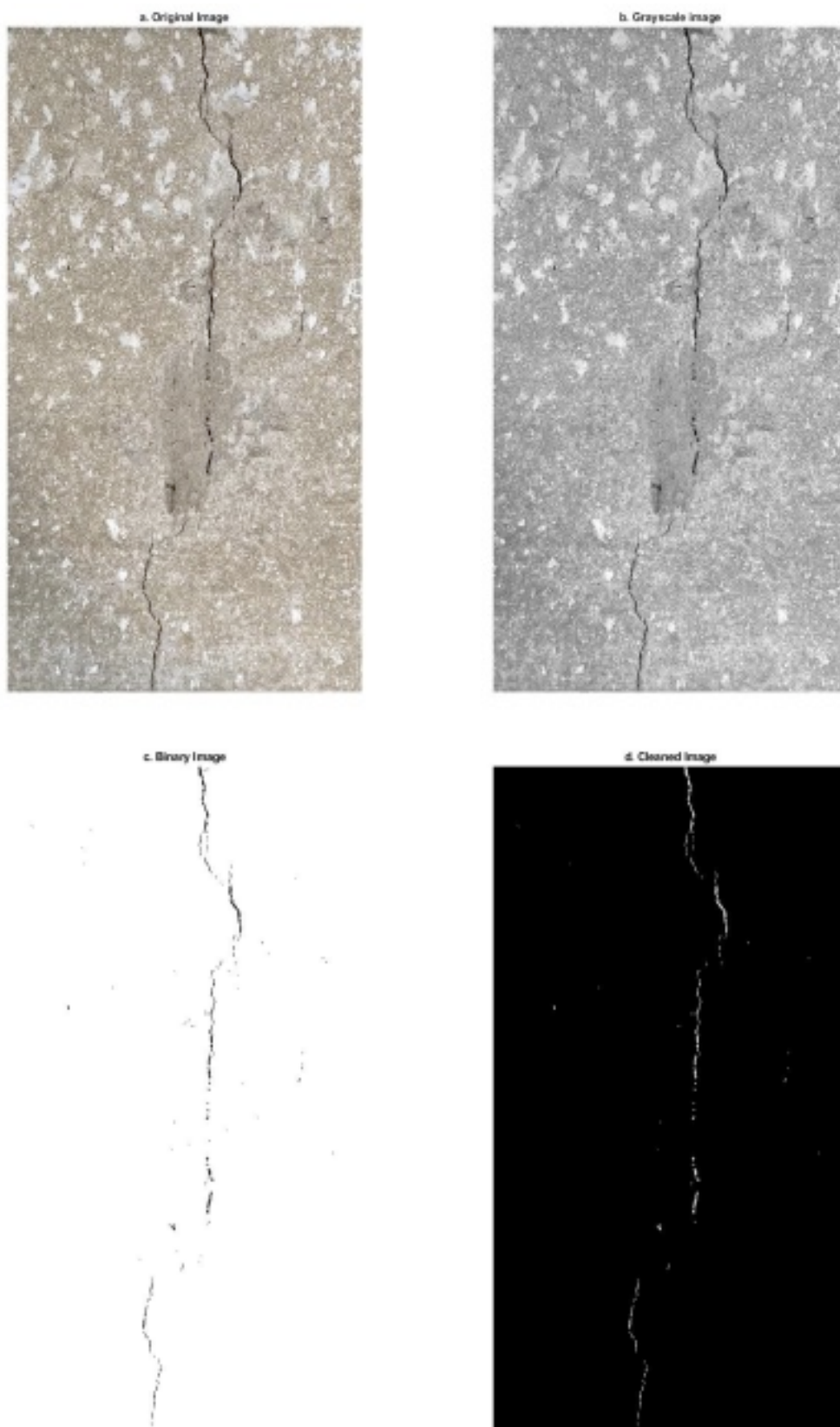


Figure C.3: MATLAB image processing steps for plain concrete.

**C.3.1.2 Optical methods measure****Table C.24** LTRTSFC30 optical measurement.

<b>Point</b>	<b>PC (mm)</b>	<b>LTRTSFC30 (mm)</b>
<b>1</b>	1	0
<b>2</b>	1	0
<b>3</b>	1	0
<b>4</b>	1	0
<b>5</b>	1	0
<b>6</b>	1	0
<b>7</b>	0.9	0
<b>8</b>	0.9	0
<b>9</b>	0.9	0
<b>10</b>	1	0
<b>11</b>	1	0
<b>12</b>	1.5	0
<b>13</b>	1.2	0
<b>14</b>	1.2	0
<b>15</b>	1.2	0
<b>16</b>	1	0
<b>17</b>	1	0
<b>18</b>	1	0
<b>19</b>	1	0
<b>20</b>	1	0
<b>21</b>	1	0
<b>22</b>	1	0
<b>23</b>	0.9	0
<b>24</b>	0.9	0
<b>25</b>	0.9	0
<b>26</b>	0.9	0
<b>Ave</b>	1.02	0

**C.3.1.3 Crack width methods measure**

<b>Concrete</b>	<b>MATLAB (mm)</b>	<b>Optical (mm)</b>
<b>PC</b>	1.10	1.02
<b>LTRTSFC30</b>	0	0



### C.3.2 MTRTSFC30

#### C.3.2.1 MATLAB and IC measure software



Figure C.4: IC crack length at 24 hours of plain concrete.

<input type="checkbox"/>	CrackArea	432.5475
<input type="checkbox"/>	CrackPixels	1.0278e+04
<input type="checkbox"/>	I	2741x680x3 uint8
<input checked="" type="checkbox"/>	Iclean	2741x680 logical
<input checked="" type="checkbox"/>	Icomp	2741x680 logical
<input type="checkbox"/>	Igray	2741x680 uint8
<input checked="" type="checkbox"/>	Ithres	2741x680 logical

Figure C.5: MATLAB crack area at 24 hours of plain concrete.

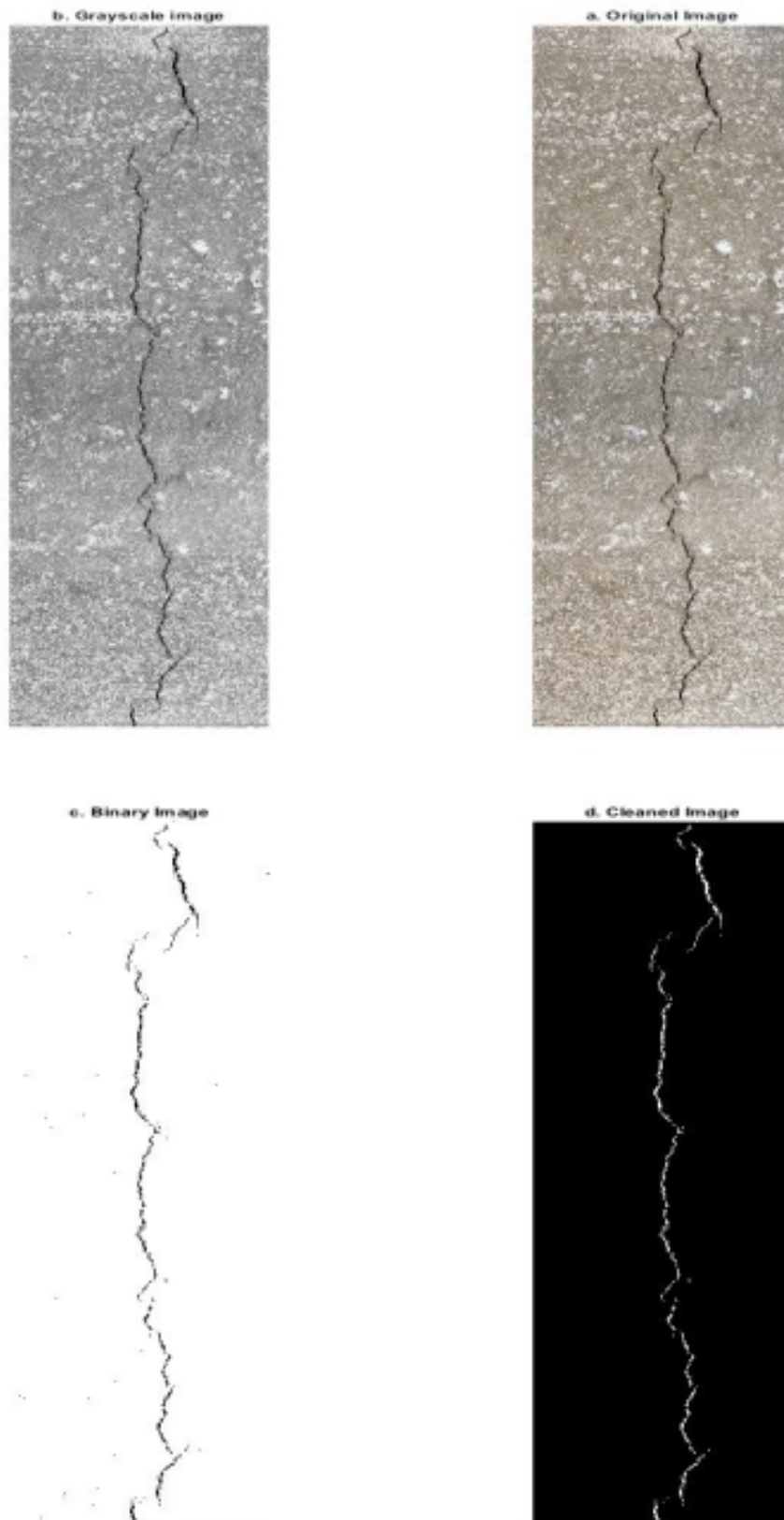


Figure C.6: MATLAB image processing steps for plain concrete.

**C.3.2.2 Optical methods measure****Table C.25** MTRTSFC30 optical measurement.

<b>Point</b>	<b>PC (mm)</b>	<b>MTRTSFC30 (mm)</b>
<b>1</b>	0.9	0
<b>2</b>	0.9	0
<b>3</b>	1	0
<b>4</b>	1	0
<b>5</b>	1	0
<b>6</b>	1.1	0
<b>7</b>	1.1	0
<b>8</b>	1.1	0
<b>9</b>	1.1	0
<b>10</b>	1.1	0
<b>11</b>	1.1	0
<b>12</b>	1.1	0
<b>13</b>	1.1	0
<b>14</b>	1.1	0
<b>15</b>	1.1	0
<b>16</b>	1.1	0
<b>17</b>	1.1	0
<b>18</b>	1.1	0
<b>19</b>	1.1	0
<b>20</b>	1	0
<b>21</b>	1	0
<b>22</b>	1	0
<b>23</b>	1	0
<b>24</b>	1	0
<b>25</b>	0.9	0
<b>26</b>	0.9	0
<b>Ave</b>	1.04	0

**C.3.2.3 Crack width methods measure**

<b>Concrete</b>	<b>MATLAB (mm)</b>	<b>Optical (mm)</b>
<b>PC</b>	1.19	1.04
<b>MTRTSFC30</b>	0	0

### C.3.3 HTRTSFC30

#### C.3.3.1 MATLAB and IC measure software



Figure C.7: IC crack length at 24 hours of plain concrete (A).

<input type="checkbox"/>	CrackArea	824.5764
<input type="checkbox"/>	CrackPixels	1.1733e+04
<input type="checkbox"/>	I	3496x766x3 uint8
<input checked="" type="checkbox"/>	Iclean	3496x766 logical
<input checked="" type="checkbox"/>	Icomp	3496x766 logical
<input type="checkbox"/>	Igray	3496x766 uint8
<input checked="" type="checkbox"/>	Ithres	3496x766 logical

Figure C.8: MATLAB crack area at 24 hours of plain concrete (A).

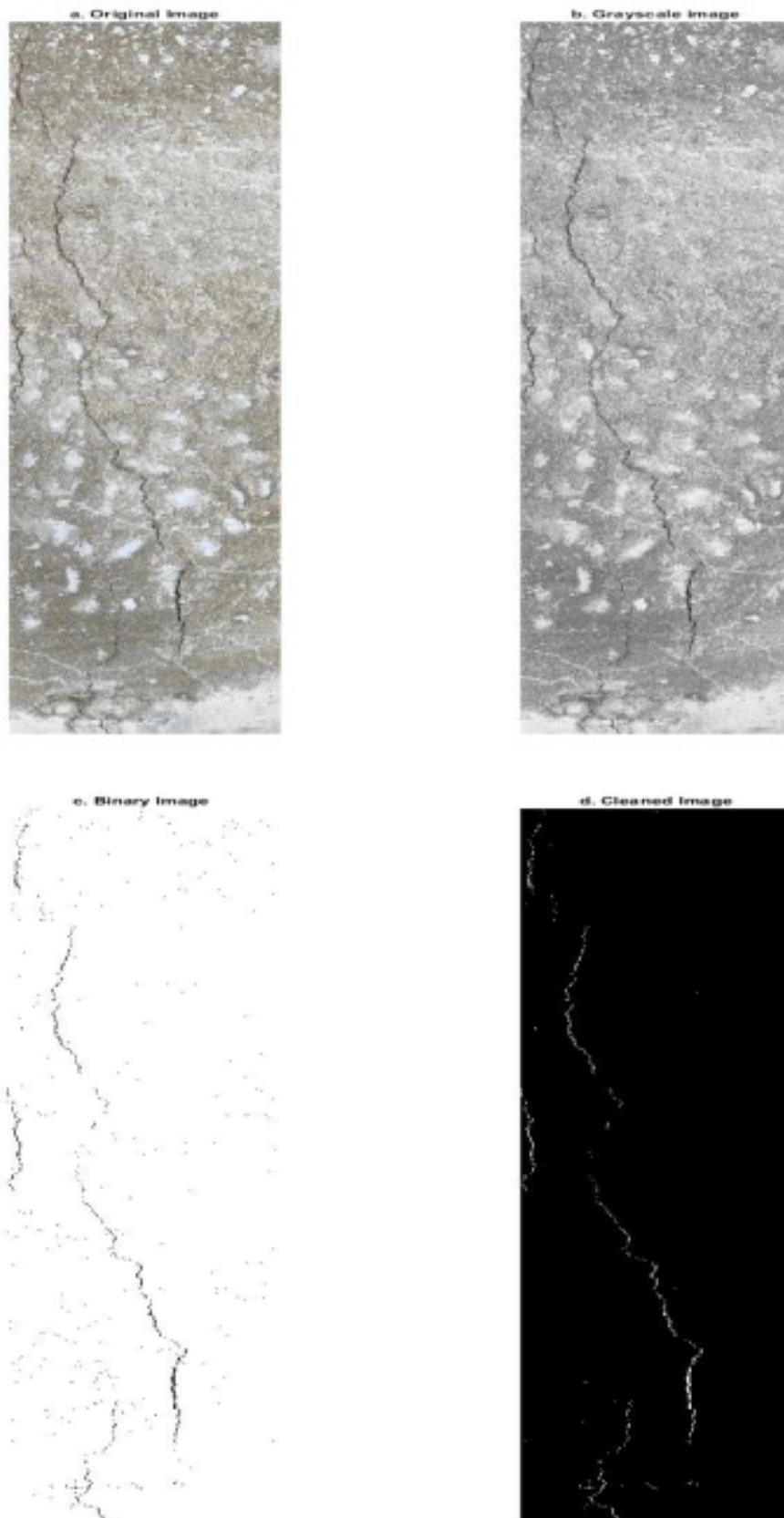


Figure C.9: MATLAB image processing steps for plain concrete (A).



Figure C.10: IC crack length at 24 hours of plain concrete (B).

<input type="checkbox"/>	CrackArea	694.1159
<input type="checkbox"/>	CrackPixels	1.1025e+04
<input type="checkbox"/>	I	3523x500x3 uint8
<input checked="" type="checkbox"/>	Iclean	3523x500 logical
<input checked="" type="checkbox"/>	Icomp	3523x500 logical
<input type="checkbox"/>	Igray	3523x500 uint8
<input checked="" type="checkbox"/>	Ithres	3523x500 logical

Figure C.11: MATLAB crack area at 24 hours of plain concrete (B).

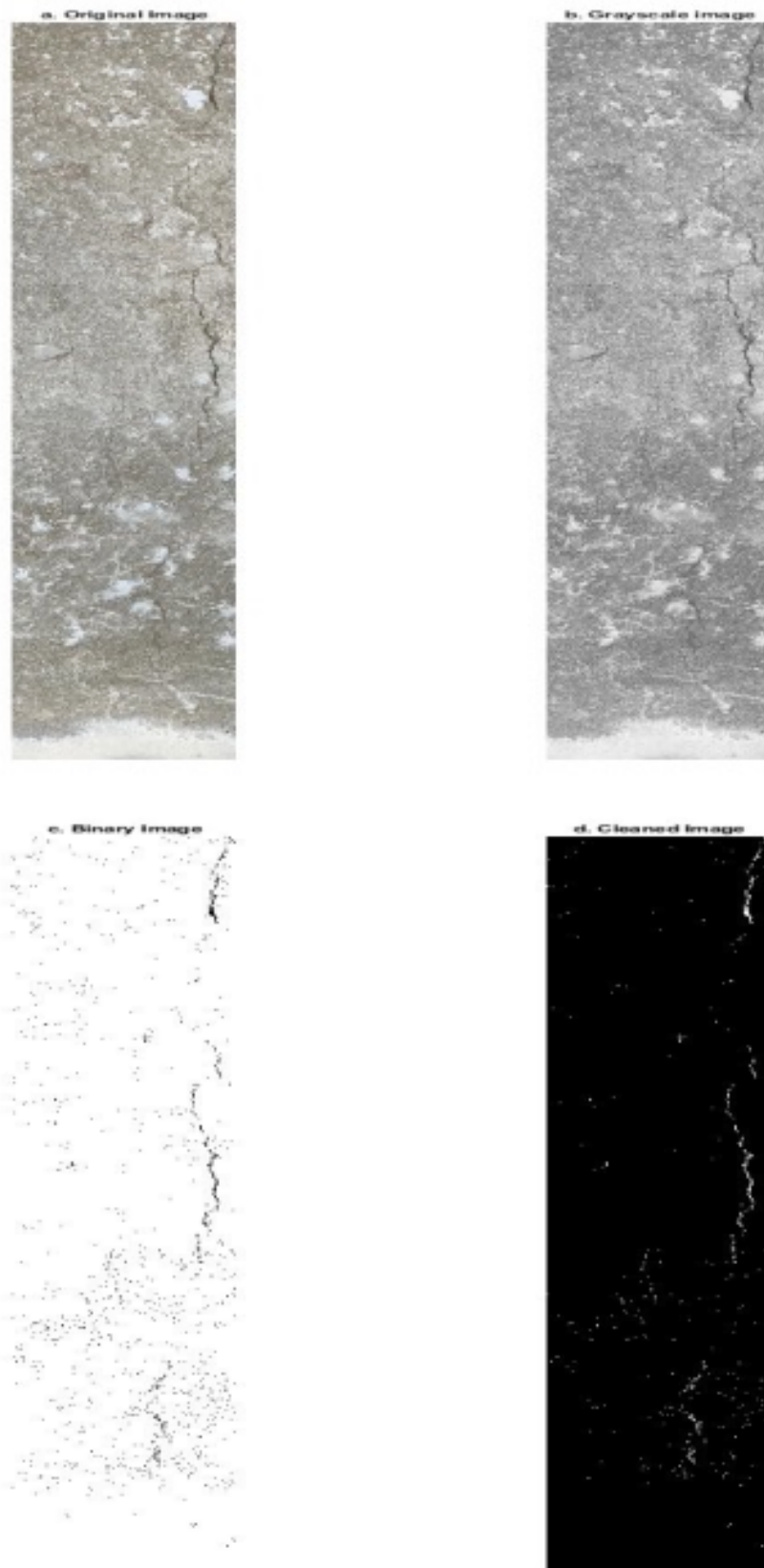


Figure C.12: MATLAB image processing steps for plain concrete (B).

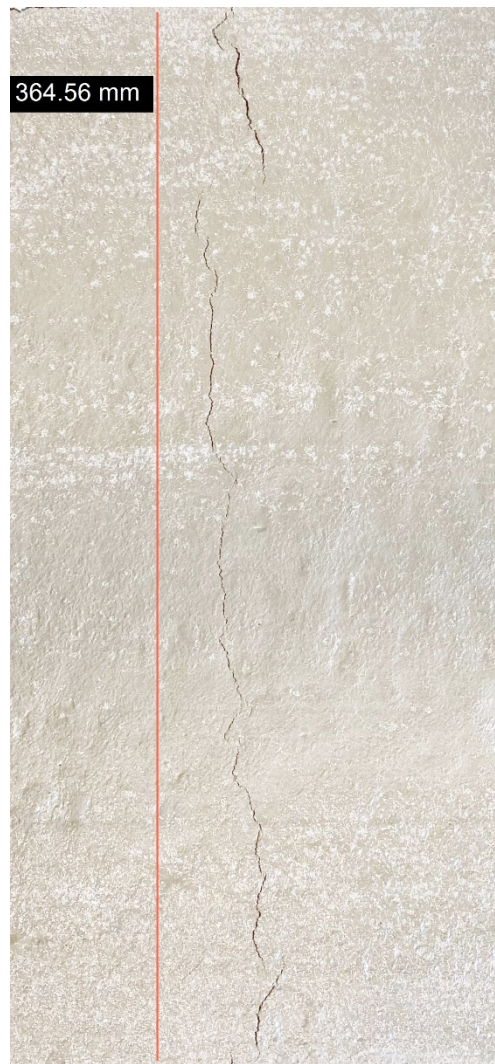


Figure C.13: IC crack length at 24 hours of HTRTSFC30.

<input type="checkbox"/>	CrackArea	392.2834
<input type="checkbox"/>	CrackPixels	7.2563e+03
<input type="checkbox"/>	I	2745x1280x3 uint8
<input checked="" type="checkbox"/>	Iclean	2745x1280 logical
<input checked="" type="checkbox"/>	Icomp	2745x1280 logical
<input type="checkbox"/>	Igray	2745x1280 uint8
<input checked="" type="checkbox"/>	Ithres	2745x1280 logical

Figure C.14: MATLAB crack area at 24 hours of HTRTSFC30.



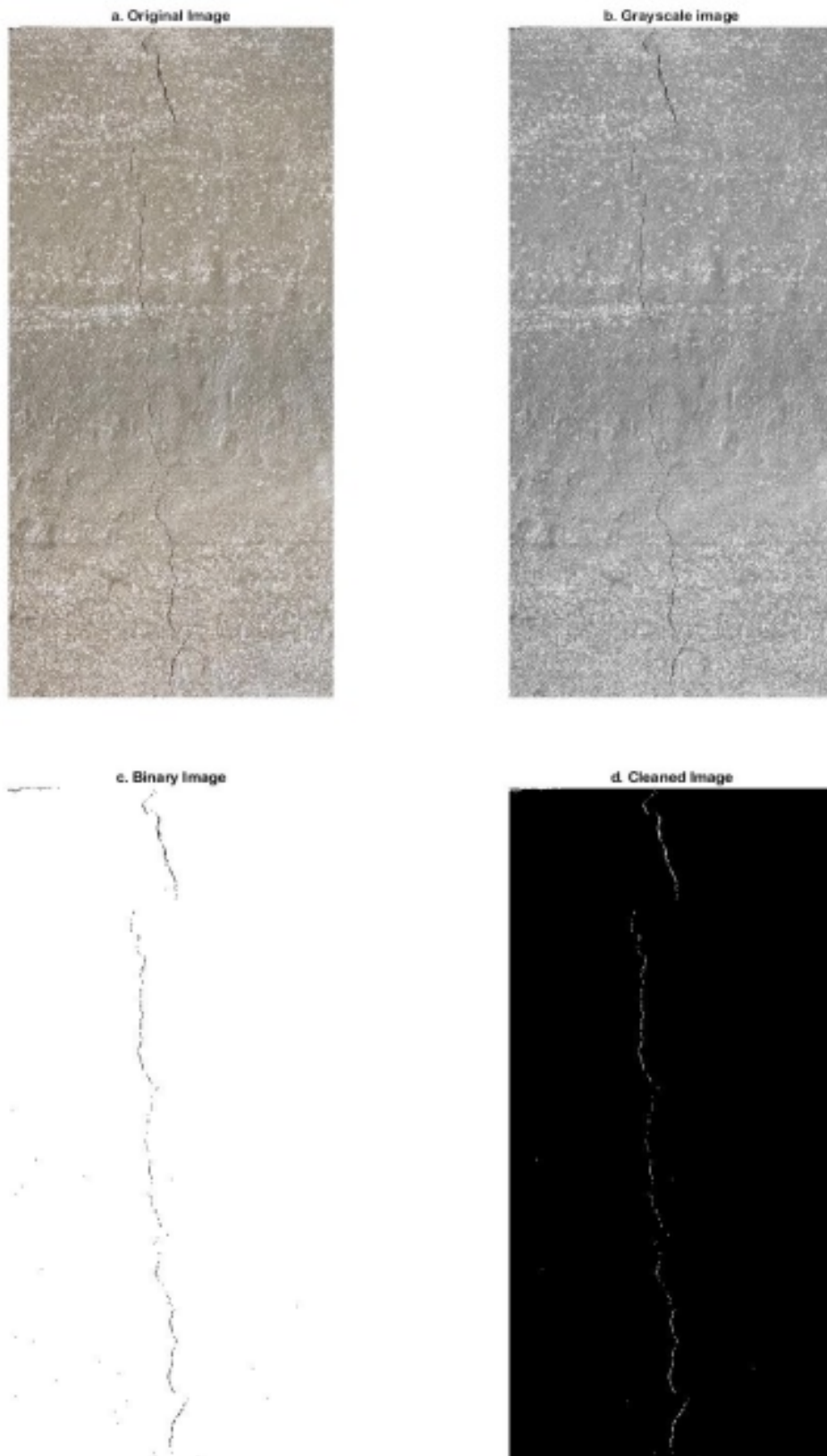


Figure C.15: MATLAB image processing steps for HTRTSFC30.

**C.3.3.2 Optical methods measure****Table C.26** HTRTSFC30 optical measurement.

<b>Point</b>	<b>PC (A) (mm)</b>	<b>PC (B) (mm)</b>	<b>HTRTSFC30 (mm)</b>
1	2	1.5	0.8
2	2.1	1.5	0.9
3	2.2	1.6	0.9
4	2	1.6	0.9
5	2.1	1.6	1
6	2	1.7	1
7	2.2	1.7	1
8	2.3	1.7	1
9	2.3	1.7	1
10	2.3	1.7	1
11	2.3	1.7	1
12	2.3	1.8	1
13	2.2	1.8	1
14	2.2	1.8	1
15	2.2	1.8	1
16	2.2	1.8	1
17	2.2	1.9	1
18	2.2	1.9	1
19	2.2	1.8	1
20	2.2	1.8	1
21	2.2	1.8	1
22	2.2	1.8	1
23	2.2	1.8	1
24	2.2	1.7	0.8
25	2.2	1.6	0.8
26	2.2	1.6	0.8
<b>Ave</b>	2.19	1.72	0.96

**C.3.3.3 Crack width methods measure**

<b>Concrete</b>	<b>MATLAB (mm)</b>	<b>Optical (mm)</b>
<b>PC (A)</b>	2.30	2.19
<b>PC (B)</b>	1.93	1.72
<b>HTRTSFC30</b>	1.07	0.96

### C.3.4 HTRTSFC40

#### C.3.4.1 MATLAB and IC measure software



Figure C.16: IC crack length at 24 hours of plain concrete.

<input type="checkbox"/>	CrackArea	731.2731
<input type="checkbox"/>	CrackPixels	1.2572e+04
<input type="checkbox"/>	I	2474x559x3 uint8
<input checked="" type="checkbox"/>	Iclean	2474x559 logical
<input checked="" type="checkbox"/>	Icomp	2474x559 logical
<input type="checkbox"/>	Igray	2474x559 uint8
<input checked="" type="checkbox"/>	Ithres	2474x559 logical

Figure C.17: MATLAB crack area at 24 hours of plain concrete.

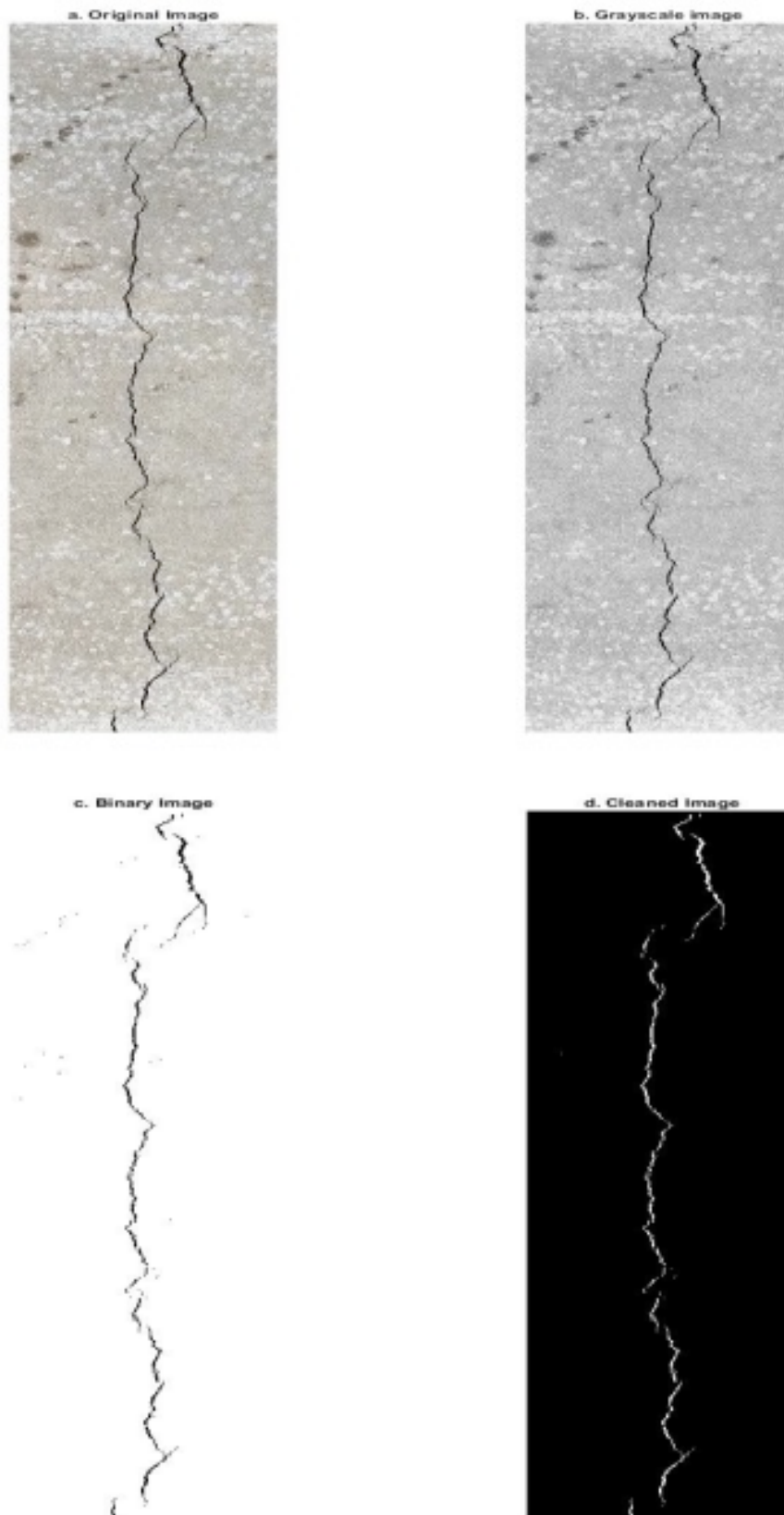


Figure C.18: MATLAB image processing steps for plain concrete.

**C.3.4.2 Optical methods measure****Table C.27** HTRTSFC40 optical measurement.

<b>Point</b>	<b>PC (mm)</b>	<b>HTRTSFC40 (mm)</b>
<b>1</b>	1.8	0
<b>2</b>	1.8	0
<b>3</b>	1.9	0
<b>4</b>	1.9	0
<b>5</b>	1.9	0
<b>6</b>	2	0
<b>7</b>	2	0
<b>8</b>	2	0
<b>9</b>	2	0
<b>10</b>	2	0
<b>11</b>	2	0
<b>12</b>	2	0
<b>13</b>	2	0
<b>14</b>	2	0
<b>15</b>	2	0
<b>16</b>	2	0
<b>17</b>	2	0
<b>18</b>	1.9	0
<b>19</b>	1.9	0
<b>20</b>	1.9	0
<b>21</b>	1.9	0
<b>22</b>	1.9	0
<b>23</b>	1.9	0
<b>24</b>	1.9	0
<b>25</b>	1.9	0
<b>26</b>	1.9	0
<b>Ave</b>	1.94	0

**C.3.4.3 Crack width methods measure**

<b>Concrete</b>	<b>MATLAB (mm)</b>	<b>Optical (mm)</b>
<b>PC</b>	2.01	1.94
<b>HTRTSFC40</b>	0	0

### C.3.5 LWSRTSFC30

#### C.3.5.1 MATLAB and IC measure software



Figure C.19: IC crack length at 24 hours of plain concrete.

<input type="checkbox"/>	CrackArea	395.6323
<input type="checkbox"/>	CrackPixels	1.9271e+04
<input type="checkbox"/>	I	2610x342x3 uint8
<input checked="" type="checkbox"/>	Iclean	2610x342 logical
<input checked="" type="checkbox"/>	Icomp	2610x342 logical
<input type="checkbox"/>	Igray	2610x342 uint8
<input checked="" type="checkbox"/>	lthres	2610x342 logical

Figure C.20: MATLAB crack area at 24 hours of plain concrete

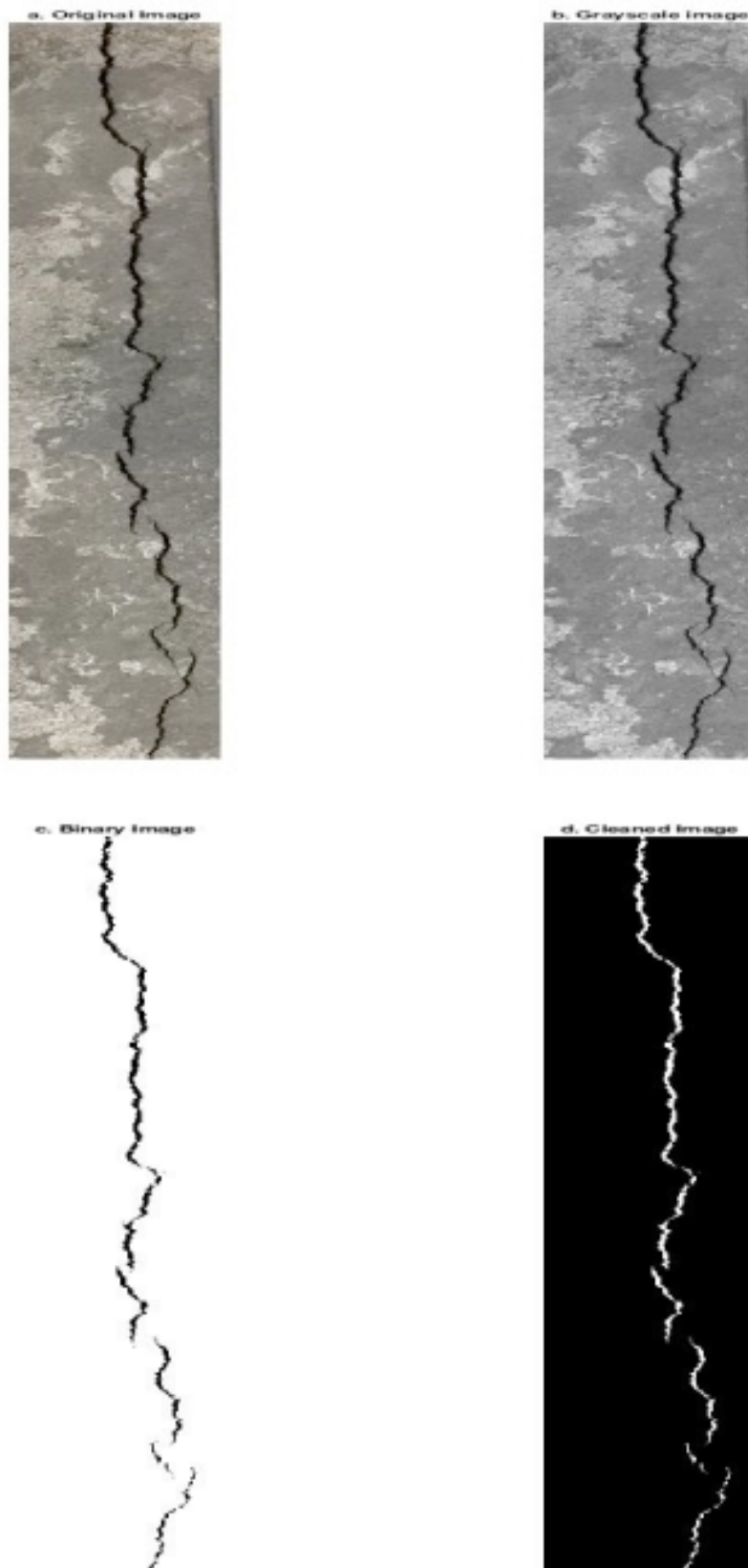


Figure C.21: MATLAB image processing steps for plain concrete.

**C.3.5.2 Optical methods measure****Table C.28** LWSRTSFC30 optical measurement.

<b>Point</b>	<b>PC (mm)</b>	<b>LWSRTSFC30 (mm)</b>
<b>1</b>	0.7	0
<b>2</b>	0.7	0
<b>3</b>	0.8	0
<b>4</b>	0.8	0
<b>5</b>	0.8	0
<b>6</b>	0.8	0
<b>7</b>	0.9	0
<b>8</b>	0.9	0
<b>9</b>	0.9	0
<b>10</b>	0.9	0
<b>11</b>	0.9	0
<b>12</b>	0.9	0
<b>13</b>	0.9	0
<b>14</b>	0.9	0
<b>15</b>	0.9	0
<b>16</b>	0.9	0
<b>17</b>	0.8	0
<b>18</b>	0.8	0
<b>19</b>	0.8	0
<b>20</b>	0.8	0
<b>21</b>	0.8	0
<b>22</b>	0.8	0
<b>23</b>	0.7	0
<b>24</b>	0.7	0
<b>25</b>	0.7	0
<b>26</b>	0.7	0
<b>Ave</b>	0.82	0

**C.3.5.3 Crack width methods measure**

<b>Concrete</b>	<b>MATLAB (mm)</b>	<b>Optical (mm)</b>
<b>PC</b>	1.09	0.82
<b>LWSRTSFC30</b>	0	0



### C.3.6 MWSRTSFC30

#### C.3.6.1 MATLAB and IC measure software



Figure C.22: IC crack length at 24 hours of plain concrete.

<input type="checkbox"/>	CrackArea	432.5475
<input type="checkbox"/>	CrackPixels	1.0278e+04
<input type="checkbox"/>	I	2741x680x3 uint8
<input checked="" type="checkbox"/>	Iclean	2741x680 logical
<input checked="" type="checkbox"/>	Icomp	2741x680 logical
<input type="checkbox"/>	Igray	2741x680 uint8
<input checked="" type="checkbox"/>	Ithres	2741x680 logical

Figure C.23: MATLAB crack area at 24 hours of plain concrete.

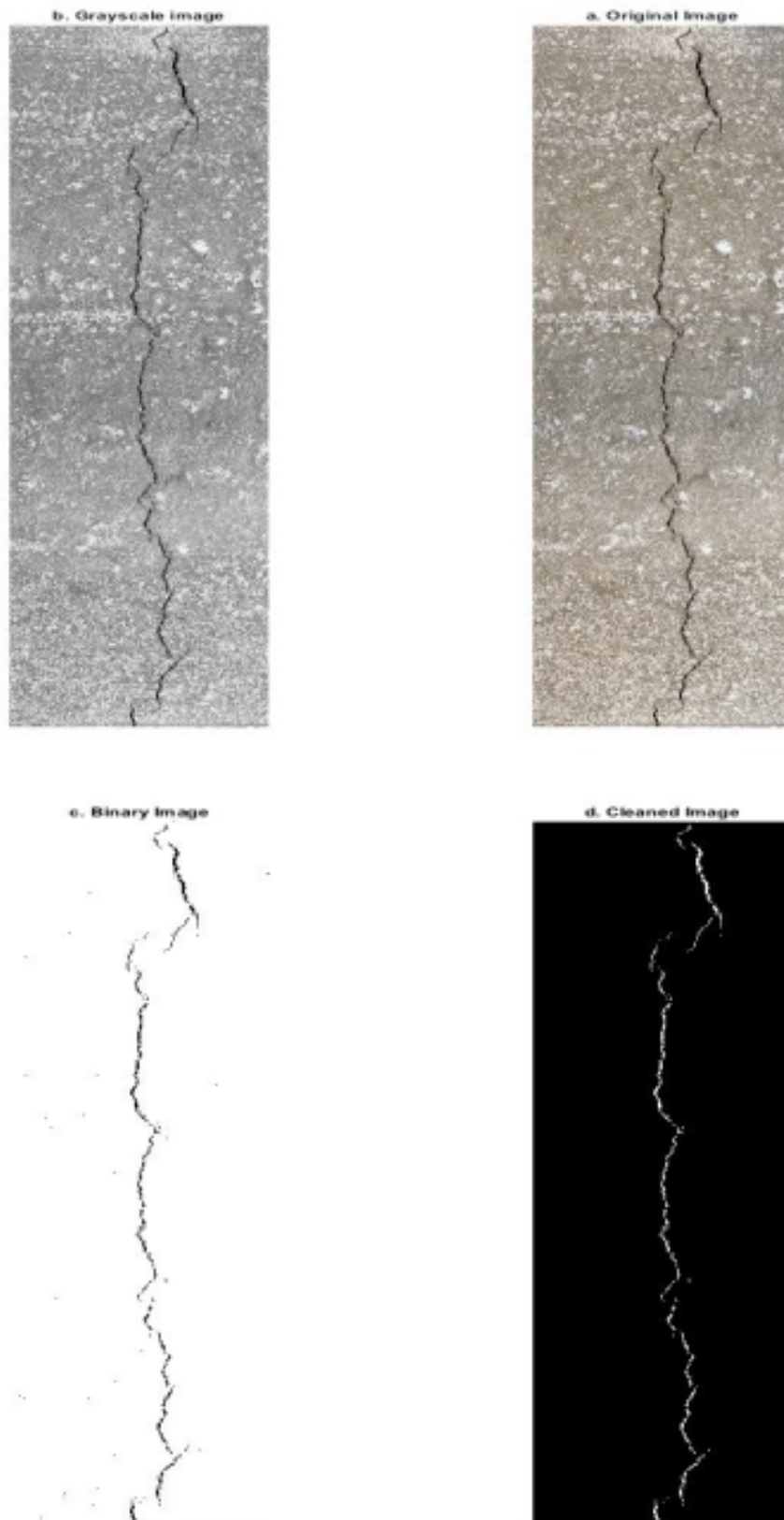


Figure C.24: MATLAB image processing steps for plain concrete.

**C.3.6.2 Optical methods measure****Table C.29** MWSRTSFC30 optical measurement.

<b>Point</b>	<b>PC (mm)</b>	<b>MWSRTSFC30 (mm)</b>
<b>1</b>	0.9	0
<b>2</b>	0.9	0
<b>3</b>	1	0
<b>4</b>	1	0
<b>5</b>	1	0
<b>6</b>	1.1	0
<b>7</b>	1.1	0
<b>8</b>	1.1	0
<b>9</b>	1.1	0
<b>10</b>	1.1	0
<b>11</b>	1.1	0
<b>12</b>	1.1	0
<b>13</b>	1.1	0
<b>14</b>	1.1	0
<b>15</b>	1.1	0
<b>16</b>	1.1	0
<b>17</b>	1.1	0
<b>18</b>	1.1	0
<b>19</b>	1.1	0
<b>20</b>	1	0
<b>21</b>	1	0
<b>22</b>	1	0
<b>23</b>	1	0
<b>24</b>	1	0
<b>25</b>	0.9	0
<b>26</b>	0.9	0
<b>Ave</b>	1.04	0

**C.3.6.3 Crack width methods measure**

<b>Concrete</b>	<b>MATLAB (mm)</b>	<b>Optical (mm)</b>
<b>PC</b>	1.19	1.04
<b>MWSRTSFC30</b>	0	0

### C.3.7 HWSRTSFC30

#### C.3.7.1 MATLAB and IC measure software

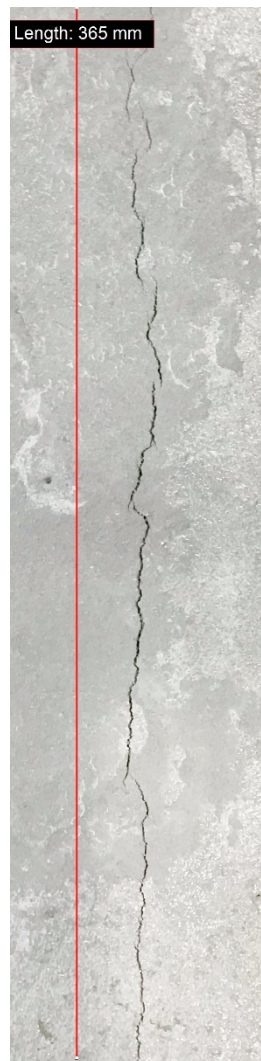


Figure C.25: IC crack length at 24 hours of plain concrete.

<input type="checkbox"/>	CrackArea	513.4432
<input type="checkbox"/>	CrackPixels	1.4210e+04
<input type="checkbox"/>	I	2887x707x3 uint8
<input checked="" type="checkbox"/>	Iclean	2887x707 logical
<input checked="" type="checkbox"/>	Icomp	2887x707 logical
<input type="checkbox"/>	Igray	2887x707 uint8
<input checked="" type="checkbox"/>	Ithres	2887x707 logical

Figure C.26: MATLAB crack area at 24 hours of plain concrete.

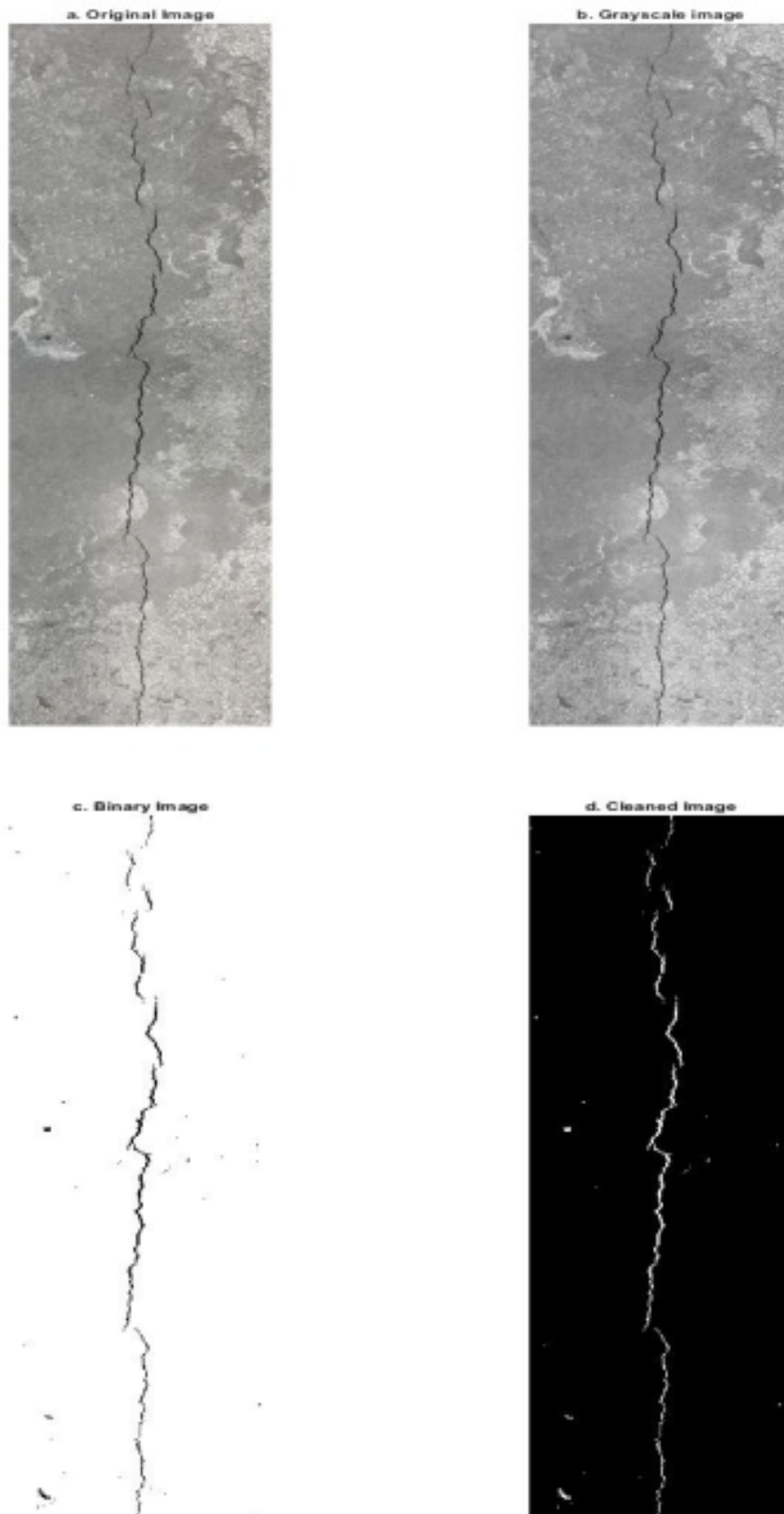


Figure C.27: MATLAB image processing steps for plain concrete.



Figure C.28: IC crack length at 24 hours of HWSRTSFC30.

<input type="checkbox"/>	CrackArea	152.7571
<input type="checkbox"/>	CrackPixels	6.9758e+03
<input type="checkbox"/>	I	2884x504x3 uint8
<input checked="" type="checkbox"/>	Iclean	2884x504 logical
<input checked="" type="checkbox"/>	Icomp	2884x504 logical
<input type="checkbox"/>	Igray	2884x504 uint8
<input checked="" type="checkbox"/>	Ithres	2884x504 logical

Figure C.29: MATLAB crack area at 24 hours of HWSRTSFC30.

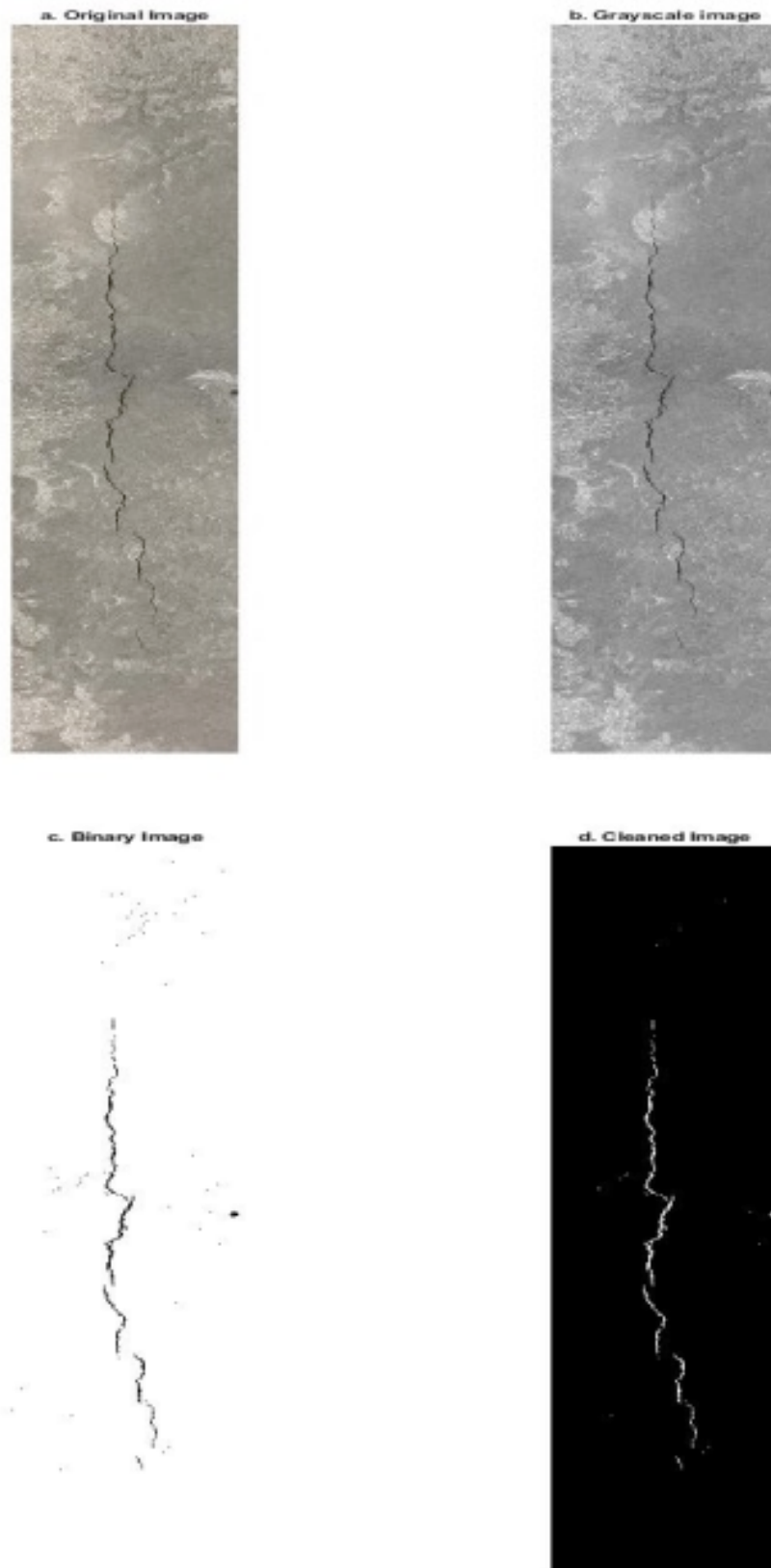


Figure C.30: MATLAB image processing steps for HWSRTSFC30.

**C.3.7.2 Optical methods measure****Table C.30** HWSRTSFC30 optical measurement.

<b>Point</b>	<b>PC (mm)</b>	<b>HWSRTSFC30 (mm)</b>
<b>1</b>	1	0.3
<b>2</b>	1	0.3
<b>3</b>	1.2	0.3
<b>4</b>	1.2	0.3
<b>5</b>	1.2	0.3
<b>6</b>	1.2	0.3
<b>7</b>	1.4	0.4
<b>8</b>	1.4	0.4
<b>9</b>	1.4	0.4
<b>10</b>	1.4	0.4
<b>11</b>	1.4	0.4
<b>12</b>	1.4	0.5
<b>13</b>	1.4	0.5
<b>14</b>	1.4	0.5
<b>15</b>	1.4	0.5
<b>16</b>	1.4	0.5
<b>17</b>	1.3	0.5
<b>18</b>	1.3	0.5
<b>19</b>	1.3	0.4
<b>20</b>	1.3	0.4
<b>21</b>	1.3	0.4
<b>22</b>	1.3	0.4
<b>23</b>	1.3	0.4
<b>24</b>	1.3	0.4
<b>25</b>	1.3	0.3
<b>26</b>	1.3	0.3
<b>Ave</b>	1.30	0.40

**C.3.7.3 Crack width methods measure**

<b>Concrete</b>	<b>MATLAB (mm)</b>	<b>Optical (mm)</b>
<b>PC</b>	1.41	1.30
<b>HWSRTSFC30</b>	0.53	0.40



### C.3.8 HWSRTSFC40

#### C.3.8.1 MATLAB and IC measure software



Figure C.31: IC crack length at 24 hours of plain concrete.

<input type="checkbox"/>	CrackArea	503.9769
<input type="checkbox"/>	CrackPixels	1.2920e+04
<input type="checkbox"/>	I	2236x787x3 uint8
<input checked="" type="checkbox"/>	Iclean	2236x787 logical
<input checked="" type="checkbox"/>	Icomp	2236x787 logical
<input type="checkbox"/>	Igray	2236x787 uint8
<input checked="" type="checkbox"/>	Ithres	2236x787 logical

Figure C.32: MATLAB crack area at 24 hours of plain concrete.

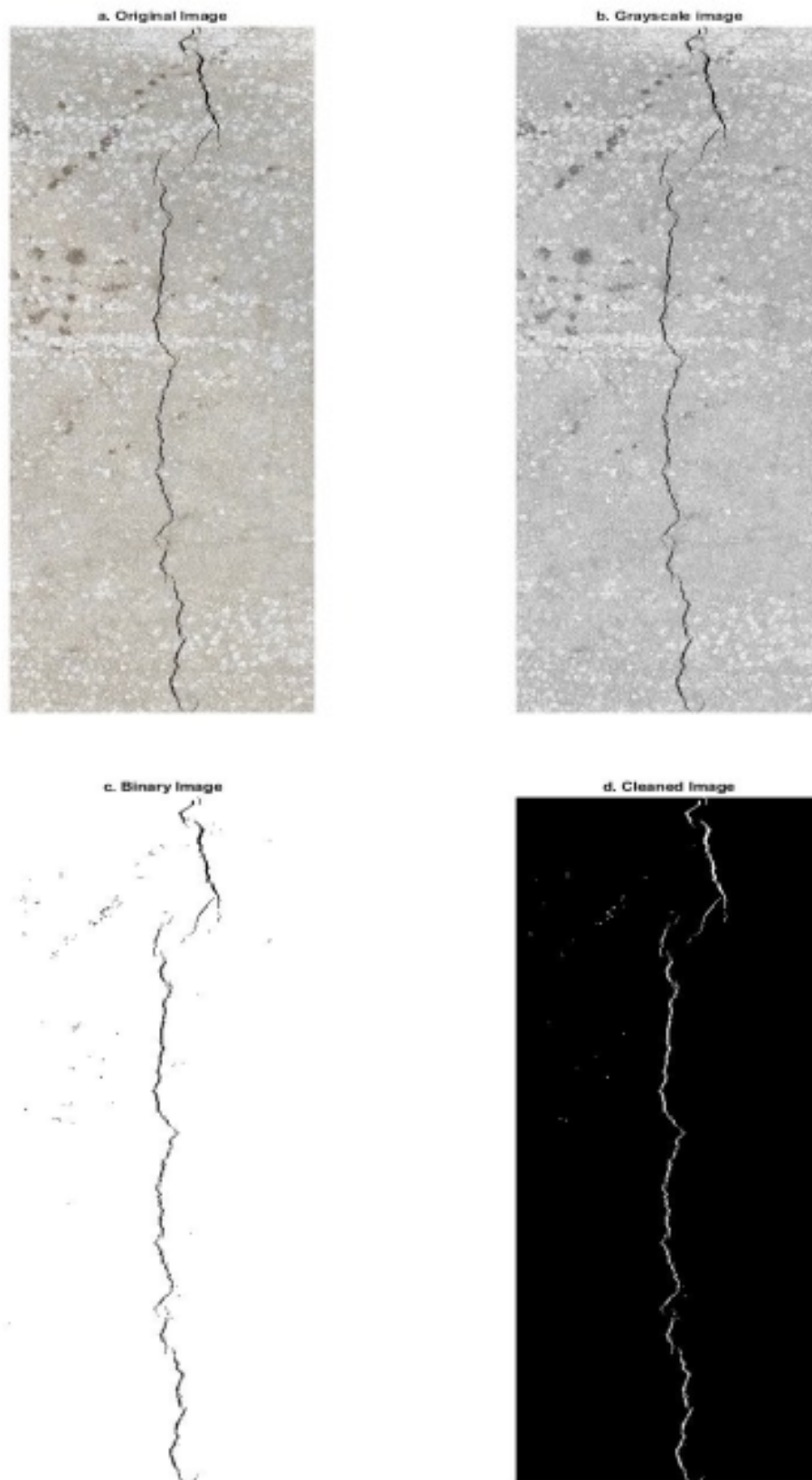


Figure C.33: MATLAB image processing steps for plain concrete.

**C.3.8.2 Optical methods measure****Table C.31** HWSRTSFC40 optical measurement.

<b>Point</b>	<b>PC (mm)</b>	<b>HWSRTSFC40 (mm)</b>
<b>1</b>	1.1	0
<b>2</b>	1.1	0
<b>3</b>	1.2	0
<b>4</b>	1.2	0
<b>5</b>	1.3	0
<b>6</b>	1.3	0
<b>7</b>	1.3	0
<b>8</b>	1.3	0
<b>9</b>	1.3	0
<b>10</b>	1.3	0
<b>11</b>	1.3	0
<b>12</b>	1.3	0
<b>13</b>	1.3	0
<b>14</b>	1.4	0
<b>15</b>	1.4	0
<b>16</b>	1.4	0
<b>17</b>	1.4	0
<b>18</b>	1.4	0
<b>19</b>	1.4	0
<b>20</b>	1.4	0
<b>21</b>	1.4	0
<b>22</b>	1.4	0
<b>23</b>	1.3	0
<b>24</b>	1.3	0
<b>25</b>	1.2	0
<b>26</b>	1.2	0
<b>Ave</b>	1.30	0

**C.3.8.3 Crack width methods measure**

<b>Concrete</b>	<b>MATLAB (mm)</b>	<b>Optical (mm)</b>
<b>PC</b>	1.38	1.3
<b>HWSRTSFC40</b>	0	0

### C.3.9 0.5W/CRTSFC30

#### C.3.9.1 MATLAB and IC measure software



Figure C.34: IC crack length at 24 hours of plain concrete.

<input type="checkbox"/>	CrackArea	404.9408
<input type="checkbox"/>	CrackPixels	1.4794e+04
<input type="checkbox"/>	I	4026x1015x3 uint8
<input checked="" type="checkbox"/>	Iclean	4026x1015 logical
<input checked="" type="checkbox"/>	Icomp	4026x1015 logical
<input type="checkbox"/>	Igray	4026x1015 uint8
<input checked="" type="checkbox"/>	Ithres	4026x1015 logical

Figure C.35: MATLAB crack area at 24 hours of plain concrete.

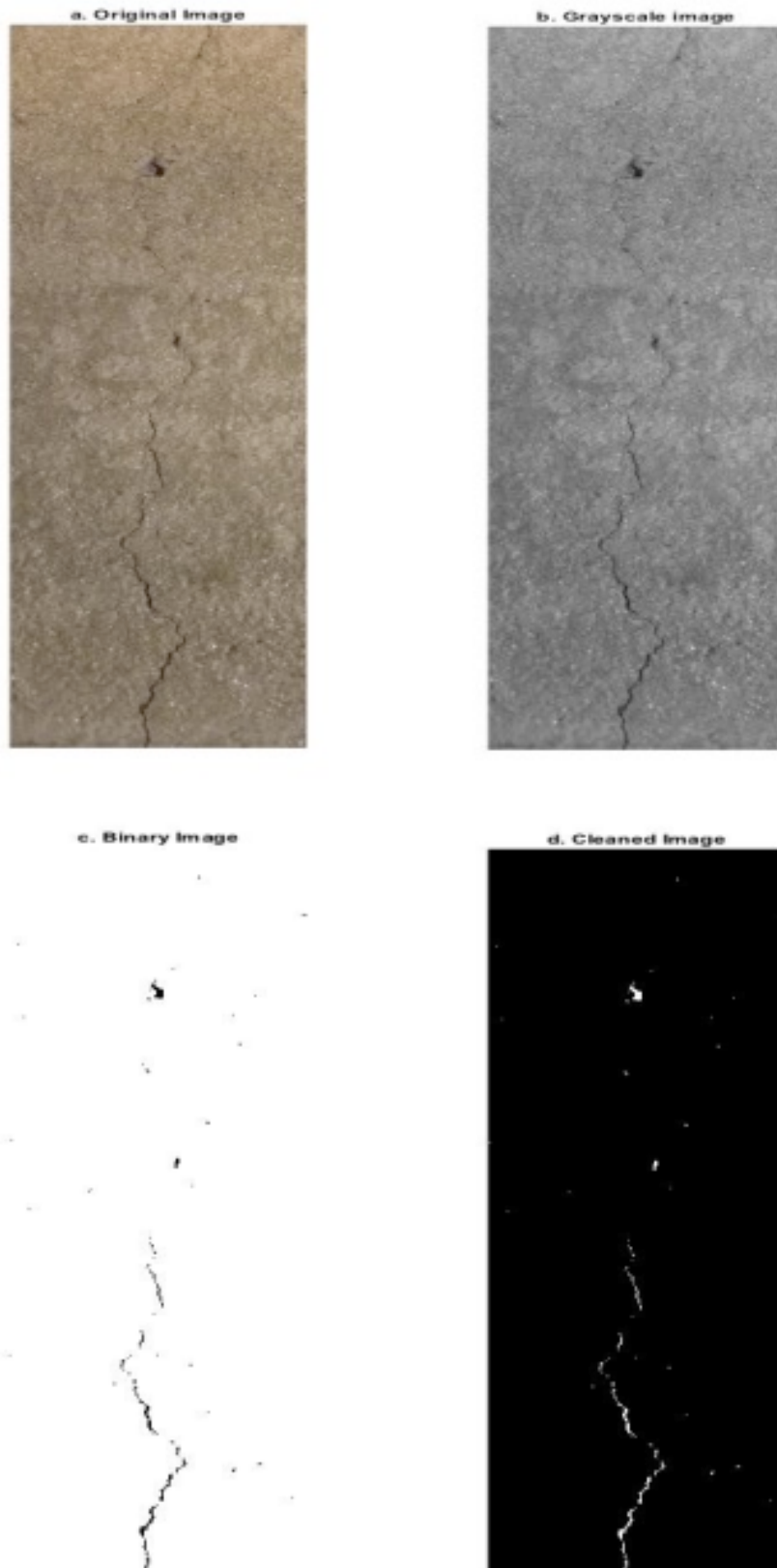


Figure C.36: MATLAB image processing steps for plain concrete.

**C.3.9.2 Optical methods measure****Table C.32** 0.5W/CRTSFC30 optical measurement.

<b>Point</b>	<b>PC (mm)</b>	<b>0.5W/CRTSFC30 (mm)</b>
1	0.7	0
2	0.7	0
3	0.7	0
4	0.8	0
5	0.8	0
6	0.9	0
7	0.9	0
8	0.9	0
9	1	0
10	1	0
11	1	0
12	1	0
13	1	0
14	1	0
15	1	0
16	1	0
17	1.1	0
18	1.1	0
19	1.2	0
20	1.2	0
21	1.2	0
22	1.2	0
23	1.2	0
24	1.2	0
25	1.1	0
26	1.1	0
Ave	1.0	0

**C.3.9.3 Crack width methods measure**

<b>Concrete</b>	<b>MATLAB (mm)</b>	<b>Optical (mm)</b>
PC	1.11	1.0
0.5W/CRTSFC30	0	0

## C.3.10 0.55W/CRTSFC30

## C.3.10.1 MATLAB and IC measure software



Figure C.37: IC crack length at 24 hours of plain concrete.

<input type="checkbox"/>	CrackArea	432.5475
<input type="checkbox"/>	CrackPixels	1.0278e+04
<input type="checkbox"/>	I	2741x680x3 uint8
<input checked="" type="checkbox"/>	Iclean	2741x680 logical
<input checked="" type="checkbox"/>	Icomp	2741x680 logical
<input type="checkbox"/>	Igray	2741x680 uint8
<input checked="" type="checkbox"/>	Ithres	2741x680 logical

Figure C.38: MATLAB crack area at 24 hours of plain concrete.

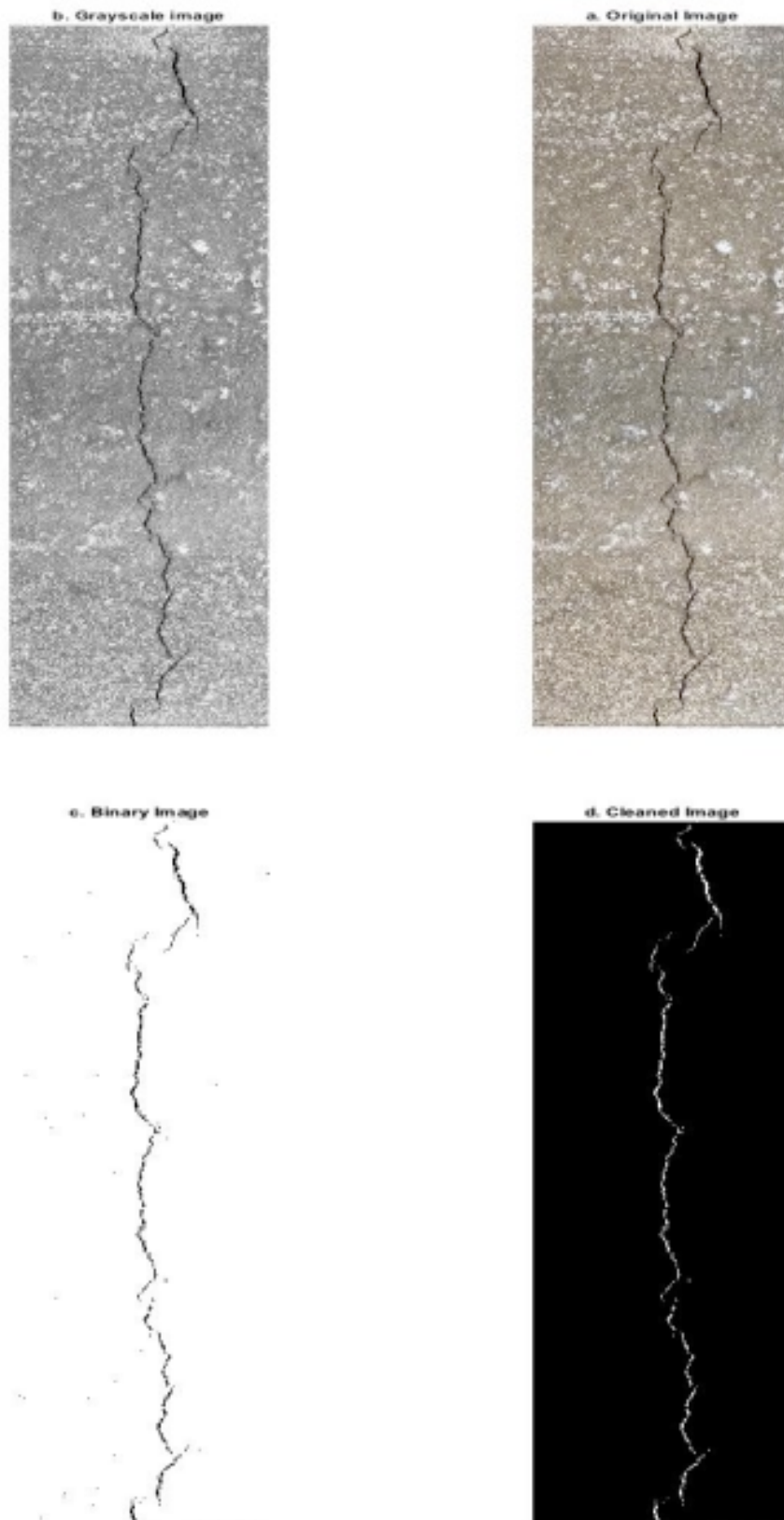


Figure C.39: MATLAB image processing steps for plain concrete.



**C.3.10.2 Optical methods measure****Table C.33** 0.55W/CRTSFC30 optical measurement.

<b>Point</b>	<b>PC (mm)</b>	<b>0.55W/CRTSFC30 (mm)</b>
<b>1</b>	0.9	0
<b>2</b>	0.9	0
<b>3</b>	1	0
<b>4</b>	1	0
<b>5</b>	1	0
<b>6</b>	1.1	0
<b>7</b>	1.1	0
<b>8</b>	1.1	0
<b>9</b>	1.1	0
<b>10</b>	1.1	0
<b>11</b>	1.1	0
<b>12</b>	1.1	0
<b>13</b>	1.1	0
<b>14</b>	1.1	0
<b>15</b>	1.1	0
<b>16</b>	1.1	0
<b>17</b>	1.1	0
<b>18</b>	1.1	0
<b>19</b>	1.1	0
<b>20</b>	1	0
<b>21</b>	1	0
<b>22</b>	1	0
<b>23</b>	1	0
<b>24</b>	1	0
<b>25</b>	0.9	0
<b>26</b>	0.9	0
<b>Ave</b>	1.04	0

**C.3.10.3 Crack width methods measure**

<b>Concrete</b>	<b>MATLAB (mm)</b>	<b>Optical (mm)</b>
<b>PC</b>	1.19	1.04
<b>0.55W/SRTSFC30</b>	0	0

### C.3.11 0.6W/CRTSFC30

#### C.3.11.1 MATLAB and IC measure software



Figure C.40: IC crack length at 24 hours of plain concrete.

<input type="checkbox"/>	CrackArea	527.2634
<input type="checkbox"/>	CrackPixels	2.7518e+04
<input type="checkbox"/>	I	2899x451x3 uint8
<input checked="" type="checkbox"/>	Iclean	2899x451 logical
<input checked="" type="checkbox"/>	Icomp	2899x451 logical
<input type="checkbox"/>	Igray	2899x451 uint8
<input checked="" type="checkbox"/>	Ithres	2899x451 logical

Figure C.41: MATLAB crack area at 24 hours of plain concrete.

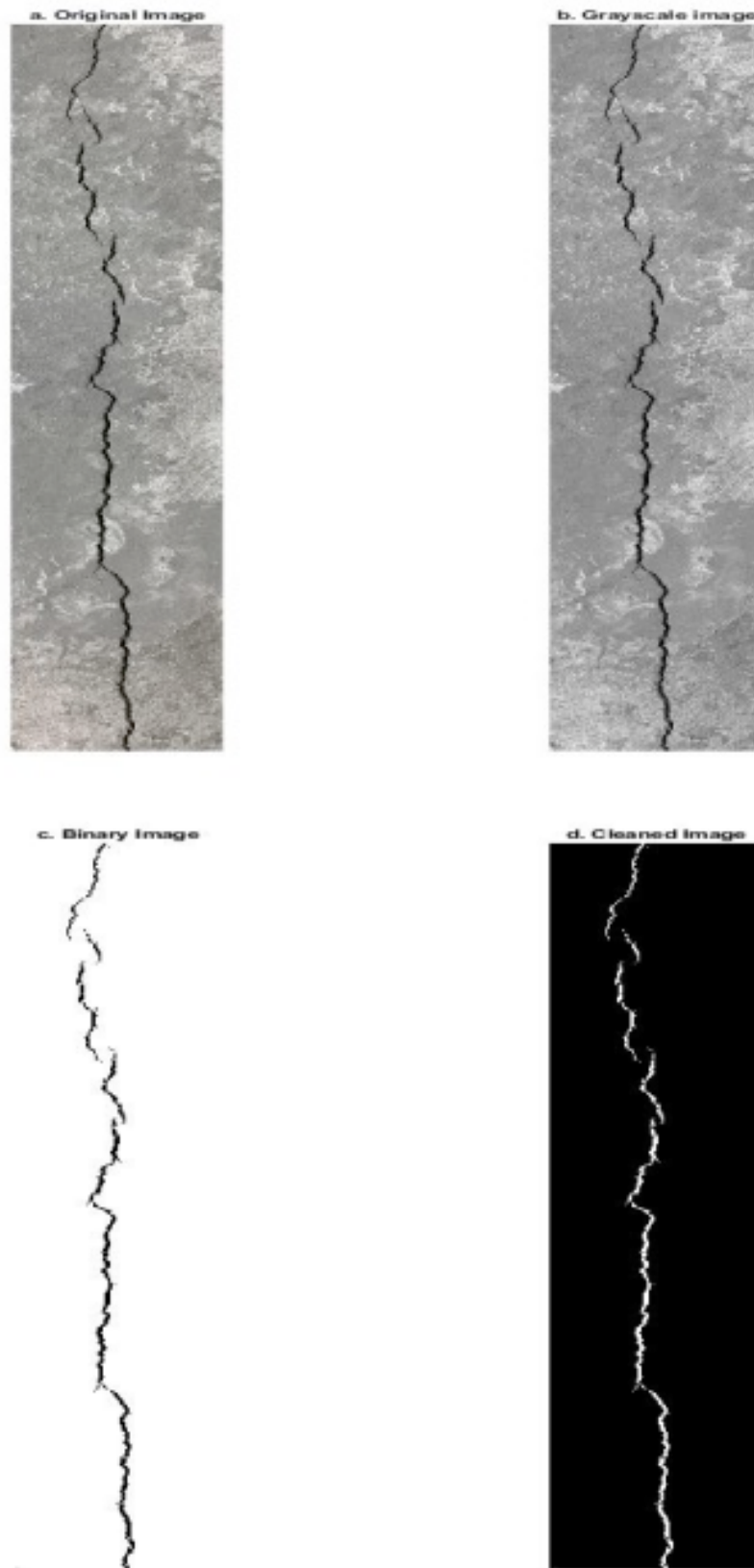


Figure C.42: MATLAB image processing steps for plain concrete.

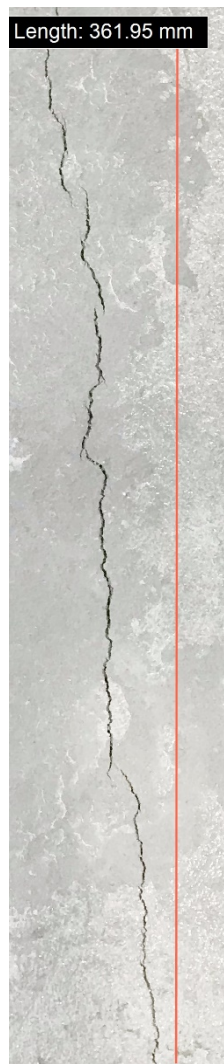


Figure C.43: IC crack length at 24 hours of 0.6W/CRTSFC30.

<input type="checkbox"/>	CrackArea	318.9220
<input type="checkbox"/>	CrackPixels	1.1799e+04
<input type="checkbox"/>	I	2464x520x3 uint8
<input checked="" type="checkbox"/>	Iclean	2464x520 logical
<input checked="" type="checkbox"/>	Icomp	2464x520 logical
<input type="checkbox"/>	Igray	2464x520 uint8
<input checked="" type="checkbox"/>	Ithres	2464x520 logical

Figure C.44: MATLAB crack area at 24 hours of 0.6W/CRTSFC30.

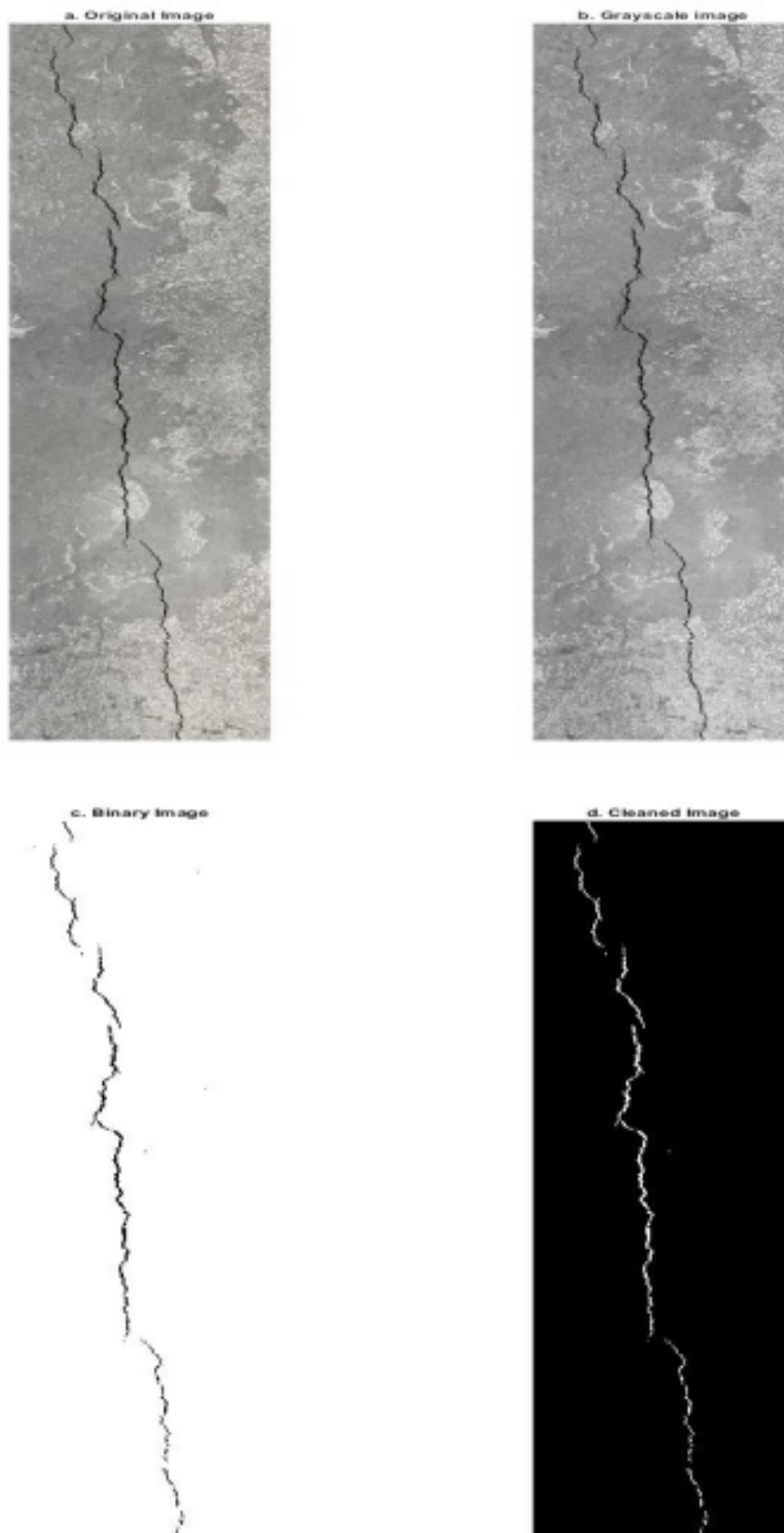


Figure C.45: MATLAB image processing steps for 0.6W/CRTSFC30.

**C.3.11.2 Optical methods measure****Table C.34** 0.6W/CRTSFC30 optical measurement.

<b>Point</b>	<b>PC (mm)</b>	<b>0.6W/CRTSFC30 (mm)</b>
<b>1</b>	1	0.5
<b>2</b>	1	0.5
<b>3</b>	1.3	0.5
<b>4</b>	1.3	0.7
<b>5</b>	1.4	0.7
<b>6</b>	1.4	0.7
<b>7</b>	1.4	0.7
<b>8</b>	1.4	0.7
<b>9</b>	1.4	0.8
<b>10</b>	1.4	0.8
<b>11</b>	1.4	0.8
<b>12</b>	1.4	0.9
<b>13</b>	1.5	0.9
<b>14</b>	1.5	0.9
<b>15</b>	1.5	0.9
<b>16</b>	1.5	0.8
<b>17</b>	1.5	0.8
<b>18</b>	1.5	0.9
<b>19</b>	1.5	0.9
<b>20</b>	1.5	0.9
<b>21</b>	1.5	0.7
<b>22</b>	1.5	0.7
<b>23</b>	1.4	0.7
<b>24</b>	1.4	0.7
<b>25</b>	1.4	0.7
<b>26</b>	1.4	0.7
<b>Ave</b>	1.40	0.75

**C.3.11.3 Crack width methods measure**

<b>Concrete</b>	<b>MATLAB (mm)</b>	<b>Optical (mm)</b>
<b>PC</b>	1.44	1.40
<b>0.6W/SRTSFC30</b>	0.88	0.75

## C.3.12 0.6W/CRTSFC40

## C.3.12.1 MATLAB and IC measure software

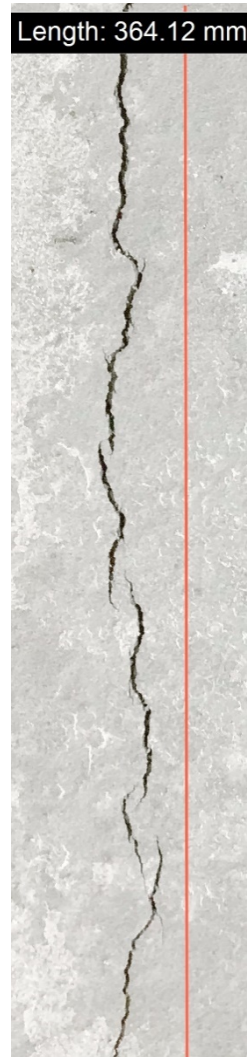


Figure C.46: IC crack length at 24 hours of plain concrete.

<input type="checkbox"/>	CrackArea	505.4883
<input type="checkbox"/>	CrackPixels	1.7178e+04
<input type="checkbox"/>	I	1915x427x3 uint8
<input checked="" type="checkbox"/>	Iclean	1915x427 logical
<input checked="" type="checkbox"/>	Icomp	1915x427 logical
<input type="checkbox"/>	Igray	1915x427 uint8
<input checked="" type="checkbox"/>	Ithres	1915x427 logical

Figure C.47: MATLAB crack area at 24 hours of plain concrete.

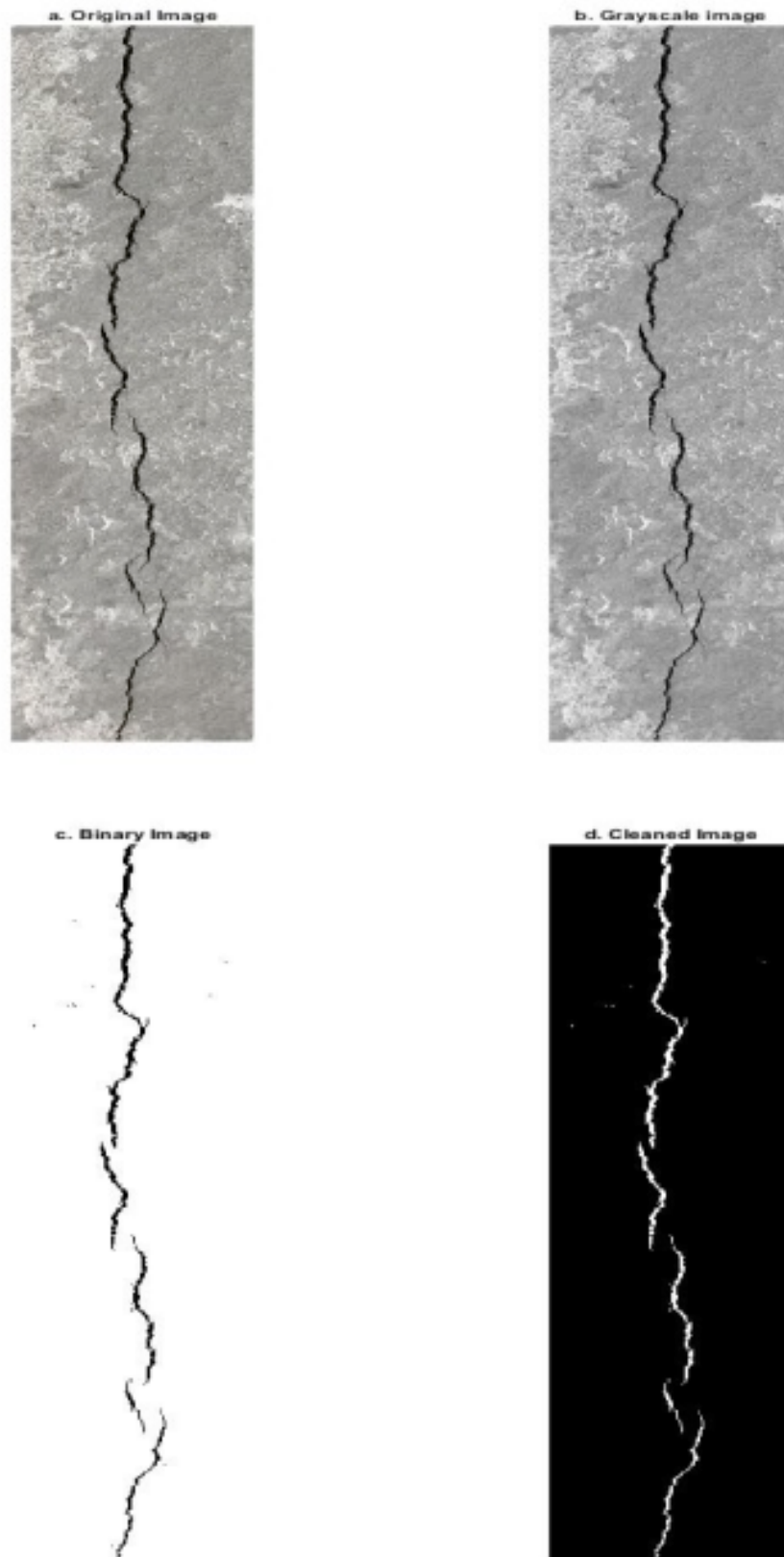


Figure C.48: MATLAB image processing steps for plain concrete.



**C.3.12.2 Optical methods measure****Table C.35** 0.6W/CRTSFC40 optical measurement.

<b>Point</b>	<b>PC (mm)</b>	<b>0.6W/CRTSFC40 (mm)</b>
1	1.4	0
2	1.4	0
3	1.4	0
4	1.3	0
5	1.3	0
6	1.2	0
7	1.2	0
8	1.2	0
9	1.2	0
10	1.4	0
11	1.4	0
12	1.4	0
13	1.4	0
14	1.4	0
15	1.4	0
16	1.3	0
17	1.3	0
18	1.3	0
19	1.3	0
20	1.2	0
21	1.2	0
22	1.1	0
23	1.1	0
24	1.1	0
25	1	0
26	1	0
<b>Ave</b>	1.27	0

**C.3.12.3 Crack width methods measure**

<b>Concrete</b>	<b>MATLAB (mm)</b>	<b>Optical (mm)</b>
<b>PC</b>	1.39	1.27
<b>0.6W/SRTSFC40</b>	0	0

**This page is intentionally left blank**


## **Appendix D:**

### **Chapter 5: Effect of Curing Methods on Plastic Shrinkage Cracking**

This appendix presents additional information regarding the results found in Chapter 5.

## D.1 Admixtures

## D.1.1 High-range Water Reducing Admixture – Sika ViscoCrete 30HE Summary Data Sheet

Construction	<b>Product Data Sheet</b> Edition 12/07/2016 Identification no: 02 13 01 01 100 0 000409 Sika® ViscoCrete® 30HE (UK)		<b>CE</b>
	<b>Sika® ViscoCrete® 30HE (UK)</b> Accelerating High Range Water Reducing/Superplasticising Concrete Admixture		
	<b>Product Description</b>	Sika® ViscoCrete® 30HE (UK) is a liquid admixture for concrete which is used as an accelerating high range water reducer or superplasticiser. It meets the requirements of BS EN 934-2.	
	<b>Uses</b>	Sika® ViscoCrete® 30HE (UK) has been specifically formulated for the production of concrete mixes which require high early strength development, powerful water reduction and excellent flowability.	
		<ul style="list-style-type: none"> <li>■ Precast concrete</li> <li>■ Fast track concrete</li> <li>■ Self compacting concrete</li> </ul>	
	<b>Characteristics / Advantages</b>	<ul style="list-style-type: none"> <li>■ Significantly increased early age strength</li> <li>■ Excellent water reduction</li> <li>■ Excellent flowability</li> <li>■ Reduced drying shrinkage</li> <li>■ Improved surface finish</li> </ul>	
	<b>Tests</b>		
	<b>Approvals / Standards</b>	Conforms to the requirements of BS EN 934-2 Tables 3.1 & 3.2 DoP 02 13 01 01 100 0 000422 1088, certified by Factory Production Control Body 0086, Certificate 541325, and provided with the CE mark	
	<b>Product Data</b>		
	<b>Form</b>		
<b>Appearance / Colour</b>	Light Brown Liquid		
<b>Packaging</b>	25 litre drum and 1000 litre IBC		
<b>Storage</b>			
<b>Storage Conditions / Shelf-Life</b>	12 months from date of production if stored in unopened and undamaged original sealed containers protected from moisture at temperatures between +5°C and +25°C.		
			

<b>Technical Data</b>	
Chemical Base	Modified Polycarboxylate
Density	1.06 kg/litre
pH Value	4.4 ± 1.0
Water Soluble Chloride Content	<0.1% w/w (chloride free)
Alkali Content	< 0.40%
<b>System Information</b>	
<b>Application Details</b>	
Consumption / Dosage	<ul style="list-style-type: none"> <li>■ 0.2 - 0.8% by weight of cement (medium workability)</li> <li>■ 1.0 – 2.0% by weight of cement (high workability/SCC)</li> </ul>
Dispensing	<ul style="list-style-type: none"> <li>■ Sika® ViscoCrete® 30HE (UK) should be dispensed through suitable calibrated equipment</li> </ul>
Application Conditions / Limitations	<ul style="list-style-type: none"> <li>■ Sika® ViscoCrete® 30HE (UK) should not be added to dry cement</li> <li>■ Sika® ViscoCrete® 30HE (UK) should be added with the mixing water</li> </ul>
Compatibility	<p>Sika® Admixtures:</p> <ul style="list-style-type: none"> <li>■ Compatibility information available on request</li> </ul> <p>Cements:</p> <ul style="list-style-type: none"> <li>■ All cement combinations</li> </ul>
Notes on Application / Limitations	Support from our Technical Service Department is recommended.
Value Base	All technical data stated in this Product Data Sheet are based on laboratory tests. Actual measured data may vary due to circumstances beyond our control.
Local Restrictions	Please note that as a result of specific local regulations the performance of this product may vary from country to country. Please consult the local Product Data Sheet for the exact description of the application fields.
Health and Safety Information	For information and advice on the safe handling, storage and disposal of chemical products, users shall refer to the most recent Material Safety Data Sheet containing physical, ecological, toxicological and other safety-related data.
Legal Notes	The information, and, in particular, the recommendations relating to the application and end-use of Sika products, are given in good faith based on Sika's current knowledge and experience of the products when properly stored, handled and applied under normal conditions in accordance with Sika's recommendations. In practice, the differences in materials, substrates and actual site conditions are such that no warranty in respect of merchantability or of fitness for a particular purpose, nor any liability arising out of any legal relationship whatsoever, can be inferred either from this information, or from any written recommendations, or from any other advice offered. The user of the product must test the product's suitability for the intended application and purpose. Sika reserves the right to change the properties of its products. The proprietary rights of third parties must be observed. All orders are accepted subject to our current terms of sale and delivery. Users must always refer to the most recent issue of the local Product Data Sheet for the product concerned, copies of which will be supplied on request.

## D.1.2 Safecure Super

# Safecure Super Adomast

## Technical Specifications

### Water Based High Efficiency Concrete Curing Compound

Applied to the surface of freshly laid concrete, SAFECURE SUPER physically 'locks' moisture into freshly cast concrete allowing full hydration of the cement thus allowing the concrete to fully cure. This is achieved by covering the surface of the concrete with a very thin temporary membrane that prevents moisture in the concrete from leaving the surface. Safecure Super has been tested, to show over 90% curing efficiency, when tested to BS 7542:1992 & ASTM C309. Safecure Super is also a WRAS approved product. Benefits of using include reduced surface shrinkage and cracking; a more durable hard wearing surface and prevention of surface dusting.

### Advantages

- Retains over 90% of hydration water—tested in accordance with BS 7542:1992 & ASTM C309
- Reduces surface shrinkage and cracking by controlling moisture loss from surfaces. Increases water resistance
- Non hazardous—suitable for outdoor & indoor use as there are no VOC's in the compound
- Prevents concrete surface from dusting and improves surface quality and reduces plastic shrinkage.
- Non-toxic and non flammable.
- Eliminates need for damp hessian, sand or polythene



WRAS Approved

### Application

SAFECURE SUPER is spray applied to the surface of newly placed concrete. The concrete should be free from surface water and the nozzle of the spray should be held approx. 450mm from the concrete surface and passed back and forth to ensure complete coverage. The pump pressure should be maintained at a level producing a fine spray. Rate of application recommended at 4–6m<sup>2</sup> per litre. Shake the Safecure Super container before using. Touch Dry Time: <1 hour dependent upon temperature and wind. Hard Dry Time: 16 to 20 hours dependent upon temperature and wind. Curing agents do not provide thermal protection. It may be advisable to provide independent thermal protection in cold weather. For any subsequent processing of the concrete surface, all traces of Safecure Super must be completely removed, by physical abrasion, prior to carrying out the next process, to ensure the optimum adhesion & performance to the concrete of that subsequent process

### Coverage

Apply the selected grade by spray at a rate of approximately 4–6 m<sup>2</sup> per litre, taking care to ensure complete coverage. Immediately after use the spraying equipment, especially the spray nozzle, should be thoroughly washed out with clean and if possible warm water. This will help ensure the nozzle does not become blocked with dried polymer latex and affect subsequent spraying.

### Storage

Keep containers sealed. Store in dry conditions at room temperature and away from direct heat. Protect from frost. When stored correctly in an unopened container, storage stability is 12 months. Please mix/agitate Safecure Super container before decanting & use.

### Shelf Life

One year in sealed containers.

### Specification

SAFECURE SUPER is manufactured by Adomast Manufacturing Ltd and shall be applied strictly in accordance with the manufacturer's instructions. For specific advice regarding any aspect of this product, please consult our Technical Department

### Health and Safety

Avoid physical contact with material. If contact with skin should occur wash with soap and water. If splashes should affect eyes, bathe immediately with clean water and if discomfort persists seek medical advice.

See separate Safety Data Sheet for further information.

## D.1.3 Safecure Super 90w-10%

# Safecure Super 90W –10% Adomast

## Technical Specifications

### Wax Emulsion Concrete Curing Compound / Evaporation Retardant

SAFECURE SUPER 90W-10% is a low viscosity water based polymeric wax emulsion. When sprayed onto freshly finished concrete it will form a thin barrier layer on the surface. The moisture barrier film created, on the surface, controls and slows the surface bleed water from evaporating too quickly to the environment, which in turn permits more efficient cement hydration. The concrete created has better durability, surface quality and compressive strength. The cast concrete also has significantly reduced levels of plastic shrinkage, surface cracking and defects.

### Advantages

- Reduces surface shrinkage and cracking by controlling moisture loss from surfaces.
- Increases water resistance.
- Enables cement to hydrate more efficiently.
- Slows the rate of water evaporation from the concrete
- Prevents dusting.
- Non-toxic and non flammable.
- Eliminates need for damp hessian, sand or polythene
- NO VOC's

### Specification

Solids Content >10%

Density 0.97-0.985 kg/m<sup>3</sup>

pH ~7.0

Colour: White

Application rate for optimum performance: 4-5m<sup>2</sup>

### Application

SAFECURE SUPER 90W –10% is spray applied to the surface of newly placed concrete. The concrete should be free from surface water and the nozzle of the spray should be held approx. 450mm from the concrete surface and passed back and forth to ensure complete coverage. The pump pressure should be maintained at a level producing a fine spray. Rate of application will be 160 to 270 ml/m<sup>2</sup> (4 - 6 m<sup>2</sup>/ltr). Touch Dry Time: 1 to 2 hours dependent upon temperature and wind. Hard Dry Time: 18 to 24 hours dependent upon temperature and wind.

Curing agents do not provide thermal protection. It may be advisable to provide independent thermal protection in cold weather. For any subsequent processing of the concrete surface, we would recommend all traces of Safecure Super 90W –10% be completely removed. The best method is by physical abrasion, prior to carrying out the next process, to ensure the optimum adhesion & performance to the concrete of that subsequent process.

### Coverage

Apply the selected grade by spray at a rate of approximately 4-6 m<sup>2</sup> per litre, taking care to ensure complete coverage. Immediately after use the spraying equipment, especially the spray nozzle, should be thoroughly washed out with clean and if possible warm water. This will help ensure the nozzle does not become blocked with dried polymer latex and affect subsequent spraying.

### Storage

Keep containers sealed. Store in dry conditions at room temperature and away from direct heat. Protect from frost. When stored correctly in an unopened container, storage stability is 12 months. If stored for more than 14 days please mix/agitate thoroughly before use

**D.2 Environmental conditions and evaporation rate****Table D.1** PSC ASTM evaporation rate.

<b>Time (hr)</b>	<b>Temp. (°C)</b>	<b>Wind speed (m/s)</b>	<b>RH (%)</b>	<b>PC water pan (g)</b>	<b>PC Eva. rate (kg/m<sup>2</sup>/h)</b>	<b>PSC water pan (g)</b>	<b>PSC Eva. rate (kg/m<sup>2</sup>/h)</b>
<b>0</b>	0	0	40	506	-	500	-
<b>1</b>	32.7	5	33	482	1.26	476	1.26
<b>2</b>	34.5	5	28	452	1.58	446	1.58
<b>3</b>	35.3	5	23	418	1.79	414	1.68
<b>4</b>	36.4	5	20	384	1.79	382	1.68
<b>5</b>	36.9	5	15	348	1.89	346	1.89
<b>6</b>	37.8	5	15	312	1.89	310	1.89

**Table D.2** PSC Menzel's formula evaporation rate

<b>Time (hr)</b>	<b>TC (PC) (°C)</b>	<b>TC (PSC) (°C)</b>	<b>PC Eva. rate (kg/m<sup>2</sup>/h)</b>	<b>PSC Eva. rate (kg/m<sup>2</sup>/h)</b>
<b>1</b>	20.18	20.4	0.50	0.51
<b>2</b>	21.5	25.22	0.72	1.04
<b>3</b>	23.7	29.7	0.91	1.49
<b>4</b>	26.3	33.4	1.20	1.95
<b>5</b>	29	36.2	1.40	2.23
<b>6</b>	31.4	37.4	1.61	2.33



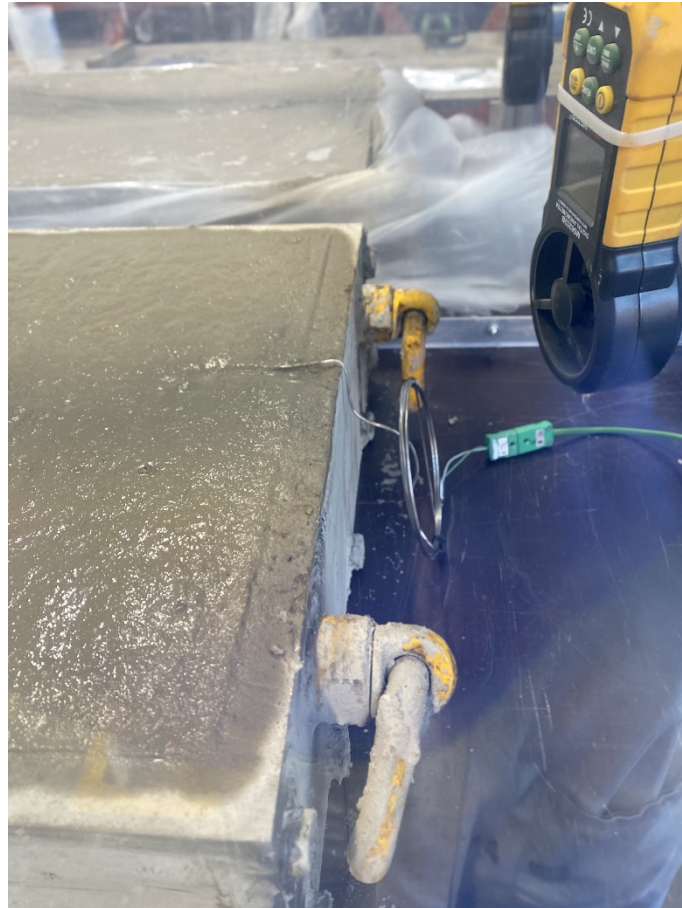


Figure D.1: Plastic sheet covering and plain concrete.

**Table D.3** HFC ASTM evaporation rate.

<b>Time (hr)</b>	<b>Temp. (°C)</b>	<b>Wind speed (m/s)</b>	<b>RH (%)</b>	<b>PC water pan (g)</b>	<b>PC Eva. rate (kg/m<sup>2</sup>/h)</b>	<b>HFC water pan (g)</b>	<b>HFC Eva. rate (kg/m<sup>2</sup>/h)</b>
<b>0</b>	0	0	40	505	-	505	-
<b>1</b>	34.1	5	36	482	1.21	483	1.16
<b>2</b>	34.5	5	25	452	1.68	452	1.63
<b>3</b>	35.1	5	20	422	1.68	421	1.63
<b>4</b>	35.6	5	18	390	1.80	387	1.79
<b>5</b>	36.3	5	15	358	1.80	353	1.79
<b>6</b>	36.9	5	15	322	1.98	316	1.95

**Table D.4** HFC Menzel's formula evaporation rate

<b>Time (hr)</b>	<b>TC (PC) (°C)</b>	<b>TC (HFC) (°C)</b>	<b>PC Eva. rate (kg/m<sup>2</sup>/h)</b>	<b>HFC Eva. rate (kg/m<sup>2</sup>/h)</b>
<b>1</b>	22.8	20.8	0.71	0.55
<b>2</b>	24.8	22.2	1.15	0.93
<b>3</b>	26.8	23.5	1.33	1.03
<b>4</b>	28.1	24.5	1.65	1.10
<b>5</b>	30.8	28.5	2	1.47
<b>6</b>	33.4	32.7	2.50	1.91

**Figure D.2:** Hessian fabric and plain concrete.

**Table D.5** PFC ASTM evaporation rate.

<b>Time (hr)</b>	<b>Temp. (°C)</b>	<b>Wind speed (m/s)</b>	<b>RH (%)</b>	<b>PC water pan (g)</b>	<b>PC Eva. rate (kg/m<sup>2</sup>/h)</b>	<b>PFC water pan (g)</b>	<b>PFC Eva. rate (kg/m<sup>2</sup>/h)</b>
<b>0</b>	0	0	40	501	-	501	-
<b>1</b>	32.5	5	32	476	1.32	476	1.32
<b>2</b>	35.5	5	25	438	1.55	447	1.52
<b>3</b>	36.5	5	20	400	1.68	414	1.68
<b>4</b>	36.8	5	15	360	1.72	376	1.71
<b>5</b>	37.3	5	15	320	1.85	337	1.81
<b>6</b>	37.7	5	15	274	1.99	295	1.98

**Table D.6** PFC Menzel's formula evaporation rate

<b>Time (hr)</b>	<b>TC (PC) (°C)</b>	<b>TC (PFC) (°C)</b>	<b>PC Eva. rate (kg/m<sup>2</sup>/h)</b>	<b>PFC Eva. rate (kg/m<sup>2</sup>/h)</b>
<b>1</b>	21	21.4	0.71	0.74
<b>2</b>	23	23.6	0.98	1.03
<b>3</b>	24.7	25.3	1.10	1.16
<b>4</b>	28.2	28.8	1.43	1.49
<b>5</b>	30.6	30.9	1.67	1.70
<b>6</b>	33.5	33.8	1.99	2.03



Figure D.3: Power floating of both scales (lab and in-situ)

Table D.7 CWC ASTM evaporation rate.

Time (hr)	Temp. (°C)	Wind speed (m/s)	RH (%)	PC water pan (g)	PC Eva. rate (kg/m <sup>2</sup> /h)	CWC water pan (g)	CWC Eva. rate (kg/m <sup>2</sup> /h)
0	0	0	40	504	-	505	-
1	28.4	5	36	480	1.26	483	1.16
2	32.9	5	25	445	1.84	453	1.58
3	35.3	5	20	410	1.84	418	1.84
4	36	5	15	375	1.84	383	1.84
5	37.1	5	15	338	1.95	348	1.84
6	37.5	5	15	300	2	310	2

Table D.8 CWC Menzel's formula evaporation rate

Time (hr)	TC (PC) (°C)	TC (CWC) (°C)	PC Eva. rate (kg/m <sup>2</sup> /h)	CWC Eva. rate (kg/m <sup>2</sup> /h)
1	20.4	15.4	0.76	0.417
2	22.5	18.4	0.98	0.67
3	25.1	20.1	1.16	0.75
4	28.7	25.3	1.50	1.17
5	30.9	27.6	1.71	1.36
6	34.8	29.8	2.03	1.58

**Table D.9** SSC ASTM evaporation rate.

<b>Time (hr)</b>	<b>Temp. (°C)</b>	<b>Wind speed (m/s)</b>	<b>RH (%)</b>	<b>PC water pan (g)</b>	<b>PC Eva. rate (kg/m<sup>2</sup>/h)</b>	<b>SSC water pan (g)</b>	<b>SSC Eva. rate (kg/m<sup>2</sup>/h)</b>
<b>0</b>	0	0	40	504	-	501	-
<b>1</b>	27.5	5	33	480	1.263	483	1.164
<b>2</b>	29	5	24	447	1.7368	453	1.578
<b>3</b>	31.3	5	20	410	1.947	418	1.842
<b>4</b>	34	5	15	373	1.947	382	1.8947
<b>5</b>	36	5	15	337	1.947	348	1.9154
<b>6</b>	36.8	5	15	298	2.05	310	2

**Table D.10** SSC Menzel's formula evaporation rate

<b>Time (hr)</b>	<b>TC (PC) (°C)</b>	<b>TC (SSC) (°C)</b>	<b>PC Eva. rate (kg/m<sup>2</sup>/h)</b>	<b>SSC Eva. rate (kg/m<sup>2</sup>/h)</b>
<b>1</b>	20.3	20	0.66	0.64
<b>2</b>	21.5	20.4	0.87	0.78
<b>3</b>	25.2	23.1	1.24	1.06
<b>4</b>	28.7	25.7	1.53	1.24
<b>5</b>	30.9	29	1.73	1.53
<b>6</b>	33.8	32	2.04	1.84



Figure D.4: Safecure Super and plain concrete.

**Table D.11** SSC90WC ASTM evaporation rate.

<b>Time (hr)</b>	<b>Temp. (°C)</b>	<b>Wind speed (m/s)</b>	<b>RH (%)</b>	<b>PC water pan (g)</b>	<b>PC Eva. rate (kg/m<sup>2</sup>/h)</b>	<b>SS90WC water pan (g)</b>	<b>SS90WC Eva. rate (kg/m<sup>2</sup>/h)</b>
<b>0</b>	0	0	40	501	-	502	-
<b>1</b>	27.5	5	33	478	1.21	477	1.20
<b>2</b>	32	5	23	449	1.55	444	1.46
<b>3</b>	33.3	5	18	420	1.74	411	1.53
<b>4</b>	34.1	5	15	391	1.74	378	1.53
<b>5</b>	35.4	5	15	361	1.85	343	1.78
<b>6</b>	36.3	5	15	331	1.98	308	1.95

**Table D.12** SSC90WC Menzel's formula evaporation rate

<b>Time (hr)</b>	<b>TC (PC) (°C)</b>	<b>TC (SS90WC) (°C)</b>	<b>PC Eva. rate (kg/m<sup>2</sup>/h)</b>	<b>SS90WC Eva. rate (kg/m<sup>2</sup>/h)</b>
<b>1</b>	19	19.4	0.67	0.70
<b>2</b>	20.6	21.6	0.73	0.81
<b>3</b>	25.3	26.7	1.22	1.35
<b>4</b>	27.1	29	1.37	1.56
<b>5</b>	29.5	31	1.60	1.76
<b>6</b>	30.1	32.1	1.64	1.86



Figure D.5: Safecure Super 90w and plain concrete.

**Table D.13** SPC ASTM evaporation rate.

<b>Time (hr)</b>	<b>Temp. (°C)</b>	<b>Wind speed (m/s)</b>	<b>RH (%)</b>	<b>PC water pan (g)</b>	<b>PC Eva. rate (kg/m<sup>2</sup>/h)</b>	<b>PC-S water pan (g)</b>	<b>PC-S Eva. rate (kg/m<sup>2</sup>/h)</b>
0	0	0	40	506	-	509	-
1	30.8	5	35	485	1.11	487	1.16
2	33.5	5	24	456	1.53	457	1.16
3	34.4	5	20	421	1.84	422	1.84
4	35.8	5	15	386	1.84	387	1.84
5	36.3	5	15	348	2	350	1.95
6	37	5	15	303	2.11	306	2.05

**Table D.14** PC-S Menzel's formula evaporation rate

<b>Time (hr)</b>	<b>TC (PC) (°C)</b>	<b>TC (PC-S) (°C)</b>	<b>PC Eva. rate (kg/m<sup>2</sup>/h)</b>	<b>PC-S Eva. rate (kg/m<sup>2</sup>/h)</b>
1	20.1	20.5	0.68	0.63
2	20.5	21.1	0.81	0.75
3	22.6	22.7	0.96	0.89
4	24.4	25.5	1.09	1.01
5	27.8	28.5	1.30	1.18
6	31.7	32.7	1.58	1.48

**Table D.15** RTSFC40 ASTM evaporation rate.

<b>Time (hr)</b>	<b>Temp. (°C)</b>	<b>Wind speed (m/s)</b>	<b>RH (%)</b>	<b>PC water pan (g)</b>	<b>PC Eva. rate (kg/m<sup>2</sup>/h)</b>	<b>RTSFC40 water pan (g)</b>	<b>RTSFC40 Eva. rate (kg/m<sup>2</sup>/h)</b>
0	0	0	40	0.504	-	0.505	-
1	28	5	32	0.48	1.48	0.483	1.47
2	30	5	20	0.445	1.59	0.453	1.58
3	34	5	15	0.41	1.90	0.418	1.88
4	36	5	15	0.375	1.95	0.383	1.93
5	37.1	5	15	0.338	2.08	0.348	2.08
6	37.5	5	15	0.3	2.15	0.31	2.15



**Table D.16** RTSFC40 Menzel's formula evaporation rate

<b>Time (hr)</b>	<b>TC (PC) (°C)</b>	<b>TC (RTSFC40) (°C)</b>	<b>PC Eva. rate (kg/m<sup>2</sup>/h)</b>	<b>RTSFC40 Eva. rate (kg/m<sup>2</sup>/h)</b>
<b>1</b>	20.1	20	0.74	0.74
<b>2</b>	21.4	21	0.94	0.91
<b>3</b>	24.8	24	1.16	1.09
<b>4</b>	27.1	26	1.34	1.23
<b>5</b>	30.4	28.5	1.65	1.45
<b>6</b>	32.9	32.4	1.93	1.87

Figure D.6: Recycled tire steel fibre (40km/m<sup>3</sup>) and plain concrete.

### D.3 Crack measurements

#### D.3.1 PSC

##### D.3.1.1 MATLAB and IC measure software



Figure D.7: IC crack length at 24 hours of plain concrete.

<input type="checkbox"/>	CrackArea	403.4413
<input type="checkbox"/>	CrackPixels	1.0623e+04
<input type="checkbox"/>	I	2498x757x3 uint8
<input checked="" type="checkbox"/>	Iclean	2498x757 logical
<input checked="" type="checkbox"/>	Icomp	2498x757 logical
<input type="checkbox"/>	Igray	2498x757 uint8
<input checked="" type="checkbox"/>	Ithres	2498x757 logical

Figure D.8: MATLAB crack area at 24 hours of plain concrete.

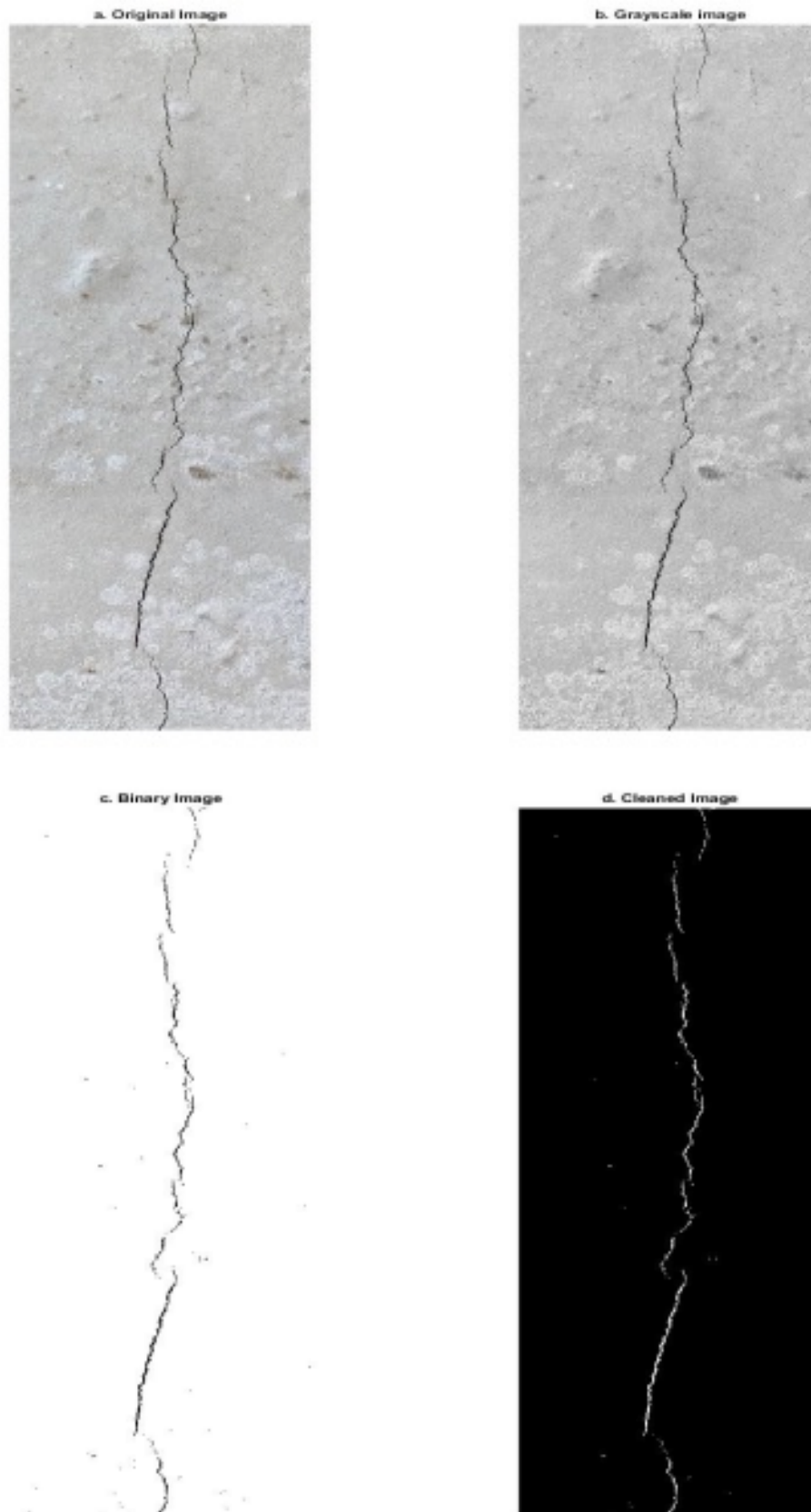


Figure D.9: MATLAB image processing steps for plain concrete.

**D.3.1.2 Optical methods measure****Table D.17** PSC optical measurement.

<b>Point</b>	<b>PC (mm)</b>	<b>PSC (mm)</b>
1	0.9	0
2	0.9	0
3	0.9	0
4	1	0
5	1	0
6	1	0
7	1	0
8	1	0
9	1	0
10	1.1	0
11	1.1	0
12	1.1	0
13	1.2	0
14	1.2	0
15	1.2	0
16	1.2	0
17	1.2	0
18	1.2	0
19	1	0
20	1	0
21	1	0
22	1	0
23	1	0
24	1	0
25	0.9	0
26	0.9	0
Ave	1.04	0

**D.3.1.3 Crack width methods measure**

<b>Concrete</b>	<b>MATLAB (mm)</b>	<b>Optical (mm)</b>
PC	1.11	1.04
SPC	0	0

## D.3.2 HFC

## D.3.2.1 MATLAB and IC measure software

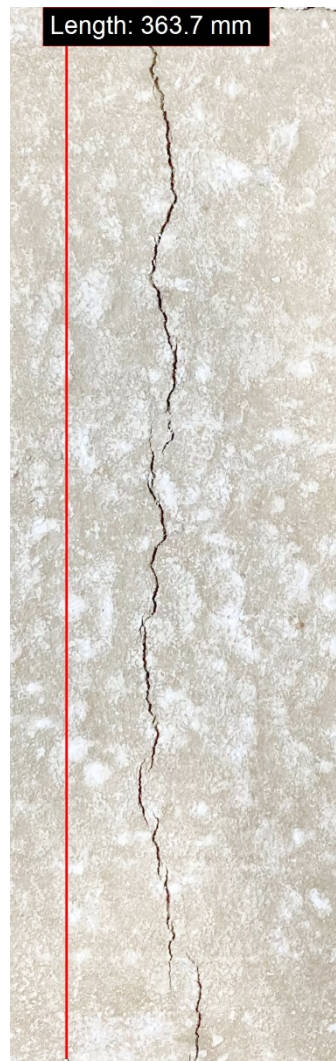


Figure D.10: IC crack length at 24 hours of plain concrete.

<input type="checkbox"/>	CrackArea	367.4476
<input type="checkbox"/>	CrackPixels	1.1932e+04
<input type="checkbox"/>	I	2041x644x3 uint8
<input checked="" type="checkbox"/>	Iclean	2041x644 logical
<input checked="" type="checkbox"/>	Icomp	2041x644 logical
<input type="checkbox"/>	Igray	2041x644 uint8
<input checked="" type="checkbox"/>	Ithres	2041x644 logical

Figure D.11: MATLAB crack area at 24 hours of plain concrete.

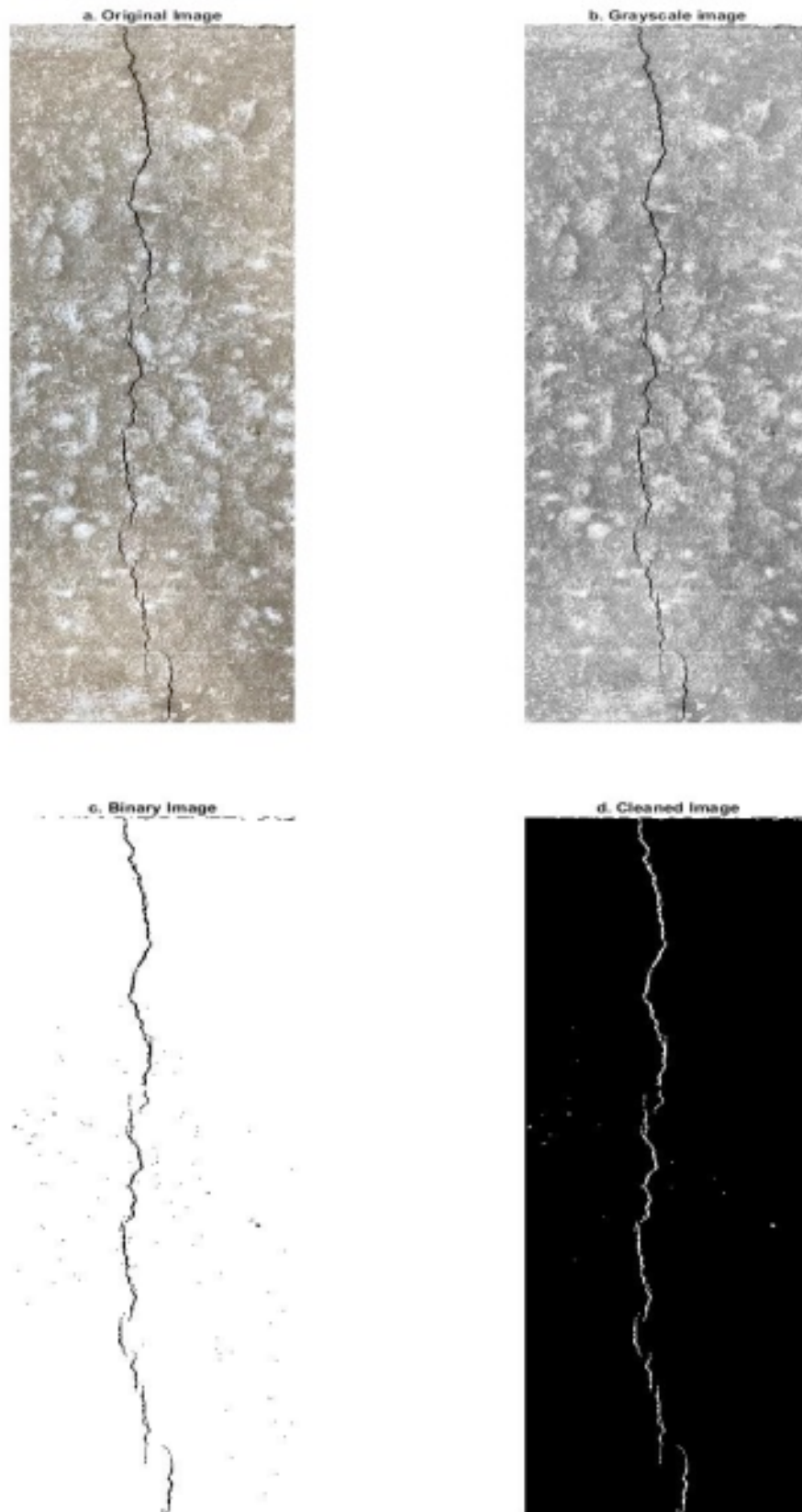


Figure D.12: MATLAB image processing steps for plain concrete.



Figure D.13: IC crack length at 24 hours of HFC.

	CrackArea	214.4366
	CrackPixels	6.2671e+03
	I	2202x476x3 uint8
	Iclean	2202x476 logical
	Icomp	2202x476 logical
	Igray	2202x476 uint8
	Ithres	2202x476 logical

Figure D.14: MATLAB crack area at 24 hours of HFC.

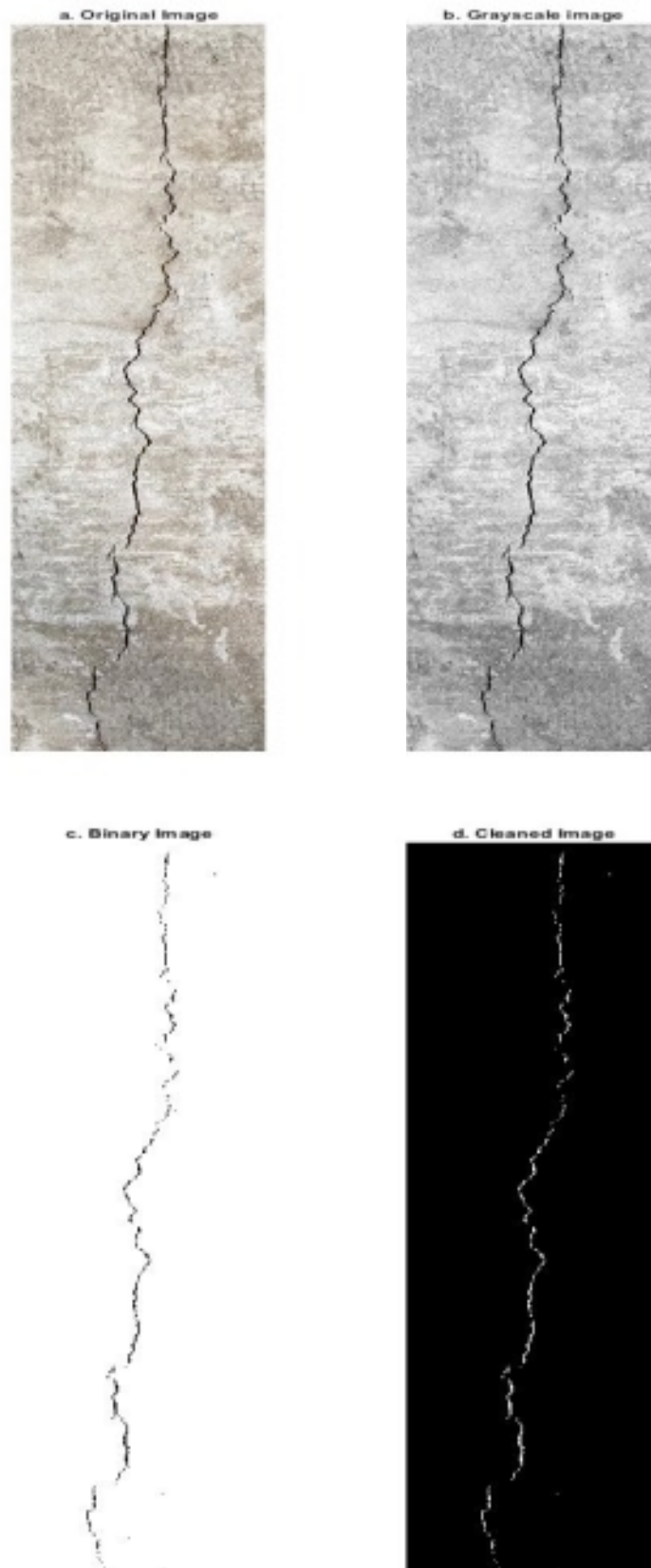


Figure D.15: MATLAB image processing steps for HFC.



**D.3.2.2 Optical methods measure****Table D.18** HFC optical measurement.

<b>Point</b>	<b>PC (mm)</b>	<b>HFC (mm)</b>
1	0.8	0.3
2	0.8	0.3
3	0.9	0.4
4	0.9	0.4
5	0.9	0.5
6	0.9	0.5
7	1	0.5
8	1	0.5
9	1	0.5
10	1	0.5
11	1	0.5
12	1	0.6
13	1	0.6
14	1	0.6
15	1.1	0.7
16	1.1	0.7
17	1.1	0.7
18	1.1	0.6
19	1.1	0.6
20	1	0.5
21	1	0.5
22	1	0.5
23	1	0.4
24	0.9	0.4
25	0.8	0.4
26	0.8	0.4
<b>Ave</b>	<b>0.97</b>	<b>0.51</b>

**D.3.2.3 Crack width methods measure**

<b>Concrete</b>	<b>MATLAB (mm)</b>	<b>Optical (mm)</b>
<b>PC</b>	1.04	0.97
<b>HFC</b>	0.59	0.51

## D.3.3 PFC

## D.3.3.1 MATLAB and IC measure software



Figure D.16: IC crack length at 24 hours of plain concrete.

<input type="checkbox"/>	CrackArea	384.1614
<input type="checkbox"/>	CrackPixels	9.3563e+03
<input type="checkbox"/>	I	2906x632x3 uint8
<input checked="" type="checkbox"/>	Iclean	2906x632 logical
<input checked="" type="checkbox"/>	Icomp	2906x632 logical
<input type="checkbox"/>	Igray	2906x632 uint8
<input checked="" type="checkbox"/>	Ithres	2906x632 logical

Figure D.17: MATLAB crack area at 24 hours of plain concrete.

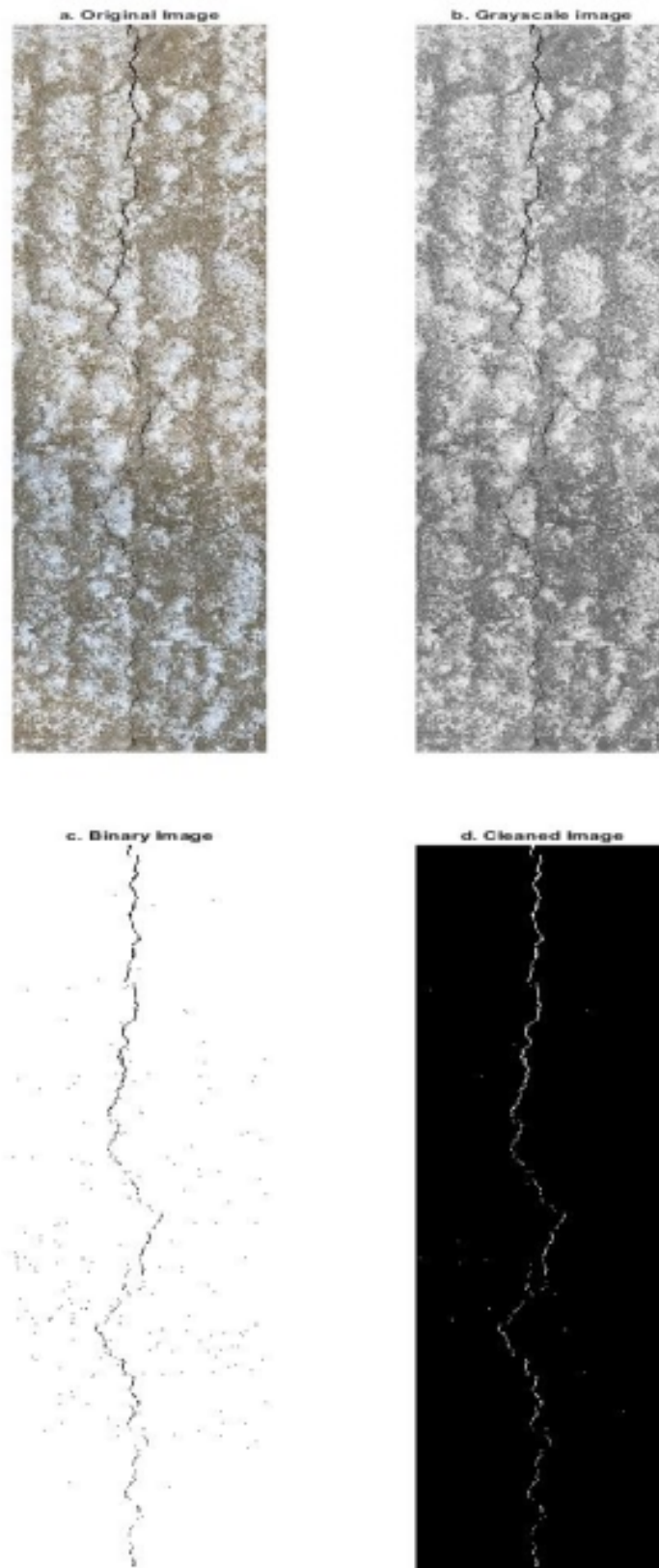


Figure D.18: MATLAB image processing steps for plain concrete.



Figure D.19: IC crack length at 24 hours of PFC.

<input type="checkbox"/>	CrackArea	108.3235
<input type="checkbox"/>	CrackPixels	3.5176e+03
<input type="checkbox"/>	I	3243x973x3 uint8
<input checked="" type="checkbox"/>	Iclean	3243x973 logical
<input checked="" type="checkbox"/>	Icomp	3243x973 logical
<input type="checkbox"/>	Igray	3243x973 uint8
<input checked="" type="checkbox"/>	Ithres	3243x973 logical

Figure D.20: MATLAB crack area at 24 hours of PFC.

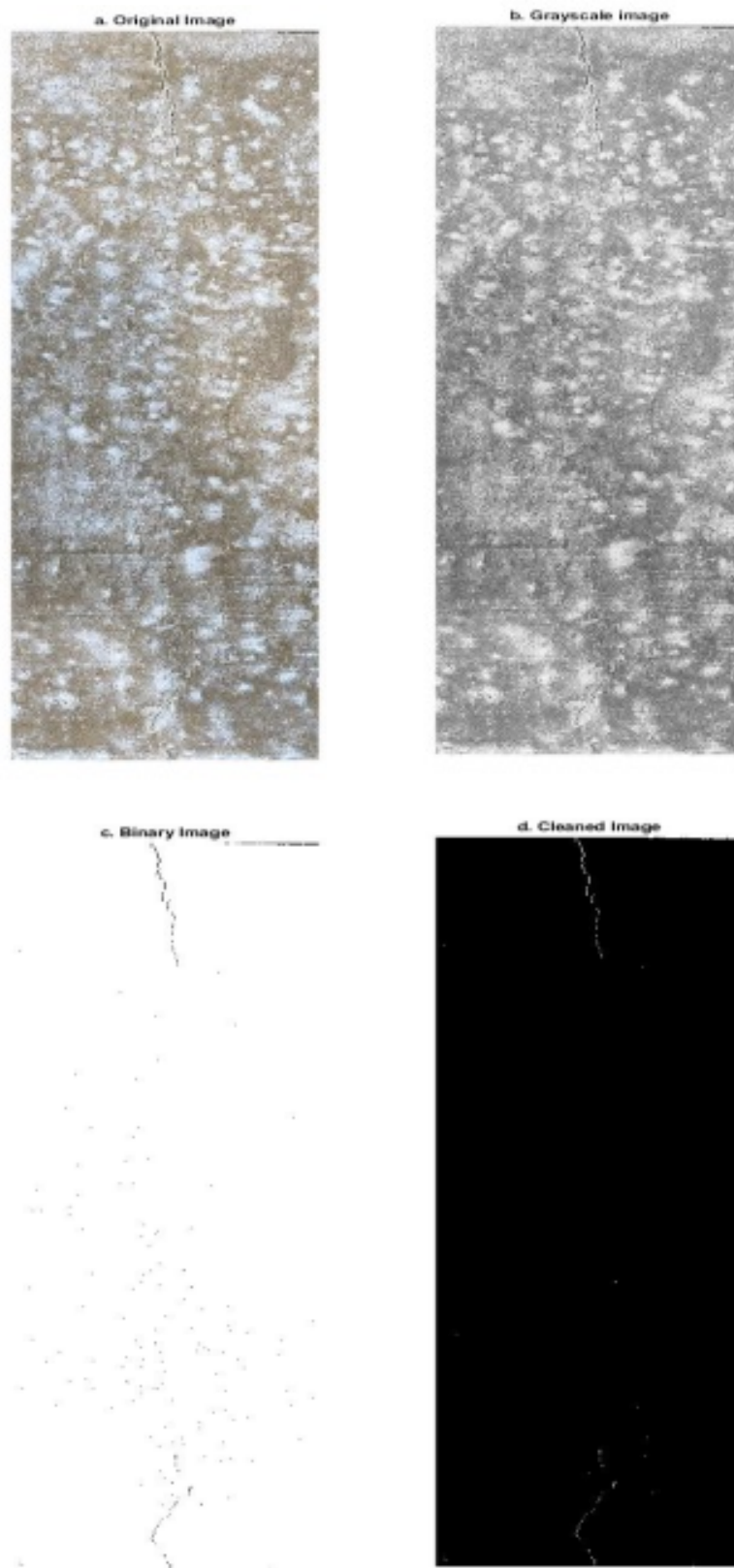


Figure D.21: MATLAB image processing steps for PFC.

**D.3.3.2 Optical methods measure****Table D.19** PFC optical measurement.

<b>Point</b>	<b>PC (mm)</b>	<b>PFC (mm)</b>
<b>1</b>	0.9	0
<b>2</b>	0.9	0
<b>3</b>	1	0
<b>4</b>	1	0
<b>5</b>	1	0
<b>6</b>	1	0
<b>7</b>	1	0
<b>8</b>	1	0
<b>9</b>	1	0
<b>10</b>	1.1	0
<b>11</b>	1.1	0
<b>12</b>	1.1	0
<b>13</b>	1.1	0
<b>14</b>	1.2	0
<b>15</b>	1.2	0
<b>16</b>	1.2	0
<b>17</b>	1.2	0
<b>18</b>	1.2	0
<b>19</b>	1.2	0
<b>20</b>	1.1	0
<b>21</b>	0.9	0
<b>22</b>	0.9	0
<b>23</b>	0.9	0
<b>24</b>	0.9	0
<b>25</b>	0.9	0
<b>26</b>	0.9	0
<b>Ave</b>	1.02	0

**D.3.3.3 Crack width methods measure**

<b>Concrete</b>	<b>MATLAB (mm)</b>	<b>Optical (mm)</b>
<b>PC</b>	1.06	1.02
<b>PFC</b>	0	0

## D.3.4 CWC

## D.3.4.1 MATLAB and IC measure software



Figure D.22: IC crack length at 24 hours of plain concrete.

<input type="checkbox"/>	CrackArea	392.9452
<input type="checkbox"/>	CrackPixels	2.0148e+04
<input type="checkbox"/>	I	2661x1149x3 uint8
<input checked="" type="checkbox"/>	Iclean	2661x1149 logical
<input checked="" type="checkbox"/>	Icomp	2661x1149 logical
<input type="checkbox"/>	Igray	2661x1149 uint8
<input checked="" type="checkbox"/>	Ithres	2661x1149 logical

Figure D.23: MATLAB crack area at 24 hours of plain concrete.

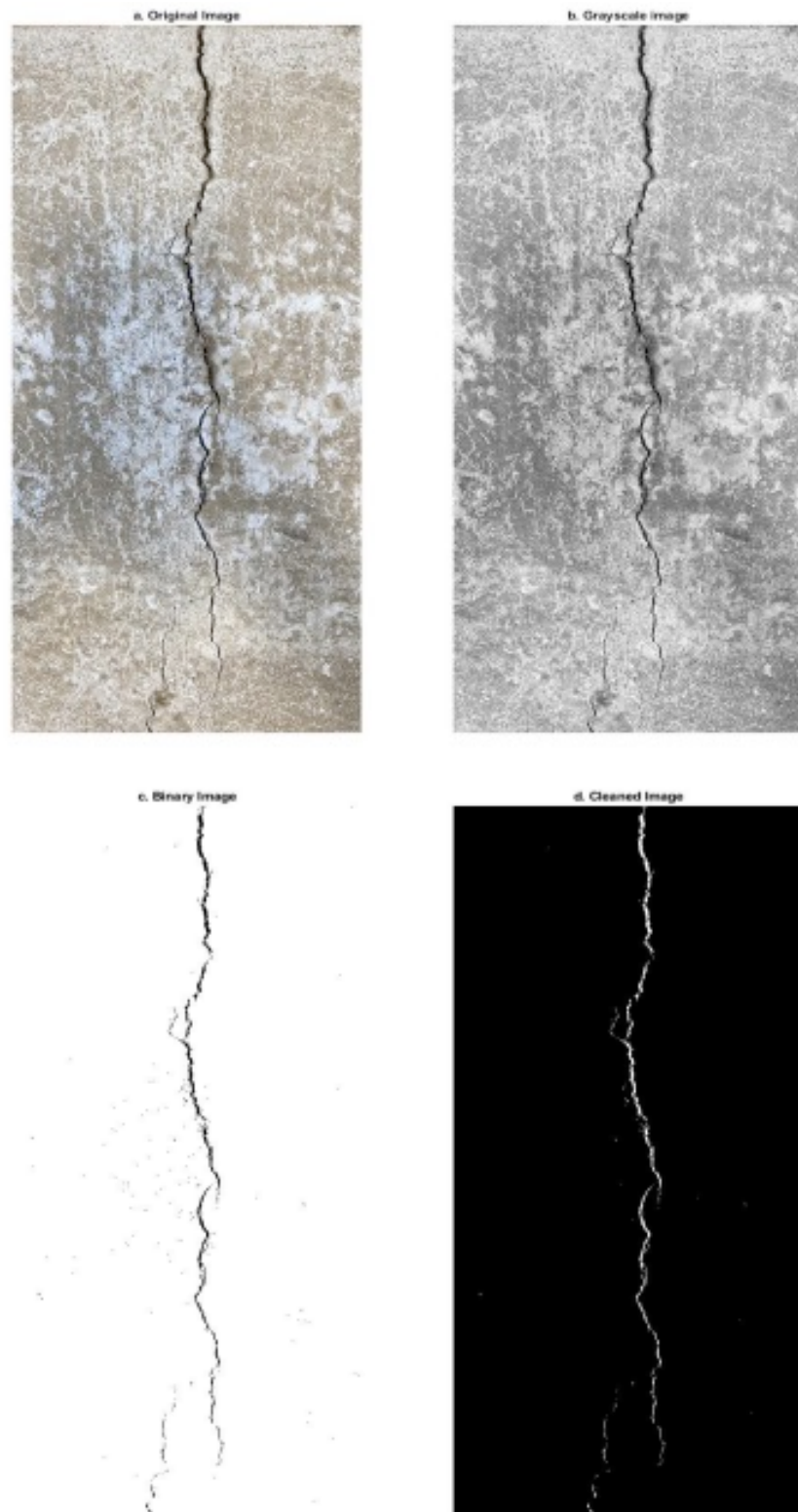


Figure D.24: MATLAB image processing steps for plain concrete.





Figure D.25: IC crack length at 24 hours of CWC.

	CrackArea	268.5965
	CrackPixels	4.9063e+03
	I	2191x550x3 uint8
	Iclean	2191x550 logical
	Icomp	2191x550 logical
	Igray	2191x550 uint8
	Ithres	2191x550 logical

Figure D.26: MATLAB crack area at 24 hours of CWC.

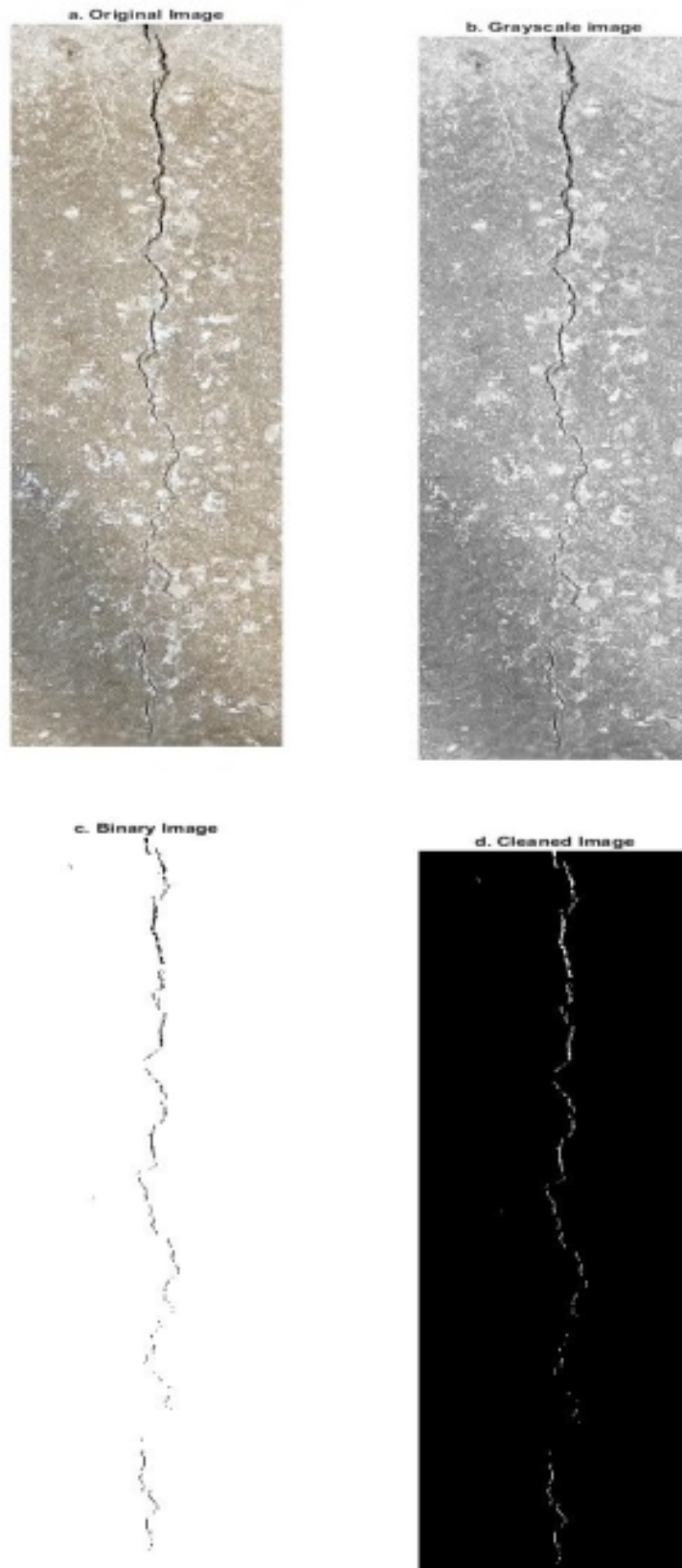


Figure D.27: MATLAB image processing steps for CWC.

**D.3.4.2 Optical methods measure****Table D.20** CWC optical measurement.

<b>Point</b>	<b>PC (mm)</b>	<b>CWC (mm)</b>
1	1.1	0.7
2	1.1	0.7
3	1.1	0.7
4	1.1	0.7
5	1.1	0.7
6	1.1	0.8
7	1.1	0.8
8	1.1	0.8
9	1.1	0.8
10	1.1	0.8
11	1.1	0.8
12	1.1	0.7
13	1.1	0.7
14	1.1	0.7
15	1.1	0.7
16	1.1	0.7
17	1	0.7
18	1	0.7
19	1	0.7
20	1	0.6
21	0.9	0.6
22	0.9	0.6
23	0.9	0.6
24	0.9	0.5
25	0.9	0.5
26	0.9	0.5
<b>Ave</b>	1.04	0.68

**D.3.4.3 Crack width methods measure**

<b>Concrete</b>	<b>MATLAB (mm)</b>	<b>Optical (mm)</b>
<b>PC</b>	1.07	1.04
<b>CWC</b>	0.74	0.68

## D.3.5 SSC

## D.3.5.1 MATLAB and IC measure software



Figure D.28: IC crack length at 24 hours of plain concrete.

<input type="checkbox"/>	CrackArea	371.8898
<input type="checkbox"/>	CrackPixels	1.2077e+04
<input type="checkbox"/>	I	2851x915x3 uint8
<input checked="" type="checkbox"/>	Iclean	2851x915 logical
<input checked="" type="checkbox"/>	Icomp	2851x915 logical
<input type="checkbox"/>	Igray	2851x915 uint8
<input checked="" type="checkbox"/>	Ithres	2851x915 logical

Figure D.29: MATLAB crack area at 24 hours of plain concrete.

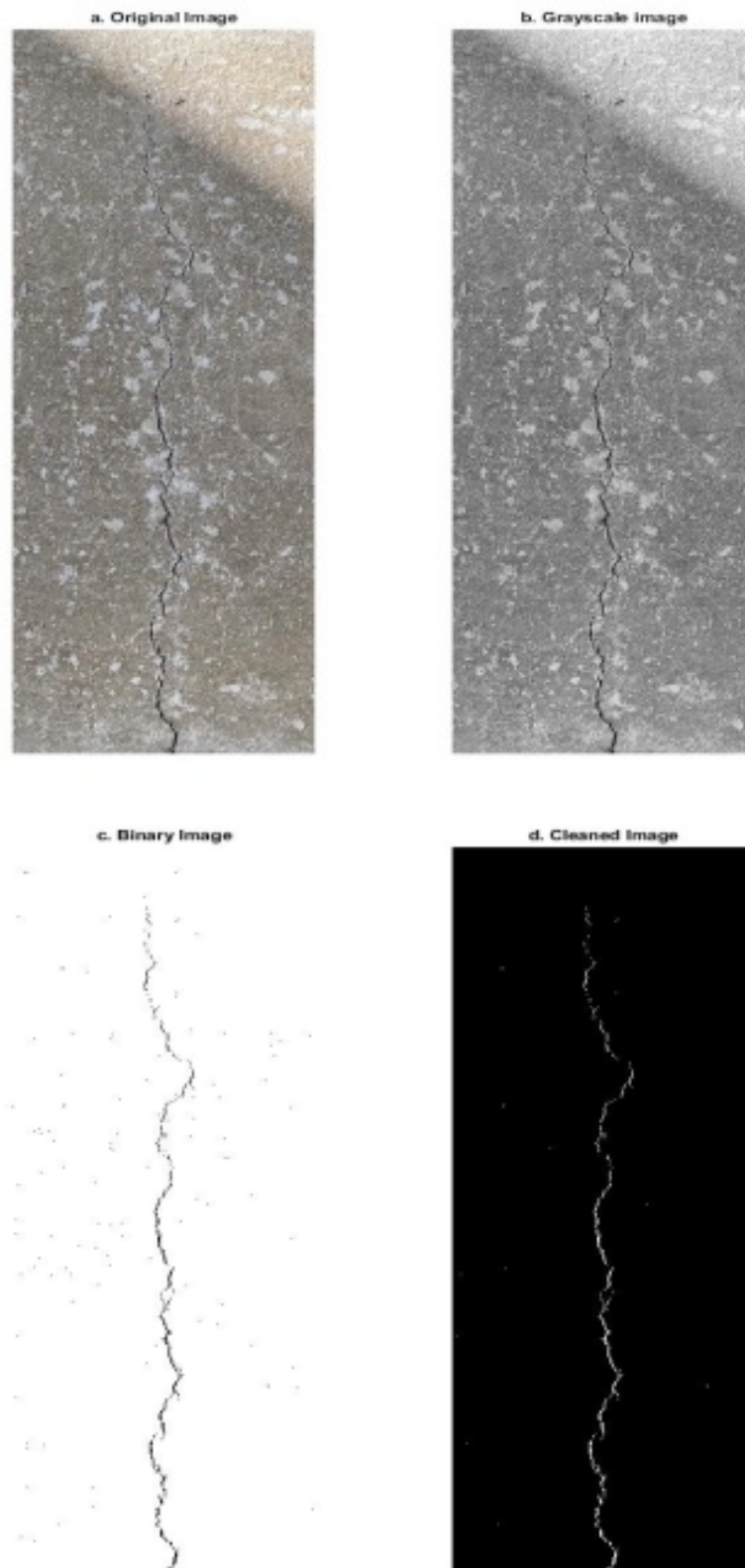


Figure D.30: MATLAB image processing steps for plain concrete.



Figure D.31: IC crack length at 24 hours of SSC.

	CrackArea	118.5994
	CrackPixels	6.9324e+03
	I	2592x688x3 uint8
	Iclean	2592x688 logical
	Icomp	2592x688 logical
	Igray	2592x688 uint8
	Ithres	2592x688 logical

Figure D.32: MATLAB crack area at 24 hours of SSC.

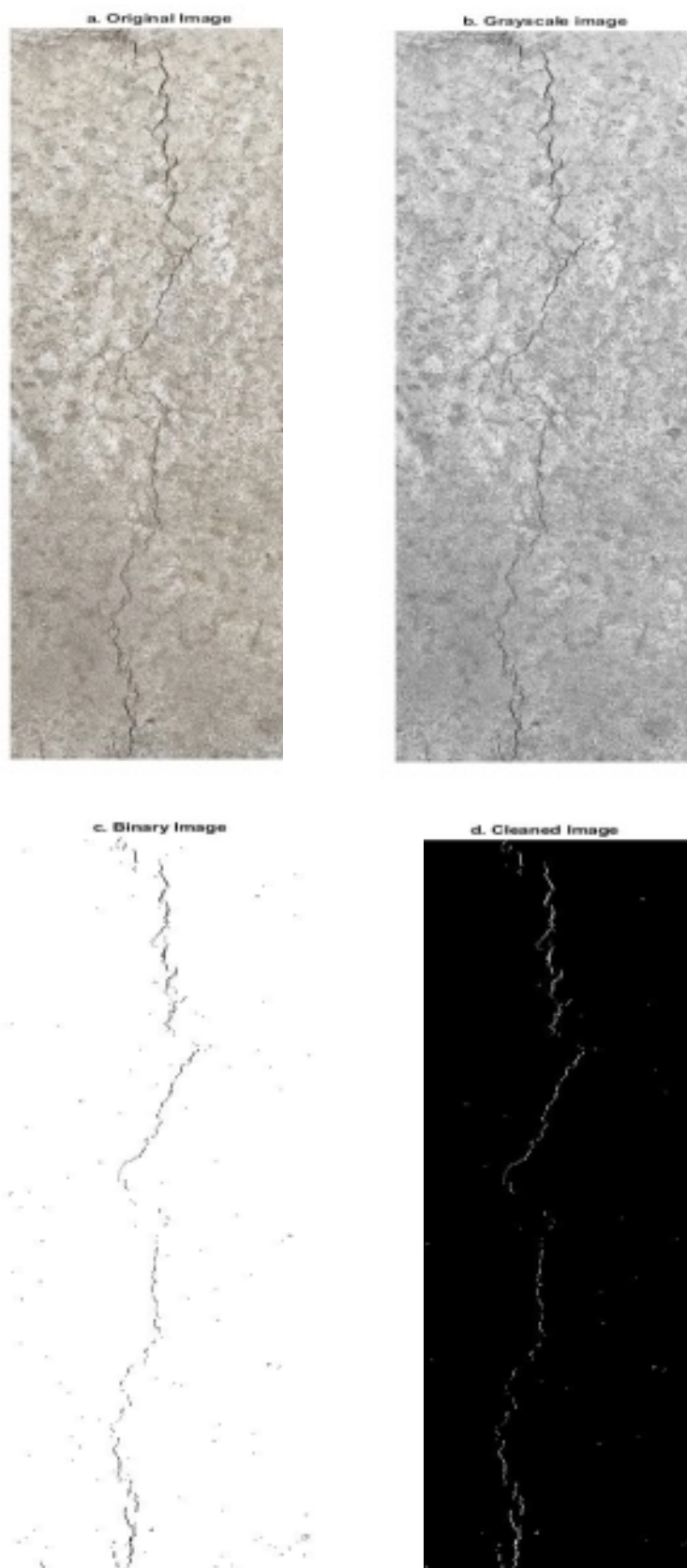


Figure D.33: MATLAB image processing steps for SSC.

**D.3.5.2 Optical methods measure****Table D.21** SSC optical measurement.

<b>Point</b>	<b>PC (mm)</b>	<b>SSC (mm)</b>
1	0.8	0.4
2	0.8	0.4
3	0.8	0.4
4	0.9	0.4
5	0.9	0.3
6	0.9	0.3
7	0.9	0.3
8	1	0.3
9	1	0.3
10	1	0.3
11	1	0.2
12	1	0.2
13	1.1	0.2
14	1.1	0.2
15	1.1	0.2
16	1.1	0.3
17	1.1	0.3
18	1.1	0.3
19	1.1	0.3
20	1.1	0.3
21	1.1	0.3
22	1.1	0.3
23	1.1	0.4
24	1.2	0.4
25	1.2	0.4
26	1.2	0.4
<b>Ave</b>	1.03	0.31

**D.3.5.3 Crack width methods measure**

<b>Concrete</b>	<b>MATLAB (mm)</b>	<b>Optical (mm)</b>
PC	1.05	1.03
SSC	0.32	0.31



## D.3.6 SS90WC

## D.3.6.1 MATLAB and IC measure software



Figure D.34: IC crack length at 24 hours of plain concrete.

<input type="checkbox"/>	CrackArea	396.0326
<input type="checkbox"/>	CrackPixels	6.8085e+03
<input type="checkbox"/>	I	1701x727x3 uint8
<input checked="" type="checkbox"/>	Iclean	1701x727 logical
<input checked="" type="checkbox"/>	Icomp	1701x727 logical
<input type="checkbox"/>	Igray	1701x727 uint8
<input checked="" type="checkbox"/>	Ithres	1701x727 logical

Figure D.35: MATLAB crack area at 24 hours of plain concrete.

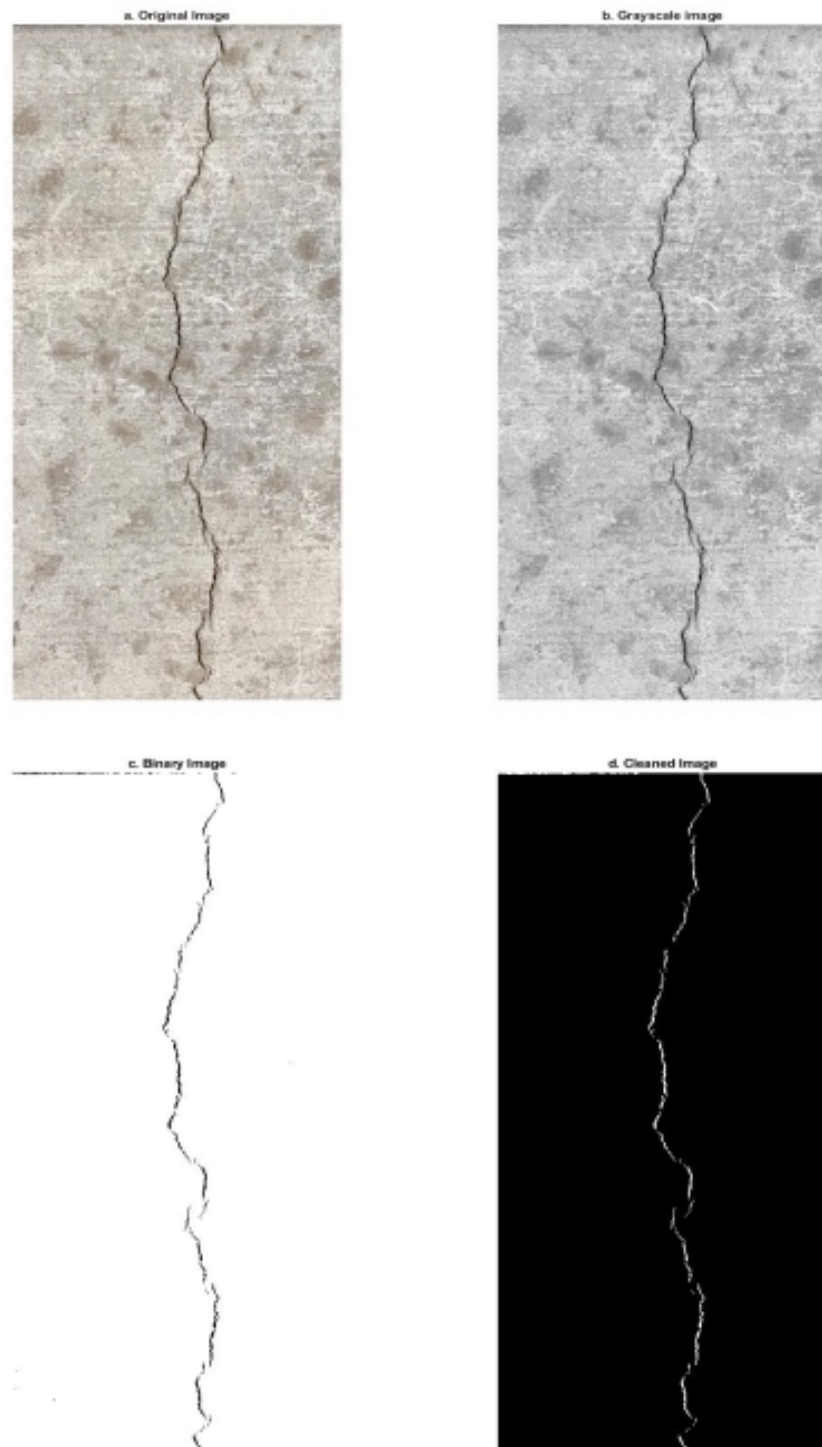


Figure D.36: MATLAB image processing steps for plain concrete.

**D.3.6.2 Optical methods measure****Table D.22** SS90WC optical measurement.

<b>Point</b>	<b>PC (mm)</b>	<b>SS90WC (mm)</b>
<b>1</b>	0.9	0
<b>2</b>	0.9	0
<b>3</b>	0.9	0
<b>4</b>	0.9	0
<b>5</b>	1	0
<b>6</b>	1	0
<b>7</b>	1	0
<b>8</b>	1	0
<b>9</b>	1	0
<b>10</b>	1.1	0
<b>11</b>	1.1	0
<b>12</b>	1.1	0
<b>13</b>	1.2	0
<b>14</b>	1.2	0
<b>15</b>	1.2	0
<b>16</b>	1.2	0
<b>17</b>	1.2	0
<b>18</b>	1.2	0
<b>19</b>	1.2	0
<b>20</b>	1.2	0
<b>21</b>	1	0
<b>22</b>	1	0
<b>23</b>	1	0
<b>24</b>	1	0
<b>25</b>	1	0
<b>26</b>	1	0
<b>Ave</b>	1.06	0

**D.3.6.3 Crack width methods measure**

<b>Concrete</b>	<b>MATLAB (mm)</b>	<b>Optical (mm)</b>
<b>PC</b>	1.09	1.06
<b>SS90WC</b>	0	0

## D.3.7 PC-S

## D.3.7.1 MATLAB and IC measure software



Figure D.37: IC crack length at 24 hours of PC.

	CrackArea	386.0614
	CrackPixels	2.0895e+04
	I	3065x773x3 uint8
	Iclean	3065x773 logical
	Icomp	3065x773 logical
	Igray	3065x773 uint8
	Ithres	3065x773 logical

Figure D.38: MATLAB crack area at 24 hours of PC.

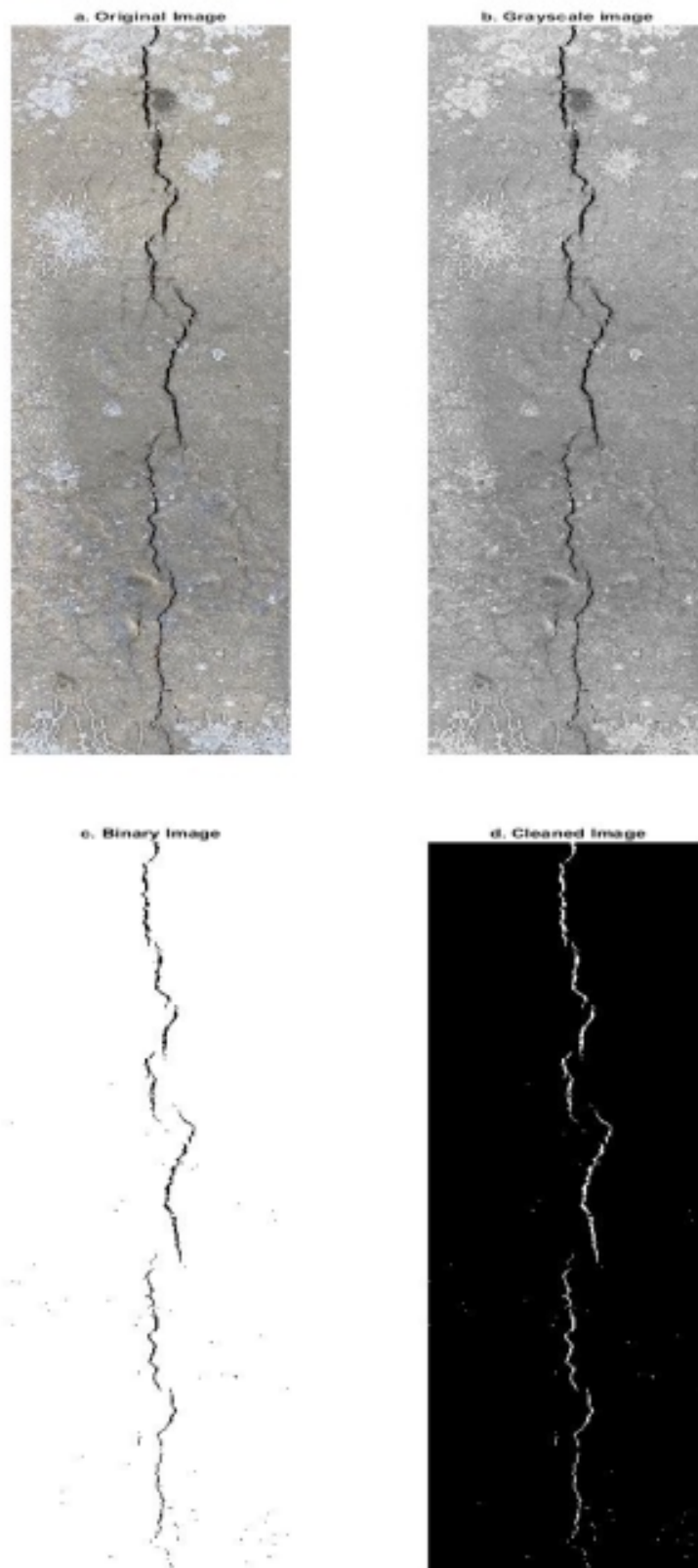


Figure D.39: MATLAB image processing steps for PC.

**D.3.7.2 Optical methods measure****Table D.23** SPC optical measurement.

<b>Point</b>	<b>PC (mm)</b>	<b>PC-S (mm)</b>
<b>1</b>	1.1	0
<b>2</b>	1.1	0
<b>3</b>	1.1	0
<b>4</b>	1.1	0
<b>5</b>	1.1	0
<b>6</b>	1.1	0
<b>7</b>	1.2	0
<b>8</b>	1.2	0
<b>9</b>	1.2	0
<b>10</b>	1.2	0
<b>11</b>	1.2	0
<b>12</b>	1.2	0
<b>13</b>	1	0
<b>14</b>	1	0
<b>15</b>	1	0
<b>16</b>	1	0
<b>17</b>	1	0
<b>18</b>	1	0
<b>19</b>	0.9	0
<b>20</b>	0.9	0
<b>21</b>	0.9	0
<b>22</b>	0.9	0
<b>23</b>	0.8	0
<b>24</b>	0.8	0
<b>25</b>	0.8	0
<b>26</b>	0.8	0
<b>Ave</b>	1.05	0

**D.3.7.3 Crack width methods measure**

<b>Concrete</b>	<b>MATLAB (mm)</b>	<b>Optical (mm)</b>
<b>PC</b>	1.02	1.01
<b>PC-S</b>	0	0

## D.3.8 RTSFC40

## D.3.8.1 MATLAB and IC measure software

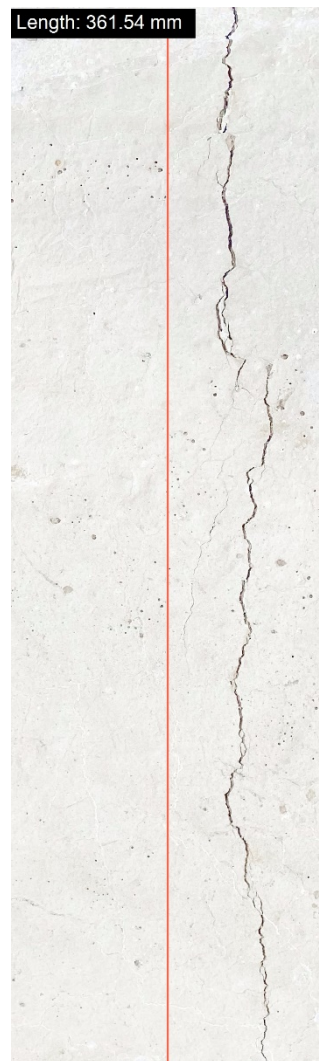


Figure D.40: IC crack length at 24 hours of plain concrete.

<input type="checkbox"/>	CrackArea	384.1833
<input type="checkbox"/>	CrackPixels	9.5154e+03
<input type="checkbox"/>	I	2653x790x3 uint8
<input checked="" type="checkbox"/>	Iclean	2653x790 logical
<input checked="" type="checkbox"/>	Icomp	2653x790 logical
<input type="checkbox"/>	Igray	2653x790 uint8
<input checked="" type="checkbox"/>	Ithres	2653x790 logical

Figure D.41: MATLAB crack area at 24 hours of plain concrete.

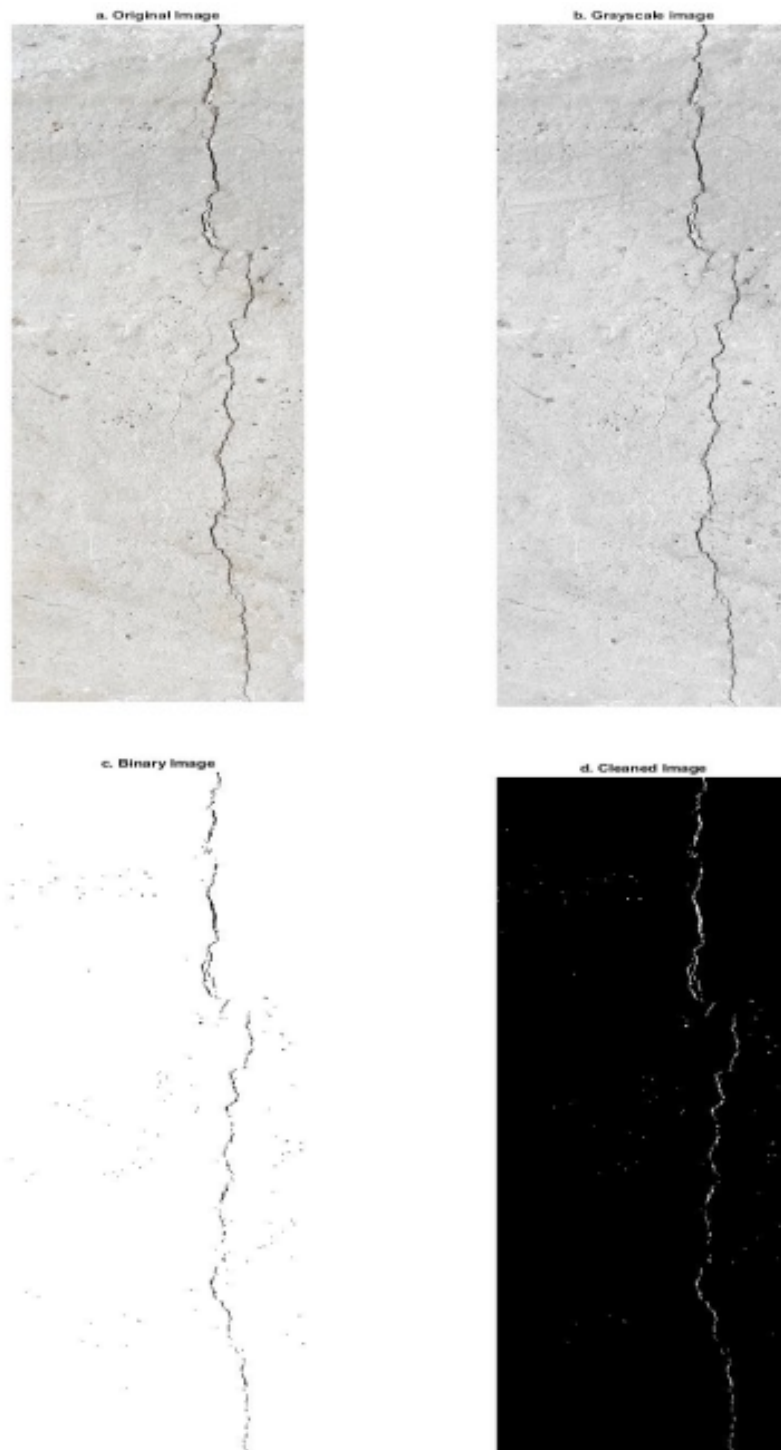


Figure D.42: MATLAB image processing steps for plain concrete.



**D.3.8.2 Optical methods measure****Table D.24** RTSFC40 optical measurement.

<b>Point</b>	<b>PC (mm)</b>	<b>SPC (mm)</b>
<b>1</b>	1	0
<b>2</b>	1	0
<b>3</b>	1	0
<b>4</b>	1	0
<b>5</b>	1.1	0
<b>6</b>	1.1	0
<b>7</b>	1.1	0
<b>8</b>	0.8	0
<b>9</b>	0.8	0
<b>10</b>	0.8	0
<b>11</b>	0.8	0
<b>12</b>	1	0
<b>13</b>	1	0
<b>14</b>	1.1	0
<b>15</b>	1.1	0
<b>16</b>	1.1	0
<b>17</b>	1.1	0
<b>18</b>	1.2	0
<b>19</b>	1.2	0
<b>20</b>	1.2	0
<b>21</b>	1.2	0
<b>22</b>	1	0
<b>23</b>	1	0
<b>24</b>	1	0
<b>25</b>	1	0
<b>26</b>	1	0
<b>Ave</b>	1.03	0

**D.3.8.3 Crack width methods measure**

<b>Concrete</b>	<b>MATLAB (mm)</b>	<b>Optical (mm)</b>
<b>PC</b>	1.06	1.03
<b>RTSFC40</b>	0	0